Effects of Low Oxygen Culture on Pluripotent Stem Cell Differentiation and Teratoma Formation

by

Jeffrey Robert Millman

Bachelor of Science in Chemical Engineering
North Carolina State University, 2005

Submitted to the Department of Chemical Engineering in Partial Fulfillment of the Requirements for the Degree of

Doctor of Philosophy in Chemical Engineering

at the

Massachusetts Institute of Technology

June 2011

Signature of Author: _____
Department of Chemical Engineering
April 28, 2011

Certified by: _____
Clark K. Colton
Professor of Chemical Engineering
Thesis Supervisor

Accepted by: _____
William M. Deen
Professor of Chemical Engineering
Chairman, Committee for Graduate Students

-Page Intentionally Left Blank-

Effects of Low Oxygen Culture on Pluripotent Stem Cell Differentiation and Teratoma Formation

by

Jeffrey Robert Millman

Submitted to the Department of Chemical Engineering on April 29, 2011 in Partial Fulfillment of the Requirements for the Degree of Doctorate of Philosophy in Chemical Engineering

Pluripotent stem cells (PSC) hold promise for the study of embryonic development and the treatment of many diseases. Most pluripotent cell research is performed in incubators with a gas-phase oxygen partial pressure (pO_2) of 142 mmHg. However, embryonic cells in early development are exposed to a local pO_2 of 0-30 mmHg, and the effects of such conditions on differentiating PSC are poorly understood. Residual PSC within differentiated populations are problematic because of their potential to form tumors *in vivo*. This is a major safety issue that must be overcome before PSC-based therapies can be used in the clinic. In this study, we differentiated mouse and human embryonic stem cells and mouse induced pluripotent stem cells at different defined pO_2 on highly oxygen-permeable silicone rubber culture dishes and assessed differentiation to the three germ layers, endoderm, ectoderm, and mesoderm and to cardiomyocytes and assessed residual PSC within differentiated populations.

Low pO_2 drastically affects differentiation of PSC to the three germ layers and cardiomyocytes. Overall, differentiation was higher to endoderm, lower to ectoderm, and higher or the same to mesoderm. Differentiation to cardiomyocytes was greatly enhanced without the need for purification, possibly by lineage selection via increased Mesp1 and Mesp2 expression. Understanding the effects of pO_2 during differentiation is an important step towards the development of protocols for regenerative medicine.

Control of pO_2 to physiological levels typical of the developing embryo reduced the fraction of PSC within, and the tumorigenic potential of, differentiated populations. Culture under differentiating conditions at low pO_2 reduced measured pluripotency markers by up to four orders of magnitude. Upon implantation into immunocompromised mice, low pO_2-differentiated PSC either did not form tumors or formed tumors at a slower rate than high pO_2 PSC. Low pO_2 differentiation could be combined with cell sorting for improved benefits. Low pO_2 culture alone or in combination with other methods is a potentially straightforward method that could be applied to future cell therapy protocols to minimize the possibility of tumor formation.

Thesis Supervisor: Clark K. Colton
Title: Professor of Chemical Engineering

Acknowledgements

This thesis would not be possible without the help, love, and support of so many people. First and foremost, I would like to thank my advisor, Prof. Clark Colton, who provided me with the freedom to explore avenues of research I found most interesting and engaged me in many spirited discussions that ultimately led to this work. I would also like to thank members of my thesis committee. Prof. William Deen provided invaluable support and advice on how to navigate the doctoral process. Prof. Susan Bonner-Weir was a continuous source of technical knowledge and assistance.

I am grateful for the wonderful environment all the members of the Colton laboratory created by their presence – Dr. Jin Dawson, Amanda Dilenno, Dr. Amy Johnson, Clarke Low, Dr. Michelle Miller, Dr. Anna Pisania, Dr. Daryl Powers, Dr. Mike Rappel, and Jit Hin Tan. I would like to particularly thank Dr. Daryl Powers, my predecessor, who left me with an exceptional experimental system and several protocols that were the foundation of my doctoral work. I leave the lab in the capable hands of Jit Hin Tan and Amanda Dilenno, both of who assisted me in experimental planning, execution, and analysis and discussed with me every aspect of our field. My undergraduate 'Army of Darkness' allowed me to investigate many more avenues of research in parallel than possible by myself - Bhargavi Chevva, Giulia Dula, Joshua Garvin, Ayushman Ghosh, Erica Griffith, Sina Omran, Julie Paul, Natalia Rodriguez, Minah Shahbaz, and Rose Yu.

I would like to thank the many outside people and laboratories that have assisted me. The Wittrup, Stephanopoulos, and Maheshri laboratories allowed me to use equipment that we could not afford. Dr. Krishanu Saha (Jaenisch laboratory, Whitehead Institute), Dr. Malgorzata Borowiak (Melton laboratory, Harvard University), Dr. Yuh-Shin Chang (Chien laboratory, Massachusetts General Hospital), and Renita Horton and Dr. E. Terry Sachlos (Auguste laboratory, Harvard University) taught me much about stem cell biology and laboratory techniques and performed joint pilot studies with me that were valuable in directing my research. I thank Randy Yerden (BioSpherix, Inc.) for the loaning me the Xvivo culture system. A special thank you goes to Dr. Kevin D'Amour and Dr. E. Edward Baetge (ViaCyte, Inc.) for allowing me to visit and work at ViaCyte for a month and teaching me so much about human embryonic stem cells and differentiation to β-cells.

I would also like to thank my family for their love and support throughout my life. My father (Don), mother (Beth), and sister (Megan) have always supported my decisions, been willing to smile and nod when I go on too long about my research, and provided me with a refuge always from 'the bubble'. Most importantly, I would like to thank my fiancée, Lily. We have shared the same path for so many years now. I am blessed to have such a wonderful, loving, and understanding person to share my life with. Not only has she been there for me personally but also intellectually, as we are able to talk to each other about our research and help each other out.

Dedicated to my mother and father for everything they have done for me

-Page Intentionally Left Blank-

Table of Contents

List of Tables

List of Figures

-Page Intentionally Left Blank-

Chapter 1. Introduction

1.1. Pluripotent stem cells

Pluripotent stem cells, such as embryonic stem cells (ESC) and induced pluripotent stem cells (iPSC), have immense clinical potential due to their ability to form all somatic cells found in the body [1-3]. These cells can potentially make major advances in human health, for example, by use in drug screening, in modeling of human disease *in vitro*, and as an unlimited supple of replacement tissue to treat heart disease, diabetes, and Parkinson's disease [3-6].

ESC are isolated from the inner cell mass of the developing blastocyst [7, 8] and are characterized by their ability to maintain their pluripotent state and differentiate. For mouse ESC (mESC), maintaining their pluripotent state is typically accomplished by the soluble factor leukemia inhibitory factor (LIF) and, for human ESC (hESC), is typically accomplished by the soluble factor basic fibroblast growth factor (bFGF) and coculture with mouse embryonic fibroblasts (MEFs) [7]. The molecular circuitry that regulates the pluripotent state of ESC is complex, involving transcription factors, chromatin modification, miRNA, and signaling pathways. The transcription factors Oct4, Nanog, and Sox2 are considered to be the master regulators of this network and lie within its core. ESC have been differentiated *in vitro* into a wide range of cell types, such as

cardiomyocytes [8], β-cells [9], and neurons [10] and then implanted into rodent models of cardiac infarct, diabetes, and Parkinson's disease to improve function.

iPSC are a promising alternative source of pluripotent stem cells that are derived from somatic cells, such as fibroblasts, via reprogramming by inserting, often by virus vectors, factors such as Oct4, Sox2, c-Myc, and Klf4 [11] or Oct4, Sox2, Nanog, and Lin28 [12]. iPSC have properties similar to those of ESC [13]. One major concern is the safety of these cells. c-Myc is a proto-oncogene that presents a tumorigenic risk. Mouse iPSCs (miPSC), derived with modified protocols without c-Myc, have reduced occurrence of tumor formation [14]. Viral insertions also possess a risk of tumor formation. Methods for generating iPSCs without viruses [15, 16], using small molecules in combination with Oct4 and Klf4 gene insertion [17], and without residual programming factors [18] have been explored. More recently, reprogramming has been achieved in mouse cells using only recombinant proteins [19].

1.2. The effects of low oxygen on self-renewal and differentiation of PSC

Adapted from Millman, J.R., J.H. Tan, and C.K. Colton, *The effects of low oxygen on self-renewal and differentiation of embryonic stem cells.* Current Opinions in Organ Transplantation, 2009. **14**(6): p. 694-700 with permission of Lippincott Williams & Wilkins

Human pluripotent cells are a renewable source of replacement tissue that have the potential to treat many diseases, including heart disease, type I diabetes, and Parkinson's disease. However, many hurdles remain before this new era of regenerative medicine can be realized. All cells of the developing embryo are exposed to oxygen levels *in vivo* far below that of atmospheric levels, and they differentiate and undergo organogenesis in a low oxygen environment [20-26]. The local oxygen environment is potentially an important variable for manipulation by researchers hoping to recapitulate specific differentiation pathways *in vitro* to produce replacement tissues from pluripotent stem cells for regenerative medicine. Here, we review recent reports investigating the effects of low oxygen on the undifferentiated phenotype and on the differentiation process, and we address the issue of control of pO_{2cell} during culture.

1.2.1. Undifferentiated phenotype

The ability to propagate pluripotent stem cells in their undifferentiated state is essential to produce sufficient cells for future applications, and the effects of oxygen levels much lower than that in a standard incubator on undifferentiated cells have been examined in a number of studies (Table 1-1). Throughout this review, we will refer to oxygen levels either as a percentage or a partial pressure in mmHg, as it was reported in the original papers, with standard incubator oxygen referred to as 20%, even though it is actually often 18.7% (142 mmHg).

1.2.1.1. Derivation of new embryonic stem cell lines

Derivation of new ES cell lines, both mouse [27, 28] and human [29], benefit from being performed in low oxygen levels. Studies examining the establishment of new ES cell lines from blastocysts under 5% oxygen have had greater success than under 20% more commonly used. The benefits of low oxygen conditions include an increase in the number of individual colonies exhibiting alkaline phosphatase activity [28], an increase in the number of proliferating cells [27], and removal of the need for undefined animal-derived products such as serum or matrices in the process [29], the last of which can be crucial in the applicability of these derived cells to clinical applications.

1.2.1.2. Pluripotency

Low oxygen affects the pluripotent phenotype of mESCs when they are cultured with leukemia inhibitory factor (LIF), a cytokine commonly used to prevent differentiation [30]. Normally, mESC colonies have smooth edges, but this morphological phenotype is lost with low oxygen exposure, instead causing the colonies to have fibroblast-like morphologies [31] or to form jagged edges [32], both signs of early differentiation despite the presence of LIF. These morphological changes are also associated with reduced levels of alkaline phosphatase activity and pluripotency gene (Oct4, Nanog, and Sox2) expression [31, 32]. One study [31] proposed that HIF-1α protein, the concentration of which

increases at low oxygen, mediates suppression of the LIF-STAT3 pathway as evidenced by a reduction in the expression of the LIF receptor under hypoxia. Interestingly, in one report [32], despite these observations, the cells maintained some potential to differentiate into cells of all three germ layers.

In contrast to mESCs, expression of Oct4, Nanog, and Sox2 in hESCs are apparently not affected by hypoxic culture (2% to 5% oxygen) [33, 34]. In one study, however, Nanog and Notch1 mRNA expression is increased in hESCs cultured over a four-week period at 5% oxygen compared to those cultured under 20% oxygen. This difference is not maintained after long term culture under the hypoxic condition, since there is no significant difference in Nanog and Notch1 mRNA levels between cells cultured for 18 months under either 5% or 20% oxygen. Consistent with earlier results, no differences in Oct4 expression are observed under both oxygen conditions with either short or long term culture [35].

Despite not affecting gene expression of Oct4, Nanog, and Sox2 directly, hypoxic culture results in wide-spread transcriptome differences in hESCs when compared to culture under ambient oxygen conditions, including downstream targets of unaffected genes Oct4, Nanog, Sox2 [34]. Amongst other affected genes, Lefty2, a member of the TGFβ family of proteins, which is hypothesized to play a role in preventing differentiation, is down-regulated at 20% oxygen compared to culture at 4%. This may lead to a greater proclivity for the hESC to differentiate. In studies on the transcriptome-wide effects of hypoxic culture on

hESCs kept under self-renewing conditions, culture at ambient pO_{2gas} results in greater heterogeneity amongst different hESC lines than when cultured under hypoxic (2-4% oxygen) conditions [33]. This heterogeneity may arise from subpopulations of cells already undergoing early differentiation when cultured at 20% oxygen.

While low oxygen appears not to affect pluripotency gene expression directly, differentiated areas of each colony expressing SSEA-1, a marker of early differentiation for hESCs, are reduced when cultured under 3% and 1% oxygen compared to normoxic culture [36]. In a different study, however, culture at 2% oxygen did not affect expression of either SSEA-4 or SSEA-1 in hESCs when compared to ambient oxygen conditions [37].

HIF-1α has been investigated as an important gene mediating hESC hypoxic response. In one report, co-culture of hESCs with transgenic human fetal liver stromal cells ectopically expressing HIF-1α protein prevents hESC differentiation and even increases Oct4 and Nanog expression [38]. Another study [39] suggests a possible link connecting HIF-1α action with Notch signaling. In mouse embryonic teratocarcinoma cells and neural stem cells, hypoxia allows for the accumulation of HIF-1α, which stabilizes the Notch intracellular domain, in turn promoting the undifferentiated phenotype. The action of Notch in promoting self-renewal appears to be conserved in hESCs in view of a recent demonstration

that self-renewal is mediated by activation of the Notch pathway and that benefits of hypoxic culture are eliminated with inhibition of Notch signaling [35].

1.2.1.3. Proliferation

Many studies have found that low oxygen affects proliferation, but this effect varies between studies and cell lines. In one study [28], proliferation of mESCs increases under 5% compared to 20% oxygen, while in another [32], no difference is observed in one cell line and a small increase in another. Culture at 1% oxygen or lower, however, reduces the rate of proliferation compared to 20% [31, 32]. mESCs are able to adapt and continue to proliferate under anoxia, albeit with a longer doubling time compared to 20% oxygen, and have the ability to utilize anaerobic respiration exclusively for their energy requirements [32]. Similarly disparate results have been reported for hESCs: In one study, proliferation rates at 5% oxygen are reduced compared to 20% [35], in another, no differences in the rates are observed at 5% and 3% and only a slight reduction at 1% [36].

1.2.1.4. Clonal recovery

Low oxygen culture improves clonal recovery after passaging. mESCs at 5% oxygen [40] and hESCs at 2% [37, 41] have improved clonal survival. Cytogenetic instability at high passages for mESCs is not reduced in culture at

5% oxygen [27], and further reductions in oxygen to even 0% do not affect the amount of oxidative DNA damage incurred by the cells [32]. In contrast for hESCs, 2% oxygen reduces chromosomal abnormalities after multiple passages [37], suggesting a further benefit of hypoxic culture.

1.2.2. Differentiation

Differentiation is a major hurdle for the successful translation of stem cell research to clinical applications. Given that low partial pressures of oxygen (pO_2) is an important physiological cue during development [42], it is not surprising that low pO_2 influences differentiation to many cell types (Table 1-2).

1.2.2.1. Neurons

Low oxygen has different effects on specific stages of differentiation of pluripotent cells to dopaminergic neurons. While low oxygen reduces differentiation from mESCs to neural stem cells (NSCs) compared to 20% oxygen [43, 44], it increases subsequent differentiation to neurons. mESCs differentiated to NSCs at standard incubator oxygen followed by differentiation at low (3.5%) oxygen have a higher number of dopaminergic neurons (tyrosine hydroxylase (TH)-expressing cells) compared to 20% oxygen. Differentiation with a neuronal differentiation-promoting cytokine mixture increases the number of dopaminergic neurons at 20% oxygen to a value equal to that at low oxygen

without the cytokine mixture, but, interestingly, combining the cytokine mixture with low oxygen culture does not further increase neural differentiation [43]. Knocking down HIF-1α expression with antisense nucleotides decreases differentiation to TH+ cells, indicating that low-oxygen enhancement of the second differentiation step is HIF-1α-mediated, which is not surprising since HIF-1α is necessary for proper brain development [45].

Even though low oxygen decreases differentiation of pluripotent cells to NSCs, differentiation of mESCs entirely at low oxygen can increase the yields of neurons compared to 20% oxygen. In one study [44], the number of beta III tubulin+ and MAP2+ (both neuron markers) cells are increased by factors of 55 and 114, respectively, when differentiated entirely at 2% compared to 20% oxygen [44]. This is related, in part, to a greater total cell number by a factor of 34 with differentiation at 2% compared to 20% oxygen.

1.2.2.2. Cardiomyocytes

Low oxygen increases the number of cardiomyoyctes from both hESCs and mESCs in bioreactors. HIF-1α is necessary for proper heart development [46], and differentiation with a HIF-1α knockout mESC line results in no observable spontaneously-beating cells [47], suggesting oxygen is an important environmental parameter. Using a strategy to selectively kill non-cardiomyocytes, the yield of cardomyocytes from mESCs is increased by a factor of 1.5 with

differentiation at 4% compared to 20% oxygen in one report [48]. However, no difference between the two oxygen levels occurs before genetic selection. With hESCs, differentiation at 4% oxygen increases the total cell number by 30-47% compared to 20% oxygen [49]. However, the fraction of spontaneously-beating EBs is the same under both oxygen conditions, and while some cardiac markers are increased, others are unaffected by low oxygen. From these reports, it is unclear if the increased cardiomyocyte number is due to preferential differentiation to cardiomyoyctes or simply to increased total number of cells. Recent unpublished data from the authors' laboratory indicates that both phenomena occur when mESCs are differentiated to cardiomyocytes at low oxygen.

1.2.2.3. Hematopoietic progenitor and endothelial cells

Low oxygen works in a complicated network to influence differentiation of pluripotent cells to blood and endothelial fates [50]. Vascular endothelial growth factor (VEGF), a growth factor secreted by cells at low oxygen, increases differentiation of mESCs to hemogenic mesoderm. These cells continue to differentiate to endothelial cells with activation of Flk-1, a VEGF receptor. Without VEGF, which is the situation if cells are cultured at 20% oxygen, Flk-1 is inactivated, resulting in the formation of hematopoietic progenitor cells. Even at low oxygen, VEGF can be inhibited by the presence of soluble Flt-1, a protein that cells express with increasing differentiation by binding VEGF and making

VEGF unavailable to activate Flk-1. VEGF secretion and inhibition results in an oxygen-dependent competitive balance between free and bound VEGF that influences differentiation of mesoderm to hematopoietic progenitor and endothelial cells. This example illustrates how understanding the mechanism by which low oxygen affects lineage selection is important for successful applications in regenerative medicine.

1.2.2.5. Chondrocytes

Chondrocytes normally reside in a low oxygen environment [51], and the effects of low oxygen on differentiation of pluripotent cells to this cell type has been investigated. Low oxygen increases collagen synthesis and biomechanical functionality of hESC-derived chondrocytes [52]. Differentiation at 2% oxygen increases collagen I and II content, tensile modulus, and compressive properties compared to differentiation at 20%. However, when these low oxygen-derived chondrocytes are used to form tissue using a scaffold-less strategy, the reverse is true: tissues formed at 20% oxygen have higher collagen content and better physical properties. Low oxygen can have different effects on different aspects (e.g. differentiation and tissue engineering) of a bioengineering strategy, and these differences must be understood to fully utilize low oxygen culture in regenerative medicine.

1.2.3. Control of pO_{2cell}

Most of the studies reviewed here implicitly make the assumption that pO_{2gas} is equal to pO_{2cell}. However, depending on the cell density, medium height, cellular oxygen consumption rate, and oxygen permeability of the culture substrate, pO_{2cell} can differ drastically from pO_{2gas} [53]. Furthermore, step changes in pO_{2gas} due to removal of culture dishes from the incubators may result in transient changes in pO_{2cell} with long time scales for equilibration. These problems are ameliorated by culturing the cells on the surface of a membrane with very high oxygen permeability, such as silicone rubber [53].

To illustrate this point, we estimate pO_{2cell} in two published studies [43, 44] (Table 1-3) using oxygen consumption rate and transport parameters combined with a model we previously developed for mESCs in monolayer [53]. The differences in pO_{2cell} and pO_{2gas} are very small (<2 mmHg) for one study and large (>20 mmHg) for the other because the cell densities and media heights are substantially different. Even though pO_{2gas} in one study (26.6 mmHg) is higher than in the other (15.5 mmHg), the order of the calculated pO_{2cell} values is reversed, 5.2 and 12.4 mmHg respectively. These results demonstrate that the assumption that pO_{2cell} is equal to pO_{2gas} is not valid for high cell densities and media heights. Knowledge of pO_{2cell} is important for successful interpretation of experimental results and comparisons between different studies.

Differences in pO_{2cell} between different experiments carried out at the same pO_{2gas} may be a possible explanation for the inconsistencies in data reported. For instance, one study [35] reports reduced proliferation of hESCs cultured at 5% oxygen, and another [36] reports no reduction in proliferation at the same oxygen condition. In the first study, there are four weeks between passages (initial and final cell numbers not reported). In the second study, $6x10^5$ cells are plated per well of standard six-well tissue culture plates, and there are only two weeks between passages, with final cell numbers of $1.5\text{-}2.5x10^6$ cells per well. It is possible that the pO_{2cell} of the first study is significantly lower than the pO_{2gas} because of higher cell densities, in particular after extended culture without passage, while pO_{2cell} in the latter study is closer to pO_{2gas}. This would help explain the differences in results because the authors of the second study report a reduced proliferation at 1% gas phase oxygen level, which may be closer in cellular oxygen level to the 5% gas phase oxygen level of the first study that also demonstrated a reduced proliferation rate. Moreover, the first group use the Xvivo system (BioSpherix, Lacona, NY), which allows for continuous culture low pO_{2gas} without interruption for media changes and passaging. The second group use a conventional sealed chamber from which cells are periodically removed for media changes and passaging, allowing for periods where pO_{2gas} is at ambient levels, disrupting the low pO_{2cell} conditions. Without information regarding the experimental conditions, especially the media height and cell density, it is impossible to draw any conclusions.

There are instances where oxygen levels higher than ambient may be beneficial for differentiation, but control and understanding of the oxygen level experienced by the cells is still essential. Mouse pancreatic bud explants cultured at 35% oxygen preferentially differentiate to β-cells [54]. This benefit is greatest when the cells are cultured on top of a membrane with enhanced oxygen permeability compared to culture on a micro-porous membrane completely immersed in culture medium, a standard method for explant culture. pO_{2cell} on the high permeability membrane is closer to pO_{2gas} than with the standard method, allowing for better control of pO_{2cell} because oxygen permeates across these membranes more rapidly than through culture media.

1.2.4. Conclusions

Although cells and tissues differentiated from pluripotent cells have the potential to treat many diseases, improvement in methods to produce these tissues is needed, and control of cell oxygen level is potentially important in addressing this issue. Under conditions maintaining the undifferentiated phenotype, low oxygen reduces spontaneous differentiation of hESCs but has the opposite effect on mESCs, although reports are conflicting. Similar disparities are reported for proliferation rates. Differentiation under low oxygen can increase yields of desired cell types through a combination of preferential differentiation and higher total cell numbers. Low oxygen can have different effects on different stages of differentiation, so detailed understanding of the phenomena and its mechanisms

is vital. One major problem in the field is the lack of recognition that pO_{2cell} is often different from pO_{2gas}, sometimes by a substantial amount, which is exacerbated because values of cell density and media height necessary for retrospective estimation of pO_{2cell} are often not reported. Knowledge of pO_{2cell} is necessary for interpreting the results of studies and comparing them to data from other studies. Efforts to estimate or control pO_{2cell} are essential for rational advancement of this field.

1.3. Differentiation to cardiomyocytes

Adapted from Horton, R.E., J.R. Millman, C.K. Colton, and D.T. Auguste, *Engineering microenvironments for embryonic stem cell differentiation to cardiomyocytes.* Regenerative Medicine, 2009. **4**(5): p. 721-32 with permission of Future Medicine Ltd

The inability of the human heart to repair itself after trauma renders it vulnerable to ischemia, viral infection, or other pathologies. Significant loss of cardiomyocytes is irreversible and may progress to heart failure. Congestive heart failure is endemic; one in three American adults suffers from one or more types of cardiovascular disease [55]. Lack of a sufficient organ supply to fulfill demand coupled with donor compatibility and organ rejection leaves a dire need for new therapeutic alternatives. Cell replacement therapies may be the solution to this deficit.

Many regenerative efforts focus on ESCs as a possible method for organ repair. ESCs are derived from the inner cell mass of blastocysts and have the potential to regenerate indefinitely and differentiate into virtually any cell type. Because of these capabilities, hESCs may be a renewable source of differentiated cells for regenerative medicine. However, embryonic differentiation is poorly understood. Of particular interest is robust cardiomyocytes for cardiovascular repair.

Cardiomyocytes are an ideal cell type for implantation to replace diseased or necrotic heart tissue because of their unique electrical, mechanical, and biological characteristics. ESC-derived cardiomyocytes display pacemaker-, atrial-, and ventricular-like characteristics [56], and spontaneously beat *in vitro*. These cardiomyocytes can integrate *in vivo* into the myocardium and improve the function of ventricles after infarction in animal models [8, 57, 58]. For example, porcine hearts exhibiting complete blockage were injected with microsectioned

hESC-derived cardiomyocytes. Electocardiogram analysis revealed that the injected cardiomyocytes successfully coupled with native heart tissue and were able to conduct electrical activity [8, 57, 58]. Concerns regarding implantation remain, including beating synchrony between implanted cells and native cells and inflammation at the injection site.

In addition to integration concerns, sufficient hESC populations are needed to repair damaged tissue. It is estimated that on the order of 10^9 replacement cells would be necessary to treat a cardiac infarct [59]. Attention has turned to the expansion of hESC and new strategies for their differentiation. Studies have focused on the use of signaling hESC through addition of morphogens and modifications to the microenvironment to increase cardiac cell generation. Here, we review strategies that give rise to increased cardiac differentiation based on controlling the stem cell microenvironment.

hESC are often induced to differentiate by generating three-dimensional suspended cellular aggregates called embryoid bodies (EBs) in the absence of MEF and bFGF [60, 61] (Figure 1-1). EBs recapitulate many aspects of embryonic development and can serve as a model for studying organ development. The complex three-dimensional environment provides temporal and spatial cues that control differentiation into all three germ layers.

Matrix-cell and cell-cell interactions are important in stem cell differentiation, which are affected by EB size. Conventional methods used to generate EBs often results in heterogeneous size and shape. Microcontact printing [62], forced aggregation [63-65], and microwells [66] are common methods for addressing heterogeneity.

Microcontact printing is a well established technique that restricts cell growth surface area, forcing cells to conform to the patterned protein regions. ECM proteins are 'inked' onto a polymer stamp containing an array of geometric designs and then printed onto a substrate. Areas without ECM protein are treated to inhibit cell adhesion, yielding a fixed array of protein islands. A cell suspension is washed over the substrate, and cells only attach to regions with protein. EBs are formed by detaching the resulting colonies from adherent surfaces and continuing culture in suspension. This technique allows for cell number control, which is dictated by the adhesive area, resulting in colony size control [67, 68].

Altering colony and EB size influences differentiation decisions to cardiomyocytes. Bauwens *et al.* demonstrated that hESC colony size, controlled using the microcontact printing technique, influences cellular gene expression. Using real-time polymerase chain reaction (PCR) quantification [69]. They show that the Gata6 (endodermal marker)/Pax6 (neural marker) ratio increases with smaller colony size and hESC with a high Gata6/Pax6 ratio preferentially differentiate to cardiomyocytes. The endoderm secretes procardiogenic factor

whereas neural signals, such as Wnt, inhibit embryonic heart development. hESC colony size and EB size are interrelated parameters that influence cell fate by altering gene expression and should be controlled in differentiation studies. In another study, Niebrugge *et al.* combined EB size and oxygen control. Using microcontact printing, uniform hESC-derived EBs were generated and exposed to hypoxic (4% oxygen) conditions, resulting in a 3.5-fold increase in overall cardiomyocyte output when compared to traditional EB formation methods [70].

Another technique for controlling EB size is forced aggregation, which typically entails the centrifugation of a defined number of cells into multiwell plates. Forced aggregation was used to deposit hESC into round bottom multi well plates to examine the effects of size on EB differentiation patterns. Ng *et al.* found that efficient blood cell formation required at least 500 hESC per well, whereas optimal erythropoiesis was achieved in wells containing 1000 hESC per well [65].

Control of colony size, the number of ESC comprising EBs, and the gene expression profiles of input cells within EBs are important in influencing cell fate decisions and is an important environmental parameter. Furthermore, controlling the size of EBs can allow for better control of biomolecular and oxygen gradients [71], which may affect differentiation mechanisms. Because many differentiation methods rely on factors to induce differentiation, molecular diffusion and gradient concentrations within cell colonies can produce heterogeneous differentiation.

Recent progress has been made differentiating hESC under two-dimensional, serum-free culture by adding exogenous factors to direct differentiation to cardiomyocytes, allowing better control of the microenvironment [8]. Passier *et al.* employs a 2D coculture method to induce differentiation of hESC towards cardiomyocytes. Replacing the typical MEF feeder layer with mitomycin C inactivated END-2 cells, which exhibit characteristics of visceral endoderm, in the presence or absence of serum led to cardiomyocyte formation. Furthermore, the absence of serum enhanced hESC differentiation towards cardiomyocytes [72].

Many studies have examined cellular responses to growth factors. In particular, studies have employed serum-free media, conditioned media, or used media additives, such as activin A [73], ascorbic acid [74], dimethyl sulfoxide (DMSO) [75], 5-azacytidine [76], retinoic acid [77], and vascular endothelial growth factor (VEGF) [29], to promote differentiation to cardiomyocytes. The *in vitro* functionality of these cardiomyocytes is assessed by visual observation of spontaneous contractions, measurement of the action potential, and measurement of intracellular Ca^{2+} oscillations [78]. Numerous signaling pathways, such as transforming growth factor beta (TGFβ), bone morphogenic protein (BMP), Wnt, and Notch, are involved in cardiogenesis [6]. Behfar *et al.* reported that TGFβ and BMP-2 activated cardiac promoters in mESC, leading to the expression of cardiac transcription factors NK2 transcription factor related, locus 5 (Nkx2.5) and myocyte enhancer factor 2C (MEF2C) and cardiomyocyte

differentiation [79]. mESC differentiation methods are often translated to hESC, but differentiation of cardiomyocytes from hESC is often less efficient. More recently, translation of differentiation strategies from hESC to iPSC has been investigated.

iPSC are a promising alternative source of autologous cells [11, 80] and are derived by reprogramming somatic cells to an ESC-like state by inserting, often by viral vectors, factors such as Oct4, Sox2, c-Myc, Klf4, Nanog, and Lin28 [81]. Cardiomyocytes derived from both mouse [82-84] and human [85] iPSC (miPSC and hiPSC) have nodal-, atrial-, and ventricular-like action potentials, similar cardiac gene and protein expression, and spontaneous contraction rates similar to ESC-derived cardiomyocytes. Some found the rate and efficiency of differentiation comparable to ESC [82], others slower [83] and less efficient [83, 85]. Persistent expression of the transgene c-Myc, a proto-oncogene that presents a tumorigenic risk, was observed with a cardiomyocyte differentiation protocol [85]. Other cardiovascular cell types reported include endothelial, smooth muscle, and hematopoietic cells [82, 84].

Methods for quantifying cardiomyocyte generation from ESC vary. The most basic approach is to count the fraction of resulting EBs containing cells that spontaneously contract, providing crude quantification of the effects of an experimental treatment on generating cardiomyocytes compared to a control. This method does not provide information on the cells within an EB. Better

quantification can be achieved by measuring the fraction of cardiomyocytes in the total cell population by immunostaining cells for cardiac-restricted proteins, such as sarcomeric myosin heavy chain, cardiac troponin T, α-sarcomeric actin, and cardiac-restricted alpha major histocompatibility complex. The fraction of cells expressing these proteins may be counted with a flow cytometer. This information can be combined with a measurement of the total cell number to calculate the number of cardiomyoyctes or, when the number of initial ESCs is known, the number of cardiomyocytes generated per input ESCs, the most useful comparison. However, most or all of this information is seldom provided, limiting rigorous comparisons between different studies.

Numerous challenges need to be addressed before hESC can be used in clinical and therapeutic applications, such as the ability to generate cardiomyocytes in clinically relevant numbers, minimization of spontaneous differentiation, and elimination of tumor-formation risk. Differentiation typically yields a mixture of cell lineages of unsuitable purity for regenerative therapies. Residual undifferentiated hESC within differentiated populations have the potential to form tumors upon implantation. If these challenges can be overcome, hESC or iPSC-derived cardiomyocytes could be used to treat heart disease, opening a door to a new era of regenerative therapies.

1.4. The tumorigenicity of pluripotent stem cells

The tumorigenicity of PSC is a major obstacle for the safe translation of stem cell biology to regenerative medicine that must be overcome [86], and the presence of any number of PSC is a potential tumor formation risk. As few as 2 m ESC have formed tumors in immunocompromised mice [87]. There have been no reported cases of undifferentiated PSC being implanted into humans, but in one case study, fetal neural stem cells implanted into a human caused the formation of a glioneuronal neoplasm, derived from donor cells [88]. Implanted iPSC can also form tumors, with a propensity that varies depending on the tissue of origin [89]. iPSC have the additional concern that inserted c-MYC genes could become reactivated and cause tumor formation [90]. In addition to the health risks to the recipient by the presence of the tumor, tumor formation could also cause a reversal of the clinical benefits of the implanted differentiated cells [91]. Preclinical testing of any stem cell-derived product for tumor formation is very important [92, 93].

Differentiation of PSC reduces the risk of tumor formation [94]. However, residual PSC can still persist, even after being subjected to a differentiation protocol, and cause tumor formation upon implantation [9, 95]. Even though studies have reported that differentiation of PSC completely avoided tumor appearance [96, 97], these experiments were not designed to sensitively detect residual PSC. A small number of residual PSC may still exist and be a safety risk for humans,

which require larger cell numbers for treatment. The experimental design of other studies has allowed for the formation of tumors with low numbers of implanted PSC [87, 98]. The fraction of animals that form tumors and the rate of tumor formation depends on the location of the implanted cells, with subcutaneous and intramuscular injections being the most convenient, sensitive, and reliable [87, 98-100].

Several methods have been used to reduce residual PSC [101]. Genetic selection has been used to kill residual PSC while retaining the desired cell type [102]. However, genetic manipulations introduce an additional hurdle to clinical translation. Positive and/or negative selection by staining cells with an fluorescently-labeled antibody against surface markers, followed by fluorescence activated cell sorting (FACS), has been used [95, 103]. An antibody, termed mAb 84, has been identified that binds to the surface protein podocalyxin-like protein-1 (PODXL) and causes cytotoxicity to human ESC (hESC) via oncosis [104], reducing the viability of undifferentiated hESC populations by a factor of 3-5 [105].

1.5. Objectives

In order for pluripotent stem cells to create a new era of regenerative medicine, they must be successfully differentiated to clinically-relevant cell types of sufficient number and purity that can be implanted into patients without the risk of tumor formation. The central hypothesis of this thesis is that oxygen is an

important parameter that greatly affects pluripotent stem cell differentiation. The objectives of this research were to investigate the effects of low oxygen culture on differentiation to the three germ layers, with particular emphasis on cardiomyocytes, and on the number and fraction of potentially-tumorigenic residual undifferentiated pluripotent cells within differentiated populations. Results and experimental details of comprehensive studies on these two objectives are described in the subsequent chapters.

1.6. Overview

Chapter 2: Extended low oxygen culture of pluripotent stem cells reduces the fraction of residual tumor-forming cells in differentiated populations

This chapter describes the effects of low oxygen culture on residual PSC within differentiated populations. mESC, miPSC, and hESC were differentiated *in vitro* for up to 90 days at 142, 36, or 7 mmHg pO_{2gas} on highly-oxygen permeable silicone rubber culture plates. Residual PSC were assessed by real-time PCR measurements of Oct4 and Nanog mRNA and by flow cytometric measurements of Oct4-GFP expression. Cells were implanted into immunocompromised mice to assess tumor formation rate. Low oxygen culture methodology was combined with fluorescence activated cell sorting (FACS) of residual Oct4-GFP+, SSEA-1+, and SSEA-4+ cells. Residual Oct4-GFP+ cells were separated from differentiated populations using FACS and characterized by morphological assessment,

immunostaining for Oct4, Nanog, and SSEA-1 protein expression, and *in vitro* differentiation. The necessity of the HIF-1α gene was assessed through use of a HIF-1α homozygous knockout mESC line.

Chapter 3: Differentiation of pluripotent stem cells under low oxygen increases generation of cardiomyocytes and influences differentiation to ectoderm, mesoderm, and endoderm

This chapter describes work that was done with Dr. Daryl E. Powers on assessing the effects of low oxygen on the differentiation of PSC to derivatives of the three germ layers, ectoderm, mesoderm, and endoderm. mESC, miPSC, and hESC were differentiated *in vitro* for up to 13 days at 142, 36, or 7 mmHg pO_{2gas} on highly-oxygen permeable silicone rubber culture plates. Real-time PCR, flow cytometry, and immunostaining for numerous markers of the three germ layers were used. The generation of cardiomyocytes was further assessed by measurements of spontaneously-beating area on the culture plate. A mathematical model was developed for the volumetric distribution of cardiomyocytes within differentiated cell aggregates. The necessity of the HIF-1α gene was assessed through use of a HIF-1α homozygous knockout mESC line.

Appendix A: Accurate control of oxygen level in cells during culture on silicone rubber membranes with application to stem cell differentiation

This appendix contains a published manuscript, of which I am a co-first author with Dr. Daryl E. Powers, demonstrating the use of silicone rubber membranes for controlling pO_{2cell}. Mass transport models of oxygen diffusion and consumption in 2- and 3-dimesional culture are described. Fibronectin and Matrigel were physically absorbed onto the membranes to promote cell attachment. mESC were differentiated 11 days *in vitro* at 142, 36, or 7 mmHg pO_{2gas} on highly-oxygen permeable silicone rubber culture plates. Flow cytometry and measurements of spontaneously-beating area on the culture plate. were used to quantitate the generation of cardiomyocytes.

Appendix B: Effects of oxygen on mouse embryonic stem cell growth, phenotype retention, and cellular energetics

This appendix contains a published manuscript, of which I am a co-author, describing the effects of oxygen on mESC growth, phenotype retention, and cellular energetics. mESC were cultured on polystyrene at pO_{2gas} values ranging from 0-285 mmHg. Cell number and viability was determined with flow cytometry. Oxygen consumption rate was determined. A comet assay was used to determine oxidative DNA damage. Pluripotency and differentiation was assessed

with morphological characterization and measurements of the expression of markers with real-time PCR and flow cytometry.

Appendix C: Differentiation of hESC to β-cells

This appendix describes work performed at ViaCyte, Inc. demonstrating my ability to replicate a protocol developed by ViaCyte differentiating hESC to insulin-secreting cells. hESC were differentiated *in vitro* for up to 29 days at 142 mmHg pO_{2gas} on polystyrene and highly-oxygen permeable silicone rubber culture plates. Real-time PCR and immunocytochemistry are used to measure the expression of pluripotency and differentiation markers. Oxygen consumption rate was determined. ELISA is used to measure c-peptide contain in the culture medium.

Appendix D: Experiments with the BioSpherix Xvivo

This appendix describes work performed with the Xvivo incubation system, fabricated by BioSpherix, Inc., demonstrating the effect of continuous oxygen exposure on VEGF secretion and cardiomyocyte differentiation and describing the use of oxygen sensors. mESC were cultured and differentiated *in vitro* for up to 10 days at 142 and 36 mmHg pO_{2gas} on polystyrene and highly-oxygen permeable silicone rubber culture plates in flush boxes or Xvivo incubations systems. VEGF secretion was measured with ELISA. Differentiation to

cardiomyocytes was assessed with flow cytometry. Oxygen sensors were assessed with finite element modeling and used in conjunction with a PID controller under a variety of cell culture scenarios.

1.7. Tables and Figures

Table 1-1. Effects of hypoxic culture on pluripotent stem cells

Species	Study	Cell Line(s)*	Culture Surface Modification	Oxygen Level (%)	Effects of low O_2 compared to standard O_2
Mouse	Wang 2008	New lines from **C57B1/6J mice**	Gelatin	5, 20	With physiological glucose levels, enhanced proliferation of cells but did not reduce rate of apoptosis. No reduction in cytogenetic stability at high passages.
	Gibbons 2006	New lines from **C57/BL6 embryos**	MEFs	5, 20	More blastocysts produced outgrowths and had AP activity. Increased proliferation.
	Jeong 2007	**CCE, R1, J1, E14TG2**	Gelatin	1, 20	Reduced AP activity and Oct4 expression. Proposed mechanism whereby HIF-1α mediates suppression of the LIF-STAT3 pathway. Reduced proliferation rates.
	Powers 2008	**CCE, D3**	Gelatin	0, 1, 5, 20, 40	Maintained pluripotency under a wide range of O_2 conditions, although high (40%) and low (0-1%) O_2 reduced Oct4/Nanog/Sox2 expression. Reduced proliferation rates at high (40%) and low (0-1%) O2. No change for intermediate values (5-20%). No effects on oxidative damage to DNA under all conditions
	Ying 2008	**E14Tg2a**	-	5, 21	Clonal propagation achieved without B27 supplement in serum-free culture.
Human	Ludwig 2006	**WA15 & WA16**	Matrigel or a combination of collagen IV, fibronectin, laminin, and vitronectin	5, 10, 20	Highest proliferation rate at 5% oxygen/10% CO_2
	Forsyth 2008	**H1, RH1, H9**	Matrigel	2, 21	Reduced heterogeneity in transcriptome. No change in expression of Oct4/Nanog/Sox2.
	Westfall 2008	**H1, H9**	MEFs or Matrigel	4, 20	Reduced heterogeneity in transcriptome. No change in expression of Oct4/Nanog/Sox2. Increased expression of Lefty2.
	Prasad 2009	**CLS1, CLS2**	HFF-1	1, 5, 10, 15, 21	No change in Oct4 expression, some increase in Nanog/Notch1 expression at 5% in culture for 4 weeks, no difference compared to 20% when cultured for 18 months. Reduced proliferation rates at 5%.
	Ezashi 2005	**H1**	MEFs or Matrigel	1, 3, 21	Reduction of differentiated areas around colonies expressing SSEA-1 at 1% and 3%. No differences in proliferation rates at 3%, slight reduction at 1%.
	Forsyth 2006	**H1, H9, RH1**	Matrigel	2, 21	No change in SSEA-1 or SSEA-4 expression. Increased clonal recovery. Decreased chromosomal abnormalities.
	Hewitt 2006	**H9**	Matrigel	2, 21	Increased clonal recovery.

*Boldface indicates main cell line(s) used.

MEFs - Mouse Embryonic Fibroblasts; AP - Alkaline Phosphatase; HIF - Hypoxia Inducible Factor; LIF - Leukaemia Inhibitory Factor; HFF - Human Foreskin Fibroblasts

Adapted from Millman, J.R., J.H. Tan, and C.K. Colton, *The effects of low oxygen on self-renewal and differentiation of embryonic stem cells.* Current Opinions in Organ Transplantation, 2009. **14**(6): p. 694-700 with permission of Lippincott Williams & Wilkins.

Table 1-2. Effects of oxygen on differentiation

Species	Study	Cell Lines	Oxygen Level (%)	Effects of low O_2 compared to standard O_2
Mouse	Kim 2008	D3	3.5	Differentiation to neurons. Number of neurons increased 35%. HIF-1α dependent.
	Mondragon-Teran 2009	E14Tg2a	2	Differentiation to neurons. Number of neurons increased factor of 55-114.
	Bauwens 2005	D3	4	Differentiation to cardiomyocytes. Total cell number increased 50%. Used bioreactor system.
	Purpura 2008	R1	4	Differentiation to hemagioblast, endothelial cells, and hematopoietic progenitor cells. Low oxygen involved in complicated network via VEGF secretion to influence differentiation to these lineages.
Human	Niebruegge 2009	H9, HES2	4	Differentiation to cardiomyocytes. Total cell number increased 30-47%. Some cardiac markers increased.
	Koay 2008	H9	2	Differentiation to chondrocytes. Collagen I and II, tensile modulus, and compressive properties increased

Adapted from Millman, J.R., J.H. Tan, and C.K. Colton, *The effects of low oxygen on self-renewal and differentiation of embryonic stem cells.* Current Opinions in Organ Transplantation, 2009. **14**(6): p. 694-700 with permission of Lippincott Williams & Wilkins.

Table 1-3. Estimated values of pO_{2cell} from published studies

Study	Cell density (10^3 cells/cm^2)	Media Height (mm)	pO_{2gas} (mmHg)	pO_{2cell} (mmHg)
Kim 2008[b]	150	3.8[c]	26.6	5.2
	150	3.8	142	99.7
Mondragon-Teran 2009[a]	28	2.1	15.2	12.4
	0.82	2.1	142	141.9

[a] Values from 8 days of differentiation

[b] Values from the beginning of differentiation of NSC to neurons

[c] Typical media height for coverslides

Adapted from Millman, J.R., J.H. Tan, and C.K. Colton, *The effects of low oxygen on self-renewal and differentiation of embryonic stem cells.* Current Opinions in Organ Transplantation, 2009. **14**(6): p. 694-700 with permission of Lippincott Williams & Wilkins.

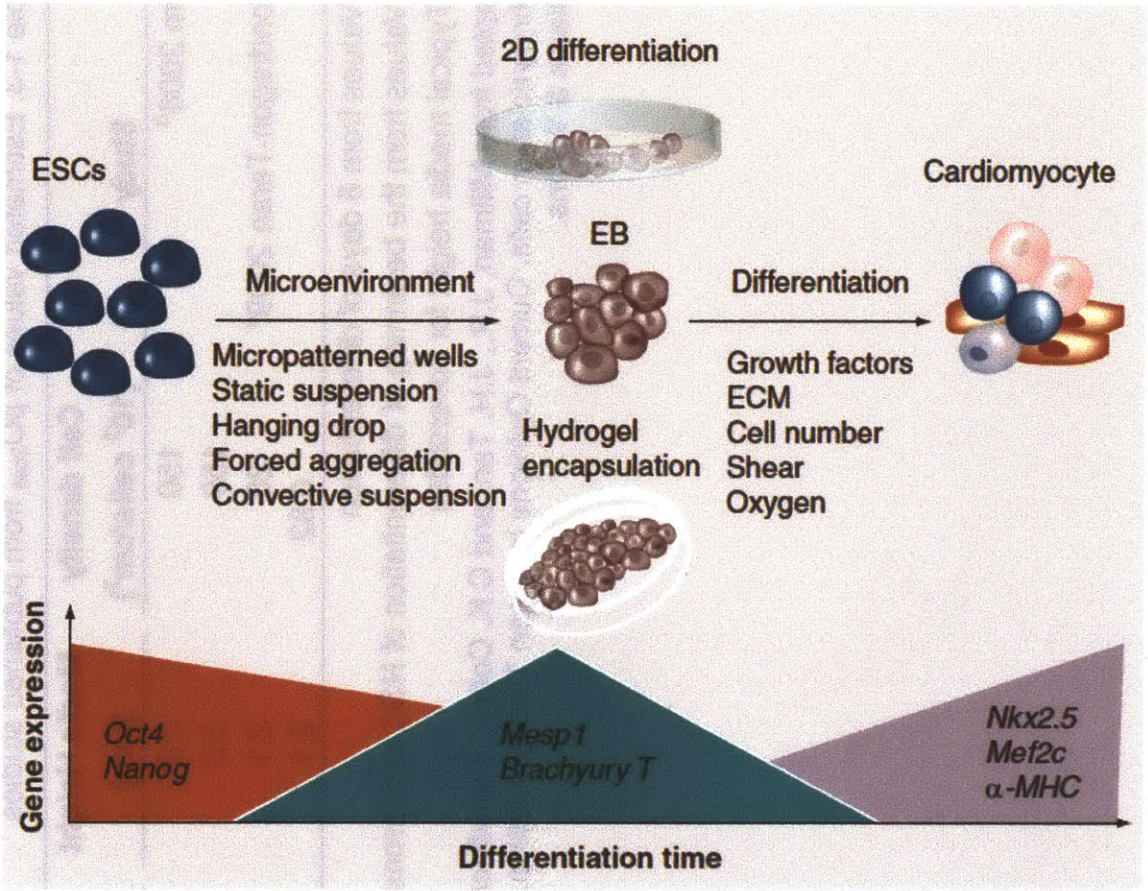

Figure 1-1. Embryonic stem cell differentiation strategies.

ESCs aggregate into EBs via hanging drop, static suspension, convective suspension, micropatterned wells or by forced aggregation. ESCs may also be cultured in 2D plates on various ECM matrices or micropatterened substrates. ESCs may also be embedded in scaffolds. These microenvironments may be subjected to shear and morphogens, for example, to promote differentiation. During differentiation, expression of pluripotency markers, such as Oct4 and Nanog, decreases, early mesodermal markers, such as Mesp1 and Brachyury T, are transiently expressed and expression of late-stage markers, such as Nkx2.5, Mef2c, and α-MHC, increases. Reproduced from Horton, R.E., J.R. Millman, C.K. Colton, and D.T. Auguste, *Engineering microenvironments for embryonic stem*

cell differentiation to cardiomyocytes. Regenerative Medicine, 2009. 4(5): p. 721-32 with permission of Future Medicine Ltd.

-Page Intentionally Left Blank-

Chapter 2. Extended Low Oxygen Culture of Pluripotent Stem Cells Reduces the Fraction of Residual Tumor-Forming Cells in Differentiated Populations

2.1. Abstract

Residual pluripotent stem cells (PSC) within differentiated populations are problematic because of their potential to form tumors. Simple methods to reduce their occurrence are needed. Here, we demonstrate that control of the oxygen partial pressure (pO_2) to physiological levels typical of the developing embryo reduces the fraction of PSC within, and the tumorigenic potential of, differentiated populations. Culture under differentiating conditions at low pO_2 reduced measured pluripotency markers by up to four orders of magnitude for mouse and human embryonic stem cells and mouse induced pluripotent stem cells. Upon implantation into immunocompromised mice, low pO_2-differentiated PSC either did not form tumors or formed tumors at a slower rate than high pO_2 PSC. Low pO_2 differentiation could be combined with cell sorting for improved benefits. Low pO_2 culture alone or in combination with other methods is a potentially straightforward method that could be applied to future cell therapy protocols to minimize the possibility of tumor formation.

2.2. Introduction

Pluripotent stem cells (PSC), such as embryonic stem cells (ESC) [106, 107] and induced pluripotent stem cells (iPSC) [11, 80], have immense clinical potential due to their ability to form many clinically-relevant cell types [1-3]. However, because of their pluripotency, ESC and iPSC have the potential to form teratomas [86], tumors composed of derivatives of the three germ layers [92], and are a serious safety risk if implanted into humans in their undifferentiated state [93].

The tumorigenicity of PSC is a major obstacle for the safe translation of stem cell biology to regenerative medicine that must be overcome [86], and the presence of any number of PSC is a potential tumor formation risk. As few as 2 mouse ESC (mESC) have formed tumors in immunocompromised mice [87]. There have been no reported cases of undifferentiated PSC being implanted into humans, but in one case study, fetal neural stem cells implanted into a human caused the formation of a glioneuronal neoplasm, derived from donor cells [88]. Implanted iPSC can also form tumors, with a propensity that varies depending on the tissue of origin [89]. iPSC have the additional concerns that inserted c-MYC genes could become reactivated and cause tumor formation [90] and that the process of reprogramming can cause genetic aberrations [108]. In addition to the health risks to the recipient by the presence of the tumor, tumor formation could also cause a reversal of the clinical benefits of the implanted differentiated cells [91].

Preclinical testing of any stem cell-derived product for tumor formation is very important [92, 93].

Differentiation of PSC reduces the risk of tumor formation [94]. However, residual PSC can still persist, even after being subjected to a differentiation protocol, and cause tumor formation upon implantation [9, 95]. Even though studies have reported that differentiation of PSC completely avoided tumor appearance [96, 97], these experiments were not designed to sensitively detect residual PSC. A small number of residual PSC may still exist and be a safety risk for humans, which require larger cell numbers for treatment. The experimental design of other studies has allowed for the formation of tumors with low numbers of implanted PSC [87, 98]. The fraction of animals that form tumors and the rate of tumor formation depends on the location of the implanted cells, with subcutaneous and intramuscular injections being the most convenient, sensitive, and reliable [87, 98-100].

Several methods have been used to reduce residual PSC [101]. Genetic selection has been used to kill residual PSC while retaining the desired cell type [102]. However, genetic manipulations introduce an additional hurdle to clinical translation. Positive and/or negative selection by staining cells with an fluorescently-labeled antibody against surface markers, followed by fluorescence activated cell sorting (FACS), has been used [95, 103]. An antibody, termed mAb 84, has been identified that binds to the surface protein podocalyxin-like protein-1

(PODXL) and causes cytotoxicity to human ESC (hESC) via oncosis [104], reducing the viability of undifferentiated hESC populations by a factor of 3-5 [105].

The oxygen partial pressure (pO_2) under which embryonic cells develop *in vivo* and PSC are cultured *in vitro* is an important parameter [2, 42]. During embryonic development, cells are exposed to pO_2 much lower than atmospheric (160 mmHg), which influences many aspects of embryogenesis, such as tracheal development, cardiovascular and bone morphogenesis, and adipogenesis, often via hypoxia inducible factors (HIF). Teratomas do not form normally, even though all differentiated cells are derived from pluripotent precursors. In addition, differentiation of PSC *in vitro* at low pO_2 affects the generation of several cell types, such as neurons, hematopoietic progenitors, endothelial cells, cardiomyocytes, and chondrocytes. pO_2 also affects many aspects of pluripotency, such as expression of the pluripotency genes Oct4, Nanog, and Sox2, in mESC and hESC. The reprogramming efficiency of mouse and human fibroblasts to iPSC is increased under low pO_2 [109, 110]. Female hESC derived under low pO_2 maintain two active X chromosomes and upon culture at atmospheric pO_2, irreversibly silences one X chromosome [111].

In this study, we show that differentiation and extended culture of mESC and mouse iPSC (miPSC), both containing a green fluorescence protein (GFP) transgene driven by an Oct4 promoter, and hESC at low pO_2 drastically reduced the fraction and number of residual PSC, which, upon implantation into nude

mice, slowed or eliminated the appearance of teratomas. Low pO_2 culture was combined with FACS removal of PSC based on GFP and PSC surface marker expression to reduce the fraction of residual PSC, more than either method alone. Residual Oct4-GFP+ mESC, after being subjected to the differentiation protocol, had *in vitro* characteristics similar to those of undifferentiated mESC.

2.3. Methods

2.3.1. Undifferentiated mESC and miPSC culture

Undifferentiated R1 mESC and miPSC, both with an inserted GFP coding sequence driven by an inserted Oct4 promoter (Oct4-GFP mESC) [112, 113] (generously donated by Professor Douglas Melton of Harvard University, Cambridge, MA, USA) and R1 mESC with a homozygous HIF-1α gene knockout (HIF-$1\alpha^{-/-}$ mESC) [114] (generously donated by Professor Peter Carmeliet of Katholieke Universiteit Leuven, Leuven, Belgium) were propagated as previously described [53] without mouse embryonic fibroblasts (MEFs) in Dulbecco's modified Eagles medium (DMEM; SCRR-2010; American Type Culture Collection (ATCC), Manassas, VA, USA) supplemented with 10% (v/v) fetal bovine serum (FBS; SCRR 30-2020; ATCC), 2 mM L-alanyl-L-glutamine (SCRR 30-2115; ATCC), 50 units/ml penicillin and 50 µg/ml streptomycin (15070; Invitrogen, Carlsbad, CA, USA), 1x MEM non-essential amino acids (SCRR 30-2116; ATCC), 100 µM 2-mercaptoethanol (M7522; Sigma-Aldrich; St. Louis, MO,

USA), and 10^3 units/mL leukemia inhibitory factor (LIF; LIF2005; Millipore, Billerica, MA, USA). Cells were passaged every two d by detaching with 0.25% trypsin (25-053-CI; Mediatech, Manassas, VA, USA) and plating at a density of $1.2x10^4$ cells cm^{-2} on cell culture flasks (353014; BD Biosciences, Bedford, MA, USA).

2.3.2. Gas phase pO_2 control

pO_2 in the gas phase (pO_{2gas}) was maintained by flowing premixed gas containing 5% CO_2 and 20%, 5%, or 1% O_2 with a balance of N_2 (certified medical gas from Airgas, Hingham, MA, USA), which corresponded under humidified conditions to 142, 36, and 7 mmHg pO_{2gas} inside chambers maintained at 37 °C as previously described [53].

2.3.3. Silicone rubber membrane-based plate

Differentiation and extended culture was performed on silicone rubber membranes having high oxygen permeability as previously described [53]. In brief, the bottoms of 24-well polystyrene plates (353047; Becton Dickinson, Franklin Lakes, NJ, USA) were replaced with silicone rubber sheets (nonreinforced vulcanized gloss/gloss 127 μm thick; Specialty Manufacturing, Saginaw, MI, USA) and sterilized by filling with 70% (v/v) ethanol (111000200; Pharmco-AAPER, Brookfield, CT, USA) in water, incubating for 1 hr, and drying

overnight under a germicidal UV lamp in a biological safety cabinet (SterilGARD III Advance; The Baker Company, Sanford, MA, USA). In use, the corners of the plate were supported on top of a 150x15 mm Petri dish (35384-326; VWR, West Chester, PA, USA), and the silicone rubber membrane was exposed directly to the gas phase. By culturing on these silicone rubber membrane-based plates, pO_2 of the cells (pO_{2cell}) at the cell-membrane interface was maintained virtually equal to pO_{2gas}, and rapid equilibration of pO_{2cell} occurred after a change in pO_{2gas}. Attachment of mESC and miPSC was achieved by incubating silicone rubber membranes at 37 °C with 2 µg/mL fibronectin (F1141; Sigma-Aldrich) in phosphate buffered saline (PBS; 21-040; Mediatech) for 24 hr, and of hESC by incubation with Matrigel (354234, Becton Dickinson) diluted 1:20 in serum-free medium for 1 hr, for hESC.

2.3.4. Differentiation of mESC and miPSC

mESC and miPSC were differentiated as previously described [53]. In brief, embryoid bodies (EBs) were formed in propagation medium without LIF with 500 cells per 20-µL hanging drops. After 2 d, 30 EBs per well were transferred to fibronectin-coated (F1141; Sigma) silicone rubber membrane-based 24-well plates filled with 2 mL of propagation medium without LIF. After 3 additional d, medium was replaced with 2.5 mL of serum-free medium, consisting of 50% (v/v) DMEM (90-133-PB; Mediatech) and 50% (v/v) Ham's F-12 (10-080-CV; Mediatech) supplemented with 0.75% (w/v) sodium bicarbonate (25-035-CI;

Mediatech), 9 mM glucose (G8769; Sigma-Aldrich), 5 μg/mL human insulin (I9278; Sigma-Aldrich), 50 μg/mL holo transferrin (T1283; Sigma-Aldrich), 31.2 nM sodium selenite (S9133; Sigma-Aldrich), 50 units/ml penicillin, and 50 μg/ml streptomycin. Cells were differentiated for a total of 10 d. As noted, pO_{2gas} was kept constant throughout differentiation in some experiments and was varied in others. In some experiments, 0.2 mM ascorbic acid (A4034; Sigma-Aldrich) was also included in the medium, as noted. At constant 142 and 7 mmHg, this protocol produced a final cell population of which approximately 10% and 30% of the cells were cardiomyocytes, respectively.

2.3.5. Extended culture of differentiated mESC and miPSC

After the 10-d differentiation protocol, cells were subjected to additional extended culture for up to 80 d. In some experiments, pO_{2gas} was identical to pO_{2gas} during differentiation, while in others, pO_{2gas} was changed. Cell samples were acquired for analysis by detachment with a 5-min incubation of 0.25% trypsin at 37 °C.

2.3.6. Flow cytometric analysis of Oct4-GFP expression

Oct4-GFP expression was measured with a flow cytometer (FACScan; Becton Dickinson) at the Koch Institute (MIT). A negative control of R1 mESC without the Oct4-GFP reporter was differentiated under the same conditions as the Oct4-GFP cells, and a gating threshold was set so that all of these cells were counted

as negative for Oct4-GFP. The fraction of cells expressing Oct4-GFP (Oct4-GFP+) was calculated as the number of cells above the threshold divided by the number of cells in the entire population at each specific measurement time and condition.

2.3.7. Real-time polymerase chain reaction (PCR)

Total RNA was isolated using the RNeasy Kit (74104, Qiagen, Valencia, CA), and RNase-Free DNase Set (79254, Qiagen), cDNA was synthesized using High Capacity cDNA Reverse Transcription Kit (4368814, Applied Biosystems, Foster City, CA). Real-time PCR was performed on a Fast Real-Time PCR System (7900HT, Applied Biosystems) using Power SYBR Green PCR Master Mix (4367659, Applied Biosystems), and 28S ribosomal RNA (rRNA) was used as an endogenous control. Primer sequences used for 28S rRNA, Oct4 (mouse), Nanog (mouse), Nestin, and Nkx2.5 have been previously reported [32]. Additional primers sequences used (in order of forward and reverse primer and 5' to 3') were Brachyury T TCCCGGTGCTGAAGGTAAAT and CCGTCACGAAGTCCAGCAA, Foxa2 TCAAGGCCTACGAACAGGTCAT and GCCCGCTTTGTTCGTGACT, cTnT AGATGCTGAAGAAGGTCCAGTAGAG and CACCAAGTTGGGCATGAAGA, cardiac-α-Actin GCTTCCGCTGTCCAGAGACT and TGCCAGCAGATTCCATACCA, OCT4 (human) TGGGCTCGAGAAGGATGTG and GCATAGTCGCTGCTTGATCG, and NANOG (human) GCAAATGTCTTCTGCTGAGATGC and

CCATGGAGGAGGGAAGAGGA. A standard calibration curve was constructed using serial dilutions of pooled cDNA from all conditions.

2.3.8. Cell enumeration

Detached cells or excised tumors were lysed to liberate nuclei by vigorous vortexing in deionized water containing 1% (v/v) Triton X-100 (T-9284; Sigma-Aldrich) and 0.1 M citric acid (0627; Mallinckrodt Specialty Chemicals Co., Paris, KY, USA). Nuclei were stained with Guava ViaCount (4000-0041; Millipore) and counted using a Guava PCA flow cytometer (Millipore) as previously described [53, 115].

2.3.9. Cell implantation into mice

Female nude mice, 43-56 d old (Charles River Laboratories International, Wilmington, MA, USA), were housed and cared for, and experiments were performed with a protocol (approved by the MIT Committee on Animal Care) based on one designed for biosafety testing of stem cell products, for which implantation of only two ES cells was sufficient to form detectable tumors [87]. Samples containing 10^5 cells (for mESC and miPSC) and 10^6 cells (for hESC) in 200 µl of 50% (v/v) Matrigel (354234; BD Biosciences) and 50% (v/v) serum-free differentiation medium were injected subcutaneously into the lower left flank of

isoflurane-anaesthetized mice using a 23G needle in a laminar-flow hood. Mice were visually observed every 3-4 d for the appearance of masses under the skin.

2.3.10. Histology

Tumors were excised from euthanized mice, fixed overnight in 4% (w/v) paraformaldehyde (36606; Alfa Aesar, Ward Hill, MA, USA) in PBS, paraffin embedded, sectioned, and stained with hematoxylin and eosin (H&E) at the Division of Comparative Medicine (DCM) at MIT. Stained histological sections were analyzed by an American College of Veterinary Pathologist board-certified pathologist.

2.3.11. Fluorescence activated cell sorting (FACS)

mESC and hESC that underwent 10 d differentiation and an additional 20 d extended culture were detached with trypsin and then sorted with an Aria 2 FACS (Becton Dickinson). mESC were sorted into Oct4-GFP+ and Oct4-GFP- populations or sorted based on surface marker expression of the mESC surface marker stage-specific embryonic antigen-1 (SSEA-1). hESC were sorted based on surface marker expression of the hESC marker SSEA-4. For SSEA-1 and SSEA-4 sorting, cells were treated with a phycoerythrin (PE)-conjugated anti-SSEA-1 antibody (12-8813; eBioscience, San Diego, CA, USA) or PE-conjugated

anti-SSEA-4 antibody (12-8843-71; eBioscience) before sorting into SSEA-1+, SSEA-1-, SSEA-4+, and SSEA-4- populations.

2.3.12. Flow cytometric analysis of immunostained cells

The fraction of Nestin+ and MF-20+ cells was measured with flow cytometry as previously described [53]. In brief, detached cells were fixed in 1% (w/v) paraformaldehyde in PBS for 20 min. Samples of $3x10^5$ fixed cells were incubated 10 min in 0.5% (w/v) saponin (S-4521; Sigma-Aldrich) in PBS to permeabilize cell membranes and incubated in 2% (v/v) FBS in PBS for 30 min to block non-specific binding. Cells were incubated with primary antibody against Nestin (MAB2736; R&D Systems, Minneapolis, MN, USA) diluted 1:50 or sarcomeric myosin heavy chain (MF-20; MF-20 supernatant; Developmental Studies Hybridoma Bank (DSHB), Iowa City, IA, USA) diluted 1:10 in 2% FBS solution for 1 hr, washed 1x with PBS, and incubated with secondary goat anti-mouse PE-conjugated antibody (Jackson ImmunoResearch, West Grove, PA) diluted 1:250 in 2% FBS solution in the dark. Stained cells were washed thrice with PBS, and fluorescence intensity data were acquired using the Guava PCA flow cytometer with the Express software module.

2.3.13. Immunocytochemistry

Cells attached to silicone rubber or polystyrene were fixed in 4% parafromaldehyde in PBS for 20 min and then permeabilized and non-specific protein binding blocked with a 45-min incubation in 3% (v/v) donkey serum (DS; D9663; Sigma-Aldrich) and 0.1% Triton X-100 in PBS. Cells were then incubated overnight at 4 °C with primary antibodies against Oct4 (sc-9081; Santa Cruz Biotechnology, Santa Cruz, CA, USA) diluted 1:100, Nanog (IHC-00205; Bethyl Laboratories, Montogomery, TX, USA) diluted 1:100, SSEA-1 (MC-480; DSHB) diluted 1:10, Foxa2 (sc-6554; Santa Cruz Biotechnology) diluted 1:200, Nestin diluted 1:50, or cardiac troponin T (cTnT; MS-295-P1; NeoMarkers, Fremont, CA, USA) diluted 1:50 in 3% DS, 0.1% Triton X-100 solution, washed once with PBS, and incubated with secondary donkey Alexa Fluor 488 (green) or 594 (red) antibodies (Invitrogen) against the appropriate species diluted 1:250 in 3% DS, 0.1% Triton X-100 solution for 2 hr in the dark. DNA was stained with a 10-min incubation with 1 µg/mL 4',6-diamidino-2-phenylindole (DAPI; 32670, Sigma-Aldrich) in PBS in the dark. Stained cells were then washed thrice with PBS and images acquired with an Axiovert 200 fluorescence microscope (Carl Zeiss, Oberkochen, Germany).

2.3.14. Differentiation of hESC

CyT49 hESC [9] (NIH Registration Number 0041; generously provided by ViaCyte, Inc, San Diego, CA, USA) were plated on Matrigel-coated silicone rubber plates at a density of $1.5x10^5$ cells cm^{-2} without MEFs, propagated 4 d in self-renewal media, and then switched to DMEM/F12 (15-090-CV; Mediatech) with 10% (v/v) Knockout serum replacement (A1099202; Invitrogen) for up to 90 d.

2.3.15. Statistics

Statistical analysis was performed using unpaired t-tests, with significant results requiring $p<0.05$. Data is presented as mean ± standard deviation.

2.4. Results

2.4.1. Low pO_2 reduces residual mESC

We differentiated and performed extended culture on Oct4-GFP mESC at various pO_{2gas} to examine the effect on residual mESC. Before differentiation, the fraction of mESC expressing Oct4-GFP (Oct4-GFP+), determined with flow cytometry, was 0.96 (Figure 1A). This fraction decreased rapidly during the 10-d differentiation, after which the fraction of total cells that were Oct4-GFP+ was

$3x10^{-3}$, $6x10^{-4}$ and $1x10^{-3}$, for culture at 142, 36, and 7 mmHg, respectively. The residual Oct4-GFP+ subpopulation had GFP intensity values similar to that of undifferentiated mESC (data not shown). We hypothesized that these cells were residual PSC that could develop into tumors upon implantation into animals.

The differentiation process was largely complete by about 10 d of culture, on the basis that no more spontaneously-contracting cells formed after that time. After differentiation, culture at each constant pO_{2gas} was extended for up to 80 additional d to further examine its effects on the reduction of Oct4-GFP+ cells. The fraction of Oct4-GFP+ cells did not change significantly at 142 mmHg but continued to decrease at 36 and 7 mmHg (Figure 1A). The greatest difference was observed at 7 mmHg after 90 total d of culture, at which point the fraction of Oct4-GFP+ cells was a factor of 1260 lower than at 142 mmHg.

Low oxygen culture also reduced the number of Oct4-GFP+ cells (Figure 1B). Each well was initially seeded with $1.44x10^4$ Oct4-GFP+ cells. After 10 d of differentiation, this number remained unchanged at 142 mmHg but decreased to $3x10^3$ and $4x10^3$ at 36 and 7 mmHg, respectively. During the next 20 d of culture, Oct4-GFP+ cell number decreased to $5x10^3$ at 142 mmHg and did not change significantly thereafter. This reduction was proportional with the total cell number (Figure 1C). In contrast, the number of Oct4-GFP+ cells decreased continuously at 36 and 7 mmHg, resulting in only 10 and 4 Oct4-GFP+ cells per well remaining by d 90, respectively. This reduction was substantially faster than the reduction in

total cell number. Gene expression of Oct4 and Nanog, measured by real-time PCR, decreased with time in a manner comparable to that observed with flow cytometry of Oct4-GFP+ cells (Figure 1D-E).

When observed with fluorescence microscopy, cells that expressed GFP after culture at 142 mmHg resided in clusters within aggregates (Figure 1F-G), whereas no cells expressing GFP were visually observed anywhere in the dish, including in aggregates, at 7 mmHg (Figure 1H-I) or at 36 mmHg (data not shown). The inability to visually observe Oct4-GFP+ cells at 36 or 7 mmHg with microscopy likely reflects the low fraction of cells expressing high enough levels of GFP to be detected by eye, rather than a complete absence of GFP-expressing cells.

Different pO_{2gas} values during differentiation and extended culture were investigated by differentiating mESC for 10 d at either 142 or 7 mmHg, followed by 20 d extended culture at the same or the other pO_{2gas} (Figure 2). After 10 d of differentiation at 142 mmHg, the fraction of Oct4-GFP+ cells was $1.4x10^{-2}$ (Figure 2A). Extended culture for 20 d at 142 mmHg did not significantly change the fraction of Oct4-GFP+ cells. However, extended culture at 7 mmHg decreased the fraction to $5x10^{-4}$. Differentiation for 10 d at 7 mmHg resulted in a fraction of Oct4-GFP+ cells of $6x10^{-4}$ (Figure 2B), a factor of 22 lower than at 142 mmHg (Figure 2A). Extended culture for 20 d at 7 mmHg further decreased the fraction

to $3x10^{-5}$. However, extended culture at 142 mmHg increased the mean fraction to $3x10^{-3}$.

After 10 d of differentiation at 142 mmHg, the number of Oct4-GFP+ cells was $3.5x10^{5}$ (Figure 2C). Extended culture for 20 d at 142 mmHg decreased the number of Oct4-GFP+ cells slightly to $1.6x10^{4}$. However, extended culture at 7 mmHg decreased the number to $9.5x10^{2}$. Differentiation for 10 d at 7 mmHg resulted in a number of Oct4-GFP+ cells of $1.1x10^{3}$ (Figure 2D), a factor of 33 lower than at 142 mmHg. Extended culture for 20 d at 7 mmHg further decreased the number to 33. However, extended culture at 142 mmHg increased the mean number to $3.1x10^{3}$. Extended culture at 142 and 7 mmHg for 20 d, at either pO_{2gas}, decreased the total cell number by approximately same proportion (Figures 2E-F).

If differentiated cells that have been previously cultured under normoxic conditions are to be cultured under hypoxic conditions in order to reduce residual PSC, it is possible that desired cell types will die if they are unable to use anaerobic metabolism. To investigate this possibility, we differentiated mESC and cultured the cells for extended time with three different sequences of pO_{2gas}: (A) Differentiate at 142 mmHg for 10 d, then extended culture at 142 mmHg for 20 d; (B) Differentiate at 142 mmHg for 10 d, then extended culture at 7 mmHg for 20 d; (C) Differentiate at 7 mmHg for 6 d, then differentiate at 142 mmHg for 4 d, then extended culture at 7 mmHg for 20 d. With all sequences, spontaneously-

contracting cells were observed. The total number of cells and the number of MF-20+ (cardiomyocyte marker) cells is tabulated in Table 1 for d 10 and 30 of culture, along with the relative decrease from each number. At d 10, sequence C maximized the number and fraction of cardiomyocytes. With all sequences, the total cell number and number of MF-20+ cells decreased from 10 to 30 d. The decreases were smallest with sequences B and C, which involved extended culture at 7 mmHg, compared to sequence A, which used extended culture at 142 mmHg.

2.4.2. Low pO_2 delays appearance of tumors after implantation of cultured mESC

pO_{2gas} culture conditions of differentiation affected the rate of tumor formation following subcutaneous injection into nude mice (Figure 3A). All animals injected with undifferentiated mESC (positive control) formed visible tumors by d 14. Differentiation for 30 d before implantation led to slower tumor formation rates and resulted in only 306, 7, and 2 Oct4-GFP+ cells being implanted per 10^5 cell injection for cells cultured at 142, 36, and 7 mmHg, respectively. Visible tumors appeared in 7/8 animals by d 17 and 8/8 by d 21 for cells cultured at 142 mmHg. Culture at lower pO_{2gas} had a greater effect. Tumors were first observed in 3/8 animals by d 31, 5/8 by d 35, and 7/8 by d 38 for cells cultured at 36 mmHg and in 5/8 animals by d 35, 6/8 animals by d 38, and 7/8 animals by d 42 for 7 mmHg. Animals (0/6) injected with only Matrigel (negative control) did not form tumors.

Tumors were excised from euthanized mice, fixed, embedded, sectioned, and H&E stained, and the resulting tissue sections histopathologically analyzed (Figure 3B). The tumors contained derivatives of all three germ layers and were identified as teratomas. These *in vivo* data are consistent with the *in vitro* Oct4-GFP and real-time PCR data and demonstrate that extended hypoxic culture of mESC greatly reduces the rate of teratoma formation *in vivo*.

2.4.3. Combination of low pO_2 culture of mESC with FACS

In a separate experimental run, mESC after 30-d differentiation at either 142 or 7 mmHg were sorted for GFP expression with FACS into Oct4-GFP+ and Oct4-GFP- populations before implantation (Figure 4). With cells cultured at 142 mmHg, the fraction of residual Oct4-GFP+ cells remaining in the sorted Oct4-GFP- population decreased compared to the unsorted population by a factor of 50, as determined by subsequent flow cytometric analysis of the sorted population (Figure 4A). With culture at 7 mmHg, all Oct4-GFP+ cells were removed from the sorted Oct4-GFP- population, as determined by subsequent flow cytometric analysis. Low pO_2 culture combined with FACS also reduced the number of Oct4-GFP+ cells (Figure 4B). Before sorting, culture at 142 mmHg resulted in 4.1×10^4 Oct4-GFP+ cells. Sorting into an Oct4-GFP+ population captured 3.8×10^4 of the Oct4-GFP+ cells. However, 9.4×10^2 Oct4-GFP+ cells were sorted into the Oct4-GFP- population. There are fewer Oct4-GFP+ cells when the Oct4-GFP+ and Oct4-GFP- populations are combined compared to the

unsorted Oct4-GFP+ cells, likely loss during sample handling or due to measurement error. For culture at 7 mmHg, each well contained 190 Oct4-GFP+ cells before sorting. Sorting into an Oct4-GFP+ population captured all the Oct4-GFP+ cells. FACS removal of Oct4-GFP+ cells decreased the total cell number by a very small fraction for both 142 and 7 mmHg cells, a factor of 1.07 and 1.0004, respectively (Figure 4C).

After FACS, unsorted cells and sorted Oct4-GFP+ and Oct4-GFP- populations, each cultured at 142 or 7 mmHg, were implanted into nude mice (Figures 4D). Each unsorted cell injection contained, on average, 1770 and 13 Oct4-GFP+ cells at 142 and 7 mmHg, respectively, each sorted Oct4-GFP+ population injection contained 1729 and 13 Oct4-GFP+ cells at 142 and 7 mmHg, respectively, and each sorted Oct4-GFP- population injection contained 41 and 0 Oct4-GFP+ cells at 142 and 7 mmHg, respectively. For cells cultured at 142 mmHg, tumors appeared at approximately the same time in the unsorted and sorted GFP+ populations; The Oct4-GFP- population had an 11-d delay in tumor appearance. For 7 mmHg, there was a 6-d delay in initial tumor appearance for the sorted GFP+ population compared to the unsorted cells, but 50% of the GFP+ cells never formed tumors. Cells cultured at 7 mmHg then sorted into Oct4-GFP- populations formed no tumors during 210 d of observation.

The combination of low pO_2 culture with FACS using an Oct4 reporter cell line reduced residual PSC compared to low pO_2 culture alone. However, sorting

based on GFP expression required genetic modifications of the cells, which might be problematic for clinical application. Therefore, we investigated low pO_2 culture combined with FACS of mESC cell surface marker stained with a PE-conjugated anti-SSEA-1 antibody (Figure 5). mESC underwent, in a separate experimental run, a 30-d differentiation at either 142 or 7 mmHg and were sorted for SSEA-1 expression with FACS into SSEA-1+ and SSEA-1- populations before implantation. The SSEA-1- populations had a fraction of Oct4-GFP+ cells that were a factor of 31 and 16 lower than unsorted cells from 142 and 7 mmHg, respectively, as determined by subsequent flow cytometric analysis of the sorted population (Figure 5A). Culture at 7 mmHg combined with FACS removal of SSEA-1+ cells resulted in a reduction in the fraction of Oct4-GFP+ cells by a factor of 1020 compared to cells culture at 142 mmHg without sorting. Low pO_2 culture combined with immunostaining for SSEA-1 and FACS also reduced the number of Oct4-GFP+ cells (Figure 5B). Before sorting, culture at 142 mmHg resulted in $6.5x10^3$ Oct4-GFP+ cells. Sorting into an SSEA-1+ population captured $6.2x10^3$ of the Oct4-GFP+ cells. However, the SSEA-1- population contained $1.9x10^2$ Oct4-GFP+ cells. For culture at 7 mmHg, each well contained 110 Oct4-GFP+ cells before sorting. Sorting into an Oct4-GFP+ population captured 95 Oct4-GFP+ cells. However, the SSEA-1- population contained 7 Oct4-GFP+ cells. There are fewer Oct4-GFP+ cells when the SSEA-1+ and SSEA-1- populations are combined compared to the unsorted Oct4-GFP+ cells, likely loss during sample handling or due to measurement error. FACS removal

of SSEA-1+ cells decreased the total cell number by a very small fraction for both 142 and 7 mmHg cells, a factor of 1.05 and 1.01, respectively (Figure 5C).

After FACS, unsorted, SSEA-1+, and SSEA-1- populations cultured at 142 or 7 mmHg were implanted into nude mice (Figure 5D). Each unsorted cell injection contained, on average, 443 and 6 Oct4-GFP+ cells at 142 and 7 mmHg, respectively, each sorted SSEA-1+ population injection contained 420 and 6 Oct4-GFP+ cells at 142 and 7 mmHg, respectively, and each sorted SSEA-1- population injection contained 13 and 0 Oct4-GFP+ cells at 142 and 7 mmHg, respectively. Unsorted cells and sorted SSEA-1+ populations produced tumors at the same time with cells cultured at 142 mmHg, whereas culture at 7 mmHg led to a delay of 4 to 12 d for the SSEA-1+ population. The 142 mmHg SSEA-1- population resulted in a 14-d delay in tumor appearance compared to unsorted cells, but the 7 mmHg SSEA-1- population resulted in no tumors during 210 d of observation.

2.4.4. Low-pO_2 differentiation of HIF-1$\alpha^{-/-}$ mESC does not reduce residual mESC and delay tumor formation

Since HIF-1α protein is present in PSC cultured at low pO_2 and has been shown to affect differentiation [2], we differentiated HIF-1$\alpha^{-/-}$ mESC for 30 d to determine what effect the absence of the HIF-1α gene would have on residual mESC and the delay in tumor appearance (Figure 6). The relative loss of Oct4 and Nanog

gene expression for HIF-1α$^{-/-}$ mESC at both 142 and 7 mmHg (Figure 6A) was similar to the relative loss of expression of wild type mESC at 142 mmHg (Figure 1E-F). In nude mice, undifferentiated HIF-1α$^{-/-}$ mESC formed tumors at d 21 (Figure 6B), 7 d later than wild type mESC (Figure 3A). Differentiated and cultured HIF-1α$^{-/-}$ mESC formed tumors at d 31 in all animals, regardless of culture pO_{2gas} (Figure 6B), 14 d later than wild type mESC cultured at 142 mmHg (Figure 3A). Although HIF-1α absence slowed tumor formation, the positive benefits of low pO_2 culture were lost.

2.4.5. Residual Oct4-GFP+ mESC *in vitro* phenotype is the same as undifferentiated mESC

We further investigated residual Oct4-GFP+ mESC by removing Oct4-GFP+ cells from differentiated mixtures, culturing them as undifferentiated mESC for two weeks, and characterizing their *in vitro* phenotype. We compared three cases: (I) Oct4-GFP+ mESC that have never undergone differentiation, (II) Oct4-GFP+ cells obtained with FACS from mESC that have undergone 30-d differentiation at 142 mmHg, and (III) cells the same as case II, but with differentiation at 7 mmHg. The distribution of Oct4-GFP intensity per cell measured by flow cytometry was similar among the three cases (Figure 7A). For all three cases, essentially all of the cells were Oct4-GFP+ and, when subjected to differentiation, for the second time for cases II and III and for the first time for case I, the fraction decreased to $9x10^{-3}$ (data not shown). Oct4-GFP+ mESC colonies for all three cases were

morphologically similar and contained Oct4, Nanog, and SSEA-1 protein (Figure 7B-E).

All three cases expressed markers for all three germ layers upon differentiation for the second time for cases II and III and for the first time for case I (Figures 8-10). All three cases (1) expressed Brachyury T, Foxa2, Nestin, cardiac Troponin T (cTnT), cardiac-α-Actin, and Nkx2.5 mRNA (Figure 8), (2) stained positive for Foxa2, Nestin, and cTnT protein (Figure 9), and (3) contained the same fraction and number of Nestin+ and MF-20+ cells (Figure 10). For all of the *in vitro* assays carried out, residual Oct4-GFP+ cells sorted from differentiated populations have the same characteristics as mESC that have never been exposed to differentiation conditions.

2.4.6. Low pO_2 reduces residual hESC and delays the appearance of tumors after implantation of differentiated and cultured hESC

We extended our investigation to hESC by differentiating hESC at various pO_{2gas} for up to 90 d (Figure 11). Before differentiation, almost all hESC stained positive for OCT4 protein with immunocytochemistry (data not shown). During differentiation, OCT4 and NANOG gene expression decreased and was lowest at reduced pO_2 (Figure 11A-B). At 142 mmHg, OCT4 and NANOG gene expression decreased until d 30, then remained constant. At 36 and 7 mmHg, expression decreased continuously and was always lower than at 142 mmHg. After 90 d,

OCT4 expression was about 360 and 100 times lower at 36 and 7 mmHg, respectively, and NANOG expression was about 2800 and 460 times lower at 36 and 7 mmHg, respectively, compared to 142 mmHg. These results are qualitatively similar to data obtained with mESC, but the loss of OCT4 expression at all pO_{2gas} is less extensive in differentiated hESC than in mESC (Figure 1F-G).

hESC differentiated for 30 d at different pO_{2gas} and injected subcutaneously into nude mice formed tumors at different rates (Figure 11C). Undifferentiated hESC (positive control) formed visible tumors by d 17. Differentiated cells had slower tumor formation rates. Cells differentiated at 142 mmHg formed tumors in 2/6 animals by d 31 and 6/6 by d 38. Tumors were not observed until d 52 with cells cultured at 7 mmHg. Cells differentiated at 36 mmHg formed tumors in 2/6 animals by d 59 and 6/6 by d 66. Tumors were histopathologically identified as teratomas (data not shown). These *in vivo* data are consistent with the *in vitro* real-time PCR data and demonstrate that hypoxic culture of hESC greatly reduces the rate of teratoma formation *in vivo*.

2.4.7. Combination of low pO_2 culture of hESC with FACS

We investigated low pO_2 culture combined with FACS of hESC cell surface marker stained with a PE-conjugated anti-SSEA-4 antibody (Figure 12). hESC underwent, in a separate experimental run, a 30-d differentiation at either 142 or 36 mmHg and were sorted for SSEA-4 expression with FACS into SSEA-4+ and

SSEA-4- populations before implantation. The SSEA-4- populations had OCT4 gene expression that were a factor of 9 and 23 lower and NANOG gene expression that were a factor of 24 and 16 lower than unsorted cells from 142 and 36 mmHg, respectively, as determined by subsequent real-time PCR analysis of the sorted population (Figure 12A-B). Culture at 36 mmHg combined with FACS removal of SSEA-4+ cells resulted in a reduction in OCT4 and NANOG gene expression by a factor of $4x10^3$ and $8x10^3$, respectively, compared to cells culture at 142 mmHg without sorting.

After FACS, unsorted, SSEA-4+, and SSEA-4- populations cultured at 142 or 36 mmHg were implanted into nude mice (Figure 12C). Unsorted cells and sorted SSEA-4+ populations first produced tumors at the same time with cells cultured at 142 mmHg, whereas culture at 36 mmHg led to a 4-d delay for the SSEA-4+ population. The 142 mmHg SSEA-4- population resulted in a 21-d delay in tumor appearance compared to unsorted cells, but the 36 mmHg SSEA-4- population resulted in no tumors during 210 d of observation.

2.4.8. Differentiation at low pO_2 reduces residual miPSC

We extended our investigation to miPSC by differentiating Oct4-GFP+ miPSC at various pO_{2gas} (Figure 13). The fraction of miPSC that were Oct4-GFP+ was 0.97, assessed with flow cytometry, before differentiation (Figure 13A). This fraction decreased during the 10 d differentiation to $4x10^{-2}$ at 142 mmHg and to $2x10^{-4}$

and $3x10^{-4}$, respectively, at 36 and 7 mmHg. The residual Oct4-GFP+ subpopulation had GFP intensity values per cell similar to that of undifferentiated miPSC (data not shown). After differentiation, culture at each constant pO_{2gas} was extended for up to 80 additional d to further examine its effects on the reduction of Oct4-GFP+ cells. The fraction of Oct4-GFP+ cells did not change significantly at 142 mmHg but continued to decrease at 36 and 7 mmHg (Figure 13A). The greatest difference was observed at 7 mmHg after 90 d of culture, at which point the fraction of Oct4-GFP+ cells as a factor of $2.3x10^4$ lower than at 142 mmHg. Though similar to data obtained with mESC, Oct4-GFP expression decreased even more dramatically at low pO_2 in miPSC (Figure 1A).

Low oxygen culture also reduced the number of Oct4-GFP+ cells (Figure 13B). Each well was initially seeded with $1.46x10^4$ Oct4-GFP+ cells. After 10 d of differentiation, this number increase to $7x10^4$ at 142 mmHg but decreased to $7x10^2$ and $1x10^3$ at 36 and 7 mmHg, respectively. During the next 20 d of culture, Oct4-GFP+ cell number decreased to $5x10^4$ at 142 mmHg and did not change significantly thereafter. This reduction was proportional with the total cell number (Figure 13C). In contrast, the number of Oct4-GFP+ cells decreased continuously at 36 and 7 mmHg, resulting in only 10 and 5 Oct4-GFP+ cells per well remaining by d 90, respectively. This reduction was substantially faster than the reduction in total cell number. At all time points, the total cell number was higher at low pO_{2gas} compared to 142 mmHg. Compared to mESC, more Oct4-GFP+ cells were present at 142 and approximately the same at 36 and 7 mmHg (Figure 1B).

Gene expression of Oct4 and Nanog, measured by real-time PCR, decreased with time in a manner comparable to that observed with flow cytometry of Oct4-GFP+ cells (Figure 13D-E). When observed with fluorescence microscopy, cells that expressed GFP after culture at 142 mmHg resided in clusters within aggregates (Figure 13F-G), albeit smaller aggregates than seen with mESC (Figure 1F and H), whereas no cells expressing GFP were visually observed anywhere in the dish, including in aggregates, at 7 mmHg (Figure 13H-I) or at 36 mmHg (data not shown).

2.4.9. Low pO_2 delays appearance of tumors after implantation of cultured miPSC

pO_{2gas} culture conditions of differentiation and extended culture affected the rate of tumor formation following subcutaneous injection of differentiated miPSC into nude mice (Figure 14A). All animals injected with undifferentiated miPSC (positive control) formed visible tumors by d 14. Differentiation and extended culture for 20 d before implantation led to slower tumor formation rates and resulted in only 4153, 1, and 0 Oct4-GFP+ cells being implanted per 10^5 cell injection for cells cultured at 142, 36, and 7 mmHg, respectively. Visible tumors appeared in 1/6 animals by d 14 and 6/6 by d 14 for cells cultured at 142 mmHg. Culture at lower pO_{2gas} resulted in no tumors during 210 d of observation. Tumors were histopathologically identified as teratomas (data not shown). These *in vivo* data are consistent with the *in vitro* Oct4-GFP and real-time PCR data and

demonstrate that extended hypoxic culture of miPSC greatly reduces the rate of teratoma formation *in vivo*.

2.4.10. Number of implanted PSC correlates with the appearance of tumors

The time required for first appearance of tumors following implantation of differentiated cell populations is plotted versus the number of implanted Oct4-GFP+ mESC or hESC in each injected sample (Figure 15). The data for each species correlated exponentially, with $R^2 = 0.90$ and $R^2 = 0.99$, respectively. This data shows that our animal model is very sensitive to small numbers of and could be used in the estimation of residual pluripotent cells.

2.5. Discussion

We performed a quantitative study on the effects of low pO_2 on the risk of residual PSC to develop tumors. mESC, hESC, and miPSC were cultured under differentiating conditions at 142, 36, and 7 mmHg pO_{2gas} on highly oxygen-permeable silicone rubber dishes and assayed for residential PSC *in vitro* by measuring Oct4 and Nanog gene expression and, for mESC and miPSC, Oct4-GFP expression. The potential of differentiated cell populations to form tumors was assessed by subcutaneous implantation into nude mice. We also investigated the effects of low pO_2 culture combined with FACS removal of residual undifferentiated cells.

Low pO_2 culture during differentiation markedly decreased the fraction of PSC, measured with Oct4-GFP, and Oct4 and Nanog gene expression. The order of magnitude of this reduction ranged from 10^2-10^4, depending on the duration of low pO_2 culture and the cell type (Figures 1, 11, 13). Residual Oct4-GFP+ cells expressed Oct4, Nanog, and SSEA1 protein and could be differentiated again *in vitro* to all three germ layers (Figures 7, 8, 9, and 10), all characteristics of PSC.

Combinations of high and low pO_2 culture could be performed and residual PSC reduced. For mESC, regardless of whether differentiation was carried out for the first 10 d at 142 or 7 mmHg, if the subsequent 20-d culture was performed at 7 mmHg, the fraction of Oct4-GFP+ cells decreased approximately by a factor of 25 compared to d 10 cells (Figure 2). Additionally, if the 20 d extended culture was performed at 142 mmHg, the fraction of Oct4-GFP+ cells either increased or stayed the same compared to d 10. These results demonstrate that differentiation can be performed at any pO_2, followed by an extended culture period at low pO_2 to reduce the fraction of Oct4-GFP+ cells without negative affecting cell number. This combination of pO_2 control strategies allows for the production of the desired differentiated cell type at the best pO_2 for producing that cell type while also reducing the fraction of potentially-tumorigenic residual PSC.

The reduction in PSC *in vitro* correlated with a reduction in the time required for tumor formation *in vivo* (Figures 3, 4, 5, 11, 12, 15). We were also able to form tumors with as few as 2 implanted mESC (Figure 2) and 100 implanted hESC (Figure 15). These values are similar to previous reports for mESC [87] and hESC [98]. The absence of tumor formation with Oct4-GFP- populations verified to contain no Oct4-GFP+ cells demonstrates that only Oct4-GFP+ mESC are likely responsible for the tumor formation in this system (Figures 4 and 5). However, if a sufficiently large number of cells had been injected, tumors would likely have formed. The possibility of other cell sources, such as multipotent progenitors, contributing to tumor or other type of undesired formation, especially with hESC, cannot be completely ruled out.

To further eliminate residual PSC, low pO_2 culture was combined with FACS removal of cells based on surface marker expression. FACS removal of SSEA-1+ cells, for mESC, and SSEA-4+ cells, for hESC, reduced Oct4-GFP+ cells or OCT4 and NANOG gene expression by approximately a factor of 10 at both high and low pO_2 (Figures 5 and 12). Combination of low pO_2 culture with FACS reduced residual PSC more than either method alone. FACS removal of residual PSC after differentiation has been reported [101], but, to the best of our knowledge, detailed quantification of its effectiveness has not, especially in cell mixtures containing a low fraction of PSC. Low pO_2 culture potentially could be used in conjunction with other selection methods, such as positive selection for

the cell type(s) of interest with FACS, selective killing of residual PSC, or differentiation protocols that better remove residual cells.

We found that low pO_2 culture of HIF-1$\alpha^{-/-}$ mESC did not decrease residual mESC (Figure 6), but the full mechanism of the phenomenon is not understood. Low pO_2 could cause residual PSC to differentiate or die. In previous studies, mESC cultured at low pO_2 display some signs of differentiation, but expression of pluripotency genes for hESC are either not affected or increased [2]. However, in those studies, cells were cultured under self-renewal conditions, which are very different than the differentiation conditions used in this study. This area deserves additional study.

We developed a model for tumor formation based on a general model of stem cell behavior (Equation 7) that better describes the kinetics of PSC-derived tumor formation than exponential (Equation 1) and Gompertz (Equation 2) mathematical models (Figures 15 and 16). According to equation 7, for both mESC and hESC implants, tumor growth progressed through two phases. At early times, there were low numbers of differentiated cells, and the dynamics were dominated by the behavior of PSC, and the rate of differentiation was greater than effective cell growth. Loss of PSC occurred much faster with mESC than hESC, consisted with *in vitro* published reports [116]. At later times, the tumors consisted of mostly differentiated cells, and the kinetics were dominated by the effective rate of cell growth of the differentiated cells. Our fitted effective

rate constant of cell growth for differentiated mESC is similar to our previously reported values for *in vitro* culture of differentiated mESC at low pO_{2gas} [32]. Overall, our model suggests that behavior of PSC during tumor formation is similar to its behavior *in vitro*.

Our mathematical analysis of tumor growth has some limitations. While our general model (Equation 7) does well at predicting the time required for tumor formation within the range of implanted cells investigated, it likely does not quantitatively reflect the growth kinetics at early time points. The model could be greatly improved with the inclusion of data from early time points. For hESC, we assumed only 1% of the implanted cells survive or contribute to the tumor. Reports have observed hESC numbering in the range of 10^2 to 10^5 are necessary to form a tumor [98, 100] while as few as 2 mESC are required [87]. Understanding the critical number PSC required to form a tumor is worthy of further investigation and is extraordinarily valuable to fully assess the safety risk of any PSC therapy.

Our work shows that *in vitro* low pO_2 culture markedly reduces the fraction of cells that are pluripotent, as measured by Oct4-GFP and Oct4 and Nanog gene expression, in differentiated mESC, hESC, and miPSC populations. The reduction correlates with reduction in the time required for tumor formation and, when all PSC are removed from differentiated populations, tumors do not form. After differentiation, sorted residual Oct4-GFP+ mESC express Oct4, Nanog, and

SSEA-1 protein and can be differentiated again, all characteristics of undifferentiated mESC. We believe that low pO_2 culture alone or in combination with other methods is a potentially straightforward method that could be applied to future cell therapy protocols to minimize the possibility of tumor formation.

2.6.Tables and Figures

Table 2-1 Comparison of changes in pO_{2gas} on total cell number and number of MF-20+ cells

pO_{2gas} (mmHg)	Ascorbic Acid	Total cell number ($x10^6$)			Number MF-20+ cells ($x10^5$)		
		Time (days)[a]		Change (%)	Time (days)[a]		Change (%)
		0	20		0	20	
142	No	1.8±0.1	0.7±0.2	63	1.4±0.1	0.5±0.01	66
142-7[b]	No	1.8±0.1	0.9±0.1	50	1.4±0.1	1.2±0.1	17
7-142-7[c]	Yes	2.1±0.4	1.0±0.2	54	3.2±0.3	2.6±0.6	19

[a] Time in extended culture

[b] Differentiation 10 d at 142 mmHg, then 20 d extended culture at 7 mmHg

[c] Differentiation 6 d at 7 mmHg followed by 4 d at 142 mmHg, then 20 d extended culture at 7 mmHg

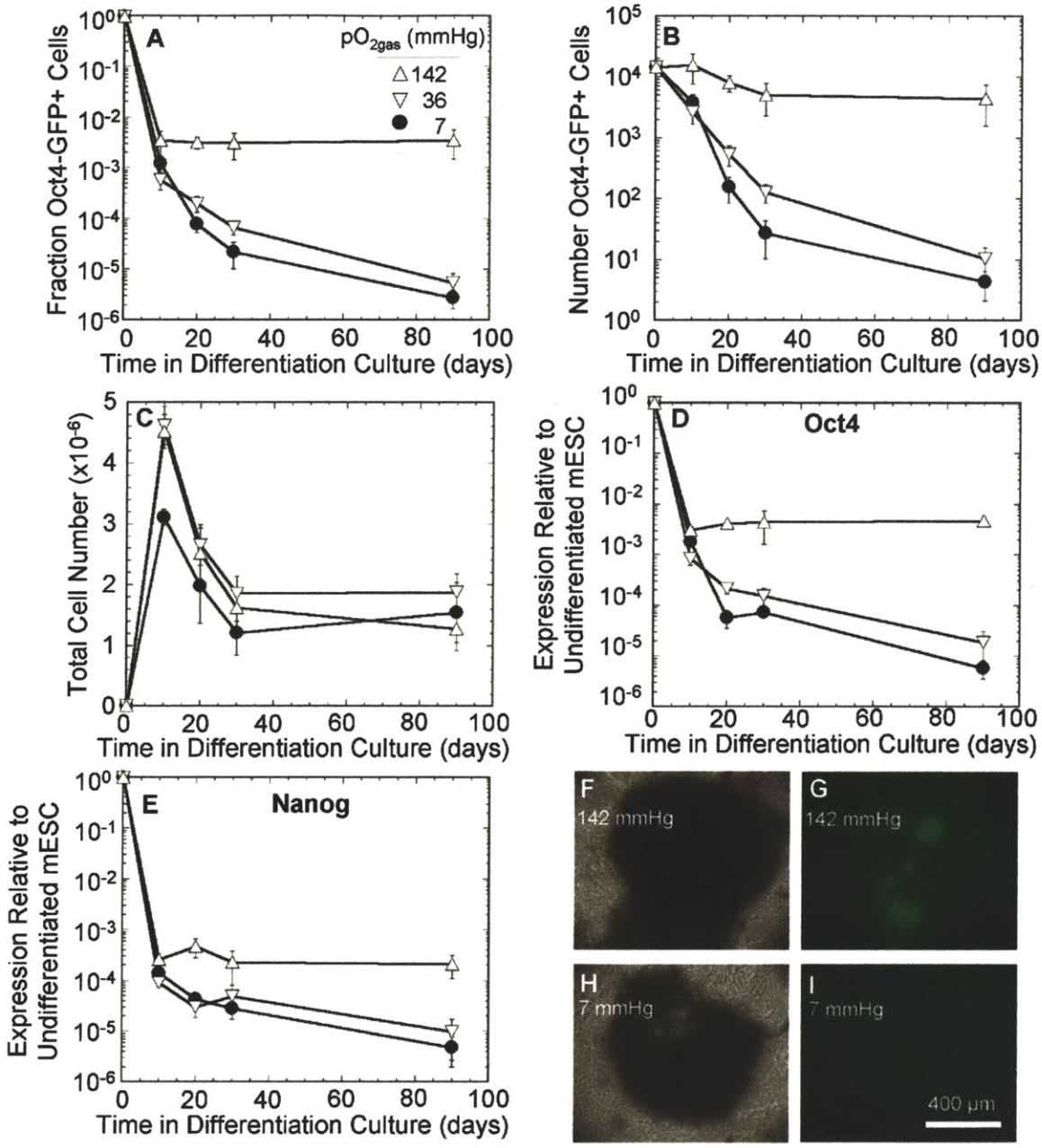

Figure 2-1. Expression of pluripotency markers in mESC having undergone differentiation and extended culture at various pO_{2gas}.

mESC were differentiated at 142, 36, or 7 mmHg pO_{2gas} then subjected to extended culture a the same pO_{2gas} used during differentiation for a total of 0, 10, 20, 30, or 90 days. (A) Fraction of cells that are Oct4-GFP+ as measured with flow cytometry (n=3). (B) The number of Oct4-GFP+ cells per well determined by

multiplying the fraction of Oct4-GFP+ cells and the total cell number (n=3). (C) The total cell number per well as measured by nuclei count (n=3). (D-E) Relative expression of Oct4 and Nanog mRNA measured with real-time PCR (n=3). (F and H) En face bright field images of cell aggregates after 30 days culture. (G and I) En face fluorescence images taken with a GFP filter corresponding with (F) and (H), respectively.

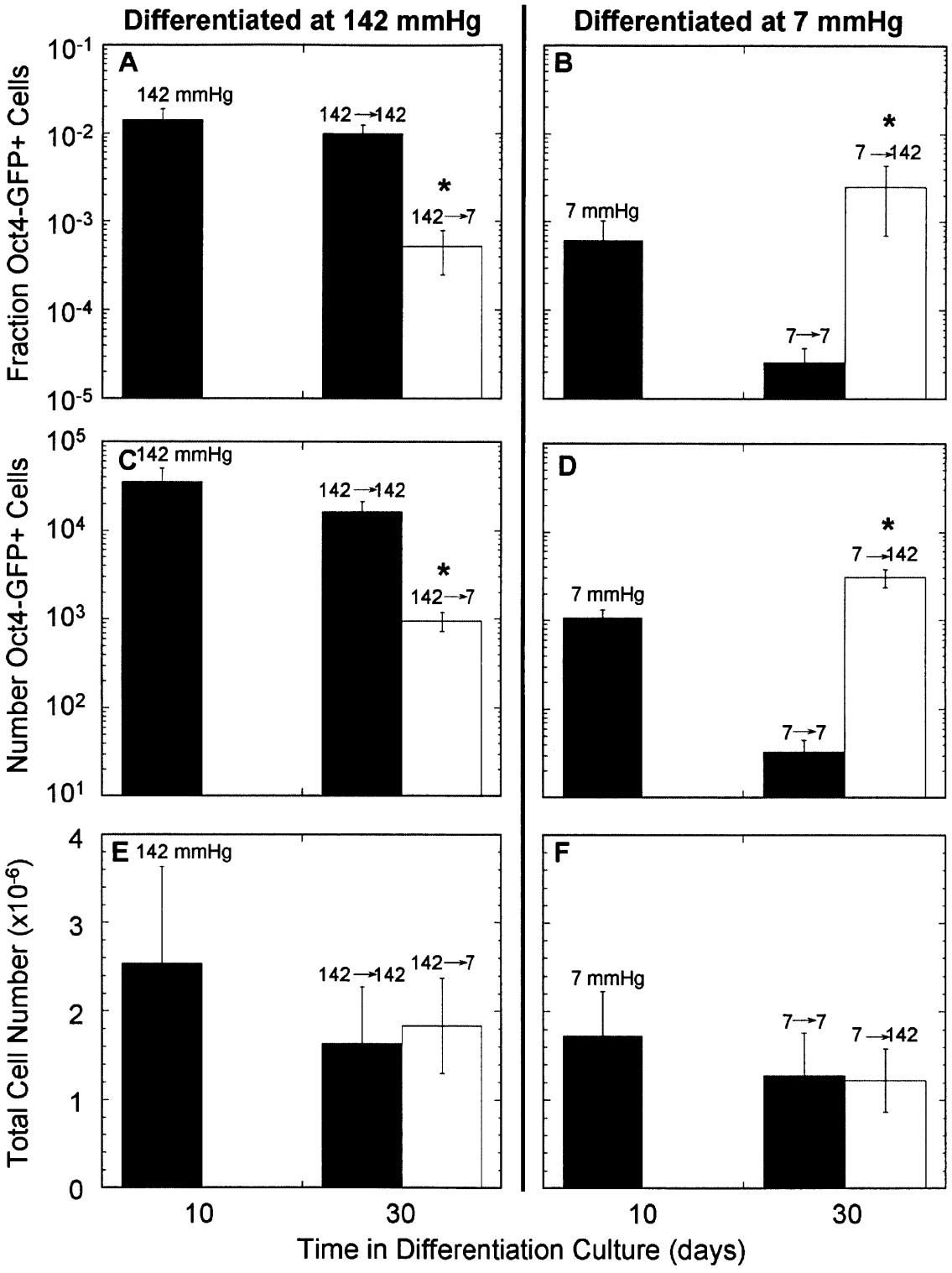

Figure 2-2. Expression of Oct4-GFP in mESC having undergone differentiation and extended culture at the same or different pO_{2gas}.

mESC were differentiated at 142 (A, C, E) or 7 (B, D, F) mmHg pO_{2gas} then subjected to extended culture at the same (black bar) or the other (white bar) pO_{2gas} used during differentiation. (A and B) Fraction of cells that are Oct4-GFP+ as measured with flow cytometry (n=3). (C and D) The number of Oct4-GFP+ cells per well determined by multiplying the fraction of Oct4-GFP+ cells and the total cell number (n=3). (E and F) The total cell number per well as measured by nuclei count (n=3). * indicates significant difference compared to the black bar of the same time.

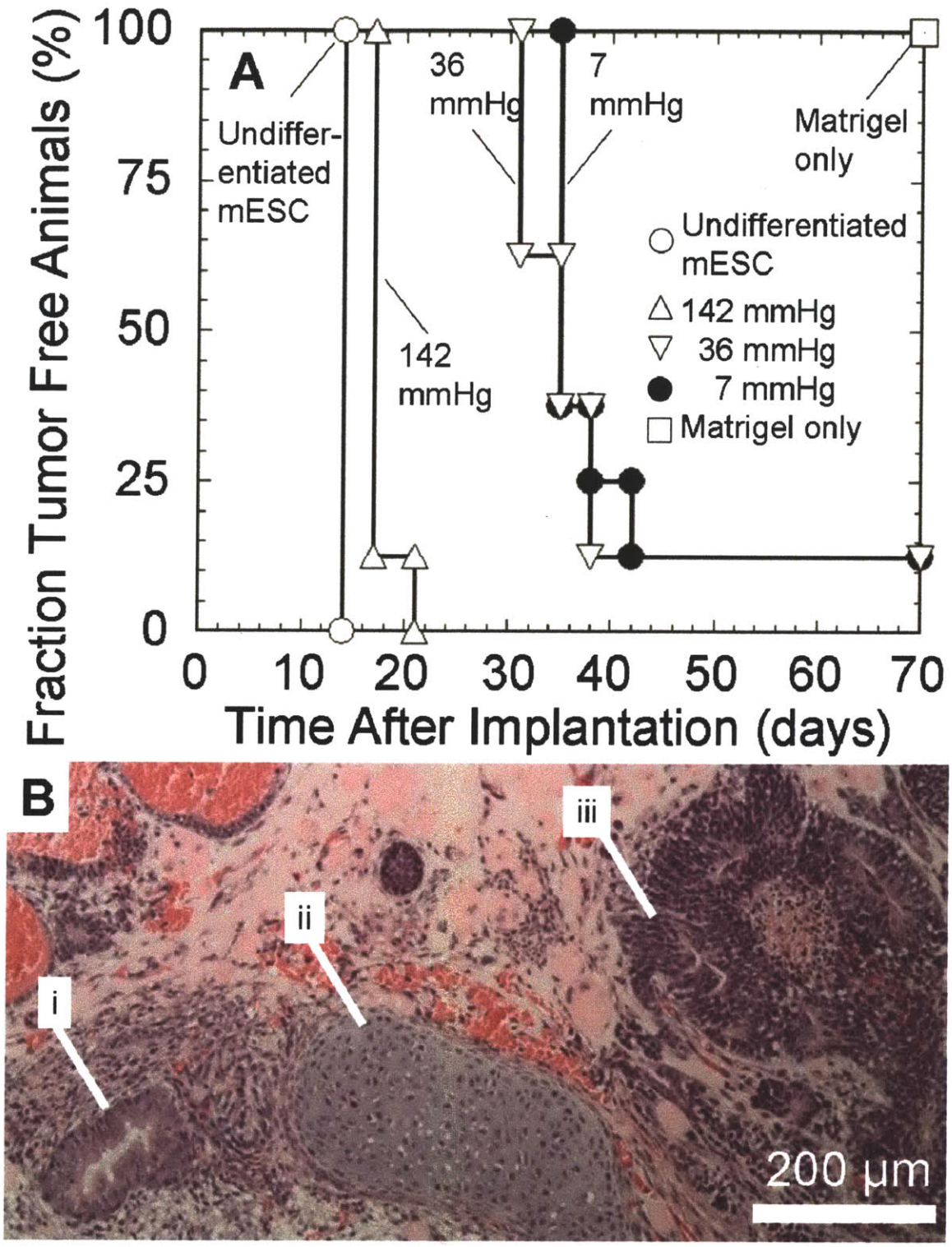

Figure 2-3. Time-course development of tumors in nude mice after subcutaneous implantation of mESC.

(A) Formation of tumors after implantation of undifferentiated mESC (n=6; positive control), mESC differentiated 10 days at 142, 36, or 7 mmHg followed by 20 days extended culture at the same pO_{2gas} (n=8) or only Matrigel (n=6; negative control). Tumor formation was determined by visual observation of the appearance of masses underneath the skin. (B) Representative H&E-stained tissue section of a tumor derived from mESC differentiated and having undergone 20 days of extended culture at 7 mmHg pO_{2gas}, with (i) small glandular structure, (ii) hyaline cartilage, and (iii) neuroepithelial structures highlighted. All animals with no tumors were monitored for a total of 210 days after implantation, during which no tumors were observed.

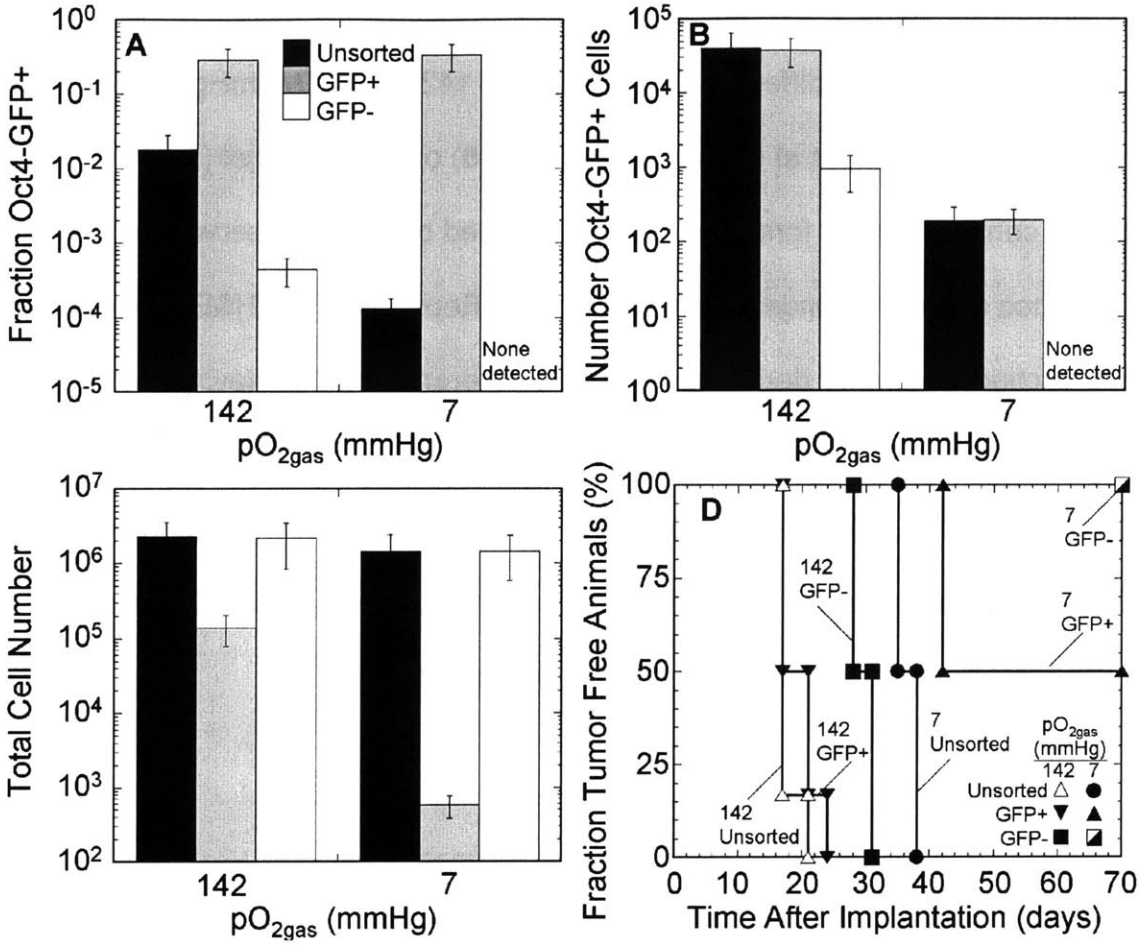

Figure 2-4. Expression of Oct4-GFP and time-course development of tumors in nude mice after subcutaneous implantation of differentiated and cultured mESC sorted into GFP+ and GFP- populations.

mESC underwent 10-day differentiation and 20-day extended culture at either 142 or 7 mmHg pO_{2gas} and cells before sorting (unsorted) and after being sorted into Oct4-GFP+ (GFP+) and Oct4-GFP- (GFP-) populations were analyzed. (A) Fraction of mESC that are Oct4-GFP+ as measured with flow cytometry (n=3). (B) The number of Oct4-GFP+ cells per well determined by multiplying the fraction of Oct4-GFP+ cells and the total cell number (n=3). (C) The total cell number per well as measured by nuclei count (n=3). (D) A sample of 10^5 cells were implanted

without sorting (unsorted; n=6) or 10^5 cells were sorted into GFP+ and GFP- populations (n=6), then implanted.

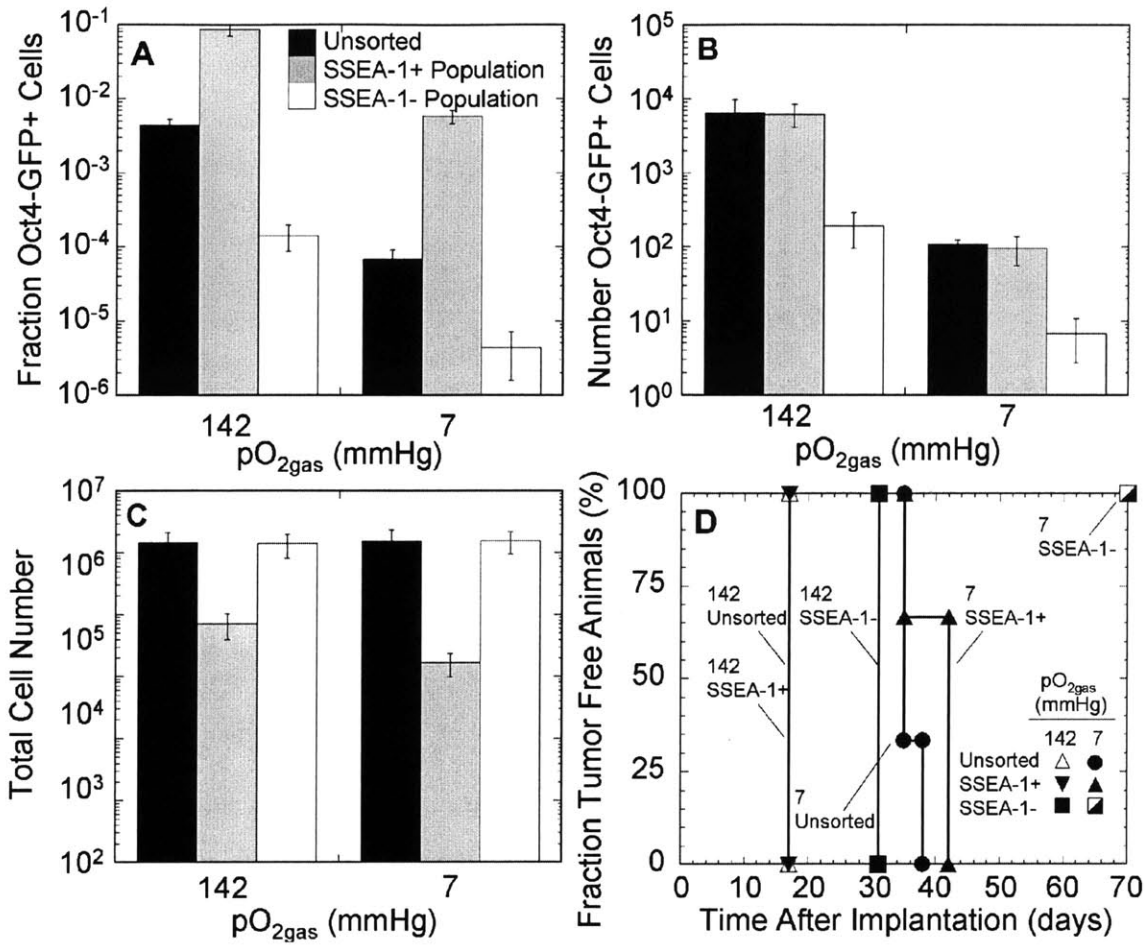

Figure 2-5. Expression of Oct4-GFP and time-course development of tumors in nude mice after subcutaneous implantation of differentiated and cultured mESC sorted into SSEA-1+ and SSEA-1- populations.

mESC underwent 10-day differentiation and 20-day extended culture at either 142 or 7 mmHg pO_{2gas}, and cells before sorting (unsorted) and after being sorted into SSEA-1+ and SSEA-1- populations were analyzed. (A) Fraction of mESC that are Oct4-GFP+ as measured with flow cytometry (n=3). (B) The number of Oct4-GFP+ cells per well determined by multiplying the fraction of Oct4-GFP+ cells and the total cell number (n=3). (C) The total cell number per well as measured by nuclei count (n=3). (D) A sample of 10^5 cells were implanted

without sorting (unsorted; n=6) or 10^5 cells were sorted into SSEA-1+ and SSEA-1- populations (n=6), then implanted.

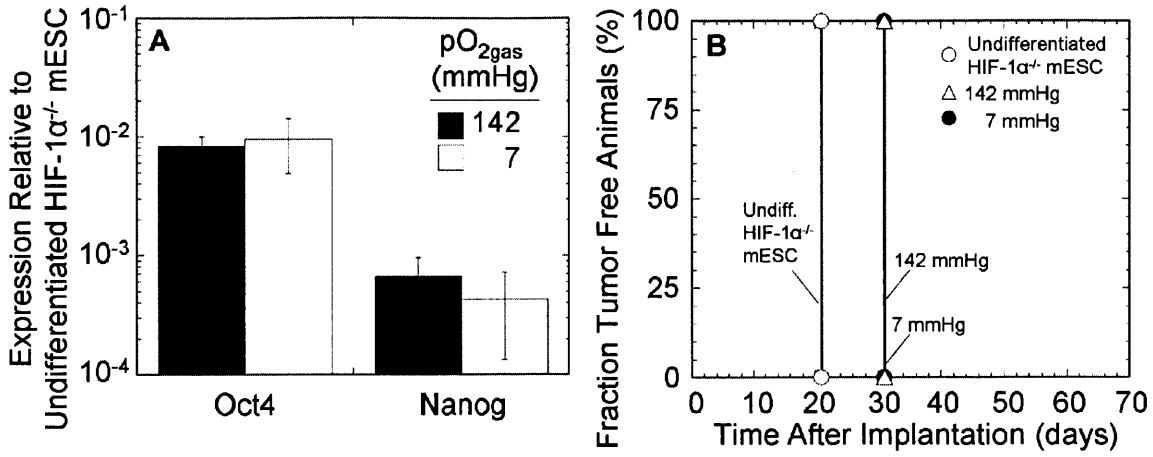

Figure 2-6. Expression of pluripotency markers and time-course development of tumors in nude mice with HIF-1α$^{-/-}$ mESC cells differentiated 10 days at 142 or 7 mmHg followed by 20-days extended culture at the same pO_{2gas}.

(A) Relative expression of Oct4 and Nanog mRNA measured with real-time PCR (n=3). (B) Formation of tumors after implantation of undifferentiated HIF-1α$^{-/-}$ mESC (n=6; positive control) and HIF-1α$^{-/-}$ mESC differentiated and cultured at 142 or 7 mmHg (n=6).

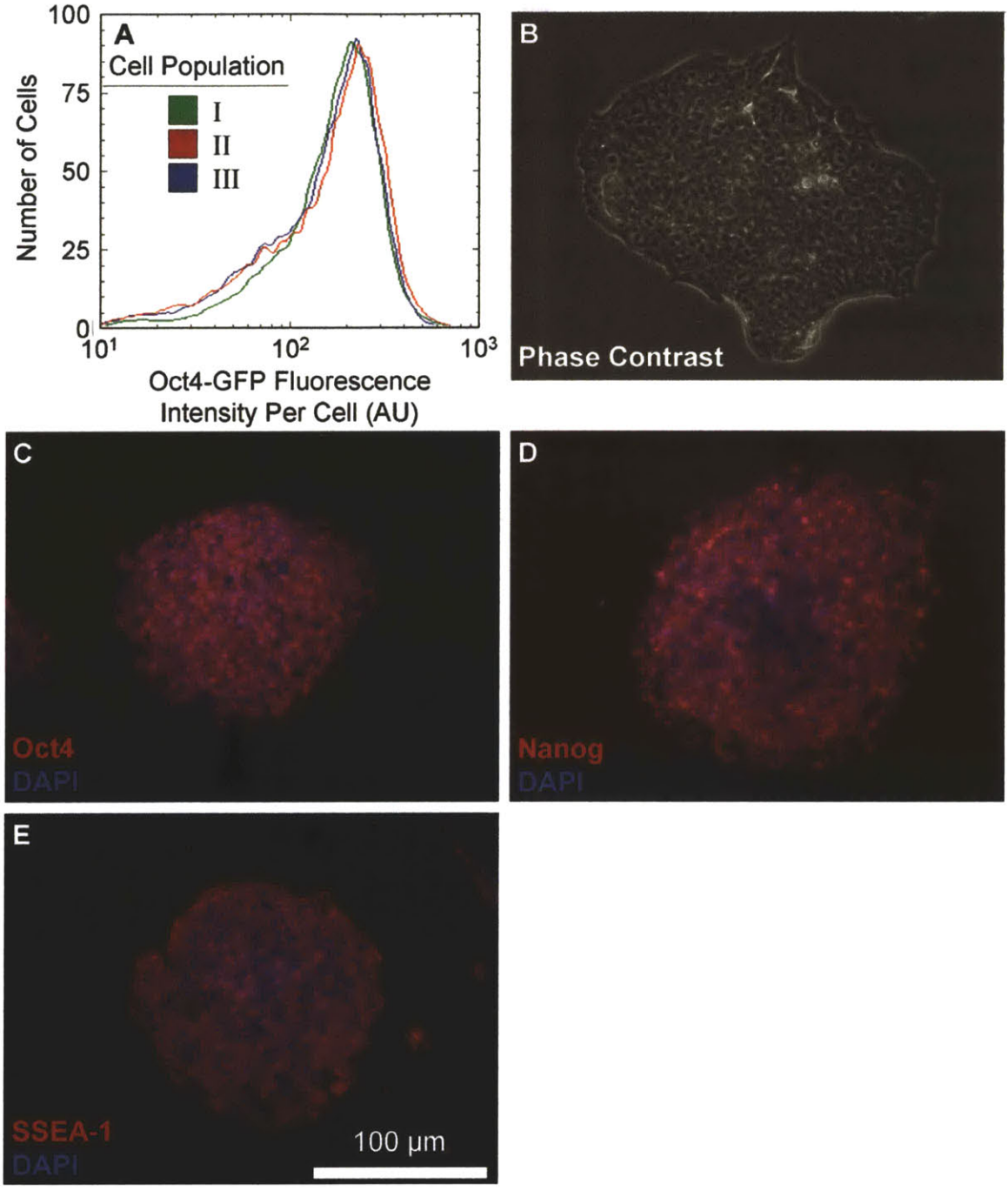

Figure 2-7. Characterization of (I) Oct4-GFP+ mESC that have never undergone differentiation and extended culture, (II) Oct4-GFP+ cells sorted with FACS from mESC that have undergone 10 days differentiation and 20 days extended culture

at 142 mmHg, and (III) Oct4-GFP+ cells cultured similar to case II, but at 7 mmHg.

(A) Histogram of the distribution of Oct4-GFP fluorescence intensity per cell, determined with flow cytometry. (B-E) En face images of colonies from cell population II. (B) Bright field image. (C-E) Cells stained with DAPI (blue) and immunostained (red) for (C) Oct4, (D) Nanog, and (E) SSEA-1.

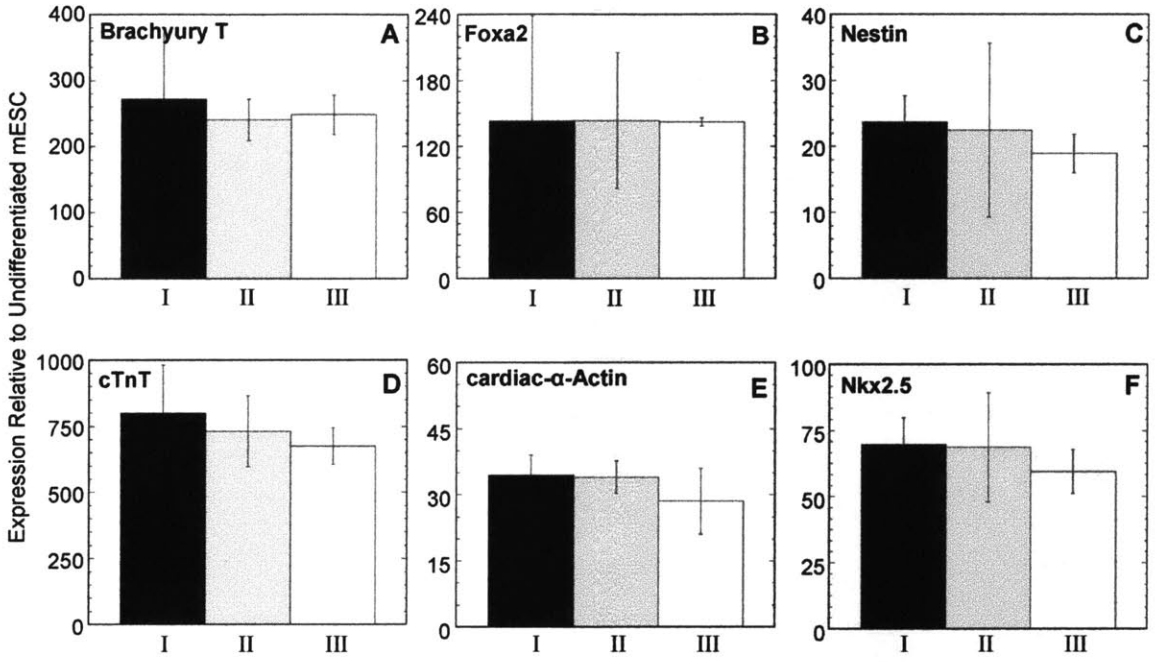

Figure 2-8. Differentiation of cases I, II, and III and assessment with real-time PCR.

Expression of (A) Brachyury T, (B) Foxa2, and (C) Nestin after 4 days of differentiation and (D) cTnT, (E) cardiac-α-Actin, and (F) Nkx2.5 after 10 days of differentiation (n=3). Expression is relative to case I before differentiation.

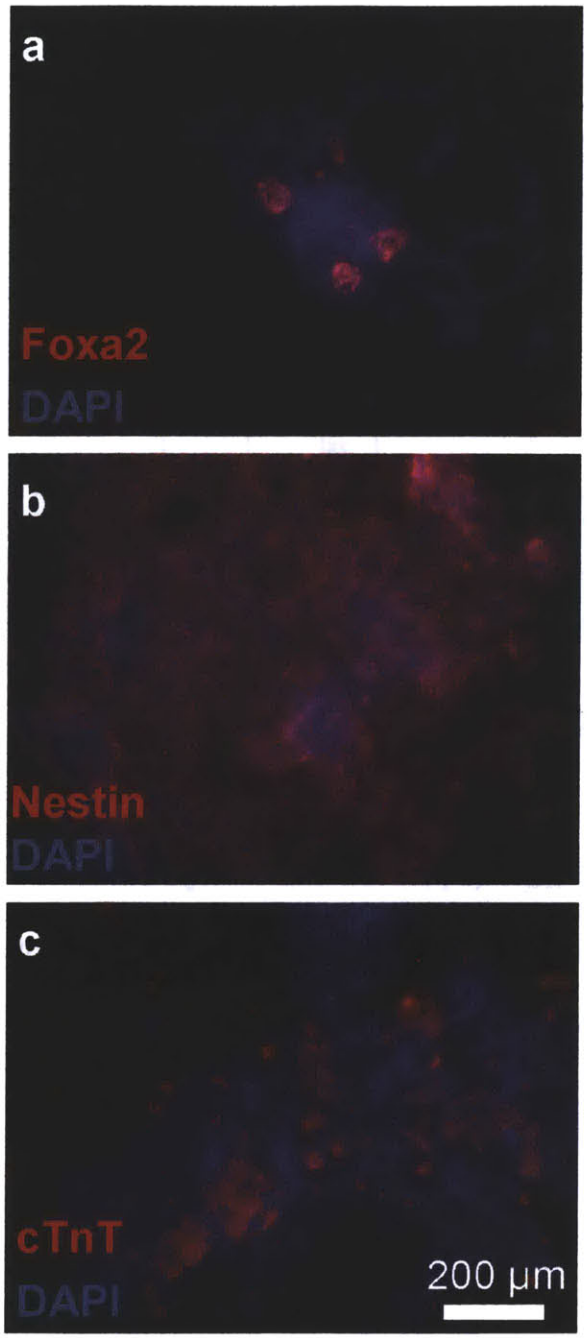

Figure 2-9. Differentiation of cases I, II, and III and assessment with immunocytochemistry.

En face images cells after (A-D) 4 days and (E-F) 10 days of differentiation stained with DAPI (A, C, E) and immunostained for (B) Foxa2, (D) Nestin, and (F) cTnT.

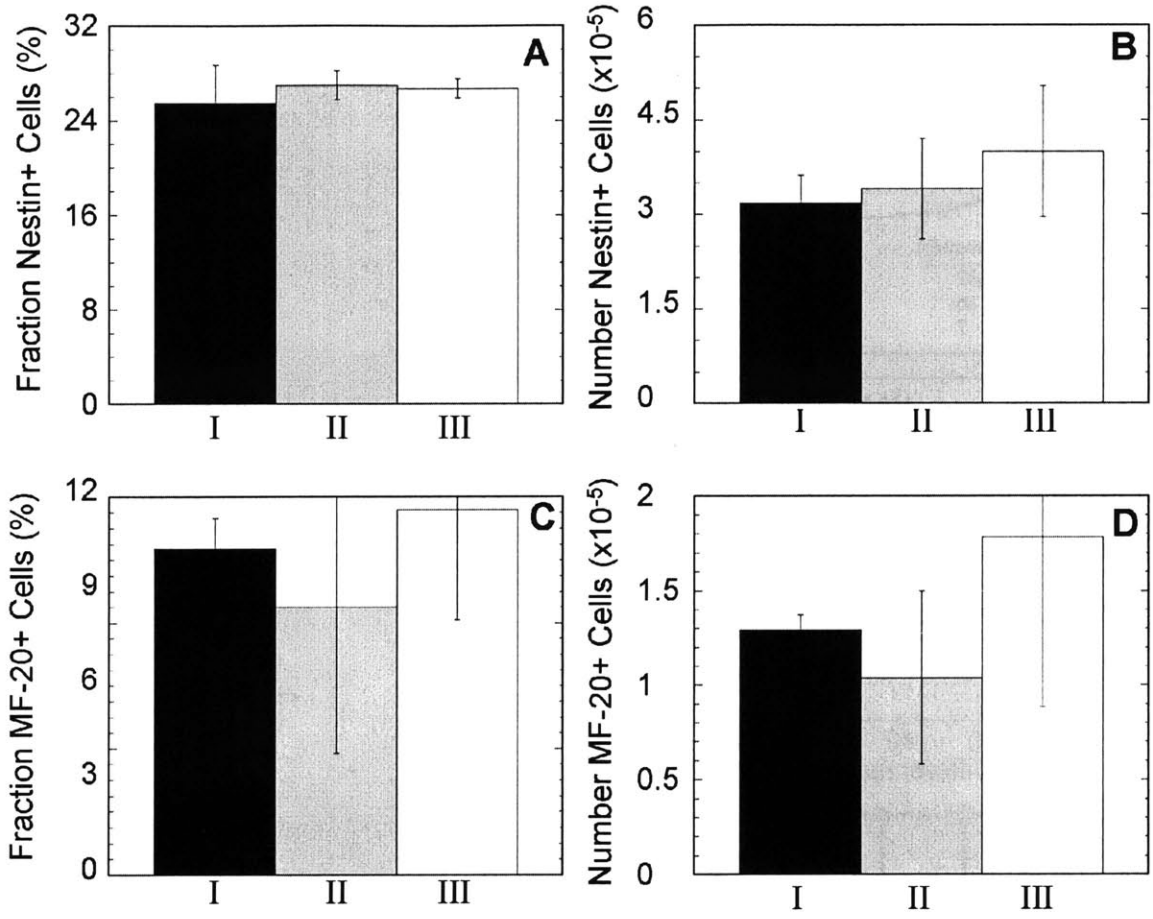

Figure 2-10. Differentiation of cases I, II, and III and assessment with flow cytometry.

(A) Fraction and (B) number of Nestin+ cells after 4 days of differentiation. (C) Fraction and (D) number of MF-20+ cells after 10 days of differentiation. (n=3).

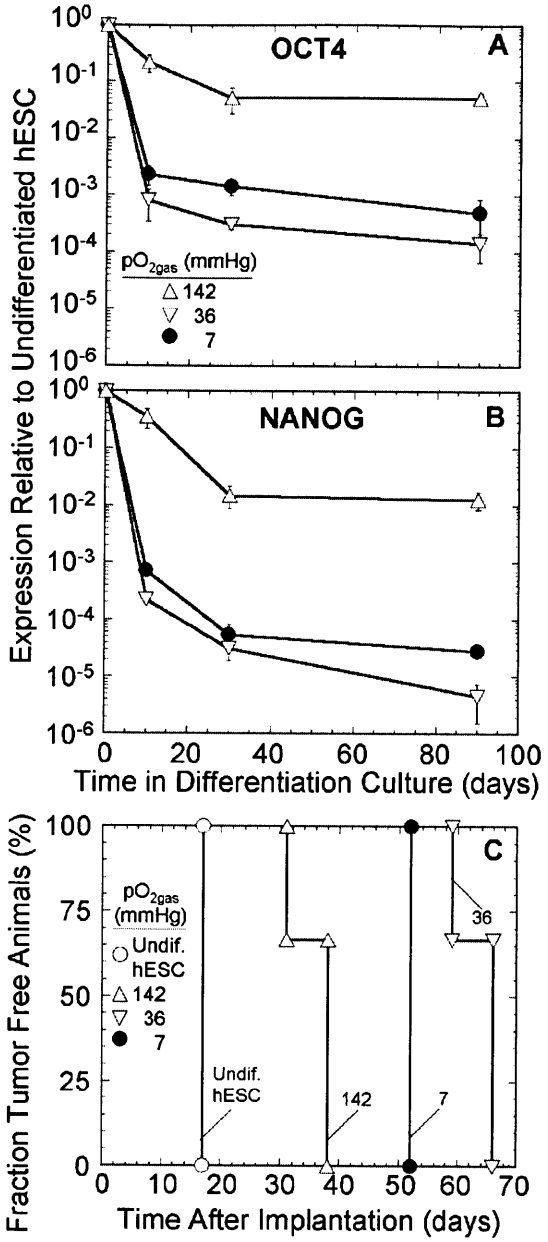

Figure 2-11. Expression of pluripotency markers and time-course development of tumors of hESC cultured under differentiation conditions at 142, 36, or 7 mmHg pO_{2gas} up to 90 days.

(A-B) Relative expression of OCT4 and NANOG mRNA measured with real-time PCR (n=3). (C) Formation of tumors after subcutaneous implantation of

undifferentiated hESC (positive control; n=6) and hESC differentiated 30 days at 142, 36, or 7 mmHg (n=6).

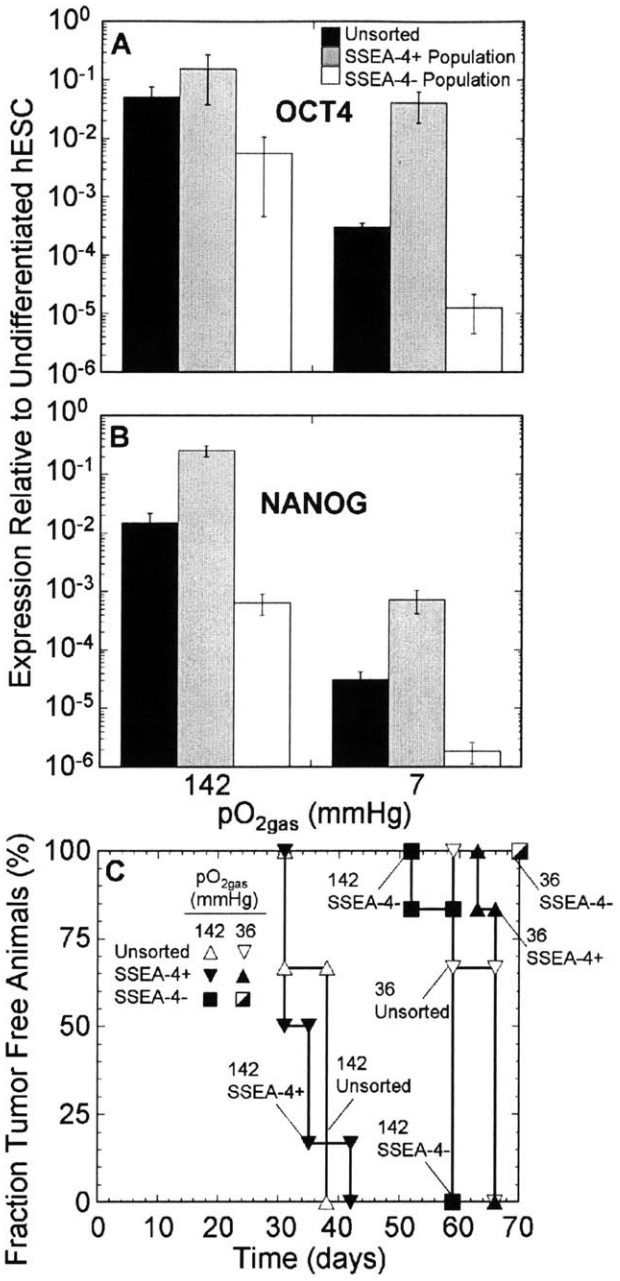

Figure 2-12. Gene expression of OCT4 and NANOG and time-course development of tumors in nude mice after subcutaneous implantation of differentiated and cultured hESC sorted into SSEA-4+ and SSEA-4- populations. hESC underwent 30-day differentiation at either 142 or 36 mmHg pO_{2gas}, and cells before sorting (unsorted) and after being sorted into SSEA-4+ and SSEA-4- populations were analyzed. (A-B) Relative expression of OCT4 and NANOG

mRNA measured with real-time PCR (n=3). (C) A sample of 10^6 cells were implanted without sorting (unsorted; n=6) or 10^6 cells were sorted into SSEA-4+ and SSEA-4- populations (n=6), then implanted.

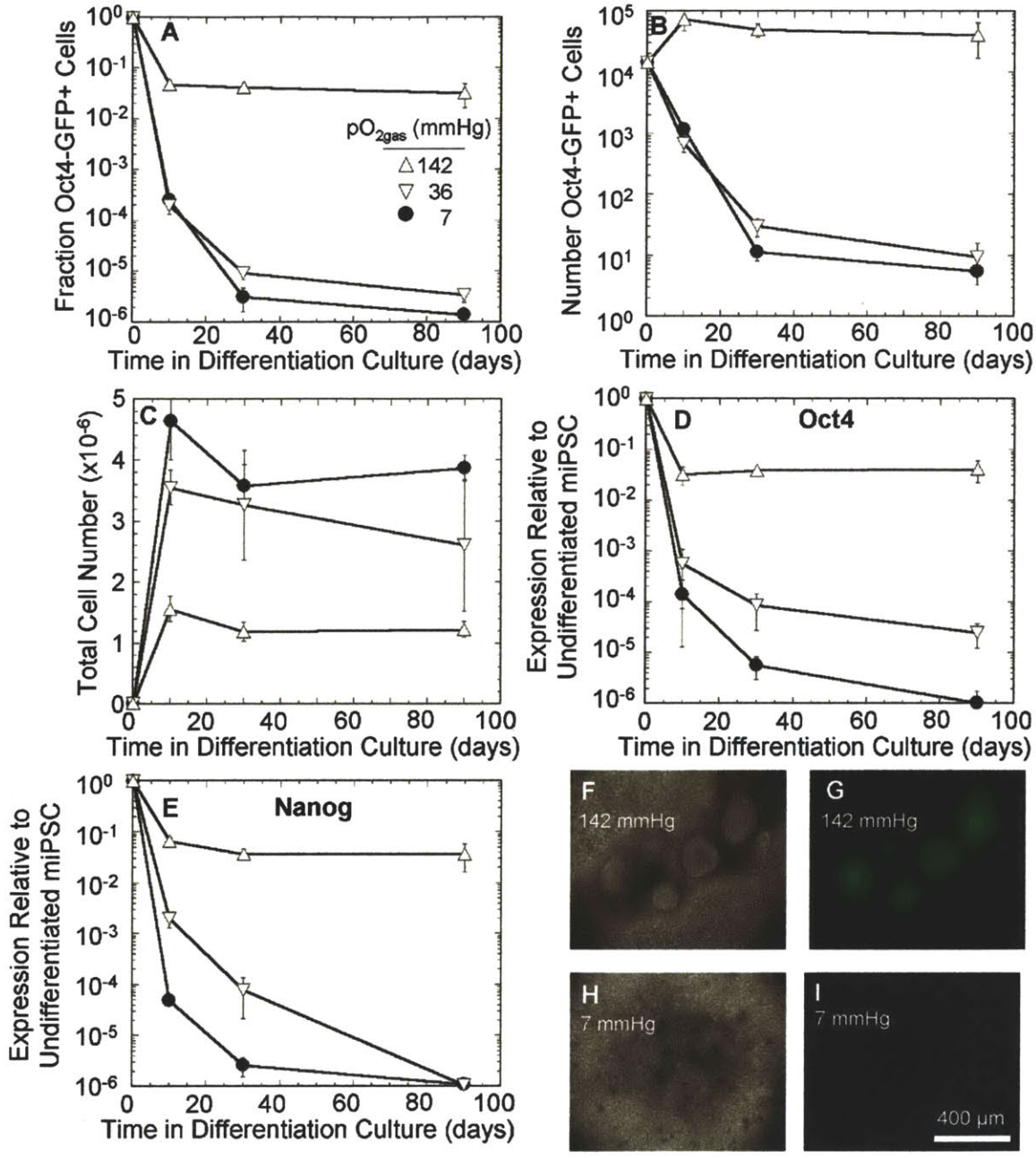

Figure 2-13. Expression of pluripotency markers in miPSC having undergone differentiation and extended culture at various pO_{2gas}.

miPSC were differentiated at 142, 36, or 7 mmHg pO_{2gas} then subjected to extended culture a the same pO_{2gas} used during differentiation for a total of 0, 10, 20, 30, or 90 days. (A) Fraction of cells that are Oct4-GFP+ as measured with flow cytometry (n=3). (B) The number of Oct4-GFP+ cells per well determined by

multiplying the fraction of Oct4-GFP+ cells and the total cell number (n=3). (C) The total cell number per well as measured by nuclei count (n=3). (D-E) Relative expression of Oct4 and Nanog mRNA measured with real-time PCR (n=3). (F and H) En face bright field images of cell aggregates after 30 days culture. (G and I) En face fluorescence images taken with a GFP filter corresponding with (F) and (H), respectively.

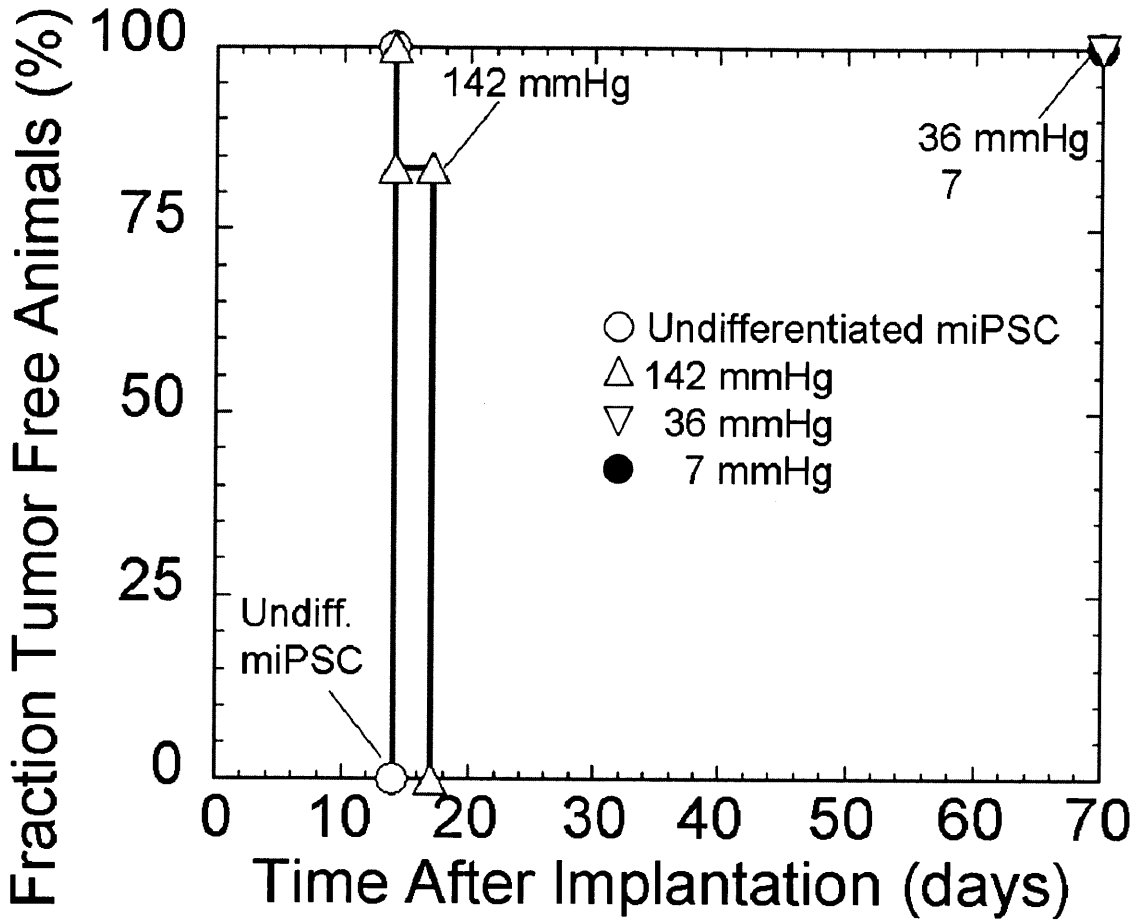

Figure 2-14. Time-course development of tumors in nude mice after subcutaneous implantation of miPSC.

Formation of tumors after implantation of undifferentiated miPSC (n=6; positive control), mipSC differentiated 10 days at 142, 36, or 7 mmHg followed by 20 days extended culture at the same pO_{2gas} (n=6). Tumor formation was determined by visual observation of the appearance of masses underneath the skin.

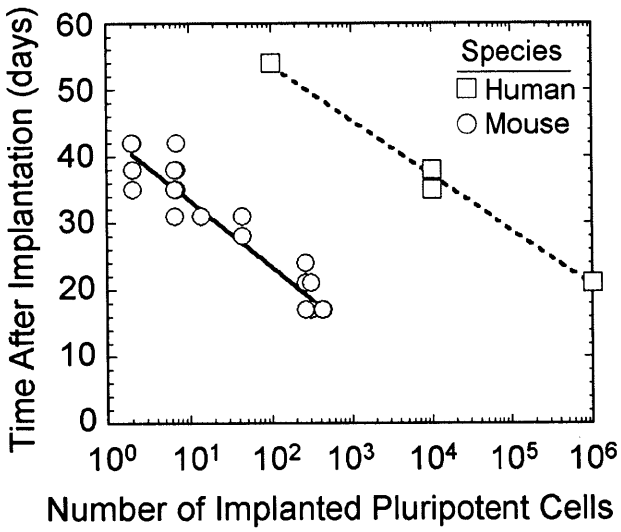

Figure 2-15. The time required for tumor appearance after implantation of different numbers mESC and hESC.

The number of implanted residual Oct4-GFP mESC, having undergone differentiation and extended culture under various conditions (Figures 1A, 4A, 5A), is plotted against the corresponding tumor formation data (Figures 3A, 4D, and 5D) (circles; n=79). 10^6, 10^4, and 10^2 undifferentiated hESC were implanted and the appearance of tumors observed (squares; n=6). The mouse (solid line) and human (dashed line) data fit the form $N_0 = Ae^{Bt}$, where N_0 is the number of implanted pluripotent cells, t is time, and $A = 1.22 \times 10^4$ and 3.03×10^8 and B = -0.209 and -0.278, respectively.

-Page Intentionally Left Blank-

Chapter 3. Differentiation of Pluripotent Stem Cells Under Low Oxygen Increases Generation of Cardiomyocytes and Influences Differentiation to Ectoderm, Mesoderm, and Endoderm

3.1. Abstract

Pluripotent stem cells (PSC) hold promise for the study of embryonic development and cell replacement therapy, but efficient differentiation to desired cell types remains a major obstacle. Most PSC research is performed in incubators with high, non-physiological partial pressures of oxygen (pO_2). However, embryonic cells in early development are exposed to much lower local pO_2, and the effects of such conditions on differentiating PSC are poorly understood. Here, low pO_2 drastically affects differentiation of mouse and human embryonic stem cells and mouse induced pluripotent stem cells to the three germ layers and cardiomyocytes. Overall, differentiation was higher to endoderm, lower to ectoderm, and higher or the same to mesoderm. Differentiation to cardiomyocytes was greatly enhanced, with our best protocol resulting in 35% cardiomyocytes and 60 cardiomyocytes being generated per input mouse embryonic stem cell without the need for purification. Understanding the effects of pO_{2gas} during differentiation is an important step towards the development of protocols for regenerative medicine.

3.2. Introduction

Pluripotent stem cells (PSC), including embryonic stem cells (ESC) and induced pluripotent stem cells (iPSC), have the potential to differentiate into any cell type found in a mature organism. The clinical potential for such PSC is immense [3], including treatments for heart disease, diabetes, Parkinson's disease, and leukemia [4-6]. For example, PSC could be differentiated to cardiomyocytes and implanted into infracted hearts to potentially replace necrotic tissue after a heart attack [117]. However, before PSC-based therapies can be used effectively in clinical applications, the ability to generate the desired differentiated cells in sufficient purity and quantity for use in humans must be developed [118].

Differentiation of PSC to the three germ layers *in vitro* is often induced with soluble signaling molecules. High and low levels of nodal signaling specify endoderm and mesoderm, respectively, while FGF signaling specifies ectoderm [119]. Numerous molecules can be used to further direct cardiomyocyte differentiation, including vascular endothelial growth factor, dickkopf homolog 1, ascorbic acid, and 5-azacytidine [120-123].

Low partial pressure of oxygen (pO_2) has been shown to increase PSC differentiation to derivatives of the ectodermal and mesodermal lineages, such as neurons, cardiomyocytes, hematopoietic progenitors, endothelial cells, and chondrocytes in separate studies [2]. In most studies, the pO_2 experienced by the

cell (pO_{2cell}) is not controlled or understood [53]. Low pO_2 is generally thought to affect cells by decreasing exposure to reactive species generated by cellular respiration [124] and by regulating the stability of the oxygen-responsive transcription factor hypoxia inducible factor-1 (HIF-1) [125], but other mechanisms may also be involved [126].

Even though pO_2 is an important culture parameter, PSC are usually cultured at relatively high pO_2, typically in a humidified atmosphere consisting of 95% air/5% CO_2, resulting in a gas phase pO_2 (pO_{2gas}) of 142 mmHg. This value is higher than that found in most mammalian tissues and *in utero*, such as rat microvasculature (25 mmHg) [20], rhesus monkey reproductive tract (15-45 mmHg) [127], and fetal human venous blood (25-30 mmHg) [21, 22]. The pO_2 in early developing embryos is likely very low because circulation is not yet occurring [128, 129].

In this study, we quantitatively investigated the effects of pO_2 on the differentiation of mouse ESC (mESC) to the three germ layers and mESC, mouse iPSC (miPSC), and human ESC (hESC) to cardiomyocytes. Cells were cultured on highly oxygen permeable silicone rubber membrane plates, which allowed us to set pO_{2cell} at the membrane-cell interface virtually to the value of pO_{2gas}. Overall, differentiation of mESC at low pO_2 increased endoderm, decreased ectoderm, and either increased or didn't change mesoderm differentiation compared to 142 mmHg. The expression of many differentiation

genes was delayed at low compared to high pO_2. Constant low pO_2 enhanced differentiation of mESC, miPSC, and hESC to cardiomyocytes, compared to 142 mmHg without the need for purification and additional soluble molecules beyond serum, but the largest cardiomyocyte yields occurred with temporal variation of pO_{2gas}. pO_{2cell} of cardiomyocytes within resulting cellular aggregates after differentiation was calculated.

3.3. Methods

3.3.1. Culture of undifferentiated mESC and miPSC

Undifferentiated J1 mESC (American Type Culture Collection (ATCC), Manassas, VA, USA), miPSC [113] and mESC harboring a Sox17-dTomato reporter [130] (Sox17-dTomato mESC) (both generously donated by Professor Douglas Melton of Harvard University, Cambridge, MA, USA), mESC with a homozygous HIF-1α, a subunit of HIF-1, gene knockout (HIF-$1\alpha^{-/-}$ mESC) [114] (generously donated by Professor Peter Carmeliet of Katholieke Universiteit Leuven, Leuven, Belgium), and mESC harboring a Brachyury T-GFP reporter (T-GFP mESC) [131] (generously donated by Professor Gordon Keller of McEwen Centre for Regenerative Medicine, Toronto, ON, Canada) were cultured without mouse embryonic fibroblasts as previously described [53] in Dulbecco's Modified Eagles Medium (DMEM; SCRR-2010; ATCC) supplemented with 10% (v/v) fetal bovine serum (FBS; SCRR 30-2020; ATCC), 1x L-alanyl-L-glutamine (SCRR 20-

2115; ATCC), 1x penicillin streptomycin (P/S; 15070; Invitrogen, Carlsbad, CA, USA), 1x MEM non-essential amino acids (SCRR 20-2116; ATCC), 100 μM 2-mercaptoethanol (M7522; Sigma-Aldrich; St. Louis, MO, USA), and 10^3 units/mL leukemia inhibitory factor (LIF; LIF2005; Millipore, Billerica, MA, USA). Cells were passaged by treatment with 0.25% trypsin (25-053-CI; Mediatech, Manassas, VA, USA) every two days and seeded at $1.2x10^4$ cells cm^{-2} on cell culture flasks (353014; Becton Dickinson, Franklin Lakes, NJ, USA).

3.3.2. Control of pO_{2gas}

pO_{2gas} was controlled by placing cells inside chambers maintained at 37 °C with premixed gas flown in containing 5% CO_2 and 20%, 5%, or 1% O_2 and a balance of N_2 (certified medical gas from Airgas, Hingham, MA, USA), which corresponded, under humidified conditions, to 142, 36, and 7 mmHg pO_{2gas}, respectively, as previously described [53].

3.3.3. Silicone rubber membrane-based plate

Differentiation was performed on custom-made highly oxygen permeable silicone rubber plates, as previously described [53]. In brief, 24-well polystyrene plate bottoms (353047; Becton Dickinson) were replaced with silicone rubber sheets (nonreinforced vulcanized gloss/gloss 127 μm thick; Specialty Manufacturing, Saginaw, MI, USA) and sterilized by 1 hr treatment with 70% (v/v) ethanol

(111000200; Pharmco-AAPER, Brookfield, CT, USA) in water and overnight drying under a biological safety cabinet germicidal UV lamp (SterilGARD III Advance; The Baker Company, Sanford, MA, USA). When in use for cell culture, a silicone rubber plate sat on top of a 150x15 mm Petri dish (35384-326; VWR, West Chester, PA, USA) with only the plate corners being supported by the Petri dish, allowing the silicone rubber membrane to be directly exposed to the gas phase. Silicone rubber membranes maintained pO_{2cell} at the cell-membrane interface at virtually the same value as pO_{2gas}, and allowed for rapid equilibration of pO_{2cell} after a change in pO_{2gas}. Treatment of silicone rubber membranes at 37 °C with 2 µg/mL fibronectin (F1141; Sigma-Aldrich) in phosphate buffered saline (PBS; 21-040; Mediatech) for 24 hr for mESC and miPSC or Matrigel (354234, Becton Dickinson) diluted 1:20 in serum-free medium for 1 hr for hESC permitted cell attachment.

3.3.4. Differentiation of mESC and miPSC

mESC and miPSC differentiation was performed as previously described [53]. In brief, embryoid bodies (EBs) were formed in 20-µL hanging drops, consisting of $2.5x10^4$ cells ml^{-1} in propagation medium without LIF. After 2 days, 30 EBs per well were transferred to fibronectin-coated silicone rubber wells filled with 2 mL of propagation medium without LIF, which was replaced with 2.5 mL of serum-free medium after 3 additional days, consisting of 50% (v/v) DMEM (90-133-PB; Mediatech) and 50% (v/v) Ham's F-12 (10-080-CV; Mediatech) supplemented

with 0.75% (w/v) sodium bicarbonate (25-035-CI; Mediatech), 9 mM glucose (G8769; Sigma-Aldrich), 5 μg/mL human insulin (I9278; Sigma-Aldrich), 50 μg/mL holo transferrin (T1283; Sigma-Aldrich), 31.2 nM sodium selenite (S9133; Sigma-Aldrich), and 1x P/S. Cells were differentiated for up to a total of 13 days. pO_{2gas} was kept constant throughout differentiation in some cases and in others, was varied, as noted. In addition, 0.2 mM ascorbic acid (A4034; Sigma-Aldrich) was also included in culture medium in some cases, as noted. Cell samples at various time points were acquired for analysis by dissociation with a 5-min exposure to 0.25% trypsin at 37 °C.

3.3.5. Real-time polymerase chain reaction (PCR)

Total RNA was extracted with the RNeasy Kit (74104, Qiagen, Valencia, CA) and RNase-Free DNase Set (79254, Qiagen), cDNA created using High Capacity cDNA Reverse Transcription Kit (4368814, Applied Biosystems, Foster City, CA), real-time PCR conducted on a Fast Real-Time PCR System (7900HT, Applied Biosystems) at the Center for Biomedical Engineering (MIT) using Power SYBR Green PCR Master Mix (4367659, Applied Biosystems) or Taqman Gene Expression Master Mix (4369016, Applied Biosystems), as appropriate, and 28S ribosomal RNA (rRNA) was measured for an endogenous control. Primer sequences used for 28S rRNA, Sox17, Nestin, and Nkx2.5 have been previously reported [32]. Additional primers sequences used (in order of forward and reverse primer and 5' to 3') were Foxa2 TCAAGGCCTACGAACAGGTCAT and

GCCCGCTTTGTTCGTGACT, Hnf4a CAGACGTCCTCCTTTTCTTGTGATA and TGTTTGGTGTGAAGGTCATGATTA, Pdx1 CGCGTCCAGCTCCCTTT and CCTGCCCACTGGCCTTT, Sox1 TGCACAGTTCAGCCCTGAGT and GCACAAACCACTTGCCAAAGA, Pax6 TGGAAACAAACGCCCTAGCT and GGACAGGGAACACACCAACTTT, Brachyury T TCCCGGTGCTGAAGGTAAAT and CCGTCACGAAGTCCAGCAA, Mesp2 TTTGGGCTGCCTTGGAAGT and AGCTAAGCAGACCTCAAAATGTCA, Tbx20 CCAGCGAAGAGATGGCTAAAA and TGTCCCAGAGCTCCTTCGTT, Mef2c TGCTGGTCTCACCTGGTAAC and ATCCTTTGATTCACTGATGGCAT, cardiac-α-Actin GCTTCCGCTGTCCAGAGACT and TGCCAGCAGATTCCATACCA, and cardiac Troponin T (cTnT) AGATGCTGAAGAAGGTCCAGTAGAG and CACCAAGTTGGGCATGAAGA. Premade primers for Mesp1 (Mm00801683_g1, Applied Biosystems), Tbx5 (Mm00803518_m1, Applied Biosystems), Titin (Mm00621005_m1, Applied Biosystems), human cTNT (Hs00165960_m1, Applied Biosystems), human MEF2C (Hs00231149_m1, Applied Biosystems), and human NKX2.5 (Hs00231763_m1, Applied Biosystems) were also used. A standard curve was constructed with pooled cDNA from all time points and pO_{2gas} serial diluted.

3.3.6. Immunocytochemistry

Attached cells were fixed with 4% (w/v) paraformaldehyde (36606; Alfa Aesar, Ward Hill, MA, USA) in PBS for 20 min, permeabilized and non-specific protein

binding blocked in a PBS solution containing 3% (v/v) donkey serum (DS; D9663; Sigma-Aldrich) and 0.1% (v/v) Triton X-100 (T9284; Sigma-Aldrich) for 45 min, and incubated overnight at 4 °C with primary antibodies against Foxa2 (sc-6554; Santa Cruz Biotechnology, Santa Cruz, CA, USA) diluted 1:200, Nestin (MAB2736; R&D Systems, Minneapolis, MN, USA) diluted 1:50, cTnT (MS-295-P1; NeoMarkers, Fremont, CA, USA) diluted 1:50, or Nkx2.5 (sc-8697; Santa Cruz Biotechnology) in 3% DS 0.1% Triton X-100 solution. After washing 1x with 3% DS 0.1% Triton X-100 solution, cells were incubated for 2 hr at room temperature in the dark with Alexa Fluor 488 (green) or 594 (red) secondary antibodies (Invitrogen, Carlsbad, CA, USA) against the appropriate primary antibody species diluted 1:200 in 3% DS 0.1% Triton X-100 solution. After washing 1x, cells were incubated with 1 µg/mL 4',6-diamidino-2-phenylindole (DAPI; 32670, Sigma-Aldrich) in PBS for 10 min in the dark to stain DNA (blue), after which cells were then washed 3x with PBS and visualized with an Axiovert 200 fluorescence microscope (Carl Zeiss, Oberkochen, Germany).

3.3.7. Flow cytometric analysis of immunostained cells

The fraction of Nestin+ and MF-20+ cells in dispersed cells was acquired with flow cytometry, as previously described [53]. In brief, samples were fixed by 20 min incubation in 1% (w/v) paraformaldehyde in PBS. Fixed cells numbering $3x10^5$ were permeabilized in 0.5% saponin (S-4521; Sigma-Aldrich) for 10 min, non-specific binding blocked 30-min incubation in 2% (v/v) FBS in PBS, and

incubated at room temperature with primary antibody against Nestin diluted 1:50 or sarcomeric myosin heavy chain (MF-20; MF-20 supernatant; Developmental Studies Hybridoma Bank, Iowa City, IA, USA) diluted 1:10 in 2% FBS solution for 1 hour. Samples were then incubated with goat anti-mouse phycoerythrin-conjugated secondary antibody (115-116-146; Jackson ImmunoResearch; West Grove, PA) diluted 1:250 in 2% FBS solution for 30 min at room temperature in the dark, washed 3x in 2% FBS solution, and staining data were measured using a Guava PCA flow cytometer (Millipore).

3.3.8. Nuclei enumeration

Dispersed cells were exposed to a lysis solution of 1% (v/v) Triton X-100 and 0.1 M citric acid (0627; Mallinckrodt Specialty Chemicals Co., Paris, KY, USA) and vortexed to obtain nuclei samples. Samples were stained with Guava Viacount (4000-0041; Millipore) and data acquired with a Guava PCA flow cytometer, as previously described [53].

3.3.9. Flow cytometric analysis of T-GFP expression

T-GFP expression was acquired with a flow cytometer (FACScan; Becton Dickinson) at the Koch Institute (MIT). Gating was set so that all of a negative control, J1 mESC without T-GFP differentiated under the same conditions as the T-GFP mESC, were counted as negative for T-GFP, and the fraction of cells

expressing T-GFP (T-GFP+) was calculated as the number of cells above this gate divided by the total number of cells at each time and condition.

3.3.10. Immunostaining of histological sections

Histological specimens obtained from cells at differentiation day 11 were fixed with 4% paraformaldehyde overnight and subsequently embedded in paraffin and sectioned by the Joslin Diabetes Center histology core to yield 5-μm sections. Samples were deparaffinized and rehydrated by 7 min rinses with xylene (8671; Mallinckrodt) (twice), 5 min rinses with 100% ethanol (twice), a 3 min rinse with 95% ethanol, a 10 min rinse with 70% ethanol, and 5 min rinses with deionized water (25-055-CM; Mediatech) (twice). Antigen retrieval was performed by boiling sections for 10 min in a 10 mM sodium citrate (0754; Mallinckrodt) solution at pH 6. Endogenous peroxidase activity was quenched by incubating the slides at room temperature for 10 min in 0.3% hydrogen peroxide (386790; Calbiochem, La Jolla, CA, USA), and slides, blocked with 1 hr incubation in 1% FBS. Samples were incubated with MF-20 (1:10) or anti-cTnT primary antibody overnight at 4 °C and, after 3 washes, were incubated with goat anti-mouse IgG (115-035-062; Jackson ImmunoResearch) diluted 1:50 in 1% FBS for 3 hr at room temperature. After 3 additional washes, samples were incubated with mouse peroxidase-anti-peroxidase complex (223-005-024; Jackson ImmunoResearch) diluted 1:500 in 1% FBS for 1 hr at room temperature. Visualized was achieved by incubating 2 min in 2 mM diaminobenzidine (D5637; Sigma-Aldrich) containing 0.015%

hydrogen peroxide, and slides were counterstained by incubating 15 sec in haematoxylin (HHS16; Sigma-Aldrich), followed by 3 washes in 30 mM sodium borate (B10267-34; EMD Chemicals, Gibbstown, NJ, USA). Slides were then dehydrated following the reverse procedure for rehydration and preserved using Permount (SP15; Fisher Chemical, Fair Lawn, NJ, USA).

3.3.11. Semi-quantitative assessments

The fractional surface coverage of spontaneously-contracting cells within 15 randomly arranged 2 mm^2 circles per well was estimated by visual observation and the average of which taken to be the fractional surface coverage of cells for that well, as previously described [53]. Histological sections of J1 mESC differentiated for 11 days with 0.2 mM ascorbic acid at 142, 36, and 7 mmHg pO_{2gas} immunostained with MF-20 were manually counted for the number of MF-20+ and MF-20- cells.

3.3.12. Calculated volumetric pO_{2cell} within MF-20+ regions

We previously reported calculating the pO_{2cell} distribution within aggregates [53]. Calculations similar to those were used to estimate the pO_{2cell} for cells positively immunostained with MF-20. For these calculations, the aggregate dimensions were measured, and MF-20+ regions were identified in the 5-μm tissue sections. The finite element model for oxygen transport was used to predict the pO_2 profile

within the entire aggregate, and the integration to determine the volume of tissue between surfaces of constant pO_2 was only performed for simulated MF-20+ regions. The volume fraction of tissue in MF-20+ regions within specific limits of pO_2 was determined by:

$$\Phi_{ab,MF20} = \frac{\sum_{j=1}^{n} V_{ab,j,MF20}}{\sum_{j=1}^{n} V_{aggregate,j,MF20}} \quad (1)$$

where $V_{ab,j,MF20}$ is the volume of tissue with a pO_2 between a and b in the j^{th} MF-20+ region and $V_{aggregate,j,MF20}$ is the total volume of the j^{th} MF-20+ region. Because no MF-20+ cells were observed in the sheet-like morphology, ϕ_{sheet} was set to 0 and does not appear in Eq. 1.

3.3.13. Differentiation of hESC

EBs were formed with 500 CyT49 hESC [9] (NIH Registration Number 0041; generously provided by ViaCyte, Inc, San Diego, CA, USA) per microwell of an Aggrewell plate (27845; Stemcell Technologies, Vancouver, BC, Canada) for 1 day, transferred to suspension culture on silicone rubber plates, previously treated with 1% (w/v) pluronic F-127 (P2443; Sigma-Aldrich) to prevent attachment for 7 days, and 30 EBs transferred to each well of a Matrigel-coated 24-well silicone rubber plate for attachment culture or 12 days. Differentiation was performed entirely in mESC and miPSC propagation medium without LIF with 0.2 mM ascorbic acid.

3.3.14. Statistics

Statistical analysis was performed with unpaired two-tailed t-tests, with $p<0.05$ being considered statistically significant. All data presented as mean ± standard deviation of biological replicates.

3.4. Results

3.4.1. The effect of pO_2 on endodermal differentiation of mESC

We differentiated J1 mESC at various, constant pO_{2gas} to examine differentiation to the endodermal lineage (Figure 1). Different pO_{2gas} values changed the timing and magnitude of endodermal gene expression, measured with real-time PCR. Expression overall was higher at low compared to high pO_{2gas}. Highest Foxa2 expression, an early endoderm marker [132], occurred on days 4, 7, and 13 for 142, 36, and 7 mmHg, respectively, with expression at 36 mmHg being 2.7 times higher than and at 7 mmHg being statistically the same as 142 mmHg (Figure 1A). Highest Sox17 expression, an early endoderm marker [133], occurred on days 8, 8, and 9 for 142, 36, and 7 mmHg, respectively, with expression at 36 mmHg being 1.9 times higher than and at 7 mmHg being statistically the same as 142 mmHg (Figure 1B). Highest Hnf4a expression, a primitive gut tube marker [134], occurred on days 7, 7, and 13 for 142, 36, and 7 mmHg, respectively, with

expression at 36 mmHg being 2.3 times higher than and at 7 mmHg being 3.0 times higher than as 142 mmHg (Figure 1C). Highest Pdx1 expression, a posterior foregut marker [135], occurred on days 12, 10, and 12 for 142, 36, and 7 mmHg, respectively, with expression at 36 mmHg being 4.5 times higher than and at 7 mmHg being 4.1 times higher than as 142 mmHg (Figure 1D).

More Foxa2+ and Sox17-dTomato+ cells were observed with microscopy at low compared to high pO_{2gas} (Figure 1E-H), qualitatively correlating with our real-time PCR data (Figure 1A-B). However, with this protocol, the fraction of Foxa2+ and Sox17-dTomato+ cells was less than 1%, assessed with visual observation, at all pO_{2gas}, and we were unable to accurately quantitate the numbers with flow cytometry.

Different pO_{2gas} values slowed or delayed endodermal gene expression, as in expression was higher at some pO_{2gas} at earlier times and higher at other pO_{2gas} at later times. Gene expression was delayed 1-2 days for Sox17 and Hnf4a at 36 mmHg and for Foxa2, Sox17, and Hnf4a at 7 mmHg, compared to 142 mmHg (Figure 1A-C). However, the trend with Pdx1 was different, with expression being first significantly higher than undifferentiated mESC on day 9 for 36 mmHg, day 10 for 142 mmHg, and day 12 for 7 mmHg (Figure 1D). We are uncertain of the cause of the difference between Pdx1 and the earlier markers.

3.4.2. The effect of pO_2 on ectodermal differentiation of mESC

We differentiated J1 mESC at various, constant pO_{2gas} to examine differentiation to the ectodermal lineage (Figure 2). Expression overall was higher at high compared to low pO_{2gas}. Highest Sox1 expression, an early ectodermal marker [136], occurred on days 13, 7, and 7 for 142, 36, and 7 mmHg, respectively, with expression at 142 mmHg being 3.2 and 8.6 times higher than 36 and 7 mmHg, respectively (Figure 2A). Highest Nestin expression, a neural stem cell marker [137], occurred on days 12, 4, and 4 for 142, 36, and 7 mmHg, respectively, with expression at 142 mmHg being 1.4 times higher than at 7 mmHg and statistically the same as 36 mmHg (Figure 2B). Highest Pax6 expression, a neurogenic marker [138], occurred on days 13, 12, and 12 for 142, 36, and 7 mmHg, respectively, with expression at 142 mmHg being 7.8 and 4.3 times higher than at 36 and 7 mmHg, respectively (Figure 2C). The fraction and number of Nestin+ cells was also lower with differentiation at low pO_{2gas} (Figure 2D-E), correlating with our real-time PCR data. After 12 days of differentiation, the fraction of Nestin+ cells was 32, 20, and 8.6% for 142, 36, and 7 mmHg, resulting in 95, 60, and 18 Nestin+ cells generated per each input mESC. More Nestin+ cells were also observed with microscopy at high compared to low pO_{2gas} (Figure 2F-G).

3.4.3. The effect of pO_2 on mesodermal differentiation of mESC

We differentiated J1 mESC at various, constant pO_{2gas} to examine mesodermal differentiation (Figure 3). pO_2 changed the timing and magnitude of mesodermal gene expression. Expression of Brachyury T, an early mesoderm marker [139], was higher at 142 mmHg on days 3 and 4 compared to 36 and 7 mmHg. Maximal Brachyury T expression was the same between 142 and 36 mmHg and slightly higher at 7 compared to 142 mmHg. The first large increase in gene expression occurred with Mesp1 and Mesp2, cardiac mesoderm markers [140], being a factor of 2 higher at 36 and 7 mmHg compared to 142 mmHg for Mesp1 and a factor of 3 and 2 higher at 36 and 7 mmHg, respectively, compared to 142 mmHg for Mesp2 on day 5.

Because of the large increase in Mesp1 and Mesp2 expression at low pO_{2gas}, we focused on differentiation to cardiomyocytes. Differentiation at 7 mmHg resulted in a delay in the expression of Tbx20, Tbx5, Nkx2.5, Mef2c, Foxh1, cardiac-α-Actin, cTnT, and Titin, cardiac markers [141-145], compared to 142 mmHg. Differentiation at 36 mmHg only delayed Foxh1 expression. After days 7-8, expression was higher at most time points at 7 compared to 142 mmHg for Tbx20, Tbx5, Nkx2.5, Mef2c, and Foxh1, and after day 9 for cardiac-α-Actin, cTnT, and Titin. Expression at 36 mmHg for most times was lower than 7 and the same or higher than 142 mmHg.

Differentiating T-GFP and J1 mESC at various constant pO_{2gas} delayed the appearance of large numbers of T-GFP+ and MF-20+ cells and increased the generation of MF-20+ cells (Figure 4). Maximal fraction of T-GFP+ cells occurred on days 4, 5, and 6 at 142, 36, and 7 mmHg, respectively but was approximately 70% at all pO_{2gas} (Figure 4A). The appearance of MF-20+ cells from J1 mESC was delayed by 2 days with differentiation at 7 compared to 142 mmHg (Figure 4B). By day 8 and later, the fraction of MF-20+ cells was higher at 36 and 7 compared to 142 mmHg. The maximal fraction of MF-20+ cells was 12, 18, and 31%, which occurred on days 7, 9, and 11, at 142, 36, and 7 mmHg, respectively. Up to day 9, total cell number was the same for most time points between 7 and 142 mmHg and higher at 36 mmHg (Figure 4C). After day 9, total cell number was approximately the same between 36 and 7 mmHg, both of which had a substantially higher cell number than 7 mmHg. Differentiation at 36 and 7 mmHg resulted in more MF-20+ cells than 142 mmHg (Figure 4D). A steady-state number of MF-20+ cells was reached by day 7 for 142 mmHg and day 8 for 36 and 7 mmHg, after which the number of MF-20+ cells was the same for most times for 36 and 7 mmHg. Differentiation at low pO_{2gas} produced 2-3x more MF-20+ cells compared to high pO_{2gas}.

We further focused our investigation on differentiation to cardiomyocytes with the addition of ascorbic acid, which has been shown to increase differentiation of mESC to cardiomyocytes [74]. Differentiating J1 mESC at various, constant pO_{2gas} for 11 days with 0.2 mM ascorbic acid resulted in a large increase in the

fraction of MF-20+ cells with decreasing values of pO_{2gas} that was reproducibly observed in 7 additional independent experimental runs (Figure 5A). The highest number fraction of MF-20+ cells was 31% with a pO_{2gas} of 7 mmHg, compared to 23% and 9% at 36 and 142 mmHg, respectively. Culture at 7 mmHg resulted in a substantial decrease in total cell number relative to 36 and 142 mmHg, respectively, both of which had comparable cell numbers (Figure 5B). As a result, the number of MF-20+ cells was higher at 36 mmHg by a factor of 2.3 and 2.9 compared to 142 and 7 mmHg, respectively, resulting in 55 MF-20+ cells being generated per initial mESC at 36 mmHg, compared to 24 and 28 at 142 and 7 mmHg, respectively (Figure 5C). Variations of this protocol without ascorbic acid, without serum-free media, with different initial cell densities in the hanging drops, and with different time periods in hanging drop also showed an enhancement in cardiomyogenesis at low compared to high pO_{2gas} (data not shown). The inclusion of ascorbic acid increased the mean fraction and number of MF-20+ cells by a factor of 2.1 and 2.4, respectively, for 142 mmHg, 1.2 and 1.3, respectively for 36 mmHg, and had no effect on 7 mmHg compared to day 11 data on Figure 4D, albeit these increases were not statistically significant. The expression of the cardiac marker genes cTnT, Mef2c, and Nkx2.5 were also higher at low compared to high pO_{2gas} (Figures 5D-F). Low pO_2-differentiated mESC immunostained positive for cTnT, which were striated, demonstrating sarcomeric organized (Figure 5G), and for Nkx2.5 (Figure 5H).

3.4.5. Verification of cardiomyocyte assessment methodology

We compared MF-20 immunostaining of histological sections, counting with flow cytometry, immunostaining of cTnT on histological sections, and the area covered with spontaneously contracting cells in each well to further assess mESC-derived cardiomyocytes (Figure 6). Immunostaining of serial sections with MF-20 and anti-cTnT antibodies showed excellent co-localization in all examined sections (Figure 6A). The fraction of MF-20+ cells assessed with histology and flow cytometry data correlated highly, with a correlation coefficient of 0.7 (Figure 6B). There was also a strong correlation (correlation coefficient of 0.8) between the number of MF-20+ cells assessed with flow cytometry and the area covered by spontaneously contracting cells (Figure 6C).

3.4.6. pO_{2cell} of cardiomyocytes after differentiation

We used MF-20-immunostained histological sections to estimate pO_{2cell} of MF-20+ cells within cellular aggregates after 11 days of differentiation with 0.2 mM ascorbic acid of J1 mESC (Figure 7). With histological examination, mESC differentiated at 7 mmHg preferentially formed thin cell sheets and smaller aggregates than were found at 36 or 142 mmHg (Figure 7A), with 90 ± 7%, 75 ± 9%, 53 ± 6% of the tissue volume being present in aggregate regions at 142, 36, and 7 mmHg, respectively. MF-20+ cells were found together in clusters at all pO_{2gas}.

We previously reported a theoretical model of oxygen consumption and diffusion to estimate the volumetric distribution of pO_{2cell} within aggregations after 11 days of differentiation [53]. Combining these results with immunostaining showing the location of MF-20+ cells (Figure 7A), we calculated the pO_{2cell} of the MF-20+ cells. Even though silicone rubber dishes were used in this study, oxygen gradients still existed within the aggregates. A comparison of the volumetric distribution of pO_{2cell} of all of the tissue and that of MF-20+ cells at 142 mmHg is shown in Figure 7B. This analysis only considered the aggregate regions (90% of the total tissue volume), since no MF-20+ cells were observed in sheet-like areas at any pO_{2gas}. MF-20+ cells represented approximately 10% of the total aggregate volume and were preferentially located in regions of moderately low pO_{2cell} (20 – 30 mmHg), with relatively fewer cardiomyocytes at high and low pO_{2cell} extremes.

3.4.7. Effect of temporal variation of pO_{2gas} on differentiation of mESC to cardiomyocytes

The effects of differentiating J1 mESC at 142 and 7 mmHg pO_{2gas} for different time periods in different orders on the fraction of MF-20+ cells, total cell number, and number of MF-20+ cells after 10 days total is shown in Figure 8. The fraction of cardiomyocytes was greater when the cells were initially started at 7 mmHg. Increased cardiomyocyte fraction was observed if days 0-6 were carried out at 7 mmHg and was not affected by increasing pO_{2gas} to 142 mmHg after day 6.

Changing pO_{2gas} from 142 to 7 mmHg after day 2 did not increase the cardiomyocyte fraction. The total cell number was greatest for cultures in which the pO_{2gas} at days 6-10 was 142 mmHg, regardless of the pO_{2gas} used prior to day 6. Therefore, the total number of cardiomyocytes present at day 10 was highest if the pO_{2gas} was 7 mmHg during the first 6 days of culture and then increased to 142 mmHg for the final 4 days. Using these pO_{2gas} conditions, 35% of cells were MF-20+ and 60 MF-20+ cells were generated for each initial mESC, both of which represent a 3x increase relative to constant culture at 142 mmHg. The mean total MF-20+ number in this case was slightly higher than that obtained using constant culture at a pO_{2gas} of 36 mmHg in the same experiments, but the difference was not statistically significant.

For cultures started at 7 mmHg, the increase in cardiomyocyte and total cell number that occurred during days 6-10 at 142 mmHg was accompanied by significant morphological changes (data not shown). The cells that were in sheet-like and small aggregate structures on day 6 proliferated and migrated to form large aggregates similar in size to those present for cultures maintained at 142 mmHg for all 10 days. These aggregates contracted vigorously and contained numerous cardiomyocytes.

3.4.8. Low pO_2 differentiation of HIF-1$\alpha^{-/-}$ mESC does not increase yield of cardiomyocytes

HIF-1$\alpha^{-/-}$ mESC were differentiated at various, constant pO_{2gas} to assess the necessity of HIF-1α in the low pO_2-mediated increase in cardiomyocytes (Figure 9). Expression of Mesp1 and Mesp2 was delayed at 36 and 7 mmHg compared to 142 mmHg (Figure 9A-B) with HIF-1$\alpha^{-/-}$ mESC, similar to J1 mESC (Figure 3). However, maximal expression, which occurred on day 4 for 142 and day 5 for 36 and 7 mmHg for both genes, was the same at all pO_{2gas} for HIF-1$\alpha^{-/-}$ mESC (Figure 9A-B), contrasting with J1 mESC, which had markedly enhanced expression at low compared to high pO_{2gas} (Figure 3). By day 11, spontaneously-contracting cells were observed with HIF-1$\alpha^{-/-}$ mESC at all pO_{2gas}. However, the number and fraction were the same at all pO_{2gas}, averaging 17 MF-20+ cells per original HIF-1$\alpha^{-/-}$ mESC and 8% of the final population, similar to the low values obtained with J1 mESC differentiated at 142 mmHg (Figure 4B and D).

3.4.9. Low pO_2 increases differentiation of hESC to cardiomyocytes

We extended our study to investigate the effects of pO_2 on differentiation of hESC to cardiomyocytes by differentiating CyT49 hESC for 21 days at constant 142, 36, or 7 mmHg pO_{2gas} (Figure 10). The gene expression of cTNT, MEF2C, and NKX2.5, measured with real-time PCR, was higher at 36 and 7 compared to 142 mmHg (Figure 10A-C). The average increase in cTNT, MEF2C, and NKX2.5

expression from 142 to 7 mmHg was similar between hESC and mESC but from 142 to 36 mmHg was higher with hESC compared to mESC (Figure 5D-F). More hESC-derived cTNT+ cells were observed with microscopy at low compared to high pO_{2gas} (Figure 10D-E). However, with this protocol, the fraction of cTNT+ cells was less than 1%, assessed with visual observation, at all pO_{2gas}, and we were unable to accurate quantitate the number with flow cytometry. A small amount of spontaneously-beating cells were also observed at 7 mmHg, but none were observed at 142 or 36 mmHg.

3.4.10. Low pO_2 increases differentiation of miPSC to cardiomyocytes

We extended our study to investigate the effects of pO_2 on differentiation of miPSC to cardiomyocytes. Differentiating miPSC at various, constant pO_{2gas} for 11 days with 0.2 mM ascorbic acid resulted in a large increase in the fraction of MF-20+ cells at low compared to high pO_{2gas} (Figure 11A). The highest fraction of MF-20+ cells was 11% with a pO_{2gas} of 36 and 7 mmHg, compared to 142 mmHg, values which were 2-3 times lower than J1 mESC (Figure 5A). Culture at 36 and 7 mmHg resulted in a substantial increase in total cell number relative to 142 mmHg (Figure 11B), unlike J1 mESC, which had the opposite trend (Figure 5B). As a result, the number of MF-20+ cells was highest at 7 mmHg by a factor of 5.2 and 1.4 compared to 142 and 36 mmHg, respectively, resulting in 34 MF-20+ cells being produced per each initial miPSC at 7 mmHg, compared to 25 and 7 at 36 and 142 mmHg, respectively (Figure 11C). The number of MF-20+ cells was higher at 142 and 36 mmHg and lower for 7 mmHg with J1 mESC compared to

miPSC (Figure 5C). The expression of the cardiac marker genes cTnT, Mef2c, and Nkx2.5 were also higher at low compared to high pO_{2gas} (Figures 11D-F). Low pO_2-differentiated miPSC immunostained positive for cTnT and Nkx2.5 (Figure 11G-H).

3.5. Discussion

We studied the effects of pO_2 on mESC differentiation to the three germ layers and mESC, miPSC, and hESC differentiation to cardiomyocytes. Throughout our studies, we used highly oxygen-permeable silicone rubber dishes to set pO_{2cell} at the membrane-cell interface. Real-time PCR was used to measure relative gene expression of cardiomyocyte and germ layer markers, and immunocytochemistry was used to verify the presence of marker protein. Flow cytometry was used to measure the fraction and number of Nestin+, T-GFP+, and MF-20+ cells. Histological analysis was used to quantitatively verify MF-20 staining and quantification with flow cytometry and to provide geometric measurements for estimations of pO_{2cell} with finite element simulations. Temporal variations in pO_{2gas} were performed to determine the time period over which a low pO_{2cell} was required to promote cardiomyocyte differentiation and to further increase MF-20+ cell fraction and number.

Low pO_2 during differentiation of mESC changed the timing and magnitude of temporal gene expression for most markers of all three germ layers. Overall, we

observed higher gene expression of endodermal genes (Figure 1), lower expression of ectodermal genes (Figure 2), and approximately the same expression of mesodermal genes at low compared to high pO_{2gas} (Figure 3-4). To our knowledge, there have been no previous reports on the effects of pO_2 on differentiation to early endoderm, although high pO_2 has been shown to affect later stages of pancreatic development [54]. Our protocol was not designed to produce large amounts of endodermal cells, so further investigating low pO_2 with a better protocol is of interest. Low pO_2 has been previously reported to affect different stages of ectodermal differentiation differently, with differentiation of PSC to neural stem cells (NSC) being reduced at low pO_2 while differentiation of NSC to neurons being enhanced [2]. pO_2 has been previously implicated in changing the timing and magnitude of the expression of the mesodermal marker Brachyury T, but this has not been shown statistically [146].

We demonstrated that control of pO_2 can result in a factor of 3 increase in cardiomyocyte fraction and number from mESC above levels typically obtained at 142 mmHg without purification (Figure 8). The best protocol reported in this study involved the addition of ascorbic acid and removal of serum after 5 days of culture. Nonetheless, the positive effect that low pO_2 culture had on mESC differentiation into cardiomyocytes was found using several variations in the differentiation protocol, such as with or without ascorbic acid or serum removal, and with miPSC and hESC, suggesting the benefits of low pO_2 are broadly applicable and not simply the artifact of using a specific differentiation protocol.

Previous studies have investigated the effects of low pO_2 on differentiation of PSC to cardiomyocytes in bioreactors. Bauwens et al. [48] reported no significant difference between 4% and 20% oxygen from mESC, likely due to the low cardiomyocyte yields without genetic selection. Only after combining low pO_2 with genetic selection to purify cardiomyocytes, 3.8 cardiomyocytes were generated per input mESC at 4% oxygen, a factor of 1.5 higher than 20% oxygen with genetic selection. This low oxygen result is a factor of 16 lower than what we achieved with our temporal modulations in pO_{2gas} protocol (Figure 8). We likely were able to achieve higher yields because our protocol consistently obtained a cardiomyocyte fraction of 5-10% from mESC at 142 mmHg, comparable to other optimized differentiation protocols [118, 147, 148], which allows for easier measurement of the effects of pO_2. Additionally, with hESC, 4% oxygen has reported to increase the expression of some cardiac markers and the total cell number compared to 20% oxygen. However, the fraction of beating EBs is the same between 20% and 4% and no information on fraction or number of cardiomyocytes was reported [49].

The mechanism by which oxygen exerted its effects in our experiments is not known. The oxygen-sensitive transcription factor HIF-1 is active in wild type PSC cultured at low pO_2 [149] and is seen in hypoxic regions of the developing chick heart [150]. We demonstrated that differentiation of HIF-1$\alpha^{-/-}$ mESC to cardiomyocytes was insensitive to pO_2 (Figure 9). HIF-1 targets hypoxic

responsive elements within the promoter regions of and increases expression of the cardiac-associated transcription factors Mef2c and Tbx5 and the sarcomere organization protein Titin [46]. HIF-1 stabilization and activity at low pO_2 therefore seems likely to be responsible for at least some of the effects observed in our experiments.

Oxygen exerted its strongest effects on cardiomyocyte differentiation during the first 6 days (Figure 8), the time period that immediately precedes the emergence of the first spontaneously-contracting and MF-20+ cells and coincides with increases Mesp1 and Mesp2 expression. Thus, we infer that pO_2 affected differentiation into cardiomyocyte progenitor cells and/or induced an increase in proliferation of such progenitor cells relative to other cells types. The increase in total cardiomyocyte number suggests a direct positive effect of reduced oxygen on differentiation or proliferation along the cardiomyocyte lineage, but the exact mechanism and cell types through which this process is occurring is not yet known. After the appearance of cardiomyocytes, high pO_{2gas} caused a higher total cell number, presumably by minimizing the oxygen or other nutrient limitations as the cell number increased.

The use of silicone rubber culture dishes to control pO_{2cell} at the membrane-cell interface was crucial for the success of our experiments. We previously reported that simply differentiating mESC on oxygen-impermeable polystyrene dishes at low pO_{2gas} does not result in more cardiomyocytes compared to high pO_{2gas} [53].

Furthermore, when polystyrene and silicone rubber dishes were compared directly, the highest cardiomyocyte fraction and number occurred with differentiation at low pO_{2gas} on silicone rubber dishes. Without control or understanding of pO_{2cell}, new important knowledge may remain hidden and apparent inconsistencies between published studies may arise [2].

Even though the cells were cultured on oxygen-permeable silicone rubber, differentiating cells preferentially formed aggregates that contained pO_2 gradients (Figure 7) [53]. The size of the aggregates was smaller with decreasing pO_{2gas} values, which may have been due to limitations on oxygen and nutrient availability, especially given that cells initially cultured at 7 mmHg would form large aggregates within 4 days of transfer to 142 mmHg (data no shown). MF-20+ cells were exclusively present in aggregates and preferentially occupied regions of moderately low local pO_2 after 11 days of differentiation at 142 mmHg (Figure 7B). However, the pO_{2cell} during differentiation (before day 11) of these cells is unknown. Oxygen gradients were large within day-11 aggregates but are certainly smaller during the first 6 days of differentiation, since the aggregates are smaller. Experiments investigating histological sections from earlier times during differentiation immunostained with antibodies to markers of cardiomyocyte progenitor cells would be worthwhile to further explore whether cardiomyocytes preferentially form in regions within a certain range of pO_{2cell}.

Our work shows that pO_{2cell} profoundly affects differentiation of PSC into cardiomyocytes and the three germ layers, which has major ramifications. One potential application of PSC is to better understand development and disease, and this work suggests that controlling pO_2 to levels experienced by the developing embryo is necessary to accurately explore this. The markedly increased yield of cardiomyocytes may enhance prospects for their therapeutic use in treating heart disease. Control of dissolved oxygen is inexpensive compared to growth factors and small molecules and can be accomplished with current technology, making our results applicable to commercial development. Reduced pO_2 culture combined with other proteins and small molecules may further enhance differentiation to cardiomyocytes and other desired cell types. Because the cells in the early embryo are exposed to pO_{2cell} that lie within the range that we observed largest effects on differentiation, pO_{2cell} may play a more important role in early embryonic development than heretofore appreciated.

3.6. Figures

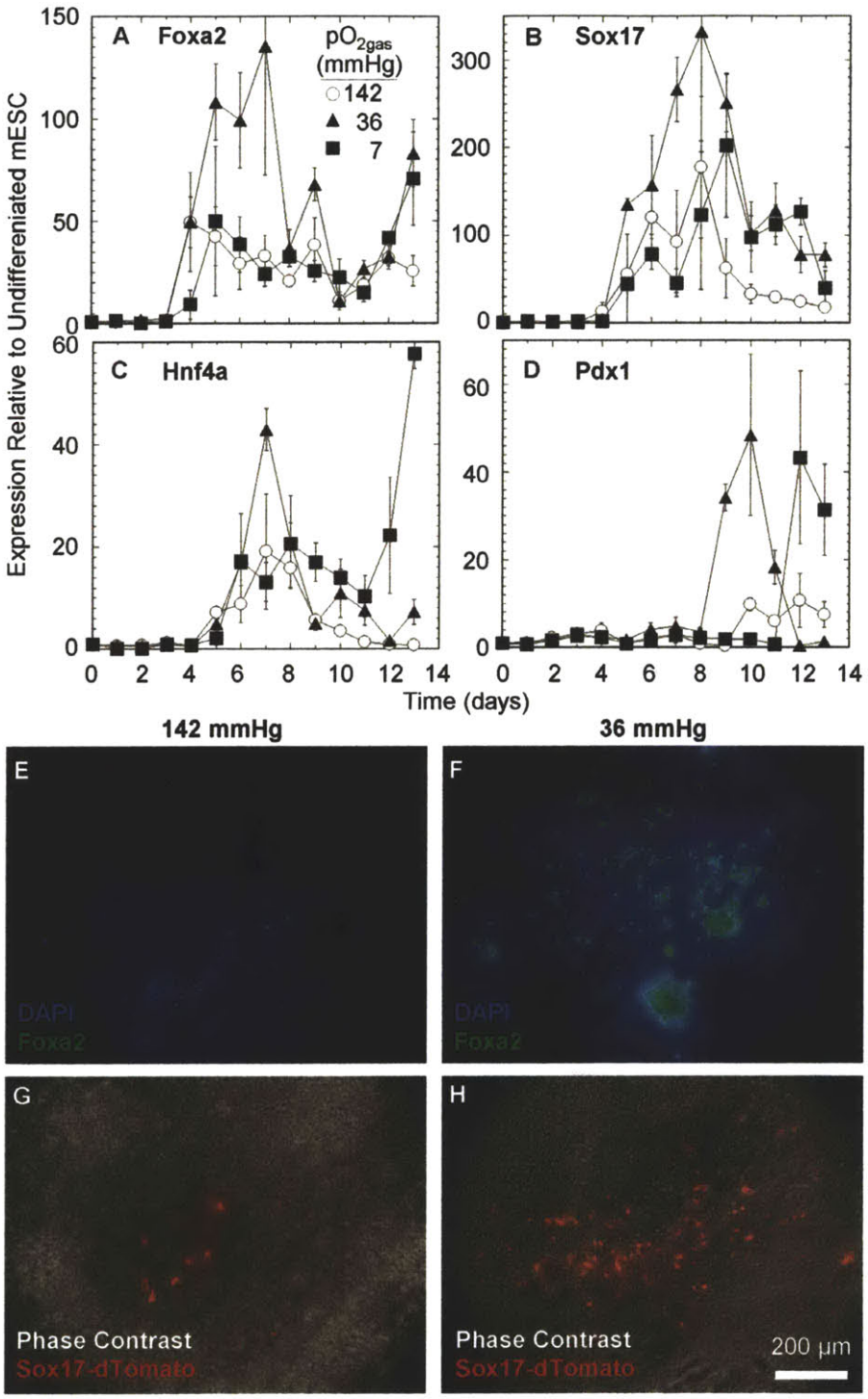

Figure 3-1. pO_2 affects differentiation to the endodermal lineage.

J1 mESC were differentiated for up to 13 days at 142, 36, or 7 mmHg pO_{2gas} without ascorbic acid. (A-D) Temporal gene expression of Foxa2, Sox17, Hnf4a,

and Pdx1 acquired with real-time PCR (n=3). (E-F) En face fluorescence images of mESC after 6 days of differentiation at 142 (E) or 36 (F) mmHg stained with DAPI (blue) and against Foxa2 (green). (G-H) En face phase contrast images of Sox17-dTomato mESC after 6 days of differentiation at 142 (G) or 36 (H) mmHg with respective Sox17-dTomato (red) fluorescence images superimposed.

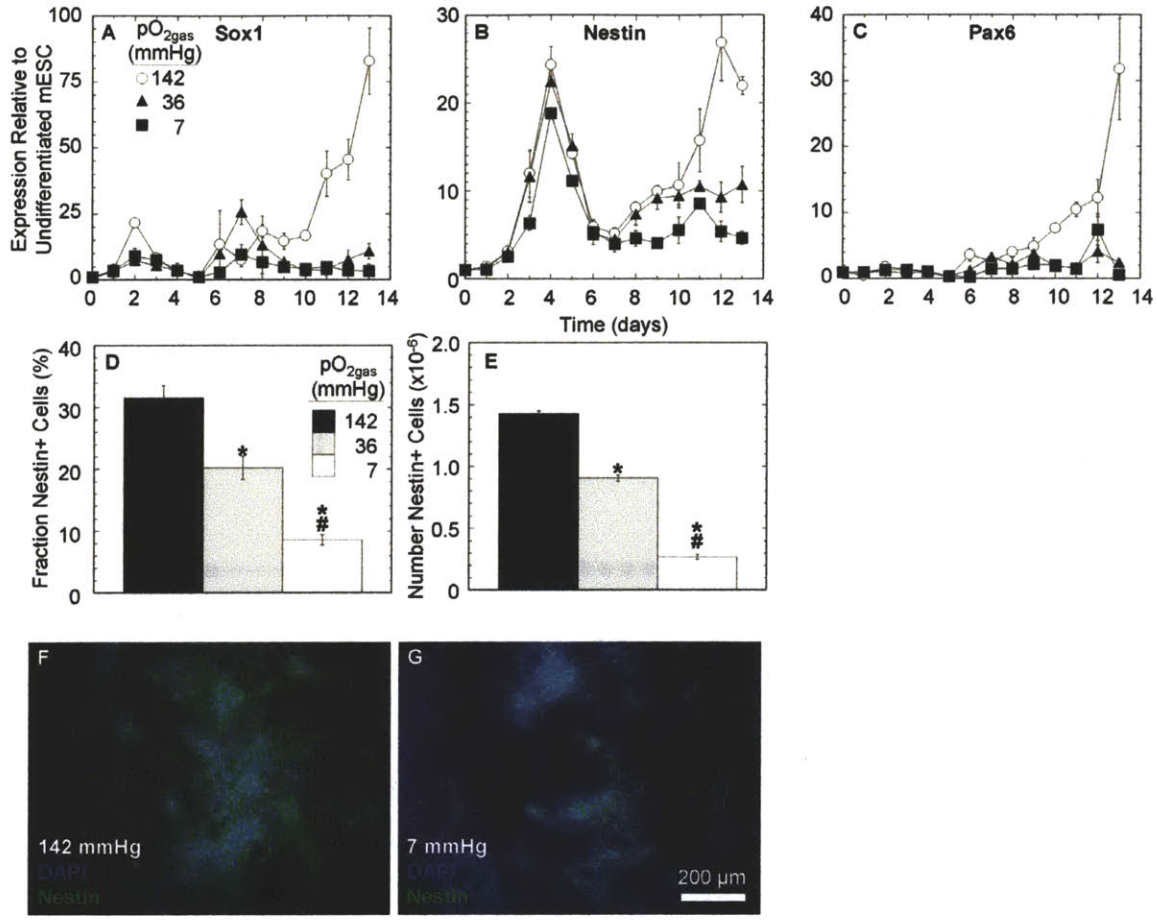

Figure 3-2. pO_2 affects differentiation to the ectodermal lineage.

J1 mESC were differentiated for up to 13 days at 142, 36, or 7 mmHg pO_{2gas} without ascorbic acid. (A-C) Temporal gene expression of Sox1, Nestin, and Pax6 acquired with real-time PCR (n=3). (D-E) Number and fraction of Nestin+ cells after 12 days of differentiation acquired with flow cytometry (n=3). (F-G) En face fluorescence images of mESC after 10 days of differentiation at 142 (F) or 7 (G) mmHg stained with DAPI (blue) or against Nestin (green). * indicates statistical difference ($p<0.05$) compared to 142 mmHg (black bar), and # indicates statistical difference compared to 36 mmHg (grey bar).

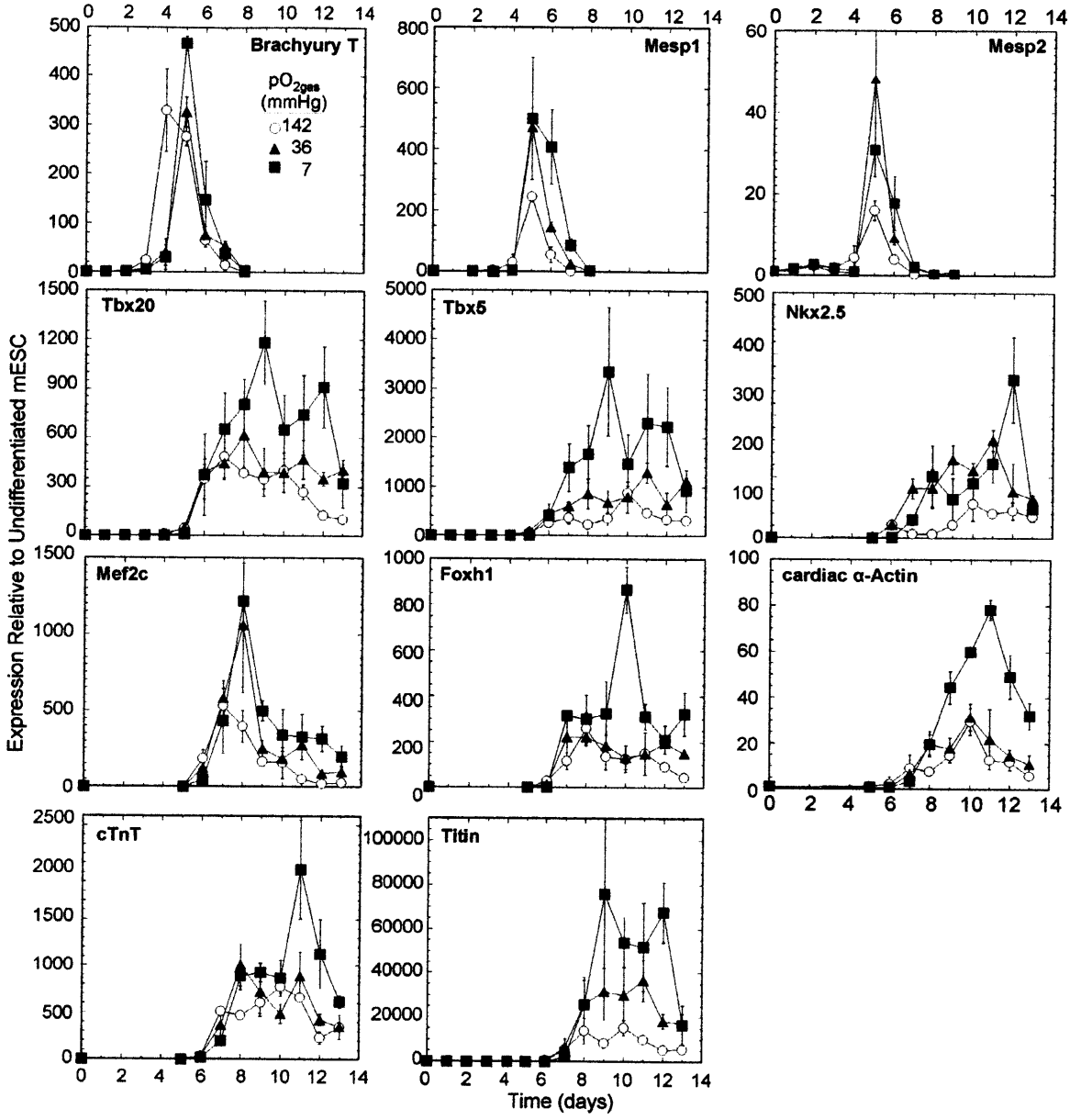

Figure 3-3. Temporal gene expression of the mesodermal and cardiac lineage markers Brachyury T, Mesp1, Mesp2, Tbx20, Tbx5, Nkx2.5, Mef2c, Foxh1, cardiac α-Actin, cTnT, and Titin for J1 mESCs differentiated for up to 13 days at 142, 36, or 7 mmHg pO_{2gas} without ascorbic acid.

All data acquired with real-time PCR (n=3).

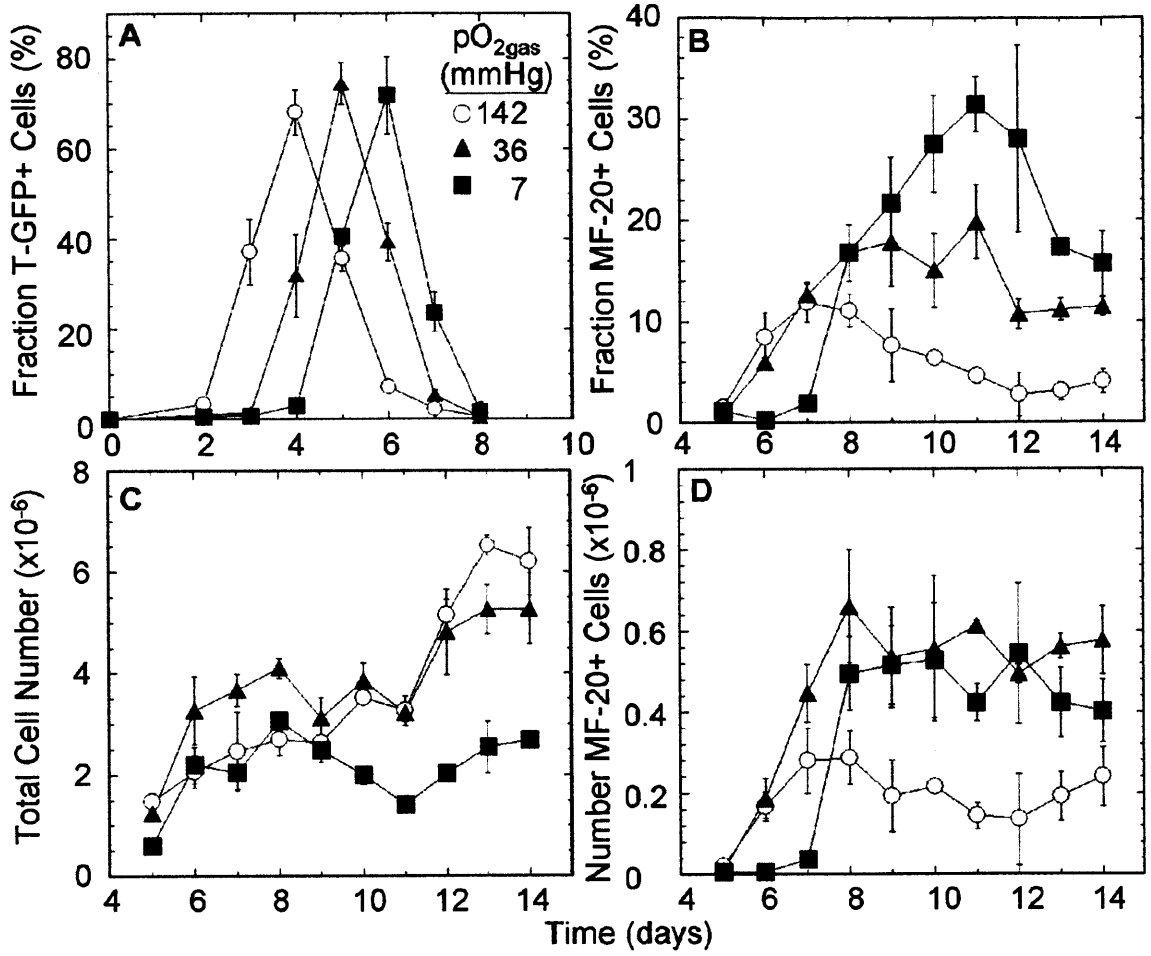

Figure 3-4. The temporal appearance of mesodermal cells and cardiomyocytes at various pO_{2gas}.

mESC were differentiated for up to 13 days at 142, 36, or 7 mmHg pO_{2gas} without ascorbic acid. (A) Fraction of T-GFP+ cells from T-GFP mESC acquired with flow cytometry (n=3). (B) Fraction of MF-20+ cells from J1 mESC acquired with flow cytometry (n=3). (C) The total cell number per well from J1 mESC acquired with nuclei counts (n=3). (D) The number of MF-20+ cells from J1 mESC calculated by multiplying the fraction of MF-20+ cells (B) and the total cell number (C) (n=3).

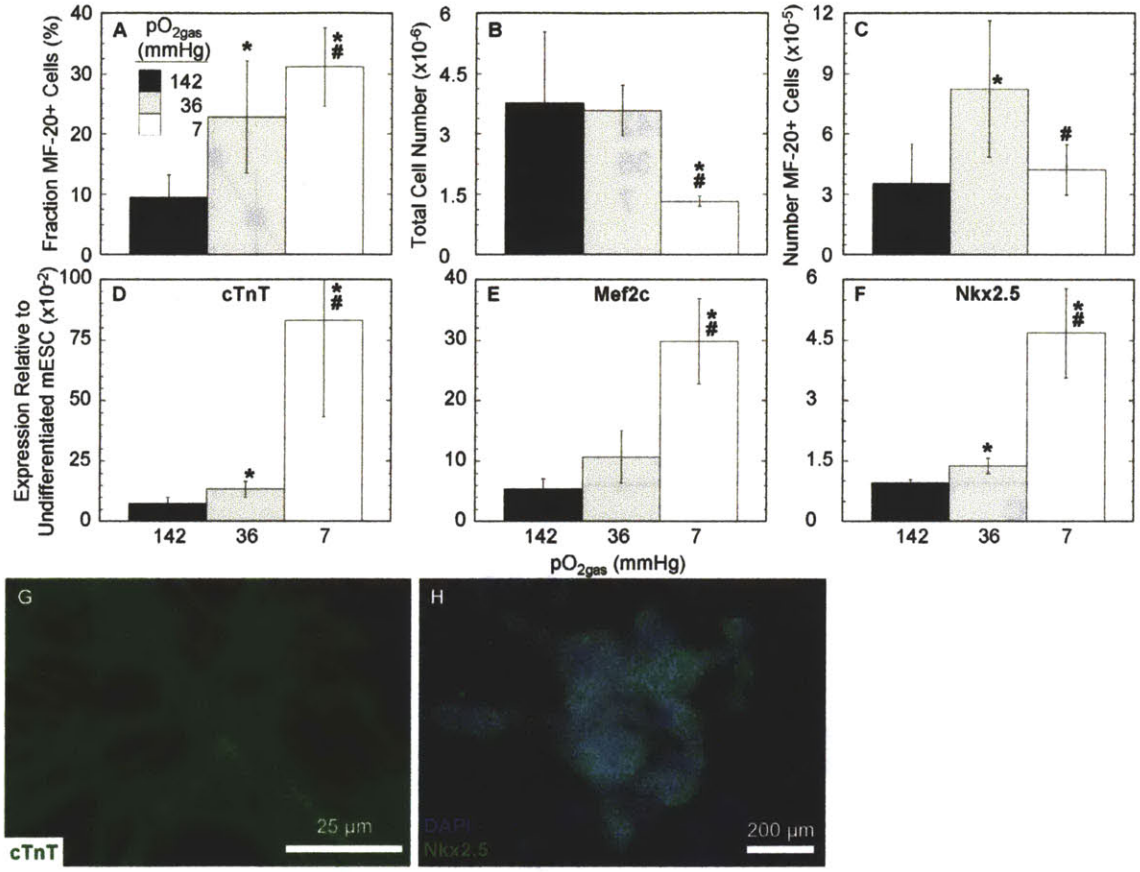

Figure 3-5. Low pO_2 increases mESC differentiation to cardiomyocytes. J1 mESC were differentiated 11 days culture at 142, 36, or 7 mmHg pO_{2gas} with ascorbic acid. (A) Fraction of MF-20+ cells from mESC acquired with flow cytometry (n=7). (B) The total cell number per well from mESC acquired with nuclei counts (n=7). (C) The number of MF-20+ cells from mESC calculated by multiplying the fraction of MF-20+ cells (A) and the total cell number (B) (n=7). (D-F) Gene expression of Nkx2.5, Mef2c, and cTnT acquired with real-time PCR for (n=4). (G-H) En face fluorescence images of mESC differentiated at 7 mmHg pO_{2gas} and stained against cTnT (green) and with DAPI (blue) and against Nkx2.5 (green). * indicates statistical difference ($p<0.05$) compared to 142 mmHg

(black bar), and # indicates statistical difference compared to 36 mmHg (grey bar).

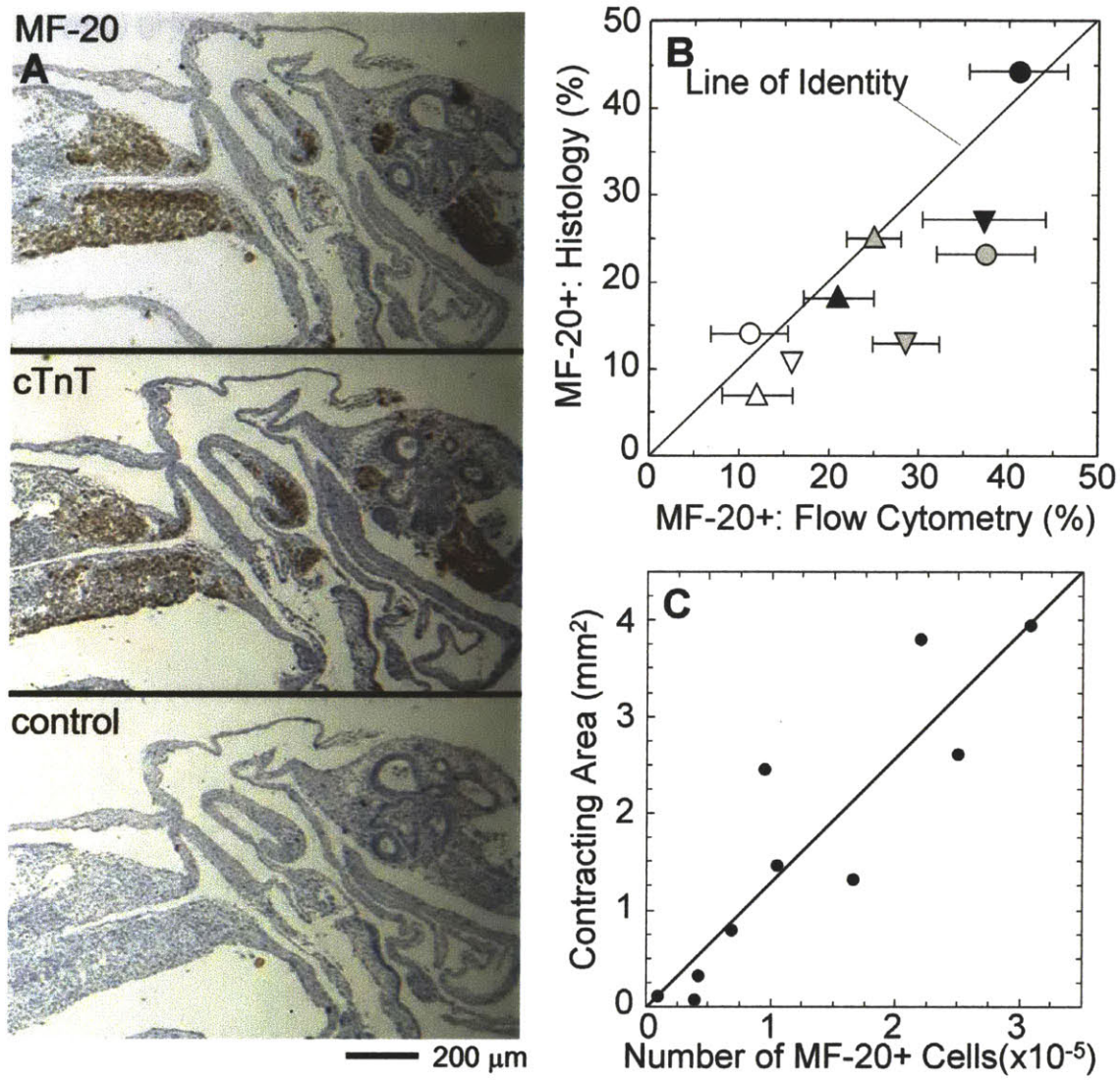

Figure 3-6. Comparison of different cardiomyocyte assessment methodologies. (A) Consecutive 5-μm tissue sections of J1 cells differentiated 11 days at 36 mmHg with ascorbic acid immunostained with a primary antibody to sarcomeric myosin heavy chain (MF-20 - top), cardiac troponin T (cTnT – middle), or no primary antibody (control – bottom). (B) Comparison of the fraction of MF-20+ cells counted from stained 5-μm sections to that measured with flow cytometry of trypsin dispersed cells. Open, gray filled, and black filled symbols represent samples taken from pO_{2gas} of 142, 36, and 7 mmHg, respectively, and each

shape (circle, triangle, upside-down triangle) represents an independent experimental run. Results for flow cytometry are the mean ± standard deviation (n=3), while the histological results are from a single section that was obtained in each experiment and pO_{2gas}. (C) Comparison between the total number of MF-20+ cells counted using flow cytometry and the total surface area of the culture dish covered with spontaneously contracting cells estimated visually. The fraction of MF-20+ cells ranged from 3 to 36% in these samples. The best-fit line was determined using linear regression, $R^2 = 0.80$.

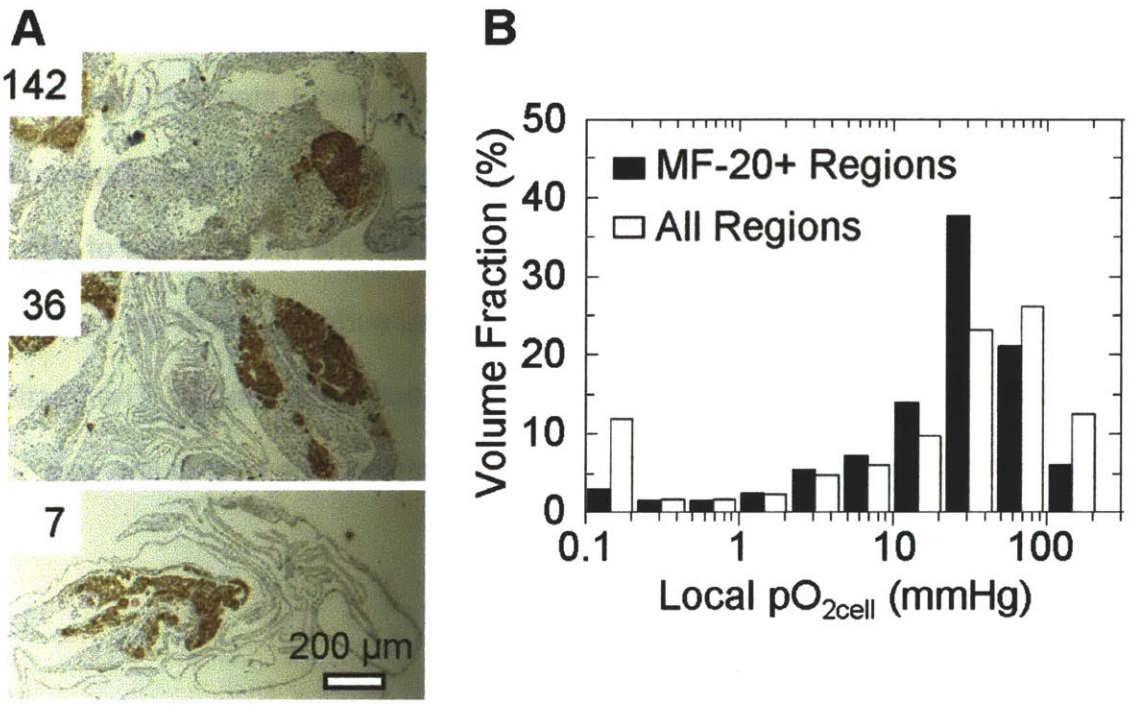

Figure 3-7. Modeling of the volumetric distribution of pO_2 within MF-20+ and all regions.

(A) Representative images of 5-μm tissue sections of J1 cells immunostained with MF-20 (brown) and counter stained with hematoxylin. (B) Volumetric distribution of pO_{2cell} values in MF-20+ regions at 142 mmHg. Filled bars represent the distribution of pO_{2cell} within MF-20+ regions, and open bars represent the distribution of pO_{2cell} in the entire volume of aggregates in the culture dish (including MF-20+ regions).

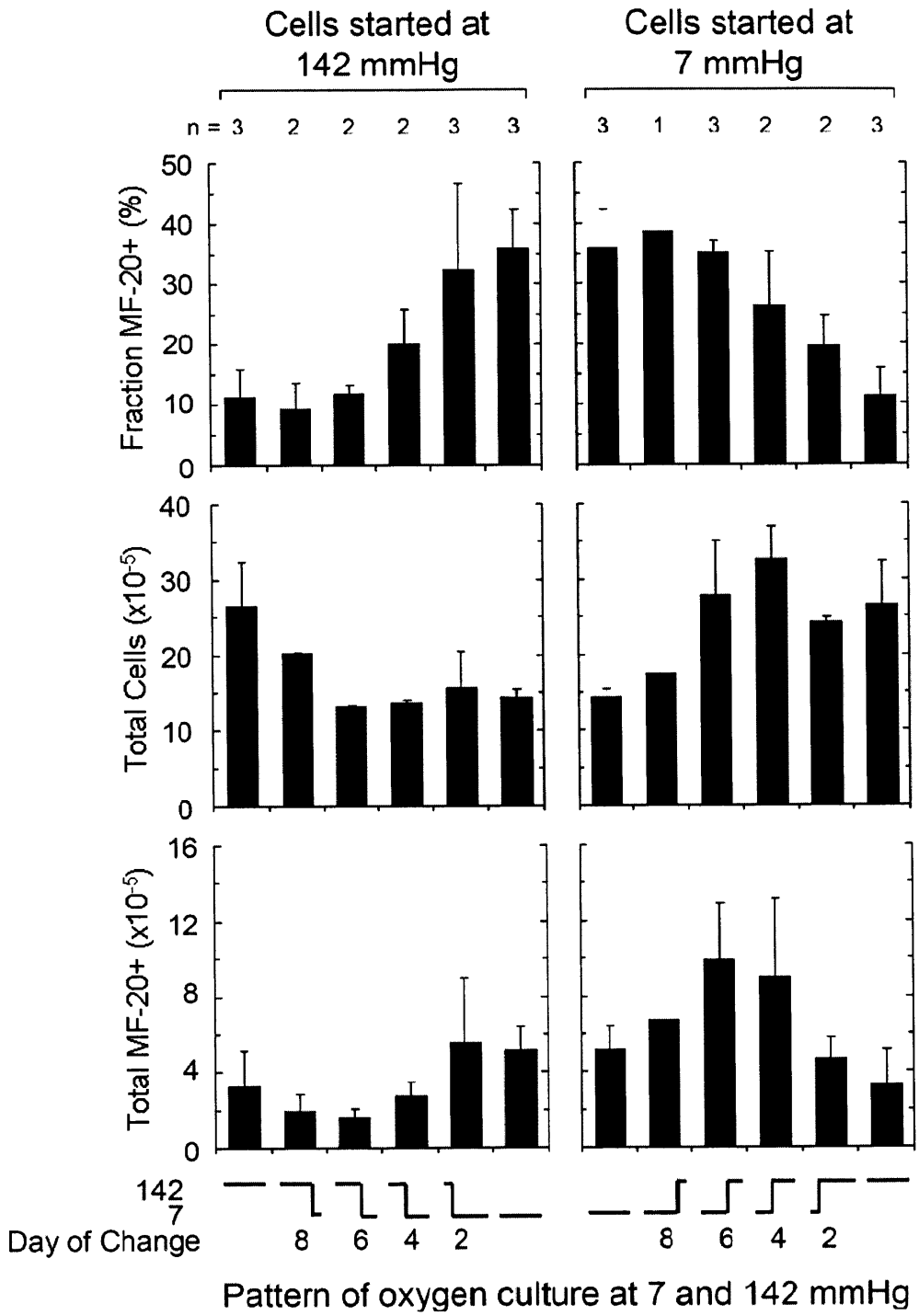

Figure 3- 8. Temporal modulation of pO_{2gas} affects differentiation to cardiomyocytes.

J1 mESC were differentiated with ascorbic acid starting at either 142 or 7 mmHg and then switched to the other condition on day 2, 4, 6, or 8 for a total of 10 days.

Fraction MF-20+, total cell number, and number of MF-20+ cells assessed with flow cytometry after 10 days of differentiation are shown (n as shown at the top of each). The 10 different pO_{2gas} histories and day of the pO_{2gas} change are shown schematically on the x-axis.

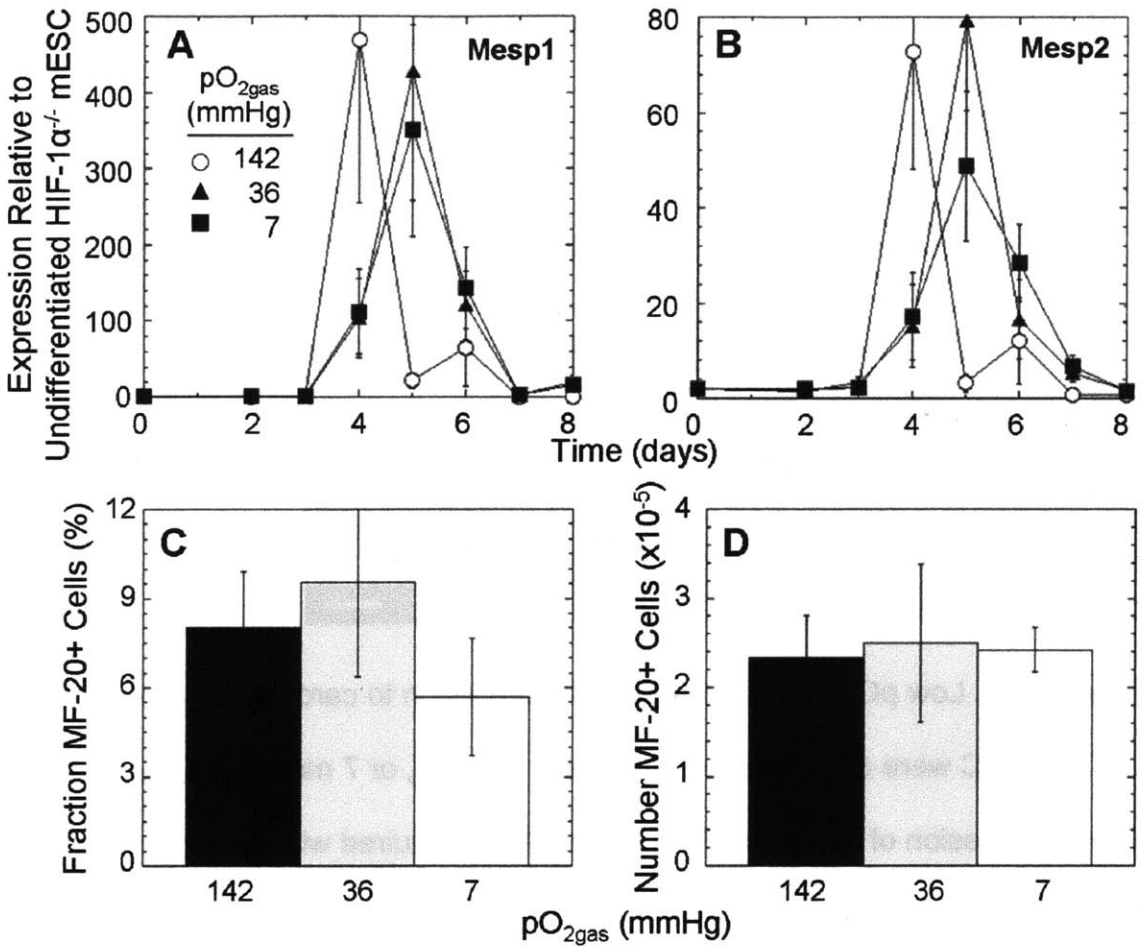

Figure 3-9. HIF-1α is necessary for low pO_2-enhancement of cardiomyocyte generation.

HIF-1$\alpha^{-/-}$ mESC were differentiated up to 10 days at 142, 36, or 7 mmHg pO_{2gas} without ascorbic acid. (A-B) Time-dependent gene expression of Mesp1 and Mesp2 acquired with real-time PCR (n=3). (C-D) The fraction and number of MF-20+ cells acquried with flow cytometry (n=6).

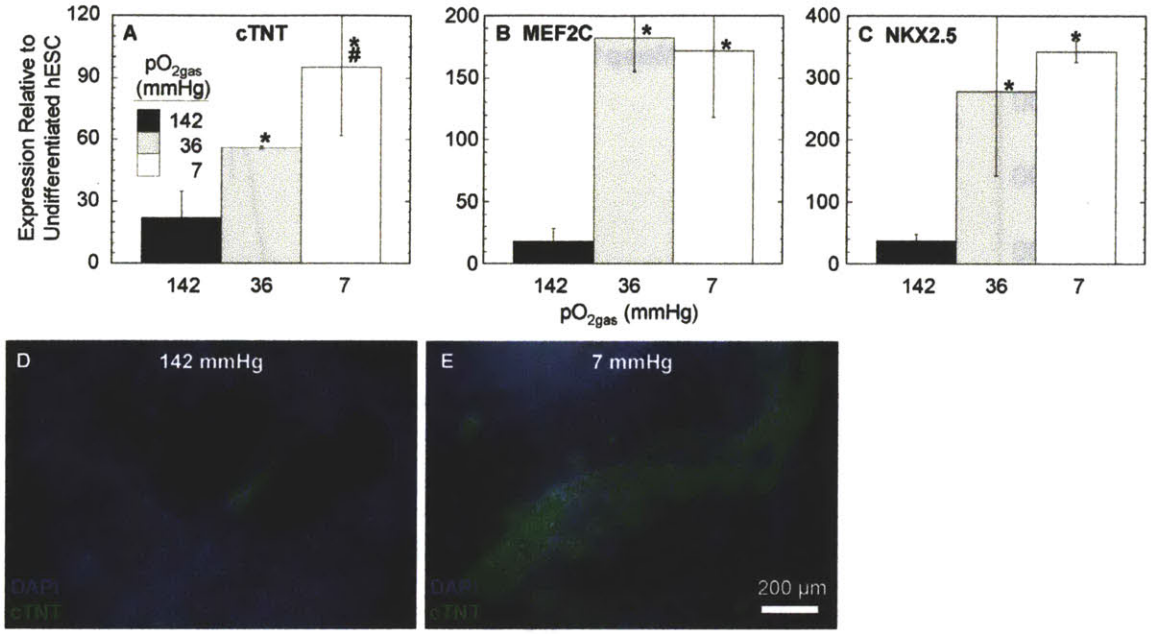

Figure 3-10. Low pO_2 increases hESC differentiation to cardiomyocytes. CyT49 hESC were differentiated 20 days at 142, 36, or 7 mmHg pO_{2gas}. (A-C) Gene expression of cTNT, MEF2c, and NKX2.5 acquired with real-time PCR (n=4). (D-E) En face fluorescence images of hESC differentiated at 142 (D) or 7 (E) mmHg and stained with DAPI and against cTNT. * indicates statistical difference ($p<0.05$) compared to 142 mmHg (black bar), and # indicates statistical difference compared to 36 mmHg (grey bar).

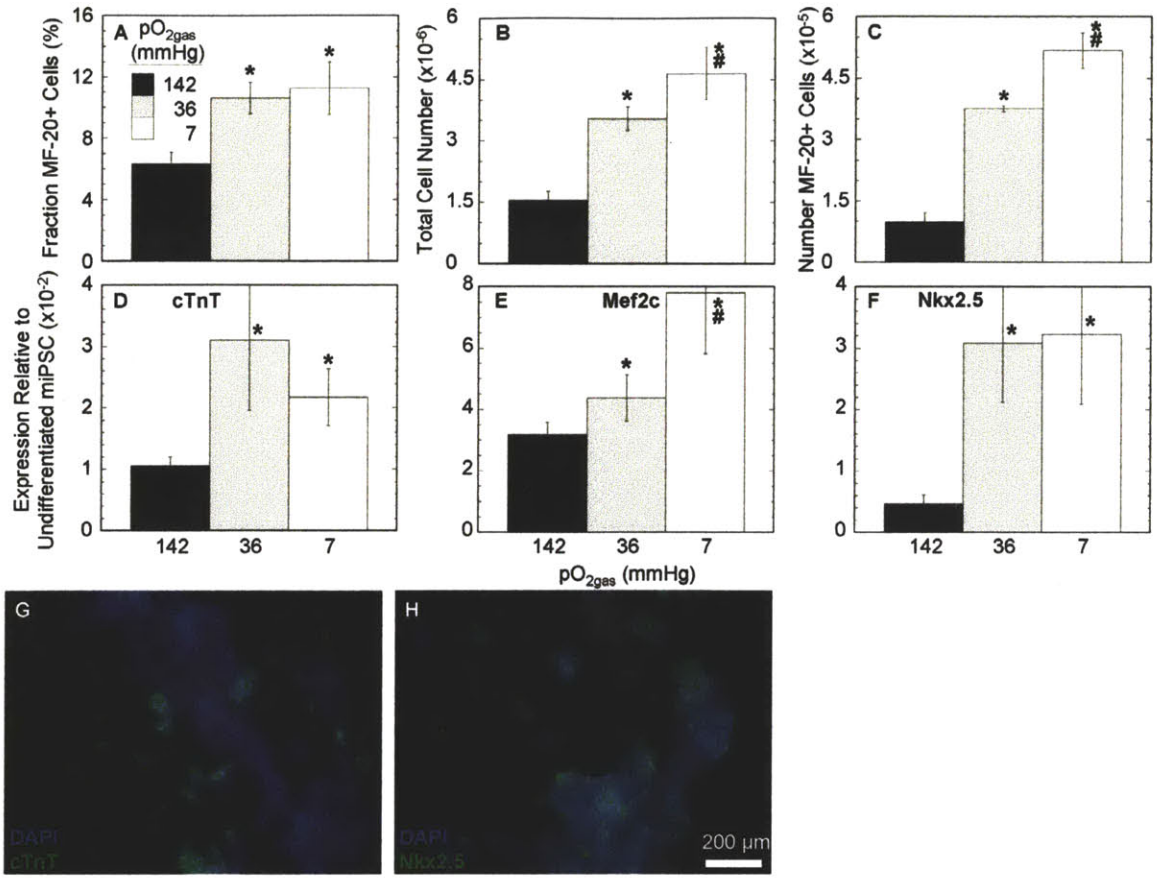

Figure 3-11. Low pO_2 increases miPSC differentiation to cardiomyocytes. miPSC were differentiated 11 days at 142, 36, or 7 mmHg pO_{2gas}. (A) Fraction of MF-20+ cells acquired with flow cytometry (n=4). (B) The total cell number per well acquired with nuclei counts (n=4). (C) The number of MF-20+ cells calculated by multiplying the fraction of MF-20+ cells (A) and the total cell number (B) (n=4). (D-F) Gene expression of cTnT, Mef2c, and Nkx2.5 acquired with real-time PCR for (n=4). (G-H) En face fluorescence images of miPSC differentiated at 7 mmHg pO_{2gas} and stained with DAPI (blue) and against cTnT and Nkx2.5 (green). * indicates statistical difference ($p<0.05$) compared to 142 mmHg (black bar), and # indicates statistical difference compared to 36 mmHg (grey bar).

-Page Intentionally Left Blank-

References

1. Horton, R.E., J.R. Millman, C.K. Colton, and D.T. Auguste, *Engineering microenvironments for embryonic stem cell differentiation to cardiomyocytes.* Regen Med, 2009. **4**(5): p. 721-32.
2. Millman, J.R., J.H. Tan, and C.K. Colton, *The effects of low oxygen on self-renewal and differentiation of embryonic stem cells.* Curr Opin Organ Transplant, 2009. **14**(6): p. 694-700.
3. Daley, G.Q., M.A. Goodell, and E.Y. Snyder, *Realistic prospects for stem cell therapeutics.* Hematology Am Soc Hematol Educ Program, 2003: p. 398-418.
4. Kaufman, D.S., E.T. Hanson, R.L. Lewis, R. Auerbach, and J.A. Thomson, *Hematopoietic colony-forming cells derived from human embryonic stem cells.* Proc Natl Acad Sci U S A, 2001. **98**(19): p. 10716-21.
5. Bonner-Weir, S., M. Taneja, G.C. Weir, K. Tatarkiewicz, K.H. Song, A. Sharma, and J.J. O'Neil, *In vitro cultivation of human islets from expanded ductal tissue.* Proc Natl Acad Sci U S A, 2000. **97**(14): p. 7999-8004.
6. Fukuda, K. and S. Yuasa, *Stem cells as a source of regenerative cardiomyocytes.* Circ Res, 2006. **98**(8): p. 1002-13.
7. Jaenisch, R. and R. Young, *Stem cells, the molecular circuitry of pluripotency and nuclear reprogramming.* Cell, 2008. **132**(4): p. 567-82.
8. Laflamme, M.A., K.Y. Chen, A.V. Naumova, V. Muskheli, J.A. Fugate, S.K. Dupras, H. Reinecke, C. Xu, M. Hassanipour, S. Police, C. O'Sullivan, L. Collins, Y. Chen, E. Minami, E.A. Gill, S. Ueno, C. Yuan, J. Gold, and C.E. Murry, *Cardiomyocytes derived from human embryonic stem cells in pro-survival factors enhance function of infarcted rat hearts.* Nat Biotechnol, 2007. **25**(9): p. 1015-24.
9. Kroon, E., L.A. Martinson, K. Kadoya, A.G. Bang, O.G. Kelly, S. Eliazer, H. Young, M. Richardson, N.G. Smart, J. Cunningham, A.D. Agulnick, K.A. D'Amour, M.K. Carpenter, and E.E. Baetge, *Pancreatic endoderm derived from human embryonic stem cells generates glucose-responsive insulin-secreting cells in vivo.* Nat Biotechnol, 2008. **26**(4): p. 443-52.
10. Ben-Hur, T., M. Idelson, H. Khaner, M. Pera, E. Reinhartz, A. Itzik, and B.E. Reubinoff, *Transplantation of human embryonic stem cell-derived neural progenitors improves behavioral deficit in Parkinsonian rats.* Stem Cells, 2004. **22**(7): p. 1246-55.
11. Takahashi, K., K. Tanabe, M. Ohnuki, M. Narita, T. Ichisaka, K. Tomoda, and S. Yamanaka, *Induction of pluripotent stem cells from adult human fibroblasts by defined factors.* Cell, 2007. **131**(5): p. 861-72.
12. Yu, J., M.A. Vodyanik, K. Smuga-Otto, J. Antosiewicz-Bourget, J.L. Frane, S. Tian, J. Nie, G.A. Jonsdottir, V. Ruotti, R. Stewart, Slukvin, II, and J.A. Thomson, *Induced pluripotent stem cell lines derived from human somatic cells.* Science, 2007. **318**(5858): p. 1917-20.
13. Daley, G.Q., *Stem cells: roadmap to the clinic.* J Clin Invest. **120**(1): p. 8-10.

14. Nakagawa, M., M. Koyanagi, K. Tanabe, K. Takahashi, T. Ichisaka, T. Aoi, K. Okita, Y. Mochiduki, N. Takizawa, and S. Yamanaka, *Generation of induced pluripotent stem cells without Myc from mouse and human fibroblasts.* Nat Biotechnol, 2008. **26**(1): p. 101-6.
15. Kaji, K., K. Norrby, A. Paca, M. Mileikovsky, P. Mohseni, and K. Woltjen, *Virus-free induction of pluripotency and subsequent excision of reprogramming factors.* Nature, 2009. **458**(7239): p. 771-5.
16. Yu, J., K. Hu, K. Smuga-Otto, S. Tian, R. Stewart, Slukvin, II, and J.A. Thomson, *Human induced pluripotent stem cells free of vector and transgene sequences.* Science, 2009. **324**(5928): p. 797-801.
17. Shi, Y., C. Desponts, J.T. Do, H.S. Hahm, H.R. Scholer, and S. Ding, *Induction of pluripotent stem cells from mouse embryonic fibroblasts by Oct4 and Klf4 with small-molecule compounds.* Cell Stem Cell, 2008. **3**(5): p. 568-74.
18. Soldner, F., D. Hockemeyer, C. Beard, Q. Gao, G.W. Bell, E.G. Cook, G. Hargus, A. Blak, O. Cooper, M. Mitalipova, O. Isacson, and R. Jaenisch, *Parkinson's disease patient-derived induced pluripotent stem cells free of viral reprogramming factors.* Cell, 2009. **136**(5): p. 964-77.
19. Zhou, H., S. Wu, J.Y. Joo, S. Zhu, D.W. Han, T. Lin, S. Trauger, G. Bien, S. Yao, Y. Zhu, G. Siuzdak, H.R. Scholer, L. Duan, and S. Ding, *Generation of Induced Pluripotent Stem Cells Using Recombinant Proteins.* Cell Stem Cell, 2009.
20. Intaglietta, M., P.C. Johnson, and R.M. Winslow, *Microvascular and tissue oxygen distribution.* Cardiovasc Res, 1996. **32**(4): p. 632-43.
21. Soothill, P.W., K.H. Nicolaides, C.H. Rodeck, and S. Campbell, *Effect of gestational age on fetal and intervillous blood gas and acid-base values in human pregnancy.* Fetal Ther, 1986. **1**(4): p. 168-75.
22. Siggaard-Andersen, O. and R. Huch, *The oxygen status of fetal blood.* Acta Anaesthesiol Scand Suppl, 1995. **107**: p. 129-35.
23. Jauniaux, E., B. Gulbis, and G.J. Burton, *Physiological implications of the materno-fetal oxygen gradient in human early pregnancy.* Reprod Biomed Online, 2003. **7**(2): p. 250-3.
24. Lee, Y.M., C.H. Jeong, S.Y. Koo, M.J. Son, H.S. Song, S.K. Bae, J.A. Raleigh, H.Y. Chung, M.A. Yoo, and K.W. Kim, *Determination of hypoxic region by hypoxia marker in developing mouse embryos in vivo: a possible signal for vessel development.* Dev Dyn, 2001. **220**(2): p. 175-86.
25. Land, S.C., *Hochachka's "Hypoxia Defense Strategies" and the development of the pathway for oxygen.* Comp Biochem Physiol B Biochem Mol Biol, 2004. **139**(3): p. 415-33.
26. Jauniaux, E., B. Gulbis, and G.J. Burton, *The human first trimester gestational sac limits rather than facilitates oxygen transfer to the foetus--a review.* Placenta, 2003. **24 Suppl A**: p. S86-93.
27. Wang, F., S. Thirumangalathu, and M.R. Loeken, *Establishment of new mouse embryonic stem cell lines is improved by physiological glucose and oxygen.* Cloning Stem Cells, 2006. **8**(2): p. 108-16.

28. Gibbons, J., E. Hewitt, and D.K. Gardner, *Effects of oxygen tension on the establishment and lactate dehydrogenase activity of murine embryonic stem cells.* Cloning Stem Cells, 2006. **8**(2): p. 117-22.
29. Ludwig, T.E., M.E. Levenstein, J.M. Jones, W.T. Berggren, E.R. Mitchen, J.L. Frane, L.J. Crandall, C.A. Daigh, K.R. Conard, M.S. Piekarczyk, R.A. Llanas, and J.A. Thomson, *Derivation of human embryonic stem cells in defined conditions.* Nat Biotechnol, 2006. **24**(2): p. 185-7.
30. Smith, A.G., J.K. Heath, D.D. Donaldson, G.G. Wong, J. Moreau, M. Stahl, and D. Rogers, *Inhibition of pluripotential embryonic stem cell differentiation by purified polypeptides.* Nature, 1988. **336**(6200): p. 688-90.
31. Jeong, C.H., H.J. Lee, J.H. Cha, J.H. Kim, K.R. Kim, D.K. Yoon, and K.W. Kim, *Hypoxia-inducible factor-1 alpha inhibits self-renewal of mouse embryonic stem cells in Vitro via negative regulation of the leukemia inhibitory factor-STAT3 pathway.* J Biol Chem, 2007. **282**(18): p. 13672-9.
32. Powers, D.E., J.R. Millman, R.B. Huang, and C.K. Colton, *Effects of oxygen on mouse embryonic stem cell growth, phenotype retention, and cellular energetics.* Biotechnol Bioeng, 2008. **101**(2): p. 241-54.
33. Forsyth, N.R., A. Kay, K. Hampson, A. Downing, R. Talbot, and J. McWhir, *Transcriptome alterations due to physiological normoxic (2% O2) culture of human embryonic stem cells.* Regen Med, 2008. **3**(6): p. 817-33.
34. Westfall, S.D., S. Sachdev, P. Das, L.B. Hearne, M. Hannink, R.M. Roberts, and T. Ezashi, *Identification of oxygen-sensitive transcriptional programs in human embryonic stem cells.* Stem Cells Dev, 2008. **17**(5): p. 869-81.
35. Prasad, S.M., M. Czepiel, C. Cetinkaya, K. Smigielska, S.C. Weli, H. Lysdahl, A. Gabrielsen, K. Petersen, N. Ehlers, T. Fink, S.L. Minger, and V. Zachar, *Continuous hypoxic culturing maintains activation of Notch and allows long-term propagation of human embryonic stem cells without spontaneous differentiation.* Cell Prolif, 2009. **42**(1): p. 63-74.
36. Ezashi, T., P. Das, and R.M. Roberts, *Low O2 tensions and the prevention of differentiation of hES cells.* Proc Natl Acad Sci U S A, 2005. **102**(13): p. 4783-8.
37. Forsyth, N.R., A. Musio, P. Vezzoni, A.H. Simpson, B.S. Noble, and J. McWhir, *Physiologic oxygen enhances human embryonic stem cell clonal recovery and reduces chromosomal abnormalities.* Cloning Stem Cells, 2006. **8**(1): p. 16-23.
38. Ji, L., Y.X. Liu, C. Yang, W. Yue, S.S. Shi, C.X. Bai, J.F. Xi, X. Nan, and X.T. Pei, *Self-renewal and pluripotency is maintained in human embryonic stem cells by co-culture with human fetal liver stromal cells expressing hypoxia inducible factor 1alpha.* J Cell Physiol, 2009. **221**(1): p. 54-66.
39. Gustafsson, M.V., X. Zheng, T. Pereira, K. Gradin, S. Jin, J. Lundkvist, J.L. Ruas, L. Poellinger, U. Lendahl, and M. Bondesson, *Hypoxia requires notch signaling to maintain the undifferentiated cell state.* Dev Cell, 2005. **9**(5): p. 617-28.

40. Ying, Q.L., J. Wray, J. Nichols, L. Batlle-Morera, B. Doble, J. Woodgett, P. Cohen, and A. Smith, *The ground state of embryonic stem cell self-renewal.* Nature, 2008. **453**(7194): p. 519-23.
41. Hewitt, Z., N.R. Forsyth, M. Waterfall, D. Wojtacha, A.J. Thomson, and J. McWhir, *Fluorescence-activated single cell sorting of human embryonic stem cells.* Cloning Stem Cells, 2006. **8**(3): p. 225-34.
42. Simon, M.C. and B. Keith, *The role of oxygen availability in embryonic development and stem cell function.* Nat Rev Mol Cell Biol, 2008. **9**(4): p. 285-96.
43. Kim, T.S., S. Misumi, C.G. Jung, T. Masuda, Y. Isobe, F. Furuyama, H. Nishino, and H. Hida, *Increase in dopaminergic neurons from mouse embryonic stem cell-derived neural progenitor/stem cells is mediated by hypoxia inducible factor-1alpha.* J Neurosci Res, 2008. **86**(11): p. 2353-62.
44. Mondragon-Teran, P., G.J. Lye, and F.S. Veraitch, *Lowering oxygen tension enhances the differentiation of mouse embryonic stem cells into neuronal cells.* Biotechnol Prog, 2009.
45. Tomita, S., M. Ueno, M. Sakamoto, Y. Kitahama, M. Ueki, N. Maekawa, H. Sakamoto, M. Gassmann, R. Kageyama, N. Ueda, F.J. Gonzalez, and Y. Takahama, *Defective brain development in mice lacking the Hif-1alpha gene in neural cells.* Mol Cell Biol, 2003. **23**(19): p. 6739-49.
46. Krishnan, J., P. Ahuja, S. Bodenmann, D. Knapik, E. Perriard, W. Krek, and J.C. Perriard, *Essential role of developmentally activated hypoxia-inducible factor 1alpha for cardiac morphogenesis and function.* Circ Res, 2008. **103**(10): p. 1139-46.
47. Ateghang, B., M. Wartenberg, M. Gassmann, and H. Sauer, *Regulation of cardiotrophin-1 expression in mouse embryonic stem cells by HIF-1alpha and intracellular reactive oxygen species.* J Cell Sci, 2006. **119**(Pt 6): p. 1043-52.
48. Bauwens, C., T. Yin, S. Dang, R. Peerani, and P.W. Zandstra, *Development of a perfusion fed bioreactor for embryonic stem cell-derived cardiomyocyte generation: oxygen-mediated enhancement of cardiomyocyte output.* Biotechnol Bioeng, 2005. **90**(4): p. 452-61.
49. Niebruegge, S., C.L. Bauwens, R. Peerani, N. Thavandiran, S. Masse, E. Sevaptisidis, K. Nanthakumar, K. Woodhouse, M. Husain, E. Kumacheva, and P.W. Zandstra, *Generation of human embryonic stem cell-derived mesoderm and cardiac cells using size-specified aggregates in an oxygen-controlled bioreactor.* Biotechnol Bioeng, 2009. **102**(2): p. 493-507.
50. Purpura, K.A., S.H. George, S.M. Dang, K. Choi, A. Nagy, and P.W. Zandstra, *Soluble Flt-1 regulates Flk-1 activation to control hematopoietic and endothelial development in an oxygen-responsive manner.* Stem Cells, 2008. **26**(11): p. 2832-42.
51. Haselgrove, J.C., I.M. Shapiro, and S.F. Silverton, *Computer modeling of the oxygen supply and demand of cells of the avian growth cartilage.* Am J Physiol, 1993. **265**(2 Pt 1): p. C497-506.
52. Koay, E.J. and K.A. Athanasiou, *Hypoxic chondrogenic differentiation of human embryonic stem cells enhances cartilage protein synthesis and*

biomechanical functionality. Osteoarthritis Cartilage, 2008. **16**(12): p. 1450-6.
53. Powers, D.E., J.R. Millman, S. Bonner-Weir, M.J. Rappel, and C.K. Colton, *Accurate control of oxygen level in cells during culture on silicone rubber membranes with application to stem cell differentiation.* Biotechnol Prog, 2010. **26**(3): p. 805-18.
54. Fraker, C.A., S. Alvarez, P. Papadopoulos, J. Giraldo, W. Gu, C. Ricordi, L. Inverardi, and J. Dominguez-Bendala, *Enhanced oxygenation promotes beta-cell differentiation in vitro.* Stem Cells, 2007. **25**(12): p. 3155-64.
55. Lloyd-Jones, D., R. Adams, M. Carnethon, G. De Simone, T.B. Ferguson, K. Flegal, E. Ford, K. Furie, A. Go, K. Greenlund, N. Haase, S. Hailpern, M. Ho, V. Howard, B. Kissela, S. Kittner, D. Lackland, L. Lisabeth, A. Marelli, M. McDermott, J. Meigs, D. Mozaffarian, G. Nichol, C. O'Donnell, V. Roger, W. Rosamond, R. Sacco, P. Sorlie, R. Stafford, J. Steinberger, T. Thom, S. Wasserthiel-Smoller, N. Wong, J. Wylie-Rosett, and Y. Hong, *Heart Disease and Stroke Statistics--2009 Update: A Report From the American Heart Association Statistics Committee and Stroke Statistics Subcommittee.* Circulation, 2009. **119**(3): p. e21-181.
56. Maltsev, V.A., J. Rohwedel, J. Hescheler, and A.M. Wobus, *Embryonic stem cells differentiate in vitro into cardiomyocytes representing sinusnodal, atrial and ventricular cell types.* Mech Dev, 1993. **44**(1): p. 41-50.
57. Kehat, I., L. Khimovich, O. Caspi, A. Gepstein, R. Shofti, G. Arbel, I. Huber, J. Satin, J. Itskovitz-Eldor, and L. Gepstein, *Electromechanical integration of cardiomyocytes derived from human embryonic stem cells.* Nat Biotechnol, 2004. **22**(10): p. 1282-9.
58. Xue, T., H.C. Cho, F.G. Akar, S.Y. Tsang, S.P. Jones, E. Marban, G.F. Tomaselli, and R.A. Li, *Functional integration of electrically active cardiac derivatives from genetically engineered human embryonic stem cells with quiescent recipient ventricular cardiomyocytes: insights into the development of cell-based pacemakers.* Circulation, 2005. **111**(1): p. 11-20.
59. Caulfield, J.B., R. Leinbach, and H. Gold, *The relationship of myocardial infarct size and prognosis.* Circulation, 1976. **53**(3 Suppl): p. I141-4.
60. Keller, G.M., *In-Vitro Differentiation of Embryonic Stem Cells* Current Opinion in Cell Biology, 1995. **7**(6): p. 862-869.
61. Itskovitz-Eldor, J., M. Schuldiner, D. Karsenti, A. Eden, O. Yanuka, M. Amit, H. Soreq, and N. Benvenisty, *Differentiation of human embryonic stem cells into embryoid bodies comprising the three embryonic germ layers.* Molecular Medicine, 2000. **6**(2): p. 88-95.
62. Bauwens, C.L., P. Raheem, S. Niebruegge, K. Woodhouse, E. Kumacheva, M. Husain, and P.W. Zandstra, *Control of Human Embryonic Stem Cell Colony and Aggregate Size Heterogeneity Influences Differentiation Trajectories.* Stem Cells, 2008. **26**(9): p. 2300-2310.
63. Burridge, P.W., D. Anderson, H. Priddle, M.D. Barbadillo Munoz, S. Chamberlain, C. Allegrucci, L.E. Young, and C. Denning, *Improved*

Human Embryonic Stem Cell Embryoid Body Homogeneity and Cardiomyocyte Differentiation from a Novel V-96 Plate Aggregation System Highlights Interline Variability. Stem Cells, 2007. **25**(4): p. 929-938.
64. Dang, S.M., S. Gerecht-Nir, J. Chen, J. Itskovitz-Eldor, and P.W. Zandstra, *Controlled, scalable embryonic stem cell differentiation culture.* Stem Cells, 2004. **22**(3): p. 275-82.
65. Ng, E.S., R.P. Davis, L. Azzola, E.G. Stanley, and A.G. Elefanty, *Forced aggregation of defined numbers of human embryonic stem cells into embryoid bodies fosters robust, reproducible hematopoietic differentiation.* Blood, 2005. **106**(5): p. 1601-1603.
66. Karp, J.M., J. Yeh, G. Eng, J. Fukuda, J. Blumling, K.Y. Suh, J. Cheng, A. Mahdavi, J. Borenstein, R. Langer, and A. Khademhosseini, *Controlling size, shape and homogeneity of embryoid bodies using poly(ethylene glycol) microwells.* Lab on a Chip, 2007. **7**(6): p. 786-794.
67. Singhvi, R., A. Kumar, G.P. Lopez, G.N. Stephanopoulos, D.I. Wang, G.M. Whitesides, and D.E. Ingber, *Engineering cell shape and function.* Science, 1994. **264**(5159): p. 696-698.
68. Tan, J.L., W. Liu, C.M. Nelson, S. Raghavan, and C.S. Chen, *Simple Approach to Micropattern Cells on Common Culture Substrates by Tuning Substrate Wettability.* Tissue Engineering, 2004. **10**(5-6): p. 865-872.
69. Bauwens, C.L., R. Peerani, S. Niebruegge, K.A. Woodhouse, E. Kumacheva, M. Husain, and P.W. Zandstra, *Control of human embryonic stem cell colony and aggregate size heterogeneity influences differentiation trajectories.* Stem Cells, 2008. **26**(9): p. 2300-10.
70. Niebruegge, S., Bauwens, Céline L. Raheem Peerani Nimalan Thavandiran Stephane Masse Elias Sevaptisidis Kumar Nanthakumar Kim Woodhouse Mansoor Husain Eugenia Kumacheva Peter W. Zandstra, *Generation of human embryonic stem cell-derived mesoderm and cardiac cells using size-specified aggregates in an oxygen-controlled bioreactor.* Biotechnology and Bioengineering, 2009. **102**(2): p. 493-507.
71. Discher, D.E., D.J. Mooney, and P.W. Zandstra, *Growth Factors, Matrices, and Forces Combine and Control Stem Cells.* Science, 2009. **324**(5935): p. 1673-1677.
72. Passier, R., D.W.-v. Oostwaard, J. Snapper, J. Kloots, R.J. Hassink, E. Kuijk, B. Roelen, A.B. de la Riviere, and C. Mummery, *Increased Cardiomyocyte Differentiation from Human Embryonic Stem Cells in Serum-Free Cultures.* Stem Cells, 2005. **23**(6): p. 772-780.
73. Laflamme, M.A., K.Y. Chen, A.V. Naumova, V. Muskheli, J.A. Fugate, S.K. Dupras, H. Reinecke, C. Xu, M. Hassanipour, S. Police, C. O'Sullivan, L. Collins, Y. Chen, E. Minami, E.A. Gill, S. Ueno, C. Yuan, J. Gold, and C.E. Murry, *Cardiomyocytes derived from human embryonic stem cells in pro-survival factors enhance function of infarcted rat hearts.* Nat Biotech, 2007. **25**(9): p. 1015-1024.
74. Takahashi, T., B. Lord, P.C. Schulze, R.M. Fryer, S.S. Sarang, S.R. Gullans, and R.T. Lee, *Ascorbic acid enhances differentiation of*

embryonic stem cells into cardiac myocytes. Circulation, 2003. **107**(14): p. 1912-6.
75. Ventura, C. and M. Maioli, *Opioid peptide gene expression primes cardiogenesis in embryonal pluripotent stem cells.* Circ Res, 2000. **87**(3): p. 189-94.
76. Yoon, B.S., S.J. Yoo, J.E. Lee, S. You, H.T. Lee, and H.S. Yoon, *Enhanced differentiation of human embryonic stem cells into cardiomyocytes by combining hanging drop culture and 5-azacytidine treatment.* Differentiation, 2006. **74**(4): p. 149-59.
77. Wobus, A.M., G. Kaomei, J. Shan, M.C. Wellner, J. Rohwedel, G. Ji, B. Fleischmann, H.A. Katus, J. Hescheler, and W.M. Franz, *Retinoic acid accelerates embryonic stem cell-derived cardiac differentiation and enhances development of ventricular cardiomyocytes.* J Mol Cell Cardiol, 1997. **29**(6): p. 1525-39.
78. Sachinidis, A., B.K. Fleischmann, E. Kolossov, M. Wartenberg, H. Sauer, and J. Hescheler, *Cardiac specific differentiation of mouse embryonic stem cells.* Cardiovasc Res, 2003. **58**(2): p. 278-91.
79. Behfar, A., L.V. Zingman, D.M. Hodgson, J.-M. Rauzier, G.C. Kane, A. Terzic, and M. Puceat, *Stem cell differentiation requires a paracrine pathway in the heart.* FASEB J., 2002. **16**(12): p. 1558-1566.
80. Takahashi, K. and S. Yamanaka, *Induction of pluripotent stem cells from mouse embryonic and adult fibroblast cultures by defined factors.* Cell, 2006. **126**(4): p. 663-76.
81. Feng, B., J.H. Ng, J.C.D. Heng, and H.H. Ng, *Molecules that Promote or Enhance Reprogramming of Somatic Cells to Induced Pluripotent Stem Cells.* Cell Stem Cell, 2009. **4**(4): p. 301-312.
82. Narazaki, G., H. Uosaki, M. Teranishi, K. Okita, B. Kim, S. Matsuoka, S. Yamanaka, and J.K. Yamashita, *Directed and systematic differentiation of cardiovascular cells from mouse induced pluripotent stem cells.* Circulation, 2008. **118**(5): p. 498-506.
83. Mauritz, C., K. Schwanke, M. Reppel, S. Neef, K. Katsirntaki, L.S. Maier, F. Nguemo, S. Menke, M. Haustein, J. Hescheler, G. Hasenfuss, and U. Martin, *Generation of functional murine cardiac myocytes from induced pluripotent stem cells.* Circulation, 2008. **118**(5): p. 507-17.
84. Schenke-Layland, K., K.E. Rhodes, E. Angelis, Y. Butylkova, S. Heydarkhan-Hagvall, C. Gekas, R. Zhang, J.I. Goldhaber, H.K. Mikkola, K. Plath, and W.R. Maclellan, *Reprogrammed mouse fibroblasts differentiate into cells of the cardiovascular and hematopoietic lineages.* Stem Cells, 2008. **26**(6): p. 1537-1546.
85. Zhang, J., G.F. Wilson, A.G. Soerens, C.H. Koonce, J. Yu, S.P. Palecek, J.A. Thomson, and T.J. Kamp, *Functional cardiomyocytes derived from human induced pluripotent stem cells.* Circ Res, 2009. **104**(4): p. e30-41.
86. Knoepfler, P.S., *Deconstructing stem cell tumorigenicity: a roadmap to safe regenerative medicine.* Stem Cells, 2009. **27**(5): p. 1050-6.

87. Lawrenz, B., H. Schiller, E. Willbold, M. Ruediger, A. Muhs, and S. Esser, *Highly sensitive biosafety model for stem-cell-derived grafts.* Cytotherapy, 2004. **6**(3): p. 212-22.
88. Amariglio, N., A. Hirshberg, B.W. Scheithauer, Y. Cohen, R. Loewenthal, L. Trakhtenbrot, N. Paz, M. Koren-Michowitz, D. Waldman, L. Leider-Trejo, A. Toren, S. Constantini, and G. Rechavi, *Donor-derived brain tumor following neural stem cell transplantation in an ataxia telangiectasia patient.* PLoS Med, 2009. **6**(2): p. e1000029.
89. Miura, K., Y. Okada, T. Aoi, A. Okada, K. Takahashi, K. Okita, M. Nakagawa, M. Koyanagi, K. Tanabe, M. Ohnuki, D. Ogawa, E. Ikeda, H. Okano, and S. Yamanaka, *Variation in the safety of induced pluripotent stem cell lines.* Nat Biotechnol, 2009. **27**(8): p. 743-5.
90. Okita, K., T. Ichisaka, and S. Yamanaka, *Generation of germline-competent induced pluripotent stem cells.* Nature, 2007. **448**(7151): p. 313-7.
91. Fujikawa, T., S.H. Oh, L. Pi, H.M. Hatch, T. Shupe, and B.E. Petersen, *Teratoma formation leads to failure of treatment for type I diabetes using embryonic stem cell-derived insulin-producing cells.* Am J Pathol, 2005. **166**(6): p. 1781-91.
92. Fink, D.W., Jr., *FDA regulation of stem cell-based products.* Science, 2009. **324**(5935): p. 1662-3.
93. FDA Center for Biologics Evaluation and Research: Cellular, Tissue, and Gene Therapeutics Advisory Committee, Summary Minutes. 2008 Meeting #45, April 10-11. http://www.fda.gov/ohrms/dockets/ac/08/minutes/2008-0471M.htm.
94. Brederlau, A., A.S. Correia, S.V. Anisimov, M. Elmi, G. Paul, L. Roybon, A. Morizane, F. Bergquist, I. Riebe, U. Nannmark, M. Carta, E. Hanse, J. Takahashi, Y. Sasai, K. Funa, P. Brundin, P.S. Eriksson, and J.Y. Li, *Transplantation of human embryonic stem cell-derived cells to a rat model of Parkinson's disease: effect of in vitro differentiation on graft survival and teratoma formation.* Stem Cells, 2006. **24**(6): p. 1433-40.
95. Wernig, M., J.P. Zhao, J. Pruszak, E. Hedlund, D. Fu, F. Soldner, V. Broccoli, M. Constantine-Paton, O. Isacson, and R. Jaenisch, *Neurons derived from reprogrammed fibroblasts functionally integrate into the fetal brain and improve symptoms of rats with Parkinson's disease.* Proc Natl Acad Sci U S A, 2008. **105**(15): p. 5856-61.
96. Kim, J.H., J.M. Auerbach, J.A. Rodriguez-Gomez, I. Velasco, D. Gavin, N. Lumelsky, S.H. Lee, J. Nguyen, R. Sanchez-Pernaute, K. Bankiewicz, and R. McKay, *Dopamine neurons derived from embryonic stem cells function in an animal model of Parkinson's disease.* Nature, 2002. **418**(6893): p. 50-6.
97. Cao, F., R.A. Wagner, K.D. Wilson, X. Xie, J.D. Fu, M. Drukker, A. Lee, R.A. Li, S.S. Gambhir, I.L. Weissman, R.C. Robbins, and J.C. Wu, *Transcriptional and functional profiling of human embryonic stem cell-derived cardiomyocytes.* PLoS One, 2008. **3**(10): p. e3474.

98. Hentze, H., P.L. Soong, S.T. Wang, B.W. Phillips, T.C. Putti, and N.R. Dunn, *Teratoma formation by human embryonic stem cells: Evaluation of essential parameters for future safety studies.* Stem Cell Res, 2009.
99. Prokhorova, T.A., L.M. Harkness, U. Frandsen, N. Ditzel, H.D. Schroder, J.S. Burns, and M. Kassem, *Teratoma formation by human embryonic stem cells is site dependent and enhanced by the presence of matrigel.* Stem Cells Dev, 2009. **18**(1): p. 47-54.
100. Lee, A.S., C. Tang, F. Cao, X. Xie, K. van der Bogt, A. Hwang, A.J. Connolly, R.C. Robbins, and J.C. Wu, *Effects of cell number on teratoma formation by human embryonic stem cells.* Cell Cycle, 2009. **8**(16): p. 2608-12.
101. Hentze, H., R. Graichen, and A. Colman, *Cell therapy and the safety of embryonic stem cell-derived grafts.* Trends Biotechnol, 2007. **25**(1): p. 24-32.
102. Xu, X.Q., R. Zweigerdt, S.Y. Soo, Z.X. Ngoh, S.C. Tham, S.T. Wang, R. Graichen, B. Davidson, A. Colman, and W. Sun, *Highly enriched cardiomyocytes from human embryonic stem cells.* Cytotherapy, 2008. **10**(4): p. 376-89.
103. Barberi, T., M. Bradbury, Z. Dincer, G. Panagiotakos, N.D. Socci, and L. Studer, *Derivation of engraftable skeletal myoblasts from human embryonic stem cells.* Nat Med, 2007. **13**(5): p. 642-8.
104. Tan, H.L., W.J. Fong, E.H. Lee, M. Yap, and A. Choo, *mAb 84, a cytotoxic antibody that kills undifferentiated human embryonic stem cells via oncosis.* Stem Cells, 2009. **27**(8): p. 1792-801.
105. Choo, A.B., H.L. Tan, S.N. Ang, W.J. Fong, A. Chin, J. Lo, L. Zheng, H. Hentze, R.J. Philp, S.K. Oh, and M. Yap, *Selection against undifferentiated human embryonic stem cells by a cytotoxic antibody recognizing podocalyxin-like protein-1.* Stem Cells, 2008. **26**(6): p. 1454-63.
106. Thomson, J.A., J. Itskovitz-Eldor, S.S. Shapiro, M.A. Waknitz, J.J. Swiergiel, V.S. Marshall, and J.M. Jones, *Embryonic Stem Cell Lines Derived from Human Blastocysts.* Science, 1998. **282**(5391): p. 1145-1147.
107. Kaufman, M.H., E.J. Robertson, A.H. Handyside, and M.J. Evans, *Establishment of pluripotential cell lines from haploid mouse embryos.* J Embryol Exp Morphol, 1983. **73**: p. 249-61.
108. Laurent, L.C., I. Ulitsky, I. Slavin, H. Tran, A. Schork, R. Morey, C. Lynch, J.V. Harness, S. Lee, M.J. Barrero, S. Ku, M. Martynova, R. Semechkin, V. Galat, J. Gottesfeld, J.C. Izpisua Belmonte, C. Murry, H.S. Keirstead, H.S. Park, U. Schmidt, A.L. Laslett, F.J. Muller, C.M. Nievergelt, R. Shamir, and J.F. Loring, *Dynamic changes in the copy number of pluripotency and cell proliferation genes in human ESCs and iPSCs during reprogramming and time in culture.* Cell Stem Cell. **8**(1): p. 106-18.
109. Yoshida, Y., K. Takahashi, K. Okita, T. Ichisaka, and S. Yamanaka, *Hypoxia enhances the generation of induced pluripotent stem cells.* Cell Stem Cell, 2009. **5**(3): p. 237-41.

110. Warren, L., P.D. Manos, T. Ahfeldt, Y.H. Loh, H. Li, F. Lau, W. Ebina, P.K. Mandal, Z.D. Smith, A. Meissner, G.Q. Daley, A.S. Brack, J.J. Collins, C. Cowan, T.M. Schlaeger, and D.J. Rossi, *Highly Efficient Reprogramming to Pluripotency and Directed Differentiation of Human Cells with Synthetic Modified mRNA.* Cell Stem Cell.
111. Lengner, C.J., A.A. Gimelbrant, J.A. Erwin, A.W. Cheng, M.G. Guenther, G.G. Welstead, R. Alagappan, G.M. Frampton, P. Xu, J. Muffat, S. Santagata, D. Powers, C.B. Barrett, R.A. Young, J.T. Lee, R. Jaenisch, and M. Mitalipova, *Derivation of pre-X inactivation human embryonic stem cells under physiological oxygen concentrations.* Cell. **141**(5): p. 872-83.
112. Zhou, Q., H. Chipperfield, D.A. Melton, and W.H. Wong, *A gene regulatory network in mouse embryonic stem cells.* Proc Natl Acad Sci U S A, 2007. **104**(42): p. 16438-43.
113. Huangfu, D., R. Maehr, W. Guo, A. Eijkelenboom, M. Snitow, A.E. Chen, and D.A. Melton, *Induction of pluripotent stem cells by defined factors is greatly improved by small-molecule compounds.* Nat Biotechnol, 2008. **26**(7): p. 795-7.
114. Brusselmans, K., F. Bono, D. Collen, J.M. Herbert, P. Carmeliet, and M. Dewerchin, *A novel role for vascular endothelial growth factor as an autocrine survival factor for embryonic stem cells during hypoxia.* J Biol Chem, 2005. **280**(5): p. 3493-9.
115. Pisania, A., K.K. Papas, D.E. Powers, M.J. Rappel, A. Omer, S. Bonner-Weir, G.C. Weir, and C.K. Colton, *Enumeration of islets by nuclei counting and light microscopic analysis.* Lab Invest, 2011. **90**(11): p. 1676-86.
116. Kehat, I., D. Kenyagin-Karsenti, M. Snir, H. Segev, M. Amit, A. Gepstein, E. Livne, O. Binah, J. Itskovitz-Eldor, and L. Gepstein, *Human embryonic stem cells can differentiate into myocytes with structural and functional properties of cardiomyocytes.* J Clin Invest, 2001. **108**(3): p. 407-14.
117. Klug, M.G., M.H. Soonpaa, G.Y. Koh, and L.J. Field, *Genetically Selected Cardiomyocytes from Differentiating Embryonic Stem Cells Form Stable Intracardiac Grafts.* 1996. p. 216-224.
118. Xu, C.H., S. Police, M. Hassanipour, and J.D. Gold, *Cardiac bodies: A novel culture method for enrichment of cardiomyocytes derived from human embryonic stem cells.* Stem Cells and Development, 2006. **15**(5): p. 631-639.
119. Murry, C.E. and G. Keller, *Differentiation of embryonic stem cells to clinically relevant populations: lessons from embryonic development.* Cell, 2008. **132**(4): p. 661-80.
120. Fukuda, K. and S. Yuasa, *Stem Cells as a Source of Regenerative Cardiomyocytes.* 2006. p. 1002-1013.
121. Chen, Y., I. Amende, T.G. Hampton, Y.K. Yang, Q.G. Ke, J.Y. Min, Y.F. Xiao, and J.P. Morgan, *Vascular endothelial growth factor promotes cardiomyocyte differentiation of embryonic stem cells.* American Journal of Physiology-Heart and Circulatory Physiology, 2006. **291**(4): p. H1653-H1658.

122. Yoon, B.S., S.J. Yoo, J.E. Lee, S. You, H.T. Lee, and H.S. Yoon, *Enhanced differentiation of human embryonic stem cells into cardiomyocytes by combining hanging drop culture and 5-azacytidine treatment.* Differentiation, 2006. **74**(4): p. 149-159.
123. Yang, L., M.H. Soonpaa, E.D. Adler, T.K. Roepke, S.J. Kattman, M. Kennedy, E. Henckaerts, K. Bonham, G.W. Abbott, R.M. Linden, L.J. Field, and G.M. Keller, *Human cardiovascular progenitor cells develop from a KDR+ embryonic-stem-cell-derived population.* Nature, 2008. **453**(7194): p. 524-8.
124. Andreyev, A.I., Y.E. Kushnareva, and A.A. Starkov, *Mitochondrial metabolism of reactive oxygen species.* Biochemistry-Moscow, 2005. **70**(2): p. 200-214.
125. Lee, J.W., S.H. Bae, J.W. Jeong, S.H. Kim, and K.W. Kim, *Hypoxia-inducible factor (HIF-1)alpha: its protein stability and biological functions.* Experimental and Molecular Medicine, 2004. **36**(1): p. 1-12.
126. Yun, Z., Q. Lin, and A.J. Giaccia, *Adaptive myogenesis under hypoxia.* Molecular and Cellular Biology, 2005. **25**(8): p. 3040-3055.
127. Fischer, B. and B.D. Bavister, *Oxygen tension in the oviduct and uterus of rhesus monkeys, hamsters and rabbits.* J Reprod Fertil, 1993. **99**(2): p. 673-9.
128. Palis, J., R.J. Chan, A. Koniski, R. Patel, M. Starr, and M.C. Yoder, *Spatial and temporal emergence of high proliferative potential hematopoietic precursors during murine embryogenesis.* Proc Natl Acad Sci U S A, 2001. **98**(8): p. 4528-33.
129. Maltepe, E. and M.C. Simon, *Oxygen, genes, and development: an analysis of the role of hypoxic gene regulation during murine vascular development.* J Mol Med, 1998. **76**(6): p. 391-401.
130. Borowiak, M., R. Maehr, S. Chen, A.E. Chen, W. Tang, J.L. Fox, S.L. Schreiber, and D.A. Melton, *Small molecules efficiently direct endodermal differentiation of mouse and human embryonic stem cells.* Cell Stem Cell, 2009. **4**(4): p. 348-58.
131. Fehling, H.J., G. Lacaud, A. Kubo, M. Kennedy, S. Robertson, G. Keller, and V. Kouskoff, *Tracking mesoderm induction and its specification to the hemangioblast during embryonic stem cell differentiation.* Development, 2003. **130**(17): p. 4217-27.
132. Sasaki, H. and B.L. Hogan, *Differential expression of multiple fork head related genes during gastrulation and axial pattern formation in the mouse embryo.* Development, 1993. **118**(1): p. 47-59.
133. Kanai-Azuma, M., Y. Kanai, J.M. Gad, Y. Tajima, C. Taya, M. Kurohmaru, Y. Sanai, H. Yonekawa, K. Yazaki, P.P. Tam, and Y. Hayashi, *Depletion of definitive gut endoderm in Sox17-null mutant mice.* Development, 2002. **129**(10): p. 2367-79.
134. Duncan, S.A., K. Manova, W.S. Chen, P. Hoodless, D.C. Weinstein, R.F. Bachvarova, and J.E. Darnell, Jr., *Expression of transcription factor HNF-4 in the extraembryonic endoderm, gut, and nephrogenic tissue of the developing mouse embryo: HNF-4 is a marker for primary endoderm in*

the implanting blastocyst. Proc Natl Acad Sci U S A, 1994. **91**(16): p. 7598-602.
135. Gu, G., J. Dubauskaite, and D.A. Melton, *Direct evidence for the pancreatic lineage: NGN3+ cells are islet progenitors and are distinct from duct progenitors.* Development, 2002. **129**(10): p. 2447-57.
136. Wood, H.B. and V. Episkopou, *Comparative expression of the mouse Sox1, Sox2 and Sox3 genes from pre-gastrulation to early somite stages.* Mech Dev, 1999. **86**(1-2): p. 197-201.
137. Lendahl, U., L.B. Zimmerman, and R.D. McKay, *CNS stem cells express a new class of intermediate filament protein.* Cell, 1990. **60**(4): p. 585-95.
138. Osumi, N., H. Shinohara, K. Numayama-Tsuruta, and M. Maekawa, *Concise review: Pax6 transcription factor contributes to both embryonic and adult neurogenesis as a multifunctional regulator.* Stem Cells, 2008. **26**(7): p. 1663-72.
139. Wardle, F.C. and V.E. Papaioannou, *Teasing out T-box targets in early mesoderm.* Curr Opin Genet Dev, 2008. **18**(5): p. 418-25.
140. Kitajima, S., A. Takagi, T. Inoue, and Y. Saga, *MesP1 and MesP2 are essential for the development of cardiac mesoderm.* Development, 2000. **127**(15): p. 3215-26.
141. Hoogaars, W.M., P. Barnett, A.F. Moorman, and V.M. Christoffels, *T-box factors determine cardiac design.* Cell Mol Life Sci, 2007. **64**(6): p. 646-60.
142. Buckingham, M., S. Meilhac, and S. Zaffran, *Building the mammalian heart from two sources of myocardial cells.* Nat Rev Genet, 2005. **6**(11): p. 826-35.
143. Labeit, S. and B. Kolmerer, *Titins: giant proteins in charge of muscle ultrastructure and elasticity.* Science, 1995. **270**(5234): p. 293-6.
144. Townsend, P.J., H. Farza, C. MacGeoch, N.K. Spurr, R. Wade, R. Gahlmann, M.H. Yacoub, and P.J. Barton, *Human cardiac troponin T: identification of fetal isoforms and assignment of the TNNT2 locus to chromosome 1q.* Genomics, 1994. **21**(2): p. 311-6.
145. Sassoon, D.A., I. Garner, and M. Buckingham, *Transcripts of alpha-cardiac and alpha-skeletal actins are early markers for myogenesis in the mouse embryo.* Development, 1988. **104**(1): p. 155-64.
146. Ramirez-Bergeron, D.L., A. Runge, K.D. Dahl, H.J. Fehling, G. Keller, and M.C. Simon, *Hypoxia affects mesoderm and enhances hemangioblast specification during early development.* Development, 2004. **131**(18): p. 4623-34.
147. Kattman, S.J., T.L. Huber, and G.M. Keller, *Multipotent Flk-1(+) cardiovascular progenitor cells give rise to the cardiomyocyte, endothelial, and vascular smooth muscle lineages.* Developmental Cell, 2006. **11**(5): p. 723-732.
148. Kanno, S., P.K.M. Kim, K. Sallam, J. Lei, T.R. Billiar, and L.L. Shears, *Nitric oxide facilitates cardiomyogenesis in mouse embryonic stem cells.* Proceedings of the National Academy of Sciences of the United States of America, 2004. **101**(33): p. 12277-12281.

149. Iyer, N.V., L.E. Kotch, F. Agani, S.W. Leung, E. Laughner, R.H. Wenger, M. Gassmann, J.D. Gearhart, A.M. Lawler, A.Y. Yu, and G.L. Semenza, *Cellular and developmental control of O2 homeostasis by hypoxia-inducible factor 1 alpha.* Genes Dev, 1998. **12**(2): p. 149-62.
150. Wikenheiser, J., Y.Q. Doughman, S.A. Fisher, and M. Watanabe, *Differential levels of tissue hypoxia in the developing chicken heart.* Developmental Dynamics, 2006. **235**(1): p. 115-123.
151. Lumelsky, N., O. Blondel, P. Laeng, I. Velasco, R. Ravin, and R. McKay, *Differentiation of embryonic stem cells to insulin-secreting structures similar to pancreatic islets.* Science, 2001. **292**(5520): p. 1389-94.
152. Bonner-Weir, S. and G.C. Weir, *New sources of pancreatic beta-cells.* Nat Biotechnol, 2005. **23**(7): p. 857-61.
153. Madsen, O.D., *Stem cells and diabetes treatment.* APMIS, 2005. **113**(11-12): p. 858-75.
154. D'Amour, K.A., A.D. Agulnick, S. Eliazer, O.G. Kelly, E. Kroon, and E.E. Baetge, *Efficient differentiation of human embryonic stem cells to definitive endoderm.* Nat Biotechnol, 2005. **23**(12): p. 1534-41.
155. D'Amour, K.A., A.G. Bang, S. Eliazer, O.G. Kelly, A.D. Agulnick, N.G. Smart, M.A. Moorman, E. Kroon, M.K. Carpenter, and E.E. Baetge, *Production of pancreatic hormone-expressing endocrine cells from human embryonic stem cells.* Nat Biotechnol, 2006. **24**(11): p. 1392-401.
156. Jiang, B.H., G.L. Semenza, C. Bauer, and H.H. Marti, *Hypoxia-inducible factor 1 levels vary exponentially over a physiologically relevant range of O2 tension.* Am J Physiol, 1996. **271**(4 Pt 1): p. C1172-80.
157. Powers, D.E., J.R. Millman, S. Bonner-Weir, M.J. Rappel, and C.K. Colton, *Accurate control of oxygen level in cells during culture on silicone rubber membranes with application to stem cell differentiation.* Biotechnol Prog. **26**(3): p. 805-18.

-Page Intentionally Left Blank-

Appendix

A. Accurate control of oxygen level in cells during culture on silicone rubber membranes with application to stem cell differentiation

Reproduced from Powers, D.E., J.R. Millman, S. Bonner-Weir, M.J. Rappel, and C.K. Colton, *Accurate control of oxygen level in cells during culture on silicone rubber membranes with application to stem cell differentiation.* Biotechnology Progress **26**(3): p. 805-18 with permission of John Wiley & Sons, Inc.

AIChE

Accurate Control of Oxygen Level in Cells During Culture on Silicone Rubber Membranes with Application to Stem Cell Differentiation

Daryl E. Powers and Jeffrey R. Millman
Dept. of Chemical Engineering, Massachusetts Institute of Technology, Cambridge, MA 02139

Susan Bonner-Weir
Section on Islet Transplantation and Cell Biology, Research Division, Joslin Diabetes Center, Boston, MA 02215

Dept. of Medicine, Harvard Medical School, Boston, MA 02215

Michael J. Rappel and Clark K. Colton
Dept. of Chemical Engineering, Massachusetts Institute of Technology, Cambridge, MA 02139

DOI 10.1002/btpr.359
Published online December 28, 2009 in Wiley InterScience (www.interscience.wiley.com).

Oxygen level in mammalian cell culture is often controlled by placing culture vessels in humidified incubators with a defined gas phase partial pressure of oxygen (pO_{2gas}). Because the cells are consuming oxygen supplied by diffusion, a difference between pO_{2gas} and that experienced by the cells (pO_{2cell}) arises, which is maximal when cells are cultured in vessels with little or no oxygen permeability. Here, we demonstrate theoretically that highly oxygen-permeable silicone rubber membranes can be used to control pO_{2cell} during culture of cells in monolayers and aggregates much more accurately and can achieve more rapid transient response following a disturbance than on polystyrene and fluorinated ethylene-propylene copolymer membranes. Cell attachment on silicone rubber was achieved by physical adsorption of fibronectin or Matrigel. We use these membranes for the differentiation of mouse embryonic stem cells to cardiomyocytes and compare the results with culture on polystyrene or on silicone rubber on top of polystyrene. The fraction of cells that are cardiomyocyte-like increases with decreasing pO_2 only when using oxygen-permeable silicone membrane-based dishs, which contract on silicone rubber but not polystyrene. The high permeability of silicone rubber results in pO_{2cell} being equal to pO_{2gas} at the tissue-membrane interface. This, together with geometric information from histological sections, facilitates development of a model from which the pO_2 distribution within the resulting aggregates is computed. Silicone rubber membranes have significant advantages over polystyrene in controlling pO_{2cell}, and these results suggest they are a valuable tool for investigating pO_2 effects in many applications, such as stem cell differentiation. © 2009 American Institute of Chemical Engineers
Biotechnol. Prog., 26: 805–818, 2010
Keywords: embryonic stem cells, oxygen, hypoxia, differentiation, silicone rubber

Introduction

Laboratory animal cell culture experiments are usually performed in glass or polystyrene dishes having zero or low oxygen permeability in an incubator having a humidified atmosphere consisting of 95% air/5% CO_2 that results in a gas oxygen partial pressure (pO_{2gas}) of 142 mm Hg. Because oxygen consumption by the cells induces oxygen concentration gradients in the medium, pO_2 at the cell surface (pO_{2cell}) is lower than pO_{2gas} and the difference (ΔpO_2), which is usually unknown, can be large, recognized using theoretical models of oxygen transport,[1,2] and experiments with microelectrodes.[3–6] These gradients have been exploited in static culture systems to measure oxygen consumption rate (OCR) of cells in monolayer culture and in embryoid bodies (EBs).[7,8] In addition to affecting steady-state values of pO_{2cell}, the long time scales associated with transient oxygen diffusion through the static medium make it nearly impossible to accurately study effects of intermittent hypoxia.[9]

To reduce ΔpO_2, cells can be cultured in gas-permeable dishes, in dishes that are mechanically mixed, or in a perfused system to induce convective transport. Mechanical mixing is preferred for oxygenation of large-scale bioreactors but introduces cumbersome equipment requirements for small-scale research. Additionally, mixing in culture vessels induces shear stresses on cells, which may affect their function.[10] Perfusion systems can avoid this problem but are complex and susceptible to contamination. In contrast,

The first two authors contributed equally to this work.
Correspondence concerning this article should be addressed to C. K. Colton at ckcolton@msit.edu.

Table 1. Oxygen Diffusivity and Solubility Parameters at 37°C

Continuous Phase	D (10^{-5} cm^2 sec^{-1})	Source	α (10^{-9} mol cm^{-3} mm Hg^{-1})	Source	$D_i\alpha_i/h_i$[a] (10^{-14} mol sec^{-1} cm^{-2} mm Hg^{-1})	$\frac{(D_i\alpha_i/h_i)}{(D_m\alpha_m/h_m)}$
Culture medium	2.78	Dionne 1990[b]	1.27	Dionne 1990[b]	7.06	1
Silicone rubber	2.19	Average value[c]	12.2	Average value[d]	2,100	298
Fluorinated ethylene-propylene copolymer	0.028	Koros et al. 1981	5.06	DuPont 1996	56.7	8.03
Polystyrene	0.011	Hodge et al. 2001	8.60	Chen et al. 1994	0.0946	0.0134
Tissue	1.53	Dionne 1990[b]	1.02	Dionne 1990[b]		

[a] Thickness h_i of 5,0.127,0.025, and 1 mm was used for culture medium, silicone rubber, fluorinated ethylene-propylene copolymer, and polystyrene, respectively. [b] Mean of published values. [c] Reitlinger et al. 1956; Robb 1968. [d] Barrer et al. 1965; Reitlinger et al. 1956; Robb 1968.

culture on a gas-permeable membrane at the bottom of a dish requires no additional equipment and no changes in the culture environment, other than the surface on which the cells are growing. Membranes previously examined include fluorinated ethylene-propylene copolymer (FEP)[6] and silicone-polycarbonate membrane copolymer.[11] FEP was selected because of its optical clarity and strength, not because it is optimal for oxygen transfer. Dishes made with this membrane are available (Lumox dishes, Greiner Bio-One, Munich) with either a hydrophobic or plasma gas-treated hydrophilic surface suitable for cell culture.[12] The oxygen permeability of silicone rubber is two orders of magnitude higher than that of FEP (Table 1).[13–15] Silicone rubber is preferred for oxygen delivery and is used in membrane-aerated bioreactors,[16–19] high density culture of hybridoma cells,[20] and cell aggregates.[21] Small-scale dishes suitable, e.g., for stem cell research that incorporate these membranes are not commercially available.

Silicone rubber surfaces must be modified prior to culture of adherent cells.[22] Treatment with plasmas of various compositions have been used,[22,23] but surfaces modified this way are not stable for extended periods of time due to migration of functional groups from the surface into the bulk material.[24–26] Modifications in which functional coatings are grafted onto the silicone rubber are more stable but infrequently used.[27,28] Recently, polyelectrolyte multilayers (PEMs) have been used for surface modification of silicone rubber because this method is inexpensive, easy to apply, and has flexible chemistry.[29–33]

Here we show theoretical justification for the superiority of silicone rubber membranes for accurate control of the pO_{2cell} during culture of both cell monolayers and aggregates. We also show that physical adsorption of fibronectin or Matrigel to silicone rubber is sufficient for robust cell adhesion of the cell line employed, mouse embryonic stem (mES) cells. These materials are used to study the effects of oxygen on the differentiation of mES cells into cardiomyocytes using an 11-day differentiation protocol, the last 9 days of which occur with the cells attached to silicone rubber membrane-based dishes. Finally, we used histology to determine the geometry of differentiated aggregates of mES cells for use in a theoretical model for predicting the pO_{2cell} distribution in these aggregates.

Materials and Methods

Silicone rubber membrane-based plate

The bottom surface of eight central wells of 24-well tissue culture treated plates (353047, Becton Dickinson, Franklin Lakes, NJ) was removed using a 3/8 × 3-in fixed handle nutdriver (Cooper Hand Tools, Apex, NC) heated in a Bunsen burner, and edges of the holes trimmed with sterile scalpel to be flush with the rest of the plate bottom. A very thin layer of silicone adhesive (Henkel Loctite Corp., Rocky Hill, CT) was spread on the base of the plate around each hole. Silicone rubber sheets (nonreinforced vulcanized gloss/gloss 0.005 in thick, Specialty Manufacturing, Saginaw, MI), cut to 8.5 × 4.5 cm and sterilized by autoclaving for 30 min at 121°C, was stretched so that it was flat (no wrinkles) and pressed onto the uncut bottom surface. After allowing the adhesive to set for 24 hr, the plates were filled with 70% (v/v) ethanol in water for 1 hr and dried overnight under a germicidal UV lamp in a biological safety cabinet. In use, the silicone rubber membrane at the bottom of the plate was placed on four layers of dry paper towels to provide access to ambient pO_{2gas}.

Coating of silicone rubber using layer-by-layer PEM film growth

PEMs were prepared by adapting a published method.[29] Solutions in Dulbecco's phosphate buffered saline (DPBS) (Mediatech, Herndon, VA) were prepared containing 3 mg/mL poly-sodium 4-styrene-sulfonate (PSS), 2 mg/mL polyethyleneimine (PEI), 0.5 mg/mL poly-D-lysine hydrobromide (PDL), 1 mg/mL type A gelatin, 1 mg/mL type B gelatin, and 50 μg/mL fibronectin (all from Sigma-Aldrich, St. Louis, MO). Coating a silicone rubber membrane at the bottom of a well was carried out at room temperature using 1 mL of solution for each step. PSS solution (polyanion) was added to an untreated plate and incubated for 1 hr, followed by a 10-min wash with DPBS, an 1-hr incubation with PEI (polycation), and a 10 min wash with DPBS. Two additional incubations with both PSS and PEI (30 min each) with intervening washes (10 min) were done to build a $(PSS\text{-}PEI)_3$ PEM. An additional three layers each of type B gelatin (polyanion) and PDL (polycation) were formed using 30-min incubations with the polyelectrolyte solution and 10-min washes with DPBS to yield $(PSS\text{-}PEI)_3$-$(type\ B\ gelatin\text{–}PDL)_3$, after which an additional 20-hr incubation with type A gelatin, type B gelatin, or fibronectin was performed. Plates were washed and incubated for 24 hr with DPBS prior to emptying the wells and adding culture medium and cells.

Coating of silicone rubber membrane by physical adsorption of proteins

Plates to be coated were incubated at 37°C in a 0.1% (w/v) solution of type A gelatin in tissue culture water for 24 hr (Mediatech, Herndon, VA), 2 μg/mL fibronectin (Sigma) in DPBS for 24 hr, or Matrigel (354234, Becton Dickinson) diluted 1:20 in serum-free medium for 1 hr. Immediately before plating cells, the solution was removed and replaced with mES cell medium.

Table 2. Composition of Undifferentiated mES Cell Maintenance and mES Cell Differentiation Medium[a]

Component	Manufacturer and Catalog Number	Volume per Liter of Medium (mL)	Notes
Dulbecco's modified eagles medium (DMEM)	ATCC SCRR 2010	868	ES cell qualified
Fetal bovine serum	ATCC SCRR 30-2020	100	ES cell qualified
L-alanyl-L-glutamine	ATCC SCRR 20-2115	10	200 mM stock solution
MEM nonessential amino acid solution	ATCC SCRR 20-2116	10	
2-mercaptoethanol solution	Sigma-Aldrich M7522	10	10 mM stock solution prepared in DMEM
Leukemia inhibitory factor[a]	Chemicon ESG 1106	1	10^6 unit/mL stock solution
L-ascorbic acid solution[a]	Sigma-Aldrich A4034	1	200 mM stock solution prepared in DPBS

[a] Leukemia inhibitory factor was added only to undifferentiated ES cell maintenance medium. Ascorbic acid was added only to ES cell differentiation medium.

Table 3. Formulation of Serum-Free ITS Medium

Component	Manufacturer and Catalog Number	Volume per Liter of Medium (mL)	Notes
Dulbecco's modified eagles medium (DMEM)	Mediatech 90-133-PB	485	8.4 mg/mL stock solution prepared in deionized water
Sodium bicarbonate	Mediatech 25-035-CI	10	7.5% (w/v) solution
F12 nutrient mixture	Invitrogen 31765-035	496	
25 M glucose solution	Sigma-Aldrich G8769	1.6	Final medium concentration of 9 mM
Human insulin solution	Sigma-Aldrich I9278	0.5	10 mg/mL solution
Holo transferrin solution	Sigma-Aldrich T1283	5	10 mg/mL stock solution prepared in DPBS
Sodium selenite solution	Sigma-Aldrich S9133	0.26	0.12 mM stock solution prepared in DPBS
L-ascorbic acid solution	Sigma-Aldrich A4034	1	200 mM stock solution prepared in DPBS

Gas phase pO_2 control

As previously described,[34] cell culture vessels were placed in sealed polystyrene chambers (Billups-Rothenburg, Del Mar, CA) inside a standard incubator (Queue Systems, Parkersburg, WV) at 37°C. Gas was bubbled through a bottle of water open only to the gas cylinder and chamber in the incubator; an open dish of deionized water in each chamber provided additional humidification. The flow rate to the chambers of premixed gas containing 20%, 5%, or 1% O_2, 5% CO_2, and the remainder N_2 (certified medical gas, Airgas, Hingham, MA) was set to 2 L/min for 15 min following closure of the chambers (after cell medium exchange) and to 30 mL/min otherwise. The corresponding pO_{2gas} in the chambers was 142, 36, or 7 mm Hg, respectively.

Measurement of transient pO_2 in culture dishes

To examine the transient response of polystyrene and silicone rubber dishes to a change in pO_{2gas}, measurements were made in an Xvivo Incubation System (BioSpherix, Lacona, NY), an oxygen-controlled incubator, using the included 2-mm diameter fiber optic oxygen-sensing probes (Model F2 OxyValidator, Kyodo International, Kawasakishi, Japan). The probe was placed vertically in each of 2 wells of a 24-well plate, one well with a polystyrene and one with a silicone rubber bottom filled with 2 mL of DBPS (medium height 10.5 cm) so that the sensing tip was in contact with the upper surface of the plate bottom inside of a sealed incubator set at pO_{2gas} = 160 mm Hg and 37°C. at $t = 0$, the incubator gas controller was set to pO_{2gas} = 7 mm Hg, and the pO_2 of each of the sensors monitored for 20 hr. Plates with silicone rubber bottoms were placed on four layers of paper towels in the same configuration as for normal cell culture.

Culture of undifferentiated mES cells

Undifferentiated J1 mES cells ATCC (SCRC 1010, ATCC, Manassas, VA) were grown in 25 cm^2 cell culture T-flasks (Becton Dickinson) using 4 mL of medium (Table 2) exchanged daily. Cells were detached with 0.25% trypsin every two days and placed in a new culture flask at a density of 1.2×10^4 cell/cm^2.

Enumeration of undifferentiated cells

Unattached cells (suspended in the supernatant medium) were mixed with an equal volume of a lysis solution containing 1% Triton X-100 (Sigma) and 0.1 M citric acid (Sigma) in deionized water and stored at 4°C for up to 1 day before analysis. Nuclei from attached cells were obtained by adding 0.5 mL of lysis solution to the well. After 10 min, solution was removed, and 0.5 mL of DPBS was added, pipetted up and down to remove any remaining nuclei, and saved for analysis. Nuclei were counted as previously described using a Guava PCA flow cytometer (Guava Technologies, Hayward, CA).[34] Viable cell counts were performed by detaching cells with 0.25% trypsin (ATCC), resuspending in 0.4% trypan blue solution (Sigma), and counting membrane-intact cells with a hemacytometer.

Differentiation of mES cells to cardiomyocytes

Differentiation. Detached undifferentiated mES cells were centrifuged, supernatant medium removed, resuspended in differentiation medium without LIF (Table 2), and diluted to 25,000 membrane-intact cells/mL. Single 20-μL drops of this cell suspension were placed on the inside surface of the lids of 10 × 10 cm Petri dishes (Becton Dickinson) using an 8-channel pipette. The lids were inverted and placed onto dish bottoms filled with 15 mL of (37°C) solution containing 75% DPBS, 25% water, and 0.002% (w/v) type A gelatin. After 2 days, the resulting EBs were manually pipetted off the lids using wide-orifice tips (Molecular BioProducts, San Diego, CA) and placed in wells with a fibronectin-coated bottom consisting of either polystyrene, a silicone rubber membrane, or a silicone rubber membrane on top of polystyrene. Exactly thirty EBs were placed in each well, and

medium was mixed by pipetting to distribute EBs uniformly across the bottom. EBs attached and spread within one day of transfer to silicone rubber. Medium was removed 48 hr after transfer and replaced with 1 mL of fresh differentiation medium. After 1 day, medium was replaced with 1 mL of serum-free differentiation medium (Table 3), which was exchanged daily for the next 4 days.

Cell Processing for Nuclei Counts and Flow Cytometry. Medium was removed from each well, attached cells were washed with DPBS, and 200 μL of trypsin solution was added. After 5 min at 37°C, 800 μL of differentiation medium was added, and the contents were vigorously pipetted up and down using a 1-mL pipette to dislodge and disperse the cells, which were transferred to a 1 mL tube and allowed to settle for 2 min. The bottom 50 μL, which contained any remaining large clumps of cells and extra-cellular matrix, was removed and discarded (or saved for later analysis). The cell sample was mixed by vortexing, and an aliquot saved for nuclei counting. The remaining cell sample was centrifuged, and the supernatant, discarded. Cells were resuspended in 750 μL DPBS, 250 μL of 4% (w/v) paraformaldehyde (Alfa Aesar, Ward Hill, MA) in DPBS was added to fix the cells, and each sample was incubated for 20 min at room temperature. Samples were then centrifuged, supernatant removed, and 1 mL of DPBS added. Samples of nuclei and of fixed cells were stored at 4°C before analysis.

Flow Cytometry. Samples containing 3×10^5 fixed cells were incubated for 10 min with an equal volume of 1% (w/v) saponin to permeabilize cell membranes, washed, and resuspended in 50 μL of 2% (v/v) fetal bovine serum (FBS, ATCC) in PBS for 30 min, then 5 μL of antisarcomeric myosin heavy chain antibody (MF-20, MF-20 supernatant, Developmental Studies Hybridoma Bank, Iowa City, IA) was added. Samples were incubated for 1 hr, 0.5 mL of 2% FBS solution was added to each tube, and the samples centrifuged. Supernatant was discarded, and the cells resuspended in 50 μL of goat anti-mouse PE-conjugated secondary antibody (Jackson ImmunoResearch, West Grove, PA) diluted 1:250 in 2% FBS. Samples were incubated 30 min in the dark, washed twice with 0.5 mL of PBS, and fluorescence intensity data were acquired using the Guava PCA flow cytometer with the Express software module.

Semiquantification of Spontaneously Contracting Areas. The fractional area of each well containing spontaneously-contracting cells was estimated by visual observation. The average beating area of fifteen random 2 mm^2 circles in each well was taken to be the fraction of beating cells for that well.

Cell Processing for Histology. Nine days after plating EBs, medium was removed from wells, and cells were washed with DPBS and incubated for 30 min with 4% (w/v) paraformaldehyde. After washing twice with 1 mL of DPBS, the sheet of cells was released from the well bottom by stretching the silicone rubber membrane and transferred into a 1.5 mL microtube. Each tube was centrifuged at 300g, all but 100 μL of the DPBS was removed, and 900 μL of 1% (w/v) agarose (Life Technologies, Gaithersburg, MD) in deionized water at 95°C was added and mixed by vortexing. Samples were centrifuged for 1 min at 20,000g, cooled for 1 hr at 4°C, and 500 μL of 4% (w/v) paraformaldehyde was added to the tubes, which were stored overnight. Agarose was removed from the tube the following day and trimmed with a razor blade so that only the pellet and a small additional amount of agarose remained. Pellets were placed in histology cassettes and embedded in paraffin. Five micrometer sections were cut, deparaffinized, and rehydrated by two 7-min rinses with xylene, two 5-min rinses with 100% ethanol, a 3-min rinse with 95% ethanol, a 10-min rinse with 70% ethanol, and two 5-min rinses with deionized water. Sections were stained by incubating for 15 sec in filtered hematoxylin (Sigma), followed by three washes in 30 mM sodium borate (EMD, Gibbstown, NJ), then dehydrated following the reverse procedure for rehydration and preserved using Permount (Fisher Chemical, FairLawn, NJ).

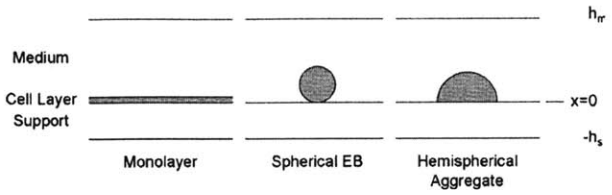

Figure 1. Schematic diagram (not to scale) of the geometries examined with theoretical models. Cells are cultured in the form of a monolayer (assumed to have negligible thickness), a spherical EB, or as cellular aggregates on a support surface of thickness h_s and overlain by medium of thickness h_m.

Both the top and bottom of the culture vessels are exposed to the incubator atmosphere.

Theory

Mathematical models were developed to estimate pO_{2cell} for (1) a monolayer of cells, common for undifferentiated cells, and (2) cells that have combined into three-dimensional aggregates, typical of cells undergoing differentiation (Figure 1). We used $c_i = \alpha_i pO_2$, where c is oxygen concentration, α is the Bunsen solubility coefficient, and i denotes the phase. OCR was assumed to depend on the local pO_2 according to Michaelis-Menten kinetics,

$$V = \frac{V_{max} pO_{2cell}}{K_m + pO_{2cell}} \tag{1}$$

where V_{max} is the maximal OCR (amol/cell sec), and K_m is the Michaelis constant, taken to be 0.44 mm Hg.[35] We previously measured V_{max} of undifferentiated CCE mouse mES cells that had been cultured at various pO_{2gas} from 0 to 285 mm Hg for a day or more[34] under conditions such that the difference between pO_{2gas} and pO_{2cell} was small. Data were fitted to a hyperbolic expression of the form

$$V_{max} = V_{max,0} + (V_{max,\infty} - V_{max,0})\left(\frac{pO_2}{K_v + pO_2}\right) \tag{2}$$

where $V_{max,0} = 10 \pm 2$ and $V_{max,\infty} = 30 \pm 2$ amol/cell sec, and the fitting constant $K_v = 16 \pm 1$ mm Hg. Preliminary measurements with EBs after two days culture and with tissue differentiated for 10 days,[36] both with J1 cells, gave results that were similar to those obtained with undifferentiated CCE cells. For analysis related to mES cells, the OCR as a function of local pO_2 was taken as the product of Eqs. 1 and 2 using the same parameters.

Cell Monolayer. We assume the cells are uniformly distributed on the surface at a density for which a one-

dimensional approximation in the medium is valid.[37] At steady state, the rate of oxygen consumption by the cells is balanced by the sum of the rates of oxygen diffusion through the stagnant medium and support layer:

$$\left(\frac{D_m\alpha_m}{h_m}+\frac{D_s\alpha_s}{h_s}\right)\left(pO_{2gas}-pO_{2cell}\right)=\rho V \qquad (3)$$

where D_i and α_i are oxygen diffusion coefficient and solubility in phase i, respectively, h_i is thickness of phase i, ρ is cell surface density, and subscripts m and s refer to medium and support layer phases, respectively. For all calculations, h_s was taken to be actual or typical values (Table 1).

If V is represented by the product of Eqs. 1 and 2, and all variables are made dimensionless, Eq. 3 becomes

$$(1-\theta)=\left[F_V+(1-F_V)\left(\frac{\theta}{\beta_V+\theta}\right)\right]\left(\frac{\theta}{\beta_M+\theta}\right)f(Da) \qquad (4)$$

where

$$f(Da)=\left(\frac{1}{Da_m}+\frac{1}{Da_s}\right)^{-1} \qquad (5)$$

and $\theta = pO_{2cell}/pO_{2gas}$, $F_V = V_{max,0}/V_{max,\infty}$, $\beta_V = K_V/pO_{2gas}$, $\beta_M = K_M/pO_{2gas}$, and $Da_i = \rho V_{max,\infty}h_i/D_i\alpha_i pO_{2gas}$, which is a Damköhler number of the second kind for phase i. If the support is impermeable ($1/Da_s = 0$), $f(Da)$ reduces to Da_m. Equation 4 applies to the most general situation, and is solved implicity for θ as a function of the dependent variables. In addition, there are several simpler cases of interest (Table 4).[38]

The transient response of pO_2 at the support-medium interface following a step change in pO_{2gas} for the situation with no cells present was examined by solving the species conservation equations for the idealized situation of a one-dimensional composite slab with equality of pO_2 and oxygen flux in each layer at the interface and pO_{2gas} specified at both external boundaries. The finite element package COMSOL Multiphysics (COMSOL, Burlington, MA) was used; an analytical solution is also available.[39]

Cell Aggregates. Steady state oxygen transport within the medium, supporter layer, and cell aggregate was modeled using the oxygen species conservation equation

$$D_i\alpha_i\nabla^2 pO_2=\frac{V_i}{v_{cell}} \qquad (11)$$

where V_i is OCR of the cell aggregate and is zero elsewhere. The boundary conditions for the model were $pO_2 = pO_{2gas}$ at the gas/liquid and gas/support interfaces, and continuity of flux and pO_2 at the support/medium, support/tissue, and medium/tissue interfaces. The conservation equations and boundary conditions were solved by the finite element method (COMSOL Multiphysics).

v_{cell}, the specific volume of a cell estimated from light microscopic measurements of EB diameters with a calibrated reticule and nuclei counts from dispersed EBs, was 10.1 ± 1.1, 11.2 ± 1.4, and 12.7 ± 1.5 × 10^{-10} cm^3/cell for day 2 EBs at pO_{2gas} of 7, 36, and 142 mm Hg, respectively. Regions of the 5-μm thick histological sections encompassing aggregated cells were examined by light microscopy, and the number of nuclei whose center point was within the volume of tissue contained in the region was estimated. Assuming that the nuclei were spheres with a diameter of 7 μm, v_{cell} was estimated to be 15 ± 4, 14 ± 6, and 14 ± 7 × 10^{-10} cm^3 for cells cultured for 11 days at pO_{2gas} of 7, 36, and 142 mm Hg, respectively. Cell size varied significantly within different regions of the tissue, and this heterogeneity was not considered in the models. Additional details are available.[36]

Geometry Used for Finite Element Model. The day 2 EB was modeled as a sphere of radius 99, 115, and 114 μm for pO_{2gas} of 7, 36, and 142 mm Hg, respectively, resting on the surface of a silicone rubber membrane, h_s = 127 μm, and with h_m = 5 mm. Each EB sphere or aggregate was modeled as being in the center of a cylindrical well with a 1.5 mm radius. Parameters for day 11 aggregates were obtained using light microscopy and stereological point counting[40] of at least 300 points in the 5-μm tissue sections from three independent experiments, such as the one shown in Figure 2. The volume fraction of tissue that was present in aggregate and sheet-like morphologies was determined. Aggregates accounted for 53, 75, and 90% of the total tissue volume for cells cultured at pO_{2gas} of 7, 36, and 142 mm Hg, respectively. Sheets were modeled as a thin slab with a thickness of 15 μm. The distance from the basal to apical surface (tissue thickness) and the length of each aggregate was recorded, and results are summarized in Table 5. Each aggregate was approximated as an oblate hemispheroid with major and minor axes that corresponded to the measured height and half width, respectively.

Distribution of pO_2 in Tissue. The numerical solution of Eq. 11 yielded the distribution of pO_2 throughout each of the individual spherical hemispheroidal and planar tissue geometries analyzed. For each geometry simulated, surfaces of constant pO_2 were determined, from which contours were plotted. In addition, numerical integration was performed to determine the volume of tissue between the surfaces of constant pO_2. For the average contribution of aggregates and sheets in an actual culture dish as determined from the 5-μm sections, the volume fraction of tissue within specific limits of pO_2 was determined from

$$\Phi_{ab}=\left[(\phi_{sheet})(\Phi_{ab,sheet})\right]+\phi_{aggregate}\frac{\sum_{j=1}^{n}V_{ab,j}}{V_{aggregate,n}} \qquad (12)$$

where Φ_{ab} is the total volume fraction with a pO_2 between a and b, $\Phi_{ab,sheet}$ is the comparable quantity for the tissue in the cell sheet, ϕ_{sheet} and $\phi_{aggregate}$ are the volume fractions of tissue in the total preparation in the sheet and aggregate geometry, respectively, $V_{ab,j}$ is the volume of tissue with a pO_2 between a and b in the jth aggregate of cells, and $V_{aggregate,n}$ is the total volume of the n aggregates analyzed.

Statistics

Statistical comparisons of data were preformed using unpaired t-tests. Results were deemed significant if the two-tailed P-value was 0.05 or less.

Results

Theoretical comparison of materials for monolayer culture

Steady State. The effect of oxygen diffusion limitations in the medium and the support layers on pO_{2cell} relative to

Table 4. Solutions to Estimate pO_{2cell} in Cell Monolayer

Case	Limits	Expression	Equations
Eq. 2: pO_2-dependent V_{max} Eq. 1: Michaelis-Menten kinetics		$(1-\theta)=\left[F_V+(1-F_V)\left(\frac{\theta}{\beta_V+\theta}\right)\right]\left(\frac{\theta}{\beta_M+\theta}\right)f(Da)$	(4)
Eq. 2: Constant V_{max} Eq. 1: Michaelis-Menten kinetics		$\theta=-\frac{1}{2}\left\{(\beta_M+f(Da)-1)+\left[(\beta_M+f(Da)-1)^2+4\beta_M\right]^{\frac{1}{2}}\right\}$	(6)[a]
	Zero order $\beta_M \ll \theta$	$\theta=1-f(Da)$	(7)
	First order $\beta_M \gg \theta$	$\theta=\frac{\beta_M}{f(Da)+\beta_M}$	(8)
Eq. 2: pO_2-dependent V_{max} Eq. 1: Zero order kinetics		$\theta=-\frac{1}{2}\left\{(\beta_V+f(Da)-1)+\left[(\beta_V+f(Da)-1)^2+4\beta_V(f(Da)f_V-1)\right]^{\frac{1}{2}}\right\}$	(9)
	Zero order $\beta_V \ll \theta$	$\theta=1-f(Da)$	(7)
	First order $\beta_V \gg \theta$	$\theta=\beta_V\frac{1-F_Vf(Da)}{1+(1-F_V)f(Da)}$	(10)

[a] The solution for this case with $Da_s = 0$ and $f(Da) = Da_m$ was previously described.[38]

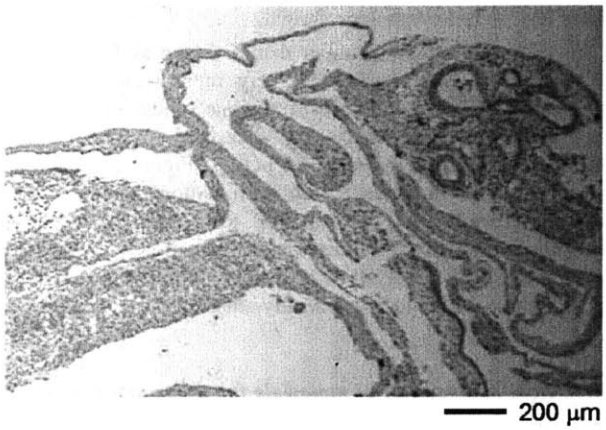

Figure 2. Representative hematoxylin-stained histological section used to estimate tissue geometry of cell aggregates for numerical solution of oxygen species conservation equation, Eq. 11.

This section shown is from tissue cultured at a pO_{2gas} of 36 mm Hg.

Table 5. Data from Sections Used for Finite Element Models

	pO_{2gas} (mm Hg)		
	7	36	142
Number of aggregates analyzed	21	19	12
Fraction of tissue in aggregates (%)	53	75	90
Aggregate height (μm)			
Mean	120	190	280
Std Dev	60	100	150
Aggregate width (μm)			
Mean	450	630	590
Std Dev	290	320	370

5-μm tissue sections from three experiments were analyzed to obtain morphology estimates that could be used in finite element models. Stereological point counting was performed to determine the volume fraction of tissue that was present in aggregates and in cell sheets. The height of each aggregate was measured as the distance from its basal to apical surface using a calibrated reticule, and the length was measured in a similar manner. The basal surface was determined by the shape of the aggregate and the surface which was continuous with the cell sheet.

pO_{2gas} is shown in Figure 3 for three values of pO_{2gas}. Da for each phase increases with increasing cell density, maximal V, and height and with decreasing oxygen diffusivity and solubility and pO_{2gas}. As Da of either phase increases, Da^{-1} decreases, $f(Da)$ increases, and the ratio $\theta = pO_{2cell}/pO_{2gas}$ decreases. The various cases begin to diverge from each other for a $f(Da)$ in the range of about 0.1–0.4 The most general case, Eq. 4, which includes both Michaelis-Menten kinetics and pO_2-dependent V_{max}, drops most slowly because it entails the largest decrease in V with decreasing pO_2. If V_{max} is constant, Eq. 6, the curve has similar shape but lower magnitude than Eq. 4. For both cases, if Michaelis-Menten is replaced by zero order kinetics, Eqs. 7 and 9, the curves drop precipitously as θ approaches zero. Equation 7 represents global zero-order kinetics.

The rates of oxygen diffusion through the medium and support relative to the rate of oxygen consumption is embodied in the function $f(Da)$, which depends on the individual Da of each phase. The phase-dependent properties are summarized by the group $D_i\alpha_i/h_i$ (the inverse of the

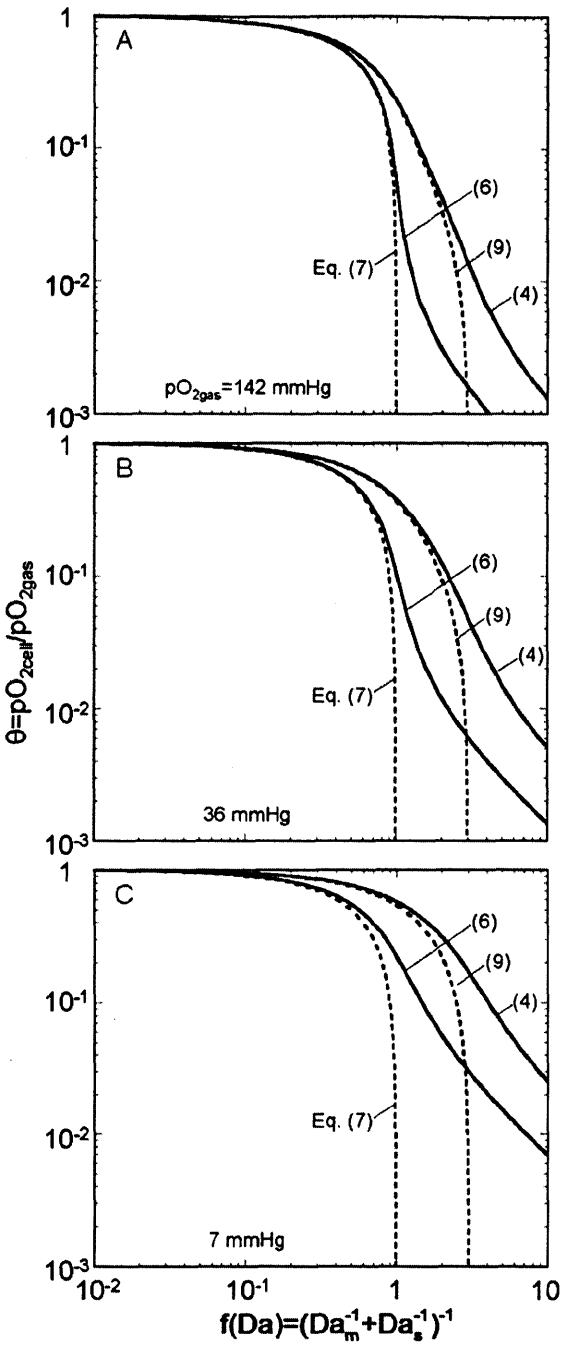

Figure 3. Steady-state reduction in pO_{2cell} relative to pO_{2gas} as a result of oxygen diffusion limitations in the support layer (s) and the medium (m) for cells in a monolayer.

θ is plotted as a function of f(Da), defined by Eq. 5, for fixed values of parameters $F_V = 1/3$, $k_V = 16$ mm Hg, $k_M = 0.44$ mm Hg at different values of pO_{2gas}, (A) 142 mm Hg, $\beta_V = 0.113$, $\beta_M = 3.1 \times 10^{-3}$; (B) 36 mm Hg, $\beta_V = 0.444$, $\beta_M = 0.012$; (C) 7 mm Hg, $\beta_V = 2.29$, $\beta_M = 0.063$. Equation numbers refer to equations in Table 4.

mass transfer resistance), which are tabulated in Table 1 together with their value relative to that of the medium. Because of its low permeability and large thickness, $D_P\alpha_P/h_P$ for polystyrene is on the order of 10^2 lower than the value for medium, oxygen is supplied almost exclusively by diffusion through the medium, and f(Da) is large, typically well in excess of 1, which is associated with low values of θ (Figure 3). The mass transfer resistances of FEP is comparable to that of medium, and f(Da) is of the order of 1. The most permeable material is silicone rubber, and $D_P\alpha_P/h_P$ is about 10^2 higher than medium. Consequently, f(Da) is typically less than 10^{-1} and θ is close to 1, so that virtually all of the oxygen is supplied by diffusion through the membrane.

The effects of the different support materials in determining actual values of pO_{2cell} calculated from Eqs. 4 or 6 are shown in Figure 4 as a function of cell density for medium heights ranging from 1 to 5 mm. Panels A, B, and C on the left apply to the OCR parameters of CCE mES cells[34] for which V_{max} decreases with pO_{2cell}; panels D, E, and F on the right are illustrative of typical adult mammalian cells, which have a higher V_{max} that is independent of pO_{2cell} and leads to even greater effects of oxygen diffusion limitations.[41] Predicted values of pO_{2cell} are very sensitive to medium height and cell surface density for culture on polystyrene, less so for FEP copolymer, and virtually not at all with silicone rubber if realistically large medium heights are used.

Transient Response. The predicted response of pO_2 at the medium-support interface of an idealized one-dimension system following a step change in pO_{2gas} was determined for each of the three support materials (Figure 5A). The equilibration time was quite long on a polystyrene dish and was highly dependent on the medium height: approximately 1, 4, and 25 $\times$ 10^3 sec were required to reach 90% of the steady state value at medium depths of 1, 2, and 5 mm, respectively, in a polystyrene dish. The time required was about 100 and 500 sec at depths of 1 and 5 mm, respectively, on an FEP-teflon membrane, and about 10 seconds in a silicone rubber dish with any medium height.

To verify that silicone rubber dishes set up as for normal cell culture reached steady-state very rapidly compared to polystyrene, pO_2 at the surface of silicone rubber membrane-based and polystyrene dishes was measured in an acellular system in response to a change in pO_{2gas} (Figure 5B) with a fiberoptic sensor in contact with each bottom surface. The incubator changed pO_{2gas} from 160 to 7 mm Hg in ~15 min; pO_2 at the silicone rubber surface lagged pO_{2gas} by several minutes. The polystyrene dish required significantly longer time, ~20 hr, to reach steady-state.

Theoretical comparison of materials for aggregate culture

In order to explore the relationships between oxygen diffusion in the medium, tissue, and different support materials, the pO_2 profile within wells containing hypothetical 100-μm radius hemispherical cell aggregates spaced 1 mm apart (2.3 $\times$ 10^5 cell/cm^2) was calculated for three different pO_{2gas} (Figure 6). In contrast to the behavior with monolayers, pO_2 varied within the aggregate. At a pO_{2gas} of 142 mm Hg (Figure 6A,B), there was a 55 mm Hg drop in pO_2 from the gas to the upper surface of the aggregate (ΔpO_{2ag}) on polystyrene dishes, which was slightly larger than the ΔpO_2 of 40 mm Hg for a cell monolayer at the same overall average density on the support. ΔpO_{2ag} was reduced to 24 and 4 mm Hg on FEP and silicone rubber membranes, respectively. The maximum pO_2 decrease within the aggregate was 45, 30, and 27 mm Hg on polystyrene, FEP and silicone rubber, respectively. The total pO_2 drop from the gas to the region of the aggregate with the lowest local pO_2 was

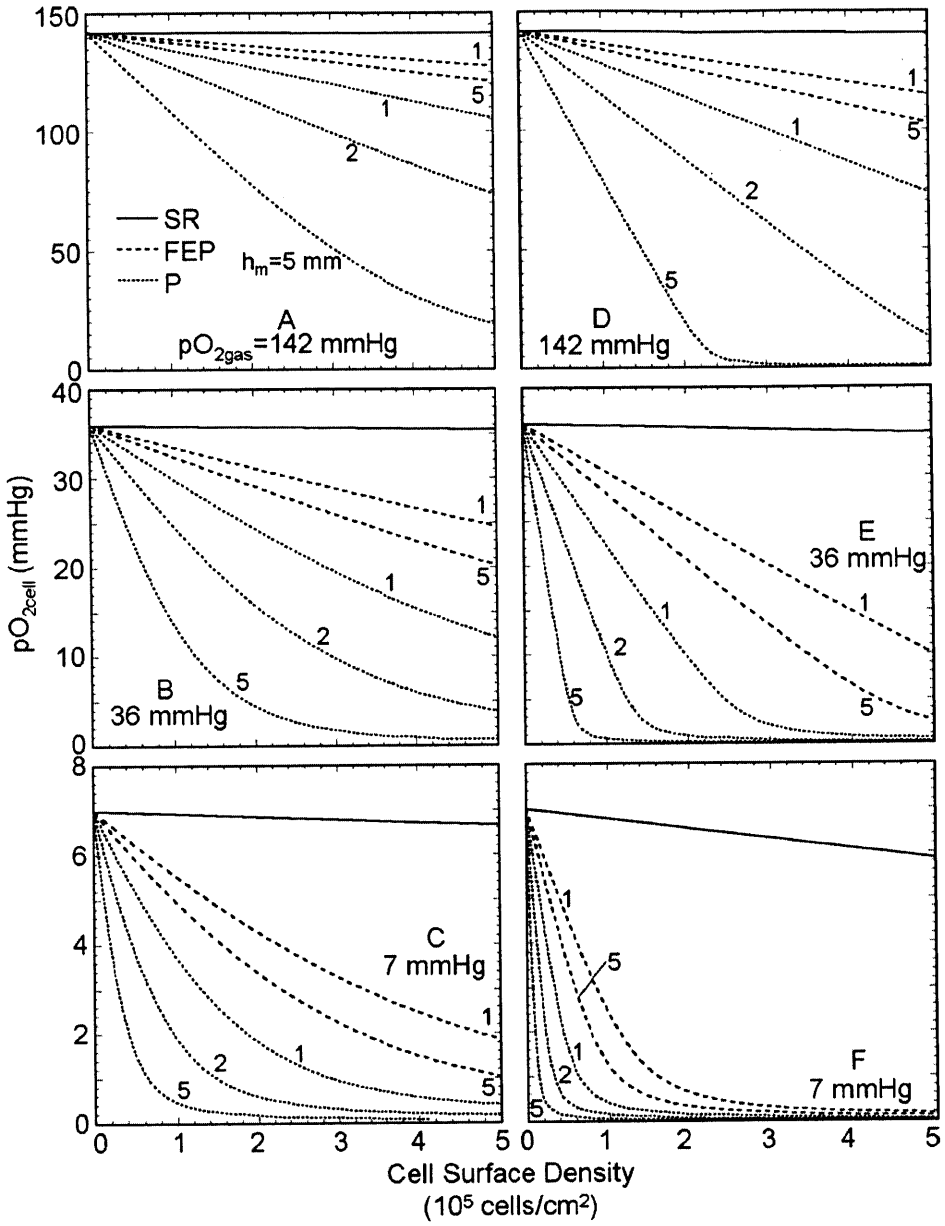

Figure 4. Predicted pO_{2cell} of cell monolayers as a function of cell density ρ and medium height h_m for culture on polystyrene (P), fluorinated ethylene-propyline copolymer (FEP) membrane, and silicone rubber (SR) membrane surfaces at pO_{2gas} of (A and D) 142, (B and E) 36, and (C and F) 7 mm Hg.

The panels on the left (A, B, and C) are for mES cells for which OCR parameters[34] are given in conjunction with Eq. 2, oxygen diffusivity and solubility parameters are from Table 1, and the pO_{2cell} was determined using Eq. 4. The panels on the right (D, E, and F) are for cells having constant V_{max} = 50 amol/sec cell, which is typical for mammalian fibroblasts.[41] pO_{2cell} was determined using Eq. 6. A single line is shown for SR because the prediction is virtually independent of h_m.

100, 54, and 31 mm Hg on polystyrene, FEP membranes, and silicone rubber membranes, respectively. When pO_{2gas} was decreased to 36 or 7 mm Hg, areas of oxygen starvation began to appear in the aggregate center. These areas were minimized by culturing on a silicone rubber membrane-based dish, but could not be eliminated because of oxygen diffusion and consumption within the aggregate itself.

Cell attachment to silicone rubber

Greater than 98% of undifferentiated mES cells were attached to uncoated polystyrene wells after a day in culture (Table 6). Coating polystyrene with fibronectin or to a lesser extent gelatin caused the cells to have a more widely spread morphology but did not affect cell proliferation (Figure 7). Cells did not attach to well bottoms made of silicone rubber that were untreated or coated with gelatin. When mES cells were placed into such wells, they formed freely floating EBs after 24 hr in culture. Exposure of the membrane to 2 μg/mL fibronectin in DPBS (or a serum-free ITS medium) for a day before addition of the cells was sufficient for attachment of 99% of the cells. There was a small but significant decrease in the total cell number on the silicone rubber treated with fibronectin relative to the polystyrene tissue culture plastic. Cells would not attach to the silicone rubber surface when

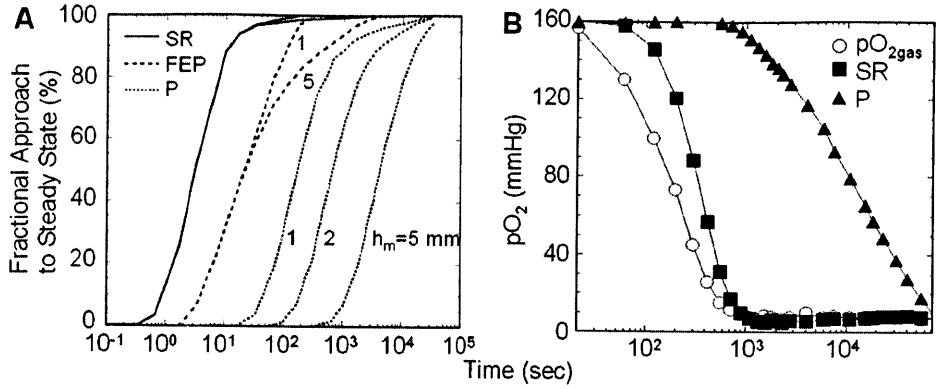

Figure 5. (A) The fractional approach of pO_2 at the medium-support interface to steady state after a step change in pO_{2gas} as estimated using numerical simulations in a cell-free system with a polystyrene (P), fluorinated ethylene-propylene copolymer (FEP), and silicone rubber (SR) bottom. Numbers refer to medium height in mm. A single line is shown for SR because the prediction is virtually independent of h_m. (B) Transient response of the pO_2 measured with a fiberoptic sensor in contact with the culture surface in acellular SR and P wells of a 24-well plate filled with 2 mL DBPS (h_m = 10.5 mm) following a change in pO_{2gas} setting from 160 to 7 mm Hg.

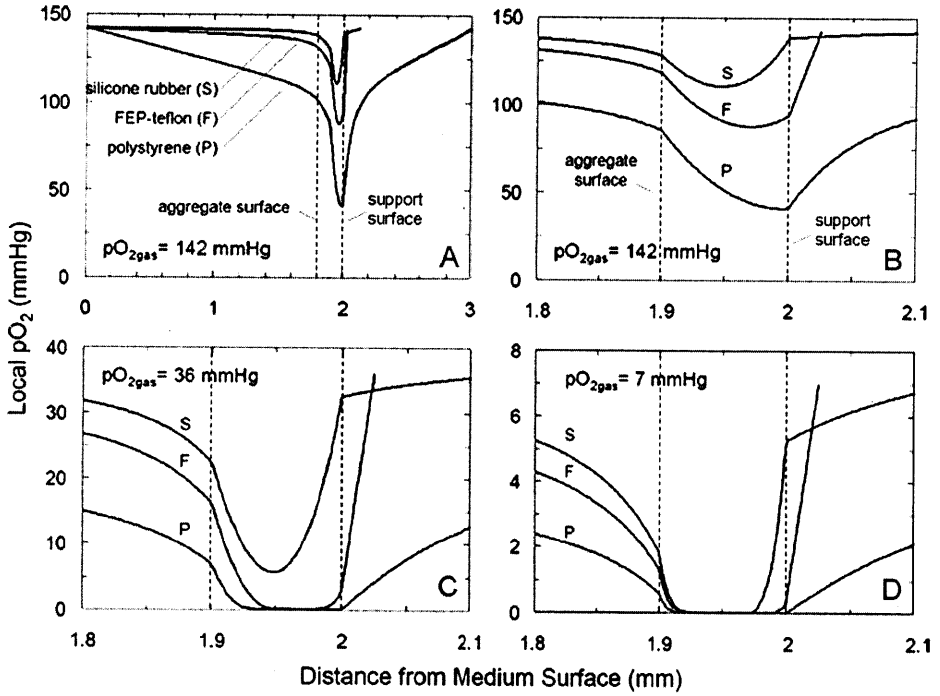

Figure 6. Theoretical predictions for pO_2 profiles within wells containing hypothetical 100-μm radius hemispherical aggregates spaced 1 mm apart (overall average on support 2.3 × 10^5 cell/cm^2) on polystyrene, FEP membranes, or silicone rubber membranes at the bottom for pO_{2gas} of 142, 36, and 7 mm Hg.

The pO_2 profile shown is on a line passing through the center of an aggregate and perpendicular to the bottom of the well. The dashed lines on the plots indicate the locations of the upper and lower aggregate surfaces. Panel (A) shows the entire distance from the top of the medium to the bottom of the culture vessel, (B), (C), and (D) are expanded to show regions within 100 μm of the top and bottom surfaces of the aggregate. Distances greater than 2 mm represent areas within the support, and the plotted lines showing the local pO_2 profiles terminate at the lower surface of the culture vessel, the location of which is different for each of the three different support materials. Parameters used in the calculations are for mES cells.

the 2 μg/mL fibronectin solution was made in DMEM with 10% FBS (data not shown). This may have resulted from competitive adsorption of other serum proteins onto the silicone surface, which limited fibronectin adsorption. Additionally, poor cell attachment was observed when cells were cultured in mES cell differentiation medium (Table 2) with 2% instead of 10% FBS, which could be rectified by absorbing Matrigel instead of fibronectin (data not shown).

Deposition of a $(PSS\text{-}PEI)_4$-$(PDL\text{-}gelatin)_3$ PEM onto silicone rubber before cell addition could be used to promote cell adhesion (Table 6). Cells adhered better to silicone rubber with a PEM than they did to unmodified silicone, but the total number of attached cells was lower on PEM-treated silicone rubber than any of the polystyrene surfaces tested. The PEM–gelatin structures did not support attachment as well as the single layer of fibronectin adsorbed

Table 6. Cell Attachment to Polystyrene and Modified Silicone Rubber Surfaces

Surface Treatment	Cell Number (% of Total on Polystyrene)			Fraction Attached (%)
	Total	Attached	Suspension	
Tissue culture polystyrene				
Unmodified[a]	100 ± 7	98 ± 7	1.7 ± 0.5	98
Gelatin A[a]	95 ± 5	95 ± 5	0.88 ± 0.07	99
Gelatin B	98 ± 2	97 ± 2	1.2 ± 0.1	99
Fibronectin[a]	110 ± 16	109 ± 16	1.0 ± 0.1	99
Silicone rubber				
Untreated[a]	69 ± 9	39 ± 18	29 ± 11	57
Gelatin A only[a]	71 ± 0	46 ± 3	24 ± 3	66
Fibronectin only[a]	91 ± 1	90 ± 1	0.8 ± 0.5	99
PEM–gelatin A	88 ± 14	85 ± 14	3.2 ± 0.4	96
PEM–gelatin B	80 ± 5	76 ± 5	3.4 ± 0.2	96
PEM–fibronectin	64 ± 5	61 ± 5	2.0 ± 0.5	97

Approximately 2×10^5 viable cells were placed into each well of a 24-well plate and cultured for about 24 hr before assessing cell attachment. Data are from two separate experiments each with an untreated polystyrene control condition. Results are reported as the mean ± SD for triplicate wells for each condition, and are normalized to the total cell number in the untreated polystyrene control for the experiment from which the data were taken.

[a] Conditions shown in Figure 7.

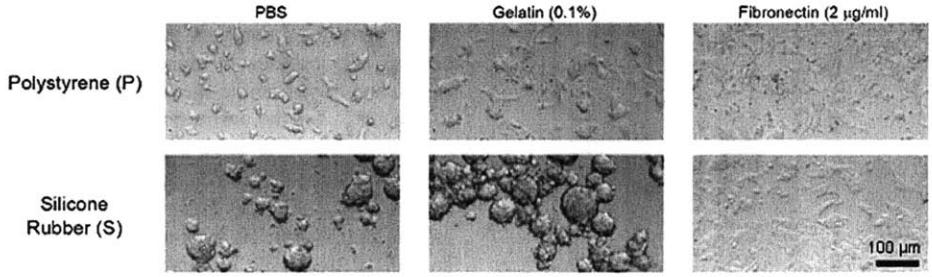

Figure 7. Adhesion of mES cells to polystyrene and silicone rubber in their native states or after incubation with PBS, 0.1% gelatin in water, or 2 μg/mL fibronectin in PBS for 24 hr before cell addition.

onto silicone rubber. Other modifications of the PEM method to examine the use of fewer layers were also tested with results comparable to those shown in Table 6 (data not shown).

Differentiation to cardiomyocytes on silicone rubber and polystyrene surfaces

Differentiation of mES cells to cardiomyocytes is an oxygen-sensitive cell culture process. We investigated if culture on gas-permeable (silicone rubber) or gas-impermeable (polystyrene alone and silicone rubber membrane glued with silicone adhesive on top of polystyrene) surfaces would lead to different results, since the cells would be exposed to different pO_{2cell}. A comparison of the results of differentiation of mES cells into cardiomyocytes for 11 days is shown in Figure 8. The fraction of cells that were positively immunostained with MF-20, a marker of cardiomyocytes, total cell number, and total MF-20+ cell number after 11 days of differentiation were each affected by pO_{2gas} differently when using wells with gas-permeable or gas-impermeable bottoms. For each of these parameters, it did not matter if the gas-impermeable bottom was silicone rubber on top of polystyrene or simply polystyrene. The fraction of MF-20+ cells was higher at 7 mm Hg, the same at 36, and lower at 142 mm Hg on pO_{2gas} for cells on gas-permeable relative compared to gas-impermeable dishes. There were significantly fewer cells on the gas-impermeable dishes relative to the gas permeable dishes at pO_{2gas} of 36 or 142 mm Hg, and the cells also adopted a much more widely spread morphology on the polystyrene dishes compared to the silicone rubber membranes (not shown). The highest number of cardiomyocyte-like cells was obtained at a pO_{2gas} of 36 mm Hg on gas-permeable dishes, a factor of 2–3 higher than all other pO_{2gas} and substrate conditions, while on gas-impermeable dishes, the highest number of cardiomyocyte-like cells was at a pO_{2gas} of 142 mm Hg.

To illustrate the difference in pO_{2cell} between the gas-permeable and gas-impermeable substrates, approximate estimates of pO_{2cell} were calculated using Eq. 4 by assuming that all of the attached cells measured at each condition were distributed in a uniform layer (Table 7). Culture on gas-permeable silicone rubber resulted in values of pO_{2cell} within 2 mm Hg of pO_{2gas}. In contrast, culture on the gas-impermeable substrates resulted in very small values of pO_{2cell} (<1 mm Hg) at all pO_{2gas}. pO_{2cell} was slightly higher for cells on silicone rubber on polystyrene compared to polystyrene alone because of slightly higher numbers of attached cells for the latter case.

Spontaneous contraction was not observed at any pO_{2gas} condition on polystyrene in multiple experiments (Table 8), even though cells stained positive with MF-20. Contractions were observed on silicone rubber membranes alone and on silicone rubber on top of polystyrene. The largest fractional area of beating cells occurred on silicone rubber alone at a pO_{2gas} of 36 mmHg, and the smallest was on silicone rubber on top of polystyrene at 7 mm Hg. Although there was substantial variation between beating area assessments, with biological replicates at the same condition, the average fraction of the entire well area covered by spontaneously contracting

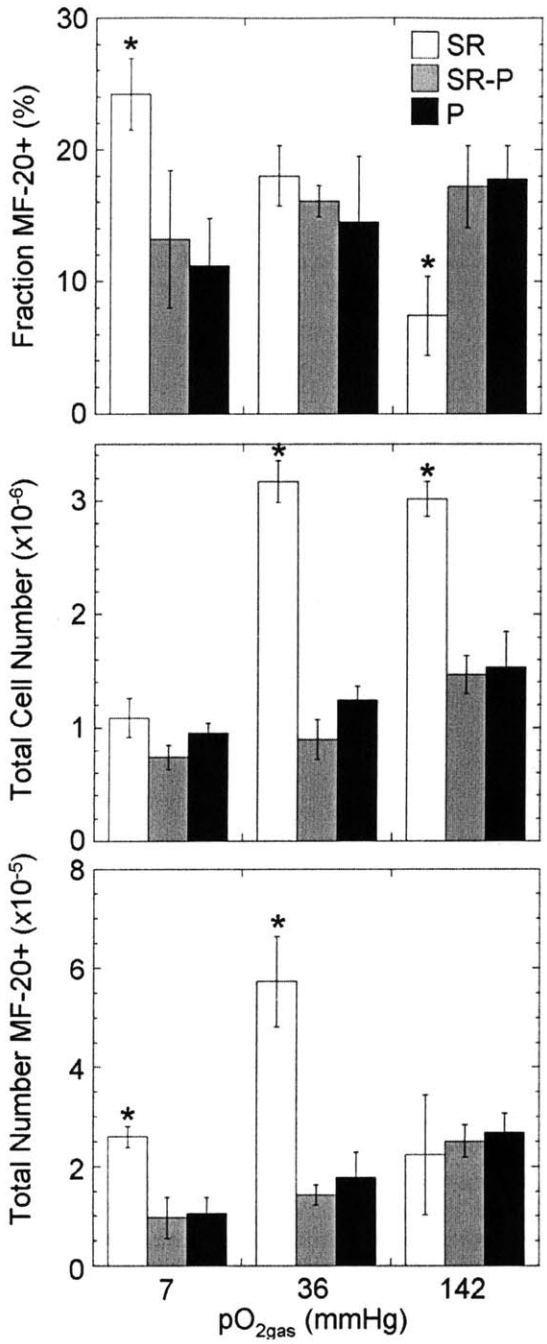

Figure 8. Differentiation in wells with silicone rubber membranes or polystyrene at the bottom. Fraction of cells that were MF-20+ (top), total number of cells (middle), and total number of MF-20+ cells (bottom) for cells cultured at constant pO_{2gas} conditions of 7, 36, or 142 mm Hg for 11 days in wells with the bottom comprised of silicone rubber membrane (SR, white bars), silicone rubber membrane on top of polystyrene (SR-P, gray bars), and polystyrene (P, black bars).

All culture surfaces were coated with fibronectin. The number fraction of MF-20+ cells was determined by flow cytometry of trypsin-dispersed cell samples. Data presented were obtained with silicone rubber glued to polystyrene with silicone adhesives. Essentially identical data was obstained when no adhesive was used. All experiments were started with 30 EBs/well (0.15×10^5 cells/well). Data are shown as mean ± SD for four replicate wells in a single experiment. * indicates statistical difference ($P < 0.05$) between value on SR compared to P and SR-P at the same pO_{2gas}.

cells correlated linearly ($R^2 = 0.90$) with flow cytometric measurements of cells immunostained with MF-20 (Figure 9).

pO_{2cell} during cardiomyocyte differentiation on silicone rubber membranes

After 2 days in hanging drops, the differentiating cells were in the form of spherical EBs of radius about 100 μm and the predicted oxygen gradients were relatively small. At times later than 2 days, the EBs were allowed to attach the fibronectin-coated silicone rubber surface. The cells spread and further proliferated on the silicone rubber membrane; the idealized spherical geometry was lost, and approximations of aggregate shapes were used in the model based on measurements from sectioned tissue (Figure 2). Cells cultured at a high pO_{2gas} grew to form larger aggregates, with a mean height after 11 days in culture of 120, 190, and 280 μm at pO_{2gas} of 7, 36, and 142 mm Hg, respectively (Table 5). The axially-symmetric three-dimensional pO_{2cell} distribution within the aggregates having mean dimensions tabulated in Table 5 was obtained by numerical solution of Eq. 11, from which the pO_{2cell} contours in Figure 10 were evaluated. Calculated pO_2 profiles in sheet-like tissue and all aggregates were used to determine the volumetric distribution of pO_{2cell} in Figure 11 for the entire tissue mass at each condition.

In spherical EBs after 2 days culture, about 60% of the tissue was exposed to pO_{2cell} less than 1 mm Hg during culture at pO_{2gas} of 7 mm Hg, whereas more than 80% of tissue cultured at 36 mm Hg was at pO_{2cell} greater than 7 mm Hg, and all of the tissue cultured at 142 mm Hg was at pO_{2cell} greater than 94 mm Hg (Figure 11). After 11 days of culture, about 28%, 26%, and 15% of the total volume of tissue was at a pO_{2cell} of less than the K_m for oxygen consumption (0.44 mmHg) at 7, 36, and 142 mmHg, respectively. However, a large portion of the tissue remained at a pO_{2cell} that was relatively near that of the gas phase (Figures 10 and 11). In contrast, if aggregates with similar dimensions and cell numbers had been cultured on a polystyrene dish at 142 mm Hg, ~80% of the aggregate volume would have been at a pO_{2cell} less than 0.44 mm Hg. Oxygen effects would therefore have been impossible to accurately study on polystyrene, because all pO_{2gas} conditions would have had extreme oxygen starvation.

Discussion

We studied silicone rubber membrane as a support for the precise control of the pO_{2cell} during culture with cell monolayers and aggregates and the extent to which it is an improvement on existing polystyrene- and FEP membrane-based dishes. We also investigated surface modifications to promote cell attachment to the silicone rubber surface, and these membranes were then used to study the effect of pO_2 on mES cell differentiation into cardiomyocytes.

Predictions of a theoretical model show that membrane-based culture dishes can dramatically improve the control of pO_{2cell} in static culture and are consistent with previous work.[6,11] FEP membranes and silicone rubber have not previously been compared, nor has the reduction in response time after a change in pO_{2gas} been examined. The differences between silicone rubber and FEP are of practical significance because the only commercially available membrane-based dish is constructed of FEP. Our results show that this dish is a significant improvement over polystyrene, but it is

Table 7. Calculation of pO_{2cell} for Day 11 Differentiated mES Cells

Material	pO_{2gas} (mm Hg)	Cell Density (10^5 cells/cm^2)	pO_{2cell} (mm Hg)[a]	$pO_{2gas} - pO_{2cell}$ (mm Hg)
P	142	7.7	0.830	141
	36	6.2	0.125	35.9
	7	4.8	0.027	6.97
SR-P	142	7.3	0.921	141
	36	4.5	0.193	35.8
	7	3.7	0.035	6.97
SR	142	15.1	140	1.96
	36	15.9	34.3	1.73
	7	5.4	6.62	0.377

P, polystyrene; SR-PS, silicone rubber on polystyrene; SR, silicone rubber.
[a] Calculated with Eq. 4.

Table 8. Comparison of Beating Areas on Different Culture Surfaces

Material	pO_{2gas} (mm Hg)	Fractional Beating Area (%)[a]
P	142	0
	36	0
	7	0
SR-P	142	1.7 ± 1.6
	36	2.5 ± 1.8
	7	0.8 ± 0.4
SR	142	3.3 ± 2.6
	36	9.6 ± 3.5
	7	2.6 ± 1.2

P, polystyrene; SR-P, silicone rubber on polystyrene; SR, silicone rubber, $n = 4$.
[a] Fraction of entire well area.

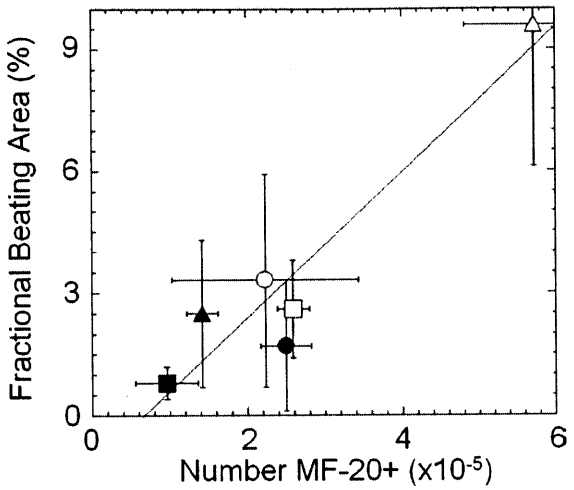

Figure 9. Beating area, expressed as a fraction of entire well area, plotted vs. the number of MF-20+ cells in the well for cells differentiated 11 days on either silicone rubber (open symbols) or silicone rubber on polystyrene (filled symbols).

Cells were differentiated at pO_2 of 7 (squares), 36 (triangles), or 142 mmHg (circles) in 24-well plates, each well having a diameter of 1.34 cm. Each symbol represents the average of four independent wells, and the line was calculated with linear regression of each averaged value ($R^2 = 0.90$).

not nearly as effective as silicone rubber for the control of pO_{2cell} (Figures 4, 5, and 6).

All cells in a monolayer cultured on a silicone rubber membrane are exposed to a value of pO_{2cell} virtually the same as pO_{2gas}. In contrast, in a thick, multicellular aggregate, pO_2 gradients are inevitable because oxygen consumed by the cells must be supplied by diffusion from the surroundings, and the magnitude of the pO_2 drop within the aggregate depends on the dimensions of the aggregate, the value of V and its dependence on pO_2, and the properties of the support. Supply of oxygen from the bottom of an aggregate by an oxygen-permeable membrane supports reduces the internal pO_2 drop (Figure 6). Silicone rubber is especially effective in this regard, because it is sufficiently permeable so that the value of pO_{2cell} at the cell-membrane interface is fixed essentially at pO_{2gas}, the highest value possible. This finding facilitates calculations of the pO_2 distribution within the aggregate (Figures 10 and 11) because it allows setting the value of pO_{2cell} at the tissue-support interface uniformly to a known value. This calculation is possible with the other supports but with much more uncertainty.

The transfer of a cell culture protocol from polystyrene dishes to FEP or silicone rubber introduces changes in cell-substrate interactions in addition to changes in cell oxygenation. A method described previously[29] using a PEM to functionalize the silicone rubber was used to promote cell attachment. Although the PEM improved cell attachment compared to native silicone rubber, the best attachment was found using simple physical adsorption of fibronectin from DPBS or serum-free medium (and of Matrigel with medium containing 2% FBS) onto the silicone rubber. The use of physical adsorption was also much easier to accomplish and required incubation of only a single solution, whereas forming a full PEM required 14 different incubation steps (with a wash between each step). We also found that incubation of the silicone rubber with fibronectin solution in PBS promoted very good cell adhesion, whereas if the fibronectin solution contained 10% FBS during the adsorption step, the subsequent cell adhesion was poor. It is not clear why others found physical adsorption of fibronectin to silicone rubber to be inefficient,[42] but it may result in part from the serum-free culture medium or protein coating solutions they used.

All fibronectin-coated wells with bottoms made of polystyrene, silicone rubber membrane, or silicone rubber membrane placed on top of polystyrene were used to study the effect of changes in pO_{2cell} on differentiation of mES cells into cardiomyocytes. These experiments were performed by forming spherical cellular aggregates in hanging drops for 2 days, then transferring them to an adherent dish for nine additional days. On gas-permeable membranes, maximal cardiomyocyte fraction occurred at the lowest pO_{2gas} condition (7 mm Hg) with decreasing fractions at 36 and 142 mm Hg, and the largest number of cardiomyocytes was obtained at a pO_{2gas} of 36 mm Hg. Culture on polystyrene, both with and without a silicone layer on top, resulted in substantially smaller numbers of cells, presumably due to oxygen limitations (Figures 6, 10, and 11), and the maximum cardiomyocyte-like cell fraction occurred at a pO_{2gas} of 142 mm Hg. There was also no increase in the total

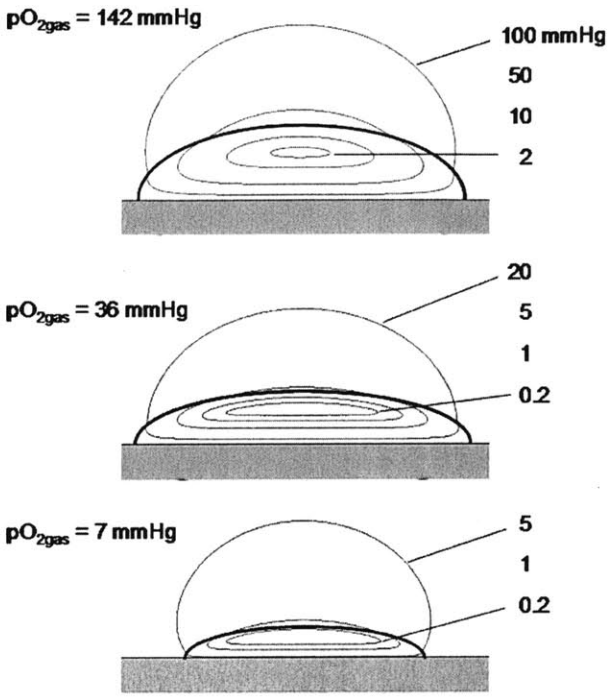

Figure 10. Predicted pO_2 profiles in day 11 differentiating aggregates cultured on gas-permeable silicone rubber membranes.

The theoretical mathematical model for oxygen consumption and diffusion in the cellular aggregates was solved numerically to yield the distribution of pO_{2cell} within tissue with heights of 120, 190, and 280 μm and radii of 450, 630, and 590 μm for pO_{2gas} of 7, 36, and 142 mm Hg, respectively. Contours of constant pO_2 are plotted for day 11 aggregates at pO_{2gas} of 142, 36, and 7 mm Hg. The numbers to the right of each shape correspond to the pO_2 values for which contour lines are plotted.

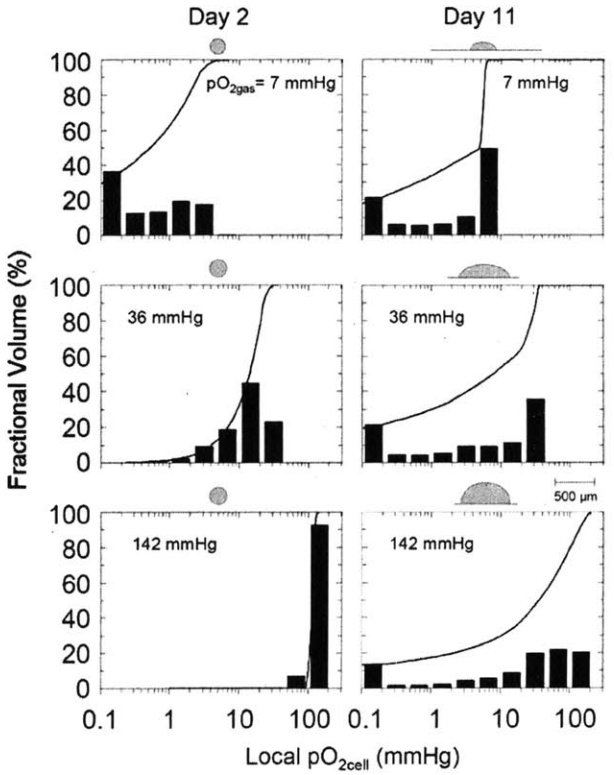

Figure 11. Volumetric distribution of pO_{2cell} within day 11 differentiating tissue.

After 2 days culture using the hanging drop method, EBs were nearly perfect spheres and were transferred to fibronectin-coated silicone rubber surfaces, to which they attached and spread. Data used to determine parameters in Table 5 was employed with the numerical model to determine the pO_{2cell} profile in each aggregate. The volume fraction of tissue exposed to specific pO_{2cell} intervals for all aggregates at each condition was estimated and combined with similar data for tissue in sheets. The line represents the cumulative volume fraction of tissue exposed to a pO_2 less than or equal to the indicated value. Each solid bar represents the fraction of the total volume of tissue that is exposed to a specific range of pO_{2cell}. These pO_{2cell} ranges span values of 1–2, 2–5, or 5–10 within each decade on a logarithmic scale.

number of cardiomyocyte-like cells in pO_{2gas} conditions less than 142 mm Hg using a gas-impermeable dish. Extensive cell contraction was observed on silicone rubber alone or on top of polystyrene, but not on polystyrene alone, for which there are at least two possible explanations: (1) the pO_2 underneath cell layers with sheets morphology (Figure 2) is higher than under adjacent aggregates, and oxygen could diffuse laterally through the silicone rubber membrane on polystyrene to raise the pO_2 under the aggregates, which contain cardiomyocyte-like cells. pO_2 affects the beating phenotype of mES cell-derived cardiomyocytes,[43] and slight differences in pO_{2cell} could explain the difference in the appearance of beating areas on polystyrene and silicone rubber on polystyrene. (2), silicone rubber is much more elastic than polystyrene, and elasticity affects the beating phenotype of embryonic cardiomyoyctes;[44] cells on more rigid substrates stop beating while cells on more elastic substrates continue to beat. This issue deserves further investigation. In this experimental system, the use of nearly gas-impermeable dishes to study oxygen effects gives misleading results as a consequence of the large differences between the pO_{2gas} and pO_{2cell}.

Our work shows that culture on silicone rubber membrane offers substantial improvements in tissue oxygenation over polystyrene and FEP membrane-based culture vessels, and that physical adsorption of fibronectin or matrigel to silicone rubber surfaces can be used to promote prolonged mES cell attachment. These findings strongly suggest that silicone rubber membrane-based dishes should be used whenever possible if oxygen is a variable of interest.

Acknowledgment

This study was supported in part by grants from the NIH (NCRR ICR U4ZPR 16606 and ROI-KD063108 OIA) and the JDRF center for Islet Transplantation at Harvard Medical School. Helpful discussions and technical assistance with aspects of the work were provided by Anna Pisania, and Jit Hin Tan (Chemical Engineering, MIT).

Literature Cited

1. Mclimans WF, Crouse EJ, Tunnah KV, Moore GE. Kinetics of gas diffusion in mammalian cell culture systems. *Biotechnol Bioeng*. 1968;10:725–740.
2. Stevens KM. Oxygen requirements for liver cells in vitro. *Nature*. 1965;206:199.
3. Metzen E, Wolff M, Fandrey J, Jelkmann W. Pericellular PO2 and O2 consumption in monolayer cell cultures. *Respir Physiol*. 1995;100:101–106.

4. Pettersen EO, Larsen LH, Ramsing NB, Ebbesen P. Pericellular oxygen depletion during ordinary tissue culturing, measured with oxygen microsensors. *Cell Prolif.* 2005;38:257–267.
5. Tokuda Y, Crane S, Yamaguchi Y, Zhou L, Falanga V. The levels and kinetics of oxygen tension detectable at the surface of human dermal fibroblast cultures. *J Cell Physiol.* 2000;182: 414–420.
6. Wolff M, Fandrey J, Jelkmann W. Microelectrode measurements of pericellular PO2 in erythropoietin-producing human hepatoma cell cultures. *Am J Physiol.* 1993;265:C1266–C1270.
7. Guarino RD, Dike LE, Haq TA, Rowley JA, Pitner JB, Timmins MR. Method for determining oxygen consumption rates of static cultures from microplate measurements of pericellular dissolved oxygen concentrations. *Biotechnol Bioeng.* 2005;91:392.
8. Lopes AS, Larsen LH, Ramsing N, Lovendahl P, Raty M, Peippo J, Greve T, Callesen H. Respiration rates of individual bovine in vitro-produced embryos measured with a novel, non-invasive and highly sensitive microsensor system. *Reproduction.* 2005;130:669–679.
9. Baumgardner JE, Otto CM. In vitro intermittent hypoxia: challenges for creating hypoxia in cell culture. *Respir Physiol Neurobiology.* 2003;136:131–139.
10. Garin G, Berk BC. Flow-mediated signaling modulates endothelial cell phenotype. *Endothelium-J Endothelial Cell. Res.* 206;13:375–384.
11. Jensen MD, Wallach DF, Sherwood P. Diffusion in tissue cultures on gas-permeable and impermeable supports. *J Theor Biol.* 1976;56:443–458.
12. Van Wachem P, Vreriks C, Beugeling T, Feijen J, Bantjes A, Detmers J, Van Aken W. The influence of protein adsorption on interactions of cultured human endothelial cells with polymers. *J Biomed Mater Res.* 1987;21:701–718.
13. Reitlinger S, Maslennikova A, Tarkho I. Gas permeability of polyorganosiloxane Resins. *Sov Phys-Tech Phys Engl Transl.* 1965;1:2467.
14. Robb W. Thin silicone membranes—their permeation properties and some applications. *Ann NY Acad Sci.* 1968;146:119–137.
15. Barrer T, Chio H. Solution and diffusion of gases and vapors in silicone rubber membranes. *J Polym Sci Part C.* 1965;10:111–138.
16. Henzler HJ, Kauling DJ. Oxygenation of cell cultures. *Bioprocess Eng.* 1993;9:61–75.
17. Rishell S, Casey E, Glennon B, Hamer G. Mass transfer analysis of a membrane aerated reactor. *Biochem Eng J.* 2004;18: 159–167.
18. Rishell S, Casey E, Glennon B, Hamer G. Characteristics of a methanotrophic culture in a membrane-aerated biofilm reactor. *Biotechnol Prog.* 2004;20:1082–1090.
19. Yoshino T, Asakura T, Toda K. Cellulose production by *Acetobacter pasteurianus* on silicone membranes. *J Ferment Bioeng.* 1996;81:32–36.
20. Falkenberg FW. Production of monoclonal antibodies in the miniPERM bioreactor: comparison with other hybridoma culture methods. *Res Immunol.* 1998;149:560–570.
21. Papas KK, Avgoustiniatos ES, Tempelman LA, Weir GC, Colton CK, Pisania A, Rappel MJ, Friberg AS, Bauer AC, Hering BJ. High-density culture of human islets on top of silicone rubber membranes. *Transplantation Proc.* 2005;37:3412–3414.
22. Hsiue GH, Lee SD, Wang CC, Shiue MHI, Chang PCT. Pphema-modified silicone-rubber film towards improving rabbit corneal epithelial-cell attachment and growth. *Biomaterials.* 1993;14:591–597.
23. Monge S, Mas A, Hamzaoui A, Kassis CM, Desimone JM, Schue F. Improvement of silicone endothelialization by treatment with allylamine and/or acrylic acid low-pressure plasma. *J Appl Polym Sci.* 2003;87:1794–1802.
24. Everaert EP, Vandermei HC, Busscher HJ. Hydrophobic recovery of repeatedly plasma-treated silicone rubber.2. A comparison of the hydrophobic recovery in air, water, or liquid nitrogen. *J Adhes Sci Technol.* 1996;10:351–359.
25. Rangel EC, Gadioli GZ, Cruz NC. Investigations on the stability of plasma modified silicone surfaces. *Plasmas Polym.* 2004;9:35–48.
26. Williams RL, Wilson DJ, Rhodes NP. Stability of plasma-treated silicone rubber and its influence on the interfacial aspects of blood compatibility. *Biomaterials.* 2004;25:4659–4673.
27. Ai H, Mills DK, Jonathan AS, Jones SA. Gelatin-glutaraldehyde cross-linking on silicone rubber to increase endothelial cell adhesion and growth. *In Vitro Cell Dev Biol Animal.* 2002; 38:487–492.
28. Okada T, Ikada Y. Surface modification of silicone for percutaneous implantation. *J Biomater Sci Polym Ed.* 1995;7:171–180.
29. Ai H, Meng HD, Ichinose I, Jones SA, Mills DK, Lvov YM, Qiao XX. Biocompatibility of layer-by-layer self-assembled nanofilm on silicone rubber for neurons. *J Neurosci Methods.* 2003;128:1–8.
30. Berg MC, Yang SY, Hammond PT, Rubner MF. Controlling mammalian cell interactions on patterned polyelectrolyte multilayer surfaces. *Langmuir.* 2004;20:1362–1368.
31. Elbert DL, Herbert CB, Hubbell JA. Thin polymer layers formed by polyelectrolyte multilayer techniques on biological surfaces. *Langmuir.* 1999;15:5355–5362.
32. Mendelsohn JD, Yang SY, Hiller J, Hochbaum AI, Rubner MF. Rational design of cytophilic and cytophobic polyelectrolyte multilayer thin films. *Biomacromolecules.* 2003;4:96–106.
33. Yang SY, Mendelsohn JD, Rubner MF. New class of ultrathin, highly cell-adhesion-resistant polyelectrolyte multilayers with micropatterning capabilities. *Biomacromolecules.* 2003;4:987–994.
34. Powers DE, Millman JR, Huang RB, Colton CK. Effects of oxygen on mouse embryonic stem cell growth, phenotype retention, and cellular energetics. *Biotechnol Bioeng.* 2008;101:241–254.
35. Wilson D, Erecinska M, Drown C, Silver I. The oxygen dependence of cellular energy metabolism archives. *Biochem Biophys.* 1979;195:485–493.
36. Powers DE. *Effects of Oxygen on Embryonic Stem Proliferation, Energetics, and Differentiation into Cardiomyocytes.* MA: Massachusetts Institute of Technology, 2007.
37. Chen B, Deen W. Analysis of the effects of cell spacing and liquid depth on nitric oxide and its oxidation products in cell cultures. *Chem Res Toxicol.* 2001;14:135–147.
38. Yarmush ML, Toner M, Dunn JC, Rotem A, Hubel A, Tompkins RG. Hepatic tissue engineering. Development of critical technologies. *Ann NY Acad Sci.* 1992;665:238–252.
39. Carslaw H, Jaeger J. *Conduction of Heat in Solids.* New York: Oxford UP, 1959.
40. Weibel E. *Stereological Methods.* London: Academic Press, 1979.
41. Brown M, Gratton T, Stuart J. Metabolic rate does not scale with body mass in cultured mammalian cells. *Am J Physiol Regul Integr Comp Physiols.* 2007;292:R2115–R2121.
42. Cunningham JJ, Nikolovski J, Linderman JJ, Mooney DJ. Quantification of fibronectin adsorption to silicone-rubber cell culture substrates. *Biotechniques.* 2002;32:876.
43. Wenzel F, Dittrich M, Hescheler J, Grote J. Hypoxia influences generation and propagation of electrical activity in embryonic cardiomyocyte clusters. *Comp Biochem Physiol A Mol Integr Physiol.* 2002;132:111–115.
44. Engler AJ, Carag-Krieger C, Johnson CP, Raab M, Tang HY, Speicher DW, Sanger JW, Sanger JM, Discher DE. Embryonic cardiomyocytes beat best on a matrix with heart-like elasticity: scar-like rigidity inhibits beating. *J Cell Sci.* 2008;121:3794–3802.

Manuscript received Mar. 23, 2009, and revision received Sept. 3, 2009.

-Page Intentionally Left Blank-

B. Effects of oxygen on mouse embryonic stem cell growth, phenotype retention, and cellular energetics

Reproduced from Powers, D.E., J.R. Millman, R.B. Huang, and C.K. Colton, *Effects of oxygen on mouse embryonic stem cell growth, phenotype retention, and cellular energetics.* Biotechnology and Bioengineering, 2008. **101**(2): p. 241-54 with permission of John Wiley & Sons, Inc.

EDITORS' CHOICE

BIOTECHNOLOGY and BIOENGINEERING

Effects of Oxygen on Mouse Embryonic Stem Cell Growth, Phenotype Retention, and Cellular Energetics

Daryl E. Powers, Jeffrey R. Millman, Ryan B. Huang, Clark K. Colton

Department of Chemical Engineering, Massachusetts Institute of Technology, 77 Massachusetts Ave., Room 66-452, Cambridge, Massachusetts 02139; telephone: 617-253-4585; fax: 617-252-1651; e-mail: ckcolton@mit.edu

Received 27 October 2007; revision received 9 May 2008; accepted 12 May 2008

Published online 3 June 2008 in Wiley InterScience (www.interscience.wiley.com). DOI 10.1002/bit.21986

ABSTRACT: Most embryonic stem (ES) cell research is performed with a gas phase oxygen partial pressure (pO_2) of 142 mmHg, whereas embryonic cells in early development are exposed to pO_2 values of 0–30 mmHg. To understand effects of these differences, we studied murine ES (mES) growth, maintenance of stem cell phenotype, and cell energetics over a pO_2 range of 0–285 mmHg, in the presence or absence of differentiation-suppressing leukemia inhibitory factor (LIF). With LIF, growth rate was sensitive to pO_2 but constant with time, and expression of self-renewal transcription factors decreased at extremes of pO_2. Subtle morphological changes suggested some early differentiation, but cells retained the ability to differentiate into derivatives of all three germ layers at low pO_2. Without LIF, growth rate decreased with time, and self-renewal transcription factor mRNA decreased further. Gross morphological changes occurred, and overt differentiation occurred at all pO_2. These findings suggested that hypoxia in the presence of LIF promoted limited early differentiation. ES cells survived oxygen starvation with negligible cell death by increasing anaerobic metabolism within 48 h of anoxic exposure. Decreasing pO_2 to 36 mmHg or lower decreased oxygen consumption rate and increased lactate production rate. The fraction of ATP generated aerobically was 60% at or above 142 mmHg and decreased to 0% under anoxia, but the total ATP production rate remained nearly constant at all pO_2. In conclusion, undifferentiated ES cells adapt their energy metabolism to proliferate at all pO_2 between 0 and 285 mmHg. Oxygen has minimal effects on undifferentiated cell growth and phenotype, but may exert more substantial effects under differentiating conditions.

Biotechnol. Bioeng. 2008;101: 241–254.

KEYWORDS: embryonic stem cells; oxygen; hypoxia; proliferation; differentiation; cellular energetics

Correspondence to: C.K. Colton

Contract grant sponsor: NIH

Contract grant numbers: NCRR ICR U4ZPR 16606; ROI-KD063108 OIA

Contract grant sponsor: JDRF Center for Islet Transplantation at Harvard Medical School

Introduction

Embryonic stem (ES) cells have the potential to generate any type of cell for transplantation to treat diseases such as diabetes, leukemia, and Parkinson's disease (Bonner-Weir et al., 2000; Kaufman et al., 2001; Kim et al., 2002; Soria, 2001). Development of efficient techniques for expansion of undifferentiated cells and subsequent directed differentiation requires an understanding of how ES cells interact with their microenvironment and methods to control these interactions. The oxygen partial pressure (pO_2) to which the cell is exposed (pO_{2cell}) is potentially one important environmental parameter.

Mammalian tissues are usually exposed to pO_2 values far below atmospheric levels, such as 25 mmHg in the rat microvasculature (Intaglietta et al., 1996), 15–45 mmHg in the reproductive tract of rhesus monkeys (Fischer and Bavister, 1993), and 25–30 mmHg in venous human fetal blood in the second and third trimester (Siggaard-Andersen and Huch, 1995; Soothill et al., 1986). Lower values occur in the gestational sac during the first trimester (Jauniaux et al., 2003b), which also provides an environment containing antioxidant molecules to further reduce oxidative damage (Jauniaux et al., 2003a). pO_2 values within early developing embryos are likely to be even lower because circulation does not occur until a well-formed vascular network is present (Maltepe and Simon, 1998; Palis et al., 2001), and there are hypoxic regions even after a well-developed vascular network exists (Land, 2004; Lee et al., 2001).

Stem cell culture is usually performed at pO_2 levels much higher than that of the embryo in vivo, typically in a humidified atmosphere consisting of 95% air/5% CO_2 that results in a gas phase pO_2 (pO_{2gas}) of 142 mmHg. Most experiments with ES cells are carried out in polystyrene culture dishes, which have very low oxygen permeability, and oxygen is supplied by diffusion through the medium. Oxygen concentration gradients exist in the medium that cause pO_{2cell} to be different from pO_{2gas} (Metzen et al., 1995;

Tokuda et al., 2000; Yarmush et al., 1992). The value of pO_{2cell} depends on several factors, including medium depth, cell density, cellular oxygen consumption rate, and pO_{2gas}, which are usually not taken into account (Csete, 2005; Metzen et al., 1995). As a consequence, the value of pO_{2cell} during ES cell culture is usually not controlled to be in the range experienced by the early embryo. The implications of this poor control are not well understood. Published data obtained with ES and other cell types suggest that cell survival and proliferation, maintenance of the stem cell phenotype, and cellular energetics are three important parameters that can be significantly affected by the magnitude of pO_{2cell}.

Cell proliferation can be adversely affected by too high or too low a pO_2. Culture at a pO_2 higher than needed exposes cells to higher concentrations of reactive oxygen species (ROS), which damage lipids, proteins, and nucleic acids (Lee and Wei, 2005; Saretzki et al., 2004) and can lead to senescence and cell death (Parrinello et al., 2003). Many cell types have a higher growth rate at pO_{2gas} conditions less than 142 mmHg, including fibroblasts (Bradley, 1978; Parrinello et al., 2003), hematopoietic cells (Bradley, 1978; Hevehan et al., 2000; Mostafa et al., 2000), neural progenitors (Milosevic et al., 2005; Morrison et al., 2000; Studer et al., 2000), muscle satellite cells (Chakravarthy et al., 2001; Csete et al., 2001), CHO and hybridoma cells (Goetz, 1975; Miller et al., 1987), as well as early embryos of both humans and mice (Dumoulin et al., 1999; Orsi and Leese, 2001; Quinn and Harlow, 1978). Providing too little oxygen can also be harmful and lead to apoptotic or necrotic cell death (Brunelle and Chandel, 2002).

In addition to growth, pO_{2gas} can affect whether stem or progenitor cells remain undifferentiated. Culture of mouse and human hematopoietic progenitor (Cipolleschi et al., 1997; Hevehan et al., 2000; Mostafa et al., 2000; Ramirez-Bergeron et al., 2004), rat CNS progenitor (Studer et al., 2000), and rat neural crest stem cells (Morrison et al., 2000) at reduced pO_{2gas} favors self-renewal, while increased pO_{2gas} favors differentiation and maturation. Some studies suggest that reduced pO_{2gas} increases the growth rate of mouse and human ES cells and may be beneficial for maintaining the undifferentiated phenotype, but usually only two or three values of pO_{2gas} were examined, and results are often not in agreement with one another (Carmeliet et al., 1998; Ezashi et al., 2005; Forsyth et al., 2006; Gibbons et al., 2006; Hopfl et al., 2002; Iyer et al., 1998; Kurosawa et al., 2006; Ludwig et al., 2006; Ording et al., 2005; Peura et al., 2005; Wang et al., 2006).

Cellular energetics are affected by pO_{2cell} (Miller et al., 1987), and survival at low oxygen requires anaerobic glycolysis for ATP generation. Mouse, bovine, and human blastocysts have high glycolytic capacity and can readily convert glucose into lactic acid (Devreker and Englert, 2000; Harvey et al., 2002; Hewitson and Leese, 1993; Houghton et al., 1996). Nonetheless, 75–85% of the ATP production in embryos occurs through oxidative phosphorylation at high pO_{2gas} (Houghton, 2006; Houghton et al., 1996; Thompson et al., 1996). The high levels of glycolytic enzymes in ES cells during culture at a pO_{2gas} of 142 mmHg are further increased at reduced pO_{2gas} conditions through the action of HIF-1α (Iyer et al., 1998; Wenger, 2002). Quantitative oxygen consumption and lactate production measurements with ES cells have not been reported, and it is unknown how these parameters are affected by the culture pO_{2cell}.

In this study we performed a systematic quantitative investigation of the effects of pO_2 on growth rate, stem cell phenotype, and energetics of murine ES (mES) cells. Varying pO_{2gas} in the range from 0 to 285 mmHg had an effect on the growth rate of undifferentiated mES cells, both with and without inclusion of the differentiation-suppressing cytokine leukemia inhibitory factor (LIF) in the culture medium. High and low pO_{2gas} reduced mRNA levels for transcription factors associated with the maintenance of the undifferentiated phenotype during culture with LIF, but only modest changes characteristic of early differentiation occurred in morphology, and cells retained the ability to differentiate into derivative of all three germ layers. Aerobic metabolism generated approximately 60% of the energy required by mES cells at high oxygen conditions, but substantially smaller fractions if cells were oxygen starved. This shift from aerobic to anaerobic respiration occurred rapidly with minimal cell death.

Materials and Methods

Cells and Media

Two mES cell lines were used, passage 22 CCE (Keller et al., 1993; Robertson et al., 1986) from Stem Cell Technologies (Vancouver, BC) and unknown passage number D3 (Doetschman et al., 1985) from ATCC (CRL-1934, Manassas, VA). Undifferentiated cells were grown in high glucose DMEM (30-2002, ATCC) supplemented to 10% (v/v) ES cell qualified fetal bovine serum (FBS) (06905, Stem Cell Technologies, or SCRR 30-2020, ATCC). The medium was further supplemented to a final concentration of 1,000 U/mL leukemia inhibitory factor (LIF, ESG1106, Chemicon, Temecula, CA) and 0.1 mM 2-mercaptoethanol (M-7522, Sigma-Aldrich, St. Louis, MO). Differentiation was carried out in an otherwise identical medium without LIF.

Cell Culture

Unless otherwise stated, cells were grown with 4 mL of medium in 25 cm^2 cell culture flasks (353109, Becton Dickinson, Franklin Lakes, NJ) that were treated for 30 min with a sterile 0.1% (w/v) solution of gelatin (G-2500, Sigma-Aldrich) in tissue culture water (25-055-CM, Mediatech, Herndon, VA). Cells were plated at a density of about 12,000 cells/cm^2. Medium was exchanged daily, and cells were detached with 0.25% trypsin (30-2101, ATCC)

every 2 days. Split fractions were chosen so that cells were always plated at 12,000 cells/cm^2. Medium was incubated in the appropriate pO_{2gas} condition for 24 h prior to use.

ES Cell Differentiation

ES cells were differentiated using the culture procedure described above (monolayer differentiation), except that medium without supplemental LIF was used. For one series of experiments, as indicated in the text and figure captions, differentiation was carried out in embryoid bodies (EBs) that were formed in 20 μL hanging drops of DMEM with 10% FBS containing 500 ES cells per drop. After 2 days, 30 EBs were transferred to each well of a gelatin-coated 24-well plate and cultured for another 3 days.

Gas Phase pO_2 Control

Cell culture vessels were placed inside polystyrene chambers (MIC-101, Billups-Rothenburg, Del Mar, CA) contained within a standard incubator (OWJ2720A, Queue Systems, Parkersburg, WV) maintained at 37°C. An open dish of deionized water in each chamber provided humidification. The desired pO_{2gas} was attained using premixed gas containing 5% CO_2 and 40%, 20%, 5%, 1%, or 0% O_2 (certified medical gas from Airgas, Hingham, MA), which corresponded under humidified conditions to 285, 142, 36, 7, and 0 mmHg. The flow rate of this gas to the chambers was 2 L/min for 15 min for an initial purge following closure of the chamber (after cell medium exchange or passage); and was 30 mL/min at all other times. To examine the response to a change in pO_2 under simulated culture conditions, a fiber optic sensor from the Micro Oxygen Monitoring System (FO/SYS2-T250, Instech Labs, Plymouth Meeting, PA) that measures oxygen fluorometrically was attached along the bottom of a 25 cm^2 flask through a hole drilled in the flask with the sensing face of the tip perpendicular to the culture surface. A volume of 4 mL of water equilibrated to room air was added, and the chamber was sealed. The gas flowing into the chamber was changed to nitrogen, and the pO_2 was measured as a function of time.

Immunocytochemistry for ES Cell-Specific Markers Analyzed by Flow Cytometry

Samples with 10^5 cells were centrifuged for 3 min at 300*g*, supernatant was removed and replaced with 750 μL of Dulbecco's phosphate buffered saline (DPBS), the cells were resuspended, and 250 μL of 4% (w/v) paraformaldehyde (Alfa Aesar, Ward Hill, MA) in DPBS was added. Cells were fixed for 20 min, washed with 1 mL DPBS, and resuspended in 100 μL of DPBS. For Oct4 staining, 100 μL of 1% (w/v) saponin (S-4521, Sigma-Aldrich) in DPBS was added to the sample, the cells were incubated for 10 min for permeabilization, then washed and resuspended in 50 μL of 1% (v/v) FBS in PBS. Samples for SSEA-1 staining were centrifuged and resuspended in 50 μL of 1% FBS in PBS without saponin treatment. All samples were incubated in the 1% FBS solution for 30 min, then 5 μL of a 1:10 dilution of either anti-Oct4 (611202, BD Transduction Laboratories, Franklin Lakes, NJ) or anti-SSEA-1 (MC-480 ascites, Developmental Studies Hybridoma Bank, Iowa City, IA) was added and the samples incubated for 1 h. To each tube 1 mL of 1% FBS solution was added, samples were centrifuged, supernatant was discarded, and the cells were resuspended in 50 μL of an appropriate PE conjugated secondary antibody (115-116-075 or 115-116-146, Jackson ImmunoResearch, West Grove, PA) diluted 1:500. Samples were incubated 30 min in the dark, then washed three times with 1 mL of PBS, and fluorescence intensity data were acquired with a flow cytometer (Guava Technologies with express software module, Hayward, CA). A negative control was prepared using cells stained only with the secondary antibody, and gating for the flow cytometry was set so that 98% or more of the unstained cells were counted as negative. The fraction of cells expressing SSEA-1 and Oct4 was measured with flow cytometry and expressed as the fraction of cells above this threshold. All steps were performed at room temperature.

Real-Time Polymerase Chain Reaction (PCR)

Total RNA was isolated using the RNeasy Kit (74104, Qiagen, Valencia, CA) and RNase-Free DNase Set (79254, Qiagen), cDNA was synthesized using High Capacity cDNA Reverse Transcription Kit (4368814, Applied Biosystems, Foster City, CA), and real-time PCR was performed on a Fast Real-Time PCR System (7900HT, Applied Biosystems), using Power SYBR Green PCR Master Mix (4367659, Applied Biosystems). 28S ribosomal RNA was used as an oxygen insensitive endogenous control (Zhong and Simons, 1999). Primer sequences used to assess gene expression are in Table I. A standard calibration curve was constructed using undifferentiated mES cells.

Table I. Primer sequences used for real-time PCR.

Target Gene	Direction	Sequence
28S rRNA	Forward	GAATCCGCTAAGGAGTGTGTAACA
	Reverse	CTCCAGCGCCATCCATTT
Oct4	Forward	CACGAGTGGAAAGCAACTCAGA
	Reverse	TCTCCAACTTCACGGCATTG
Nanog	Forward	CCTGATTCTTCTACCAGTCCCA
	Reverse	GGCCTGAGAGAACACAGTCC
Sox2	Forward	GACAGCTACGCGCACATGA
	Reverse	GGTGCATCGGTTGCATCTG
Nkx2.5	Forward	CAGTGGAGCTGGACAAAGCC
	Reverse	TAGCGACGGTTCTGGAACCA
Sox17	Forward	GCTGGCGGGTCTGAAGTG
	Reverse	TAACTTCTGCTGACCATTCTCTTGA
Nestin	Forward	GCTGGAACAGAGATTGGAAGG
	Reverse	CCAGGATCTGAGCGATCTGAC

Sequences reported 5′–3′.

Cell Enumeration, Membrane Integrity, and Apoptosis Assessment

After detachment with trypsin, the total number of cells and the number of viable cells (assayed by membrane integrity measurements) in a sample were evaluated by staining cells using a Guava Viacount assay kit (Guava Technologies) and acquiring data with the Guava PCA flow cytometer. Apoptotic cell fraction was determined using an Annexin V assay kit (Guava Technologies).

Oxygen Consumption Rate

Cells were detached with trypsin and resuspended at a density of between 6 and 12×10^6 viable cells/mL in fresh culture medium equilibrated to 37°C and ambient oxygen, leading to a reoxygenation of hypoxic cells. The oxygen consumption rate (OCR) of this suspension was measured with a Micro Oxygen Monitoring System (FO/SYS2-T250, Instech Labs) as described previously (Papas et al., 2007). Briefly, a 200 μL aliquot of the cell suspension was sealed within the titanium chamber stirred with a glass-coated magnetic stirring bar. The time-dependent pO_2 within the chamber was recorded with a fluorescence-based oxygen sensor, and the data at pO_2 values greater than 30 mmHg were fit to a straight line by linear regression analysis. The oxygen consumption rate (OCR) was evaluated from the following equation:

$$\mathrm{OCR} = V_{\mathrm{ch}} \alpha \frac{\Delta \mathrm{pO}_2}{\Delta t} \tag{1}$$

where V_{ch} is the chamber volume (200 μL), $\alpha = 1.19 \times 10^{-9}$ mol/cm^3/mmHg is the Bunsen solubility coefficient for oxygen in medium (Avgoustiniatos, 2002), and $\Delta pO_2/\Delta t$ is the slope of the fitted line. OCR/cell was determined by dividing the total OCR by the total number of viable cells that were loaded into the chamber.

Lactate Concentration

Assay reagent, prepared fresh for each test, consisted of 1 U/mL lactate oxidase (L-0638, Sigma-Aldrich), 0.025 U/mL peroxidase (P-6782, Sigma-Aldrich), and 0.1 mg/mL of *o*-dianisidine (F-5803, Sigma-Aldrich) in DPBS. Samples of supernatant medium from cell cultures were collected, and lactate concentration was measured by adding 100 μL of assay reagent to 50 μL of diluted sample (final concentration 0.1–0.3 mM lactate) in wells of a 96-well plate. The plate was incubated for 30 min at 37°C, 100 μL of 12 N sulfuric acid was added to stop the reaction, absorbance was measured at 540 nm using a microplate reader (Molecular Devices, Sunnyvale, CA), and lactate concentration was determined with a standard curve prepared for each test using lactic acid (L-1750, Sigma-Aldrich). DPBS (21-030-CM, Mediatech) was used as a diluent throughout.

Lactate Production Rate

We assumed that the lactate production rate (LPR) is proportional to the number of cells (N) at any instant of time (t), which can be represented by

$$\mathrm{LPR} = V_{\mathrm{m}} \frac{\mathrm{d}C}{\mathrm{d}t} = \lambda N \tag{2}$$

where V_m is the medium volume, C is the lactate concentration in the medium, and the coefficient λ is the LPR per cell, which is assumed to be constant during an experiment. Rearranging and integrating yields

$$V_{\mathrm{m}}(C_{\mathrm{f}} - C_0) = \lambda \int_0^{t_{\mathrm{f}}} N \mathrm{d}t \tag{3}$$

where subscripts 0 and f represent the initial and final conditions, and t_f is the duration of the experiment. When cells are in exponential growth, which applied in all of our experiments, we can write

$$N = N_0 \exp(\mu t) \tag{4}$$

where N_0 is the initial number of cells, and μ is the specific growth rate. Substituting Equation (4) into Equation (3) and integrating leads to

$$\lambda = \frac{V_{\mathrm{m}}(C_{\mathrm{f}} - C_0)}{(N_0/\mu)[\exp(\mu t_{\mathrm{f}}) - 1]} \tag{5}$$

from which λ is evaluated, since all quantities in Equation (5) were known. In our experiments, we measured final cell number N_f at $t = t_f$, which was used to estimate N_0 with Equation (4).

Lactate Dehydrogenase (LDH) Activity

A 100-μL aliquot containing 10^5 cells was added to a 1.5 mL tube containing 1 mL of DPBS and centrifuged for 3 min at 300*g* to obtain a cell pellet. To lyse the cells, the supernatant was removed, and 1 mL of 1% (v/v) Triton X-100 (T-9284, Sigma-Aldrich) in DPBS was added to each sample. The tubes were then briefly mixed using a vortex mixer and kept at room temperature for 1 h. LDH activity in the samples was measured with an Ektachem Vitros DT 60 II analyzer (Johnson and Johnson Clinical Diagnostics, Rochester, NY), which monitored the kinetics of the change in reflection density on a test slide as pyruvate and NADH were enzymatically converted into lactate and NAD by LDH in the test sample.

Estimation of pO_{2cell}

pO_{2cell} was estimated by equating the rate of diffusion of oxygen through the stagnant medium to the rate of oxygen consumption:

$$\frac{D\alpha}{L}[pO_{2gas} - pO_{2cell}] = \rho\left[\frac{V_{max}pO_{2cell}}{K_m + pO_{2cell}}\right] \quad (6)$$

where D and α are the diffusivity and solubility of oxygen in cell culture medium, respectively, L is the medium depth, pO_{2gas} and pO_{2cell} are the gas phase and cell surface pO_2 values, respectively, ρ is the viable cell density on the surface, K_m is the Michaelis constant for oxygen consumption, and V_{max} is the experimentally measured OCR/cell. The presence of a small pO_2 drop across the layer of cultured cells was ignored. For our calculations we used $D = 2.97 \times 10^{-5}$ cm^2/s, $\alpha = 1.19 \times 10^{-9}$ mol/cm^3/mmHg, $L = 0.15$ cm, and $K_m = 0.44$ mmHg (Avgoustiniatos, 2002; Wilson et al., 1979). Equation (6) was solved for pO_{2cell} by iterative solution (Excel solver).

Estimation of Specific Growth Rate

The cell specific growth rate, μ, was approximately constant during culture of undifferentiated cells. The specific growth rate was determined for these cultures using linear regression of the cumulative cell number versus time plotted on a semi-log arithmetic scale (as in Fig. 2A). The specific growth rate varied with time in culture when ES cells were differentiating (as in Fig. 3A). The instantaneous specific growth rate at a given time t was determined by numerically differentiating the data using the average of the forward, backward, and central differences, according to the following equation:

$$\mu = \frac{\ln(N/N_0)}{3(t - t_0)} + \frac{\ln(N_1/N)}{3(t_1 - t)} + \frac{\ln(N_1/N_0)}{3(t_1 - t_0)} \quad (7)$$

where N_0, N, and N_1 are the cumulative cell numbers at successive times t_0, t, and t_1, respectively.

Assessment of Oxidative DNA Damage

A single cell gel electrophoresis (comet) assay (Tice et al., 2000) was used to detect DNA damage. This assay was done with and without the use of formamidopyrimidine DNA glycosylase (FPG, F-3174, Sigma-Aldrich), which creates strand breaks at sites of 8-oxoguanine (Collins and Dusinska, 2002), a well-documented product of oxidative DNA damage (Helbock et al., 1999). Undifferentiated mES cells were cultured at specified pO_{2gas} for 72 h, then detached with trypsin and resuspended at a concentration of 200 cell/μL in 37°C, 1% (w/v) low melting point agarose (A-6560, Sigma-Aldrich) in DPBS. Methods for alkaline single-cell gel electrophoresis were subsequently followed (Collins and Dusinska, 2002). Comets were stained with 50 nM Sytox Orange dye (S11368, Molecular Probes, Eugene, OR), images were acquired with a 10× objective on a Zeiss epifluorescence microscope, and image analysis was performed using NIH image (Helma and Uhl, 2000). Samples with oxidative DNA damage (positive controls) were prepared by treating cells with 25, 85, and 150 μM hydrogen peroxide for 30 min immediately before embedding them in low melting point agarose.

Statistics

Statistical comparisons of data were performed using t-tests (paired or unpaired as appropriate), and results were deemed significant if the two-tailed P-value was 0.05 or less.

Results

Characterization of pO_2 Control in Experimental Apparatus

The time-dependent response of the liquid phase pO_2 to a step change in pO_2 of the gas flowing into the flask under simulated culture conditions is shown in Figure 1. The pO_2 in the region near the bottom of the water layer dropped from 160 to about 10 mmHg within 1 h and to less than 1 mmHg after 100 min. The pO_2 continued to drop at longer times, but it could not be measured when it was below the resolution of the sensor. The presence of oxygen-consuming cells at the bottom of the flask under actual culture conditions would have accelerated the decrease of pO_{2cell} and would have brought it to values substantially smaller than 1 mmHg in less than 2 h. Thus, the response time for liquid phase pO_2 was much smaller than the time of the

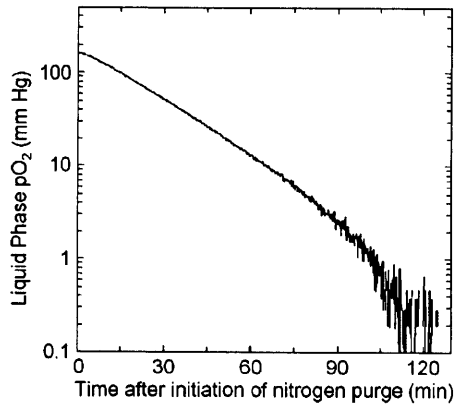

Figure 1. Response of liquid pO_2 to a change in ambient pO_{2gas}. The pO_2 at the bottom of 4 mL of water contained within a 25 cm^2 tissue culture flask is plotted as a function of time. The flask was initially equilibrated with room air. At $t = 0$, the gas flowing into the flask was changed to nitrogen. The time dependence of the inlet gas flow rate was identical to that used in all cell culture experiments.

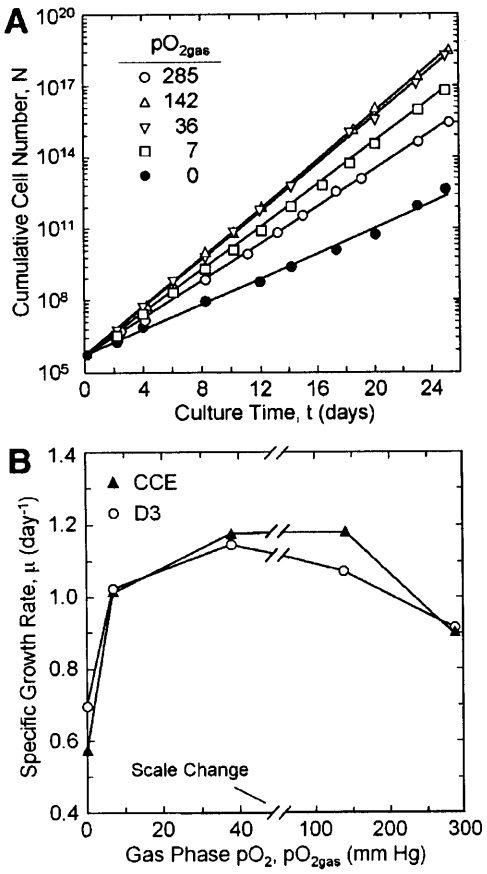

Figure 2. A: Cumulative cell number versus time for undifferentiated mES cells (CCE) maintained at different pO_{2gas} conditions. Data are from an experiment that is representative of results obtained with both CCE and D3 cells. B: Specific growth rates of the two cell lines as determined from an exponential fit of data, such as that plotted in **panel A**. The uncertainty of the slope was less than 0.04 day^{-1} for all conditions; error bars are not plotted. Cell densities between passages ranged from 0.1 to 2.0 × 10^5 cell/cm^2 in these experiments.

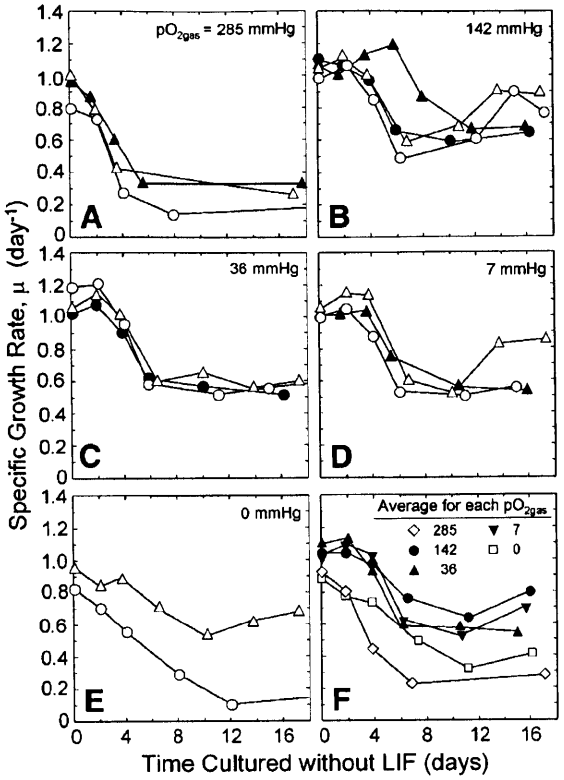

Figure 3. Specific growth rate of CCE mES cells grown in culture medium without LIF beginning on day 0. Results from up to four independent experiments at different pO_{2gas} conditions are shown in **panels A–E**. Data obtained from comparable times for each pO_{2gas} were averaged, and the result is plotted in **panel F**.

experiment in all experiments carried out. Cells cultured at low pO_2 would be exposed to higher pO_2 for a period of at most 3 h once every two days as the result of passaging.

Cellular pO_2

Estimates of pO_{2cell}, calculated from Equation (6) for cell densities ranging from 0.1 to 2.0 × 10^5 cell/cm^2, corresponding to the lowest and highest cell density present before and after passaging cells, respectively, are tabulated in Table II. Although the magnitude of the pO_2 drop across the culture medium was small in all cases, the difference between pO_{2gas} and pO_{2cell} was large relative to pO_{2gas} at very low oxygen concentrations, for example, cells cultured using a pO_{2gas} of 7 mmHg were often exposed to pO_{2cell} values that approached 0.

Cell Growth

Undifferentiated CCE and D3 mES cells at pO_{2gas} of 0, 7, 36, 142, and 285 mmHg grew exponentially for up to 25 days (Fig. 2A). There were no temporal changes that suggested senescence, differentiation, or long-term conditioning to the culture conditions. The fraction of cells with intact cell

Table II. Experimental pO_{2gas} conditions and the corresponding pO_{2cell} for undifferentiated mES cell monolayers.

Gas phase[a]			
% Oxygen	pO_{2gas} (mmHg)	Maximal OCR;[b] V_{max} (amol/sec cell)	Cellular pO_2;[c] pO_{2cell} (mmHg)
40	285	28	262–284
20	142	29	118–141
5	36	23	18–35
1	7	17	0.5–6.5
0	0	10	0

[a]The oxygen content in the pre-mixed gas cylinders (containing 5% CO_2) was specified, and the pO_{2gas} was determined from pO_{2gas} = (% oxygen) × ($Patm - P_{H_2O}$), where $Patm$ is the atmospheric pressure and P_{H_2O} = 47 mmHg is the vapor pressure of water at 37°C.

[b]OCR measured experimentally (Fig. 9).

[c]pO_{2cell} calculated with Equation (6) for extreme low and high densities of 0.1 and 2.0 × 10^5 cell/cm^2 (about 2–50% confluence), respectively.

membranes was between 94% and 98%, which further suggested that undifferentiated mES cells survived and proliferated in all conditions tested. Both CCE and D3 cells had roughly the same specific growth rate (Fig. 2B) and were tolerant of a wide range of oxygen conditions. Growth was significantly suppressed under anoxia, but the cells continued to grow exponentially with a doubling time between 24 and 27 h. Elevated pO_{2gas} of 285 mmHg also caused a decrease in growth rate in both cell lines relative to that at 142 mmHg. D3 cells consistently grew faster at a pO_{2gas} of 36 mmHg compared to 142 mmHg. The specific growth rate μ in four experiments was 1.05 ± 0.12 day^{-1} at 142 mmHg and 1.15 ± 0.10 day^{-1} at 36 mmHg. This small, but statistically significant difference ($P < 0.01$, paired t-test) would lead to a threefold difference in cell number after 10 days of culture. No difference in growth at these same two pO_{2gas} conditions was observed with CCE cells.

Without LIF in the culture medium, CCE cells readily differentiated, and the specific growth rate (Fig. 3) decreased with increasing time after LIF withdrawal. After a time lag of about 2 days, the specific growth rate, on average, decreased at a similar rate for pO_{2gas} conditions ranging from 7 to 142 mmHg, and reached a minimum after about 10 days (Fig. 3F). Changing pO_{2gas} in this range did not significantly delay or accelerate the onset or rate of differentiation. Individual experiments were reproducible at 285, 36, and 7 mmHg, less so at other conditions. The specific growth rate at 285 mmHg was suppressed to a greater extent, relative to that at other values of pO_{2gas}, than was observed in the presence of LIF. A small number of experiments with D3 cells suggested similar trends (data not shown), which occurred more slowly due to a decreased rate of spontaneous differentiation.

Oxidative DNA Damage

Comet assays run with and without FPG using cells cultured for 72 h at each pO_{2gas} produced similar values of tail length (Table III) and tail moment, both measures of the relative amount of DNA damage, and there was no trend of increased damage with increased pO_{2gas}. Cells treated with hydrogen peroxide displayed dose-dependent increases in mean tail length and moment, and a further dose-dependent increase occurred when the assay was performed with FPG. These results suggest that pO_{2gas} did not significantly affect the amount of oxidative DNA damage detectable with a comet assay, a result consistent with growth rate data (Fig. 2A).

Table III. Relative tail length from a Comet assay.

		Relative tail length[a]	
pO_{2gas} (mmHg)	H_2O_2 (μM)	Without FPG	With FPG
0	0	1.4	1.8
7	0	1.3	1.7
36	0	1.4	1.8
142	0	1.0	1.6
285	0	1.2	1.1
142	25	0.9	1.9
142	85	1.8	2.9
142	150	2.2	4.2

[a]Assay was carried out with and without FPG, which induces DNA strand breaks at 8-oxoguanine sites and increases comet tail lengths. Relative tail length is the measured tail length divided by the value at 142 mmHg. Data tabulated are from a single experiment.

Retention of Undifferentiated Stem Cell Phenotype at Different pO_{2gas}

Protein and Gene Expression

When using culture medium containing LIF, which suppresses mES cell differentiation (Viswanathan et al., 2002), pO_{2gas} did not affect the fraction of cells that expressed SSEA-1 and Oct4 using flow cytometry. Both proteins were expressed by 85–95% of all cells over a 25-day period at all pO_{2gas}. When gene expression of several transcription factors (Oct4, Sox2, and Nanog) typically associated with the undifferentiated ES cell phenotype was measured with real-time PCR, there were no changes after 8 days from the undifferentiated stem cells with cells cultured at 142 and 36 mmHg. However, other values of pO_{2gas} led to differences in the amount of mRNA present (Fig. 4). After 8 days in culture (3 passages), both high (285 mmHg) and low (7 and 0 mmHg) pO_{2gas} resulted in significant decreases of Oct4, Sox2, and Nanog mRNA to levels ranging from 10% to 40% of those in the undifferentiated stem cells after at day 0, and the levels of each transcription factor were sequentially lower at 7 and 0 mmHg.

Without LIF in the culture medium, the fraction of CCE cells expressing Oct4 protein, as measured by flow cytometry, also decreased with time except for pO_{2gas} of 285 mmHg and some experiments at 142 mmHg, at which the fraction decreased and then rebounded (Fig. 5A and B). Individual experiments were reproducible at 7 and 285 mmHg but less so at 142 and 36 mmHg, similar results were observed at 0 and 7 mmHg. The averaged data (Fig. 5F) demonstrate a decrease in the fraction of Oct4 positive cells with decreasing pO_{2gas}. Because of the scatter in the data, this trend was only significant ($P < 0.04$) when 142 and 7 mmHg were compared at day 6, and 285 and 7, 36, or 0 mmHg were compared on day 16. After about 16 days, the average fraction of Oct4 positive cells converged to about 30% at 0, 7, and 36 mmHg and was about 55% and 70% at 142 and 285 mmHg, respectively.

With the exception of inconsistent behavior at 285 mmHg, the data for gene expression of Oct4, Nanog, and Sox2 (Fig. 4) displayed several trends when LIF was absent. (1) The relative gene expression of all transcription factors decreased as pO_{2gas} decreased from 142 to 0 mmHg. The relative magnitude of the decline decreased in the order Nanog > Oct4 > Sox2. The overall trend for Oct4 was consistent with that of the flow cytometry measurements in

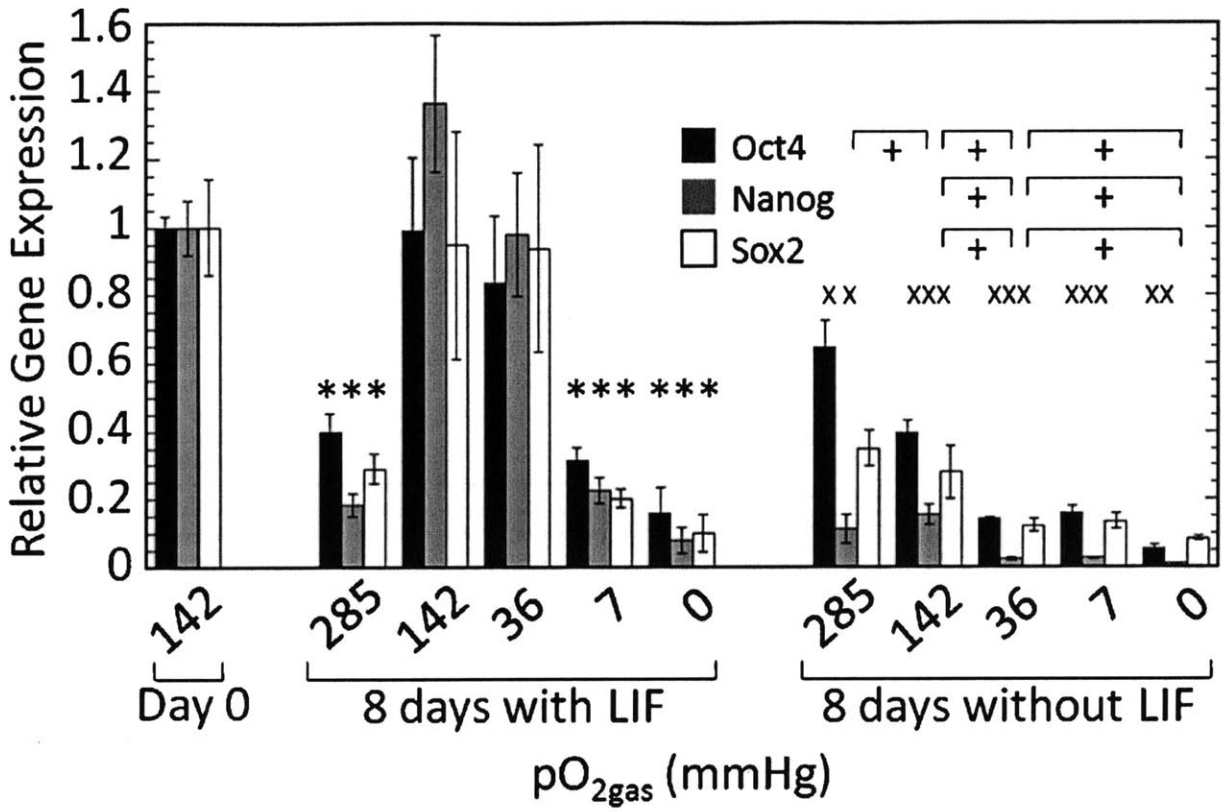

Figure 4. Real-time PCR analysis of ES cell markers Oct4, Sox2, and Nanog in CCE cells cultured for 8 days with and without LIF in the culture medium. Results reported are mean ± SD of data obtained with four different cultures carried out with the same undifferentiated stem cells starting at day 0. All data is normalized to that for the cells at day 0. Gene expression for conditions with LIF that are significantly different from the day 0 undifferentiated cells are indicated with an asterisk (*). For conditions without LIF, the X denotes a significant difference in gene expression between cultures with LIF and without LIF at identical pO_{2gas} conditions, and the plus sign (+) denotes significant difference between pO_{2gas} conditions indicated by the brackets, all without LIF.

Figure 3. (2) At any given pO_{2gas}, gene expression was lower in the absence than in the presence of LIF, and the relative difference depended on pO_{2gas}. By assuming that the effects ascribed to reduced oxygen in the presence of LIF and to the elimination of LIF at any pO_{2gas} are independent and multiplicative, it was possible to estimate the relative reduction in gene expression associated with each phenomenon (Table IV). The effect of LIF removal on reduction of gene expression was the dominant factor at higher pO_{2gas}, but the effect of reduced pO_{2gas} became most important at low pO_{2gas}.

Morphology

Cells cultured with LIF at reduced pO_{2gas} displayed altered morphology in comparison to culture at 142 mmHg (Fig. 6A). By 48 h of culture at 7 mmHg, cells at the periphery of the colony developed more jagged edges and contracted, indicating the initiation of differentiation. This morphology was maintained with little change for up to 8 days of culture. In contrast, when LIF was removed (Fig. 6B), the cells became expanded and flattened, consistent with overt differentiation.

Differentiation to Germ Layer Derivatives

To examine the pluripotency of mES cells cultured with LIF at reduced pO_{2gas} for 8 days, cells were subsequently subjected to a differentiation protocol involving EB formation followed by attached culture. Gene expression measurements (Fig. 7) after 5 days of culture for Nkx2.5, Sox17, and Nestin, demonstrated a 1–2 order of magnitude increase in these markers for mesoderm, endoderm, and ectoderm, respectively, relative to undifferentiated mES cells.

Continuous Culture Without Passaging

In experiments described to this point, medium was exchanged daily, and cells were passaged every 2 or 3 days. Fresh medium was pre-equilibrated to the desired pO_2 so that there was minimal disturbance associated with medium exchange; however, during passaging the mES cells were exposed to ambient oxygen for about 1 h and to the stress of trypsin detachment, which may have selectively harmed either differentiated or undifferentiated cells. To study effects of pO_{2gas} on mES cell growth and differentiation without these potential artifacts, D3 and CCE cells were

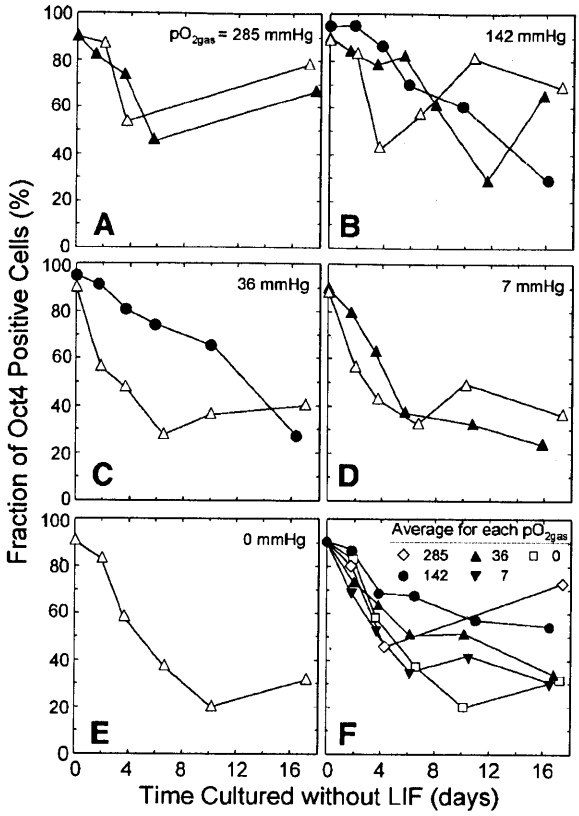

Figure 5. Fraction of Oct4 positive CCE cells during culture in medium without LIF beginning on day 0. Results from up to three independent experiments at different pO_{2gas} conditions are shown in **panels A–E**. Data obtained from comparable times for each pO_{2gas} were averaged, and the result is plotted in **panel F**.

plated at a density of 100 cells/well in 6-well plates containing 3 mL of culture medium (three wells for each condition) both with and without supplemental LIF. The plates were maintained for 8 days without passaging the cells or changing the medium. Plates were kept at a pO_{2gas} of 142 or 7 mmHg continuously (24 h/day) or at a pO_{2gas} of 7 mmHg for 23 h/day and 142 mmHg for 1 h/day. With and without LIF, exposure of D3 and CCE ES cells to a pO_{2gas} of 7 mmHg for 23 h and 142 mmHg for 1 h each day did not significantly affect specific growth rate or the fraction of cells expressing SSEA-1 and Oct4 protein (measured by flow cytometry), relative to culture at 7 mmHg continuously (data not shown), although it is possible that a more sensitive method such as real-time PCR might detect differences.

Temporal Response to Anoxia

The ability of mES cells to grow in anoxia with a doubling time of about 24 h indicated that mES cells are well suited to, or can readily adapt to, low oxygen conditions. To further explore this behavior, undifferentiated mES cells were

Table IV. Relative effect of reduced oxygen and LIF removal on gene expression of transcription factors associated with self-renewal and pluripotency.

mRNA	pO_{2gas} (mmHg)	+LIF/Day 0	−LIF/+LIF
Oct4	285	**0.39 ± 0.06**	1.6 ± 0.2
	142	1.0 ± 0.2	**0.4 ± 0.04**
	36	0.8 ± 0.2	**0.170 ± 0.006**
	7	**0.32 ± 0.04**	0.51 ± 0.07
	0	**0.16 ± 0.08**	0.35 ± 0.06
Nanog	285	**0.19 ± 0.03**	0.6 ± 0.2
	142	1.4 ± 0.2	**0.11 ± 0.02**
	36	1.0 ± 0.2	**0.027 ± 0.004**
	7	0.23 ± 0.04	**0.12 ± 0.01**
	0	**0.08 ± 0.04**	0.14 ± 0.03
Sox2	285	**0.29 ± 0.05**	1.2 ± 0.2
	142	1.0 ± 0.3	**0.29 ± 0.08**
	36	0.9 ± 0.3	**0.13 ± 0.02**
	7	**0.20 ± 0.03**	0.7 ± 0.1
	0	**0.10 ± 0.05**	0.85 ± 0.07

Day 0 represents the mRNA level of the indicated transcription factor in mES cells at the start of the experiment. +LIF represents cells cultured with LIF at the indicated pO_{2gas} for 8 days. −LIF represents cells cultured without LIF at the indicated pO_{2gas} for 8 days. Tabulated ratios were calculated from data in Figure 3 and from the assumption that the effects of (a) reduced oxygen with LIF present and (b) LIF removal could be separated according to the relation (−LIF/Day 0) = (+LIF/Day 0) × (−LIF/+LIF). The value in boldface for each entry denotes the greater of the two relative effects in decreasing gene expression.

subjected to a change in pO_{2gas} from 142 to 0 mmHg. The fraction of cells with intact membranes, the fraction of apoptotic cells, OCR/cell immediately after reoxygenation, and LDH activity were measured at various times up to 50 h after the transition to anoxia (Fig. 8).

Exposure to anoxia decreased the fraction of cells with intact membranes by about 2–5%. Similarly, there was a very small increase in the fraction of cells that were apoptotic which never exceeded 9% under anoxia compared to about 4% in cells exposed to 142 mmHg. Thus, exposure to anoxia caused only a small fraction of cells to become apoptotic and die, and more than 90% remained alive. Oxygen deprivation caused mES cells to rapidly down-regulate aerobic metabolic pathways as indicated by a decrease in OCR that began immediately after the initiation of anoxia and was nearly complete within 1 day. There was little change in the intracellular LDH activity for the first 10 h of exposure to anoxia, after which it increased to more than twice that found in cells cultured at 142 mmHg.

Cellular Energy Metabolism

The data in Figure 8 provide evidence that mES cells increased anaerobic metabolism when exposed to hypoxia or anoxia. To quantify this further, we estimated the rate of ATP produced aerobically and anaerobically under each of the pO_2 conditions tested. OCR/cell was used as a measure of oxidative phosphorylation and LPR/cell as a measure of anaerobic glycolysis. ATP production rate was estimated by assuming production of 6 mol of ATP per mol of oxygen

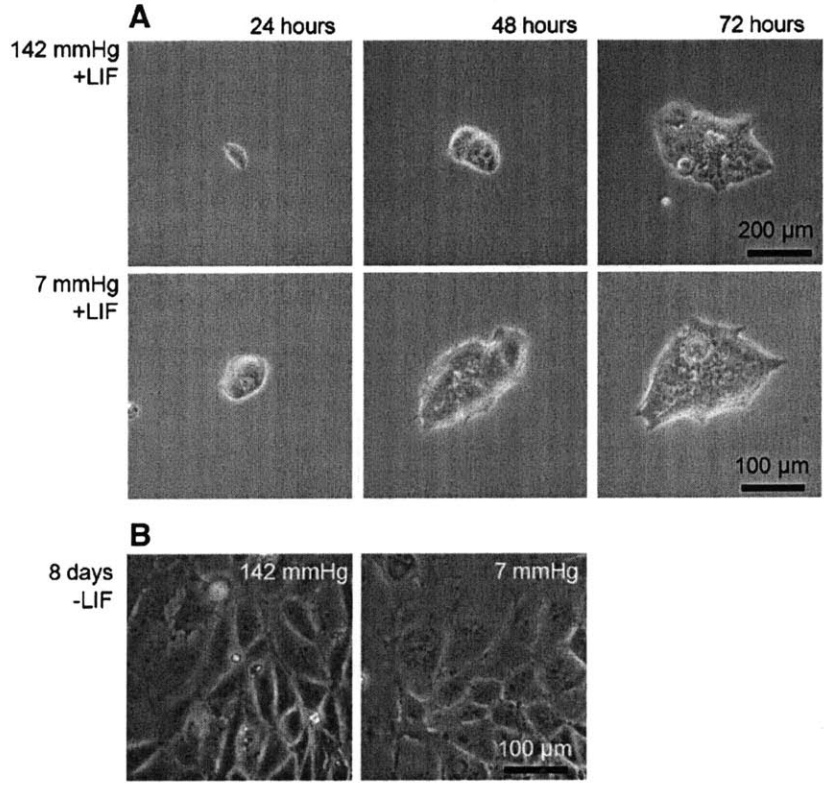

Figure 6. Phase contrast photomicrographs of CCE cells cultured **(A)** for up to 72 h with 1,000 U/mL LIF at pO_{2gas} of 142 mmHg **(top panels)** or 7 mmHg **(middle panels)** or **(B)** 8 days without LIF **(bottom two panels)** at a pO_{2gas} of 142 or 7 mmHg.

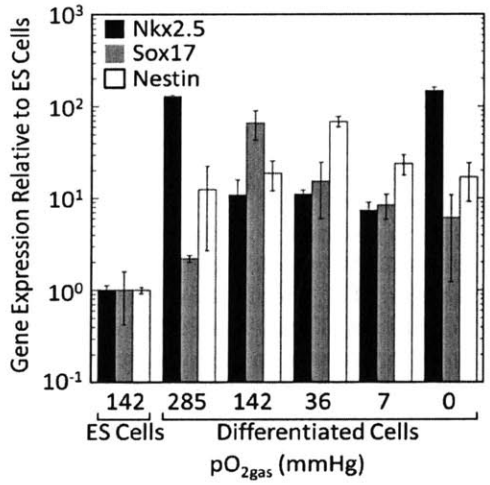

Figure 7. Real-time PCR analysis of the differentiation markers Nkx2.5, Sox17, and Nestin of CCE cells cultured at the indicated pO_2 for 8 days with 1,000 U/mL LIF and then differentiated without LIF in hanging drop EBs for 2 days and in attached culture for an additional 3 days at the same pO_2. Nkx2.5, Sox17, and Nestin are markers for mesoderm, endoderm, and ectoderm, respectively. Results reported are mean ± SD of data obtained with four different cultures carried out with the same undifferentiated stem cells starting at day 0, and all of the results were significantly different from the control (undifferentiated ES cells at 142 mmHg).

consumed and 1 mol of ATP per mol of lactate formed (Lindqvist et al., 2002; Miller et al., 1987).

A relatively high level of anaerobic metabolism occurred in the mES cells, even at high pO_{2gas} at which there was a plentiful supply of oxygen to the cells (Fig. 9). Nearly 40% of the ATP production was provided by anaerobic metabolism of glucose into lactate at 142 mmHg or greater. When pO_{2gas} was reduced to 36 mmHg, a small but significant decrease in OCR and increase in LPR was observed. This shift to increased anaerobic metabolism became more pronounced as the pO_{2gas} decreased to 0 mmHg, a condition in which no significant aerobic ATP production could occur. Overall, the total estimated ATP production rate remained nearly constant as long as oxygen was present, and decreased about 10% at 0 mmHg.

Discussion

In order to determine whether oxygen level affected proliferation and maintenance of undifferentiated phenotype in differentiation-suppressing and -permissive conditions, we measured the growth rate, Oct4, Sox2, and Nanog mRNA expression, the potential to differentiate into derivatives of all three germ layers, and the cell and colony

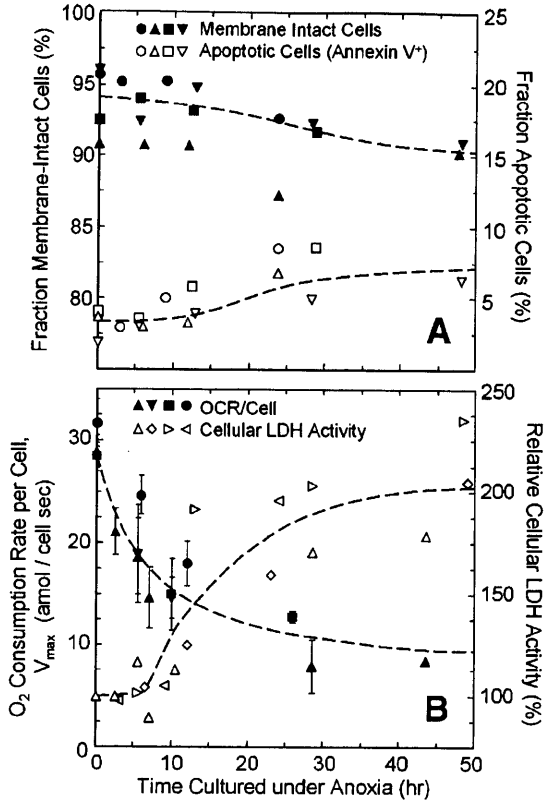

Figure 8. **A**: The fraction of membrane intact and apoptotic cells (Annexin V positive) and (**B**) cellular oxygen consumption rate (measured under normoxic conditions) and intracellular LDH activity plotted as a function of the time spent in anoxia. Undifferentiated CCE cells were initially grown at pO_{2gas} of 142 mmHg before being cultured under anoxia for periods of time shown, all in the presence of LIF. Each point represents a single measurement except for the OCR measurements, which represent the mean ± SD of at least three replicates. Each symbol represents data taken with the same initial batch of cells. The dashed lines in both panels represent an approximate fit of the data that was performed by eye.

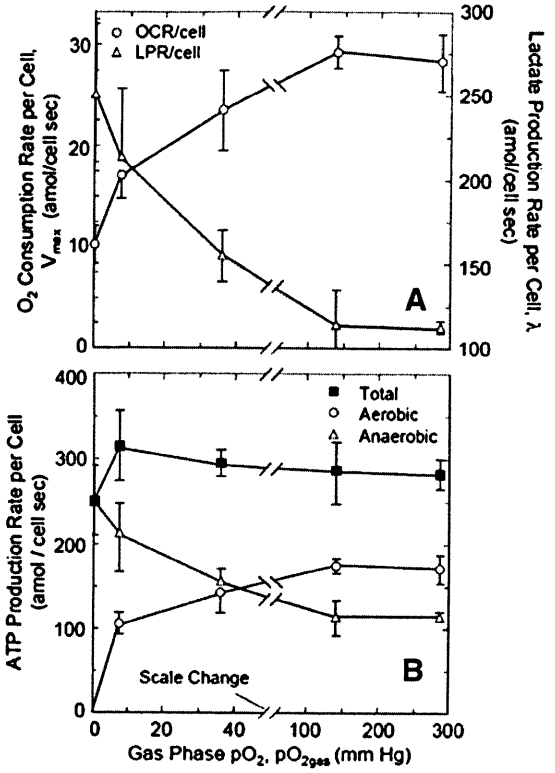

Figure 9. **A**: Oxygen consumption rate per cell and lactate production rate per cell and (**B**) the corresponding ATP production rates for undifferentiated mES cells cultured at different pO_{2gas} conditions. Each data point is the mean ± SD of at least three independent experiments. No differences between CCE and D3 cells were observed, and the plotted data were obtained from experiments with both cell lines. All cells were cultured at least 50 h at the indicated pO_2 prior to assessment.

morphology of undifferentiated mES cells cultured with LIF, and a subset of these characteristics for mES cells cultured without LIF, at pO_{2gas} in the range of 0–285 mmHg. We also studied mES cell energetics over the same range of pO_{2gas} to gain further insight into the extent to which mES cells adapt to different environmental oxygen conditions.

When LIF was present in the culture medium, growth of undifferentiated mES cells was sensitive to pO_2 (Fig. 2), but the growth rate was constant at any fixed pO_{2gas} up to 24 days. When compared to culture at a pO_{2gas} of 142 mmHg, the specific growth rate (Fig. 2B) was similar at 36 mmHg, moderately reduced at 7 and 285 mmHg as others have found for mES cells (Iyer et al., 1998; Saretzki et al., 2004) and hES cells (Ezashi et al., 2005; Ludwig et al., 2006) and further reduced at 0 mmHg. D3 cells had a slightly higher growth rate at a pO_{2gas} of 36 relative to 142 mmHg, while growth rates for CCE cells were the same. The fraction of cells expressing Oct4 and SSEA-1 protein as quantified with flow cytometry was not affected by pO_{2gas}, but measurements of mRNA levels using real-time PCR revealed a decrease in gene expression of Oct4, Sox2, and Nanog at pO_{2gas} of 285, 7, and 0 mmHg (Fig. 4). Compared to 142 mmHg, photomicrographs of cells grown at pO_{2gas} of 7 mmHg revealed subtle changes indicating initiation of differentiation (Fig. 6A). Nonetheless, cells cultured at low pO_{2gas} in the presence of LIF retained the ability to subsequently different into derivatives of all three germ layers (Fig. 7).

When LIF was removed from the culture medium, the cells differentiated. The growth rate decreased with time and was not affected by pO_{2gas} from 7 to 142 mmHg (Fig. 3), but there were differences at the extremes of 0 and 285 mmHg as there were for growth in the undifferentiated state. Differentiation occurred much faster in the CCE cell line than it did in the D3 cell line. Such variations between ES cell lines have been observed by others in many different aspects of culture (Ward et al., 2004). The rate at which CCE cells lost Oct4 protein expression increased with decreasing pO_{2gas} in the range of 0–285 mmHg (Fig. 5). For 0–142 mmHg pO_{2gas}, gene expression of Oct4, Nanog, and Sox2 decreased with decreasing pO_{2gas} and was always lower than when LIF was present at the same pO_{2gas} (Fig. 4). At pO_{2gas} of 7 and 0 mmHg, the effect on gene expression of reduced oxygen was comparable to or greater than the

separate effect of LIF removal (Table IV). Gross changes in cell and colony morphology were evident when LIF was not present (Fig. 6B).

Taken together, our observations suggest that hypoxic culture of mES cells causes initiation of differentiation, even in the presence of LIF. This finding is consistent with that of Jeong et al. (2007), who observed that hypoxia inhibits mES cell self-renewal and induces early differentiation. Their data suggested that hypoxia-induced in vitro differentiation of mES cells is triggered at least in part by the HIF-1α-mediated suppression of LIF-STAT3 signaling. Jeong et al. observed a 50% reduction in Oct4 gene expression after CCE cells were cultured for 48 h with pO_{2gas} of 7 mmHg, which is consistent with our data. They also observed much more dramatic morphological changes after 48 h than we did, which may be due to their use of a defined serum replacement in place of FBS used in our study. Niwa et al. (2001) used conditional expression to reduce Oct4 by a factor of 2 in mES cells. With cells under normoxia, they observed cell compaction at 48 h, as did we, but found extensive flattening with enlarged nuclei at 96 h, which we did not.

Although we observed substantial reduction in gene expression of transcription factors associated with self-renewal after culture at 7 or 0 mmHg in the presence of LIF, all other measurements—constancy of growth rate with time, morphological changes, pluripotency—demonstrated only modest or no departure from the behavior of undifferentiated stem cells under the conditions we studied. Such paradoxical behavior suggests that the hypoxia-induced early differentiation was self-limiting. We hypothesize that it could result from the simultaneous presence of self-renewal promoting characteristics of hypoxia that counterbalance the HIF-1α-mediated suppression of LIF-STAT3 signaling. Because this signaling pathway is important for maintenance of mES but not hES cells in an undifferentiated state (Daheron et al., 2004), our speculation draws support from a previous study (Ezashi et al., 2005) that found pO_{2gas} of 36 or 21 mmHg promoted self-renewal of hES cells, although other studies have not reported significant effects on hES cell self-renewal (Forsyth et al., 2006; Ludwig et al., 2006; Peura et al., 2005).

Further research is needed to explore the effects of hypoxic culture on mES cells in the presence of LIF on subsequent differentiation. There are situations where ES cell growth and survival are enhanced at moderately low pO_2 conditions, such as during the establishment of new mES cell lines (Gibbons et al., 2006; Wang et al., 2006) and during culture of hES cells at very low cell densities or sub-optimal culture conditions (Forsyth et al., 2006; Ording et al., 2005). Reduced pO_{2gas} conditions may also reduce the occurrence of chromosomal abnormalities in hES cells (Forsyth et al., 2006), but similar results have not been observed with mES cells (Wang et al., 2006). We found no effect of culture pO_2 in the range of 0–285 mmHg on the amount of oxidative DNA damage in undifferentiated mES cells using the comet assay.

The limited effects of culture pO_2 on ES cell proliferation, particularly under anoxia, led us to further investigate ES cellular energetic (Figs. 8 and 9). We measured the rates of lactate production and oxygen consumption (Fig. 9A) as indicators of the contributions of aerobic and anaerobic metabolism to the total cellular ATP production rate at all pO_{2gas} conditions (Fig. 9B). With excess oxygen, 40% of the ATP demand of ES cells was satisfied through anaerobic glycolysis, which is higher than the 15–25% reported for early embryos (Houghton, 2006; Houghton et al., 1996; Thompson et al., 1996). The reliance on anaerobic metabolism increased further with oxygen depletion, and all of the ATP was produced anaerobically under anoxia. The total ATP production rate remained nearly constant during this change, and ES cells could complete this adaptation in less than 2 days without significant loss of viability (Fig. 4).

Use of anaerobic metabolism of glucose and the ability of ES cells to adapt to reduced pO_2 conditions including anoxia is logical from a developmental viewpoint, since fetal development occurs in a very low pO_2 environment. The pO_2 in the maternal endometrium supporting an early embryo is about 40 mmHg, which in turn produces an oxygen concentration of about 0.05 mM in the surrounding tissue (Rodesch et al., 1992). Compared to oxygen, glucose is in substantial excess, with a fasting plasma concentration of approximately 3–4 mM (Weijers et al., 2002). An early embryo can therefore maximize its energy production rate by using both aerobic and anaerobic metabolism of glucose. The fact that mES cells utilize anaerobic metabolism to a substantial extent even at high pO_2 may also partially explain their ability to survive hyperoxia, since such a metabolic profile reduces the generation of harmful ROS (Andreyev et al., 2005). This profile is also observed in tumor cells (Gatenby and Gawlinski, 2003), and it has been shown that the glycolytic and the cancer phenotypes are very closely linked to one another (Kondoh et al., 2005; Ramanathan et al., 2005).

Many other cells increase anaerobic metabolism when confronted with hypoxia, which was first observed by Pasteur during yeast fermentation (Berg et al., 2002). The Pasteur effect has been particularly well documented in CHO and hybridoma cultures (Lin and Miller, 1992; Miller et al., 1987). Although the Pasteur effect is commonly observed, not all cells can adapt equally well to survive hypoxic/anoxic insult. As ES cells differentiate into mature cells, a shift to aerobic metabolism will occur for many lineages (Sharma et al., 2006), and some of the resulting cells will become sensitive to oxygen deprivation. Study of the energetics of differentiated cells obtained from ES cells could potentially be used as an evaluative tool for determination of cell maturation.

Our work shows that for bioprocess development with cells having the properties of undifferentiated mES cells, pO_2 control is not likely to be a critical parameter. The ideal pO_{2cell} is about 40 mmHg, which is likely to maximize growth without leading to excessive lactate formation and might also provide some protection from DNA damage.

However, both lower and higher pO_{2cell} conditions can be tolerated without excessive cell death or undesired changes in cell phenotype, although there may be effects on subsequent differentiation with LIF removal. We have observed a large effect of reduced pO_2 during the directed differentiation of ES cells to cardiomyocytes (Powers, 2007). Under these conditions pO_2 control is a much more important area that warrants further study.

This study was supported in part by grants from the NIH (NCRR ICR U4ZPR 16606 and ROI-KD063108 OIA) and the JDRF Center for Islet Transplantation at Harvard Medical School. Helpful discussions and technical assistance with aspects of the work were provided by Dr. Susan Bonner-Weir (Joslin Diabetes Center, Harvard Medical School), Anna Pisania, and Michael J. Rappel (MIT, Chemical Engineering), and Dr. Yuh-Shin Chang (Massachusetts General Hospital).

References

Andreyev AY, Kushnareva YE, Starkov AA. 2005. Mitochondrial metabolism of reactive oxygen species. Biochemistry (Mosc) 70(2):200–214.

Avgoustiniatos ES. 2002. Oxygen diffusion limitations in pancreatic islet culture and immunoisolation. Cambridge: MIT.

Berg JM, Tymoczko JL, Stryer L. 2002. Biochemistry. New York: W.H. Freeman and Company. p 974.

Bonner-Weir S, Taneja M, Weir GC, Tatarkiewicz K, Song KH, Sharma A, O'Neil JJ. 2000. In vitro cultivation of human islets from expanded ductal tissue. Proc Natl Acad Sci USA 97(14):7999–8004.

Bradley TR. 1978. The effect of oxygen tension on hematopoietic and fibroblastic cell proliferation in vitro. J Cell Physiol 97:517–522.

Brunelle JK, Chandel NS. 2002. Oxygen deprivation induced cell death: An update. Apoptosis 7(6):475–482.

Carmeliet P, Dor Y, Herbert JM, Fukumura D, Brusselmans K, Dewerchin M, Neeman M, Bono F, Abramovitch R, Maxwell P, Koch CJ, Ratcliffe P, Moons L, Jain RK, Collen D, Keshet E. 1998. Role of HIF-1alpha in hypoxia-mediated apoptosis, cell proliferation and tumour angiogenesis. Nature 394(6692):485–490.

Chakravarthy MV, Spangenburg EE, Booth FW. 2001. Culture in low levels of oxygen enhances in vitro proliferation potential of satellite cells from old skeletal muscles. Cell Mol Life Sci 58(8):1150–1158.

Cipolleschi MG, D'Ippolito G, Bernabei PA, Caporale R, Nannini R, Mariani M, Fabbiani M, Rossi-Ferrini P, Olivotto M, Dello Sbarba P. 1997. Severe hypoxia enhances the formation of erythroid bursts from human cord blood cells and the maintenance of BFU-E in vitro. Exp Hematol 25(11):1187–1194.

Collins AR, Dusinska M. 2002. Oxidation of cellular DNA measured with the comet assay. In: D A, editor. Oxidative stress biomarkers and antioxidant protocols. Totowa, N.J.: Humana Press. p 147–159.

Csete M. 2005. Oxygen in the cultivation of stem cells. Ann NY Acad Sci 1049:1–8.

Csete M, Walikonis J, Slawny N, Wei Y, Korsnes S, Doyle JC, Wold B. 2001. Oxygen-mediated regulation of skeletal muscle satellite cell proliferation and adipogenesis in culture. J Cell Physiol 189(2):189–196.

Daheron L, Opitz SL, Zaehres H, Lensch WM, Andrews PW, Itskovitz-Eldor J, Daley GQ. 2004. LIF/STAT3 signaling fails to maintain self-renewal of human embryonic stem cells. Stem Cells 22(5):770–778.

Devreker F, Englert Y. 2000. In vitro development and metabolism of the human embryo up to the blastocyst stage. Eur J Obstet Gynecol Reprod Biol 92(1):51–56.

Doetschman TC, Eistetter H, Katz M, Schmidt W, Kemler R. 1985. The invitro development of blastocyst-derived embryonic stem-cell lines—Formation of Visceral Yolk-Sac, Blood Islands and Myocardium. J Embryol Exp Morphol 87:27–45.

Dumoulin JC, Meijers CJ, Bras M, Coonen E, Geraedts JP, Evers JL. 1999. Effect of oxygen concentration on human in-vitro fertilization and embryo culture. Hum Reprod 14(2):465–469.

Ezashi T, Das P, Roberts RM. 2005. Low O2 tensions and the prevention of differentiation of hES cells. Proc Natl Acad Sci USA 102(13):4783–4788.

Fischer B, Bavister BD. 1993. Oxygen tension in the oviduct and uterus of rhesus monkeys, hamsters and rabbits. J Reprod Fertil 99(2):673–679.

Forsyth NR, Musio A, Vezzoni P, Simpson AH, Noble BS, McWhir J. 2006. Physiologic oxygen enhances human embryonic stem cell clonal recovery and reduces chromosomal abnormalities. Cloning Stem Cells 8(1):16–23.

Gatenby RA, Gawlinski ET. 2003. The glycolytic phenotype in carcinogenesis and tumor invasion: Insights through mathematical models. Cancer Res 63(14):3847–3854.

Gibbons J, Hewitt E, Gardner DK. 2006. Effects of oxygen tension on the establishment and lactate dehydrogenase activity of murine embryonic stem cells. Cloning Stem Cells 8(2):117–122.

Goetz IE. 1975. Oxygen toxicity in normal and neoplastic hamster cells in culture. In Vitro 11(6):382–394.

Harvey AJ, Kind KL, Thompson JG. 2002. REDOX regulation of early embryo development. Reproduction 123(4):479–486.

Helbock HJ, Beckman KB, Ames BN. 1999. 8-hydroxydeoxyguanosine and 8-hydroxyguanine as biomarkers of oxidative DNA damage. Oxidants Antioxidants B 300:156–166.

Helma C, Uhl M. 2000. A public domain image-analysis program for the single-cell gel-electrophoresis (comet) assay. Mutat Res Genet Toxicol Environ Mutagen 466(1):9–915.

Hevehan DL, Papoutsakis ET, Miller WM. 2000. Physiologically significant effects of pH and oxygen tension on granulopoiesis. Exp Hematol 28(3):267–275.

Hewitson LC, Leese HJ. 1993. Energy metabolism of the trophectoderm and inner cell mass of the mouse blastocyst. J Exp Zool 267(3):337–343.

Hopfl G, Wenger RH, Ziegler U, Stallmach T, Gardelle O, Achermann R, Wergin M, Kaser-Hotz B, Saunders HM, Williams KJ, et al. 2002. Rescue of hypoxia-inducible factor-1alpha-deficient tumor growth by wild-type cells is independent of vascular endothelial growth factor. Cancer Res 62(10):2962–2970.

Houghton FD. 2006. Energy metabolism of the inner cell mass and trophectoderm of the mouse blastocyst. Differentiation 74(1):11–18.

Houghton FD, Thompson JG, Kennedy CJ, Leese HJ. 1996. Oxygen consumption and energy metabolism of the early mouse embryo. Mol Reprod Dev 44(4):476–485.

Intaglietta M, Johnson PC, Winslow RM. 1996. Microvascular and tissue oxygen distribution. Cardiovasc Res 32(4):632–643.

Iyer NV, Kotch LE, Agani F, Leung SW, Laughner E, Wenger RH, Gassmann M, Gearhart JD, Lawler AM, Yu AY, et al. 1998. Cellular and developmental control of O2 homeostasis by hypoxia-inducible factor 1 alpha. Genes Dev 12(2):149–162.

Jauniaux E, Gulbis B, Burton GJ. 2003a. The human first trimester gestational sac limits rather than facilitates oxygen transfer to the foetus—A review. Placenta 24(Suppl A):S86–S93.

Jauniaux E, Gulbis B, Burton GJ. 2003b. Physiological implications of the materno-fetal oxygen gradient in human early pregnancy. Reprod Biomed Online 7(2):250–253.

Jeong C-H, Lee H-J, Cha J-H, Kim JH, Kim KR, Kim J-H, Yoon D-K, Kim K-W. 2007. HIF-1 alpha inhibits self-renewal of mouse embryonic stem cells in vitro via negative regulation of the LIF-Stat3 pathway. J Biol Chem 282(19):13672–13679.

Kaufman DS, Hanson ET, Lewis RL, Auerbach R, Thomson JA. 2001. Hematopoietic colony-forming cells derived from human embryonic stem cells. Proc Natl Acad Sci USA 98(19):10716–10721.

Keller G, Kennedy M, Papayannopoulou T, Wiles MV. 1993. Hematopoietic commitment during embryonic stem-cell differentiation in culture. Mol Cell Biol 13(1):473–486.

Kim JH, Auerbach JM, Rodriguez-Gomez JA, Velasco I, Gavin D, Lumelsky N, Lee SH, Nguyen J, Sanchez-Pernaute R, Bankiewicz K, et al. 2002.

Dopamine neurons derived from embryonic stem cells function in an animal model of Parkinson's disease. Nature 418(6893):50–56.

Kondoh H, Lleonart ME, Gil J, Wang J, Degan P, Peters G, Martinez D, Carnero A, Beach D. 2005. Glycolytic enzymes can modulate cellular life span. Cancer Res 65(1):177–185.

Kurosawa H, Kimura M, Noda T, Amano Y. 2006. Effect of oxygen on in vitro differentiation of mouse embryonic stem cells. J Biosci Bioeng 101(1):26–30.

Land SC. 2004. Hochachka's "Hypoxia Defense Strategies" and the development of the pathway for oxygen. Comp Biochem Physiol B Biochem Mol Biol 139(3):415–433.

Lee HC, Wei YH. 2005. Mitochondrial biogenesis and mitochondrial DNA maintenance of mammalian cells under oxidative stress. Int J Biochem Cell Biol 37(4):822–834.

Lee YM, Jeong CH, Koo SY, Son MJ, Song HS, Bae SK, Raleigh JA, Chung HY, Yoo MA, Kim KW. 2001. Determination of hypoxic region by hypoxia marker in developing mouse embryos in vivo: A possible signal for vessel development. Dev Dyn 220(2):175–186.

Lin AA, Miller WM. 1992. CHO cell response to low oxygen: Regulation of oxygen consumption and sensitization to oxidative stress. Biotechnol Bioeng 40(4):505–516.

Lindqvist A, Dreja K, Sward K, Hellstrand P. 2002. Effects of oxygen tension on energetics of cultured vascular smooth muscle. Am J Physiol Heart Circ Physiol 283(1):H110–H117.

Ludwig TE, Levenstein ME, Jones JM, Berggren WT, Mitchen ER, Frane JL, Crandall LJ, Daigh CA, Conard KR, Piekarczyk MS, et al. 2006. Derivation of human embryonic stem cells in defined conditions. Nat Biotechnol 24(2):185–187.

Maltepe E, Simon MC. 1998. Oxygen, genes, and development: An analysis of the role of hypoxic gene regulation during murine vascular development. J Mol Med 76(6):391–401.

Metzen E, Wolff M, Fandrey J, Jelkmann W. 1995. Pericellular PO_2 and O_2 consumption in monolayer cell cultures. Respir Physiol 100(2):101–106.

Miller WM, Wilke CR, Blanch HW. 1987. Effects of dissolved oxygen concentration on hybridoma growth and metabolism in continuous culture. J Cell Physiol 132(3):524–530.

Milosevic J, Schwarz SG, Krohn K, Poppe M, Storch A, Schwarz J. 2005. Low atmospheric oxygen avoids maturation, senescence, and cell death of murine mesencephalic precursors. J Neurochem 92:713–729.

Morrison SJ, Csete M, Groves AK, Melega W, Wold B, Anderson DJ. 2000. Culture in reduced levels of oxygen promotes clonogenic sympathoadrenal differentiation by isolated neural crest stem cells. J Neurosci 20(19):7370–7376.

Mostafa SS, Miller WM, Papoutsakis ET. 2000. Oxygen tension influences the differentiation, maturation and apoptosis of human megakaryocytes. Br J Haematol 111(3):879–889.

Niwa H, Miyazaki J, Smith AG. 2001. Quantitative expression of Oct-3/4 defines differentiation, dedifferentiation or self-renewal of ES cells. Nat Genet 24(4):372–376.

Ording CJ, Josephson HK, Auerbach JM. 2005. Effects of reduced oxygen tension on HUES-7 hES cells. ATCC Connect 17(2):1–5.

Orsi NM, Leese HJ. 2001. Protection against reactive oxygen species during mouse preimplantation embryo development: Role of EDTA, oxygen tension, catalase, superoxide dismutase and pyruvate. Mol Reprod Dev 59(1):44–53.

Palis J, Chan RJ, Koniski A, Patel R, Starr M, Yoder MC. 2001. Spatial and temporal emergence of high proliferative potential hematopoietic precursors during murine embryogenesis. Proc Natl Acad Sci USA 98(8):4528–4533.

Papas KK, Pisania A, Wu H, Weir GC, Colton CK. 2007. A stirred microchamber for oxygen consumption rate measurements with pancreatic islets. Biotechnol Bioeng 98(5):1071–1082.

Parrinello S, Samper E, Krtolica A, Goldstein J, Melov S, Campisi J. 2003. Oxygen sensitivity severely limits the replicative lifespan of murine fibroblasts. Nat Cell Biol 5(8):741–747.

Peura T, Bosman A, Stojanov T. 2005. Improved growth of hES cells in a reduced oxygen atmosphere. Reprod Fertil Dev 17(2):238–239.

Powers DE. 2007. Effects of dissolved oxygen on embryonic stem cell growth, energetics, and differentiation into cardiomyocytes. Cambridge: Massachusetts Institute of Technology. p 100.

Quinn P, Harlow GM. 1978. The effect of oxygen on the development of preimplantation mouse embryos in vitro. J Exp Zool 206(1):73–80.

Ramanathan A, Wang C, Schreiber SL. 2005. Perturbational profiling of a cell-line model of tumorigenesis by using metabolic measurements. Proc Natl Acad Sci USA 102(17):5992–5997.

Ramirez-Bergeron DL, Runge A, Dahl KD, Fehling HJ, Keller G, Simon MC. 2004. Hypoxia affects mesoderm and enhances hemangioblast specification during early development. Development 131(18):4623–4634.

Robertson E, Bradley A, Kuehn M, Evans M. 1986. Germ-line transmission of genes introduced into cultured pluripotential cells by retroviral vector. Nature 323(6087):445–448.

Rodesch F, Simon P, Donner C, Jauniaux E. 1992. Oxygen measurements in endometrial and trophoblastic tissues during early pregnancy. Obstet Gynecol 80(2):283–285.

Saretzki G, Armstrong L, Leake A, Lako M, von Zglinicki T. 2004. Stress defense in murine embryonic stem cells is superior to that of various differentiated murine cells. Stem Cells 22(6):962–971.

Sharma NS, Shikhanovich R, Schioss R, Yarmush ML. 2006. Sodium butyrate-treated embryonic stem cells yield hepatocyte-like cells expressing a glycolytic phenotype. Biotechnol Bioeng 94(6):1053–1063.

Siggaard-Andersen O, Huch R. 1995. The oxygen status of fetal blood. Acta Anaesthesiol Scand Suppl 107:129–135.

Soothill PW, Nicolaides KH, Rodeck CH, Campbell S. 1986. Effect of gestational age on fetal and intervillous blood gas and acid-base values in human pregnancy. Fetal Ther 1(4):168–175.

Soria B. 2001. In-vitro differentiation of pancreatic beta-cells. Differentiation 68(4–5):205–219.

Studer L, Csete M, Lee SH, Kabbani N, Walikonis J, Wold B, McKay R. 2000. Enhanced proliferation, survival, and dopaminergic differentiation of CNS precursors in lowered oxygen. J Neurosci 20(19):7377–7383.

Thompson JG, Partridge RJ, Houghton FD, Kennedy CJ, Pullar D, Leese HJ. 1996. Oxygen consumption by day 7 blastocysts: Determination of ATP production. Anim Reprod Sci 43:241–247.

Tice RR, Agurell E, Anderson D, Burlinson B, Hartmann A, Kobayashi H, Miyamae Y, Rojas E, Ryu JC, Sasaki YF. 2000. Single cell gel/comet assay: Guidelines for in vitro and in vivo genetic toxicology testing. Environ Mol Mutagen 35(3):206–221.

Tokuda Y, Crane S, Yamaguchi Y, Zhou L, Falanga V. 2000. The levels and kinetics of oxygen tension detectable at the surface of human dermal fibroblast cultures. J Cell Physiol 182(3):414–420.

Viswanathan S, Benatar T, Rose-John S, Lauffenburger DA, Zandstra PW. 2002. Ligand/receptor signaling threshold (LIST) model accounts for gp130-mediated embryonic stem cell self-renewal responses to LIF and HIL-6. Stem Cells 20(2):119–138.

Wang F, Thirumangalathu S, Loeken MR. 2006. Establishment of new mouse embryonic stem cell lines is improved by physiological glucose and oxygen. Cloning Stem Cells 8(2):108–116.

Ward CM, Barow KM, Stern PL. 2004. Significant variations in differentiation properties between independent mouse ES cell lines cultured under defined conditions. Exp Cell Res 293(2):229–238.

Weijers RN, Bekedam DJ, Smulders YM. 2002. Determinants of mild gestational hyperglycemia and gestational diabetes mellitus in a large Dutch multiethnic cohort. Diabetes Care 25(1):72–77.

Wenger RH. 2002. Cellular adaptation to hypoxia: O_2-sensing protein hydroxylases, hypoxia-inducible transcription factors, and O_2-regulated gene expression. FASEB J 16(10):1151–1162.

Wilson DF, Erecinska M, Drown C, Silver IA. 1979. The oxygen dependence of cellular energy metabolism. Arch Biochem Biophys 195(2):485–493.

Yarmush ML, Toner M, Dunn JC, Rotem A, Hubel A, Tompkins RG. 1992. Hepatic tissue engineering. Development of critical technologies. Ann NY Acad Sci 665:238–252.

Zhong H, Simons JW. 1999. Direct comparison of GAPDH, beta-actin, cyclophilin, and 28S rRNA as internal standards for quantifying RNA levels under hypoxia. Biochem Biophys Res Commun 259(3):523–526.

-Page Intentionally Left Blank-

C. Differentiation of hESC to β-cells

C.1. Introduction

Pluripotent stem cells are a potential source of insulin-secreting β-cells that has been explored for the past decade with both mouse and human cells [151-153]. ViaCyte, Inc. has recently developed a four-stage protocol for differentiating hESC *in vitro* in successive stages that mimic *in vivo* pancreatic organogenesis, inducing (1) definitive endoderm (DE), (2) primitive gut tube (PGT), (3) posterior foregut (PF), and (4) pancreatic endoderm (PE) and endocrine precursor (EP) [154, 155] and was the first to show that implantation of hESC-derived PE into mice resulted in the formation of insulin-secreting cells that can cure diabetic mice [9]. The Melton laboratory is also following an approach similar to ViaCyte but with the addition of small molecules, which are identified with a high-throughput screening assay at each stage. These small molecules result in an increased fraction of DE cells derived from mESC and hESC [130].

In 2009, the Colton and Melton laboratories along with ViaCyte, Inc. were awarded a research grant from the Juvenile Diabetes Research Foundation to increase the efficiency of differentiating human pluripotent stem cells into β-cells to cure type 1 diabetes and to improve characteristics of these cells for implantation. As part of this grant, I worked at ViaCyte, Inc. for one month to learn hESC culture and β-cell differentiation protocols and to begin to merge

these protocols with our low oxygen culture methodologies. The following are the results from my time at ViaCyte, Inc.

C.2. Differentiation of CyT49 hESCs with ViaCyte protocol

The ViaCyte protocols employed culture at 142 mmHg pO_{2gas} on standard polystyrene culture dishes, as described in Kroon et al [9]. When expanded in the pluripotent state, almost all CyT49 hESC cultured remained undifferentiated (Figure C-1). Two CyT49 clones, 304d and 511b, were differentiated. Assays were carried out for all markers and with all methods normally used by ViaCyte and cells were periodically observed by light microscopy. During stage 1, expression of BRACHYURY T, CER, SOX17, AND FOXA2 were detected with real-time PCR, and by the end of stage 1, most cells expressed FOXA2 and few expressed OCT4 (Figure C-2). HNF4A expression was detected during stage 2 (Figure C-3). PDX1 expression was detected during stage 3 (Figure C-4). During stage 4, expression of NKX6.1, PTF1A, NGN3, NKX2.2 was detected with qPCR (Figure C-5). Many cells expressed PDX1, and a subset of these cells coexpressed NKX6.1 (Figure C-6). After 16 days of differentiation, insulin-, glucagon-, and somatostatin-expression cells were observed (Figure C-7); some of these cells expressed more than one of these hormones, and c-peptide was detected in the culture medium (Figure C-8). These results are consistent with previous results from ViaCyte Inc and demonstrate that all aspects of the ViaCyte protocol were replicated, which is a necessary and critical first step in completing

all subsequent aims and milestones in the proposal. Cells from clone 304d were maintained in extended culture under stage 4 conditions for an additional 17 d. OCT4 expression decreased by four orders of magnitude during the 12-day differentiation and by another two orders of magnitude after 29 d (Figure C-9).

C.3. OCR of differentiating CyT49 hESC

We measured the OCR of cells differentiated with the ViaCyte protocol after 0, 2, 8, and 14 days of differentiation (Table C-1). The OCR for undifferentiated CyT49 cells was 21 amol $cell^{-1}$ s^{-1}, a value about 2/3 that of undifferentiated mouse embryonic stem cells, which we reported in Powers et al. [32], and the OCR remained unchanged with differentiation time.

C.4. Culture and differentiation of CyT49 cells on silicone rubber

One of the major aspects of the JDRF grant is to perform studies in well-defined oxygen environments by culturing in dishes having a silicone rubber membrane culture surface. Because of rapid progress made with the standard ViaCyte protocol, there was some time available to begin studies with these dishes. We plated undifferentiated CyT49 cells on silicone rubber membranes pretreated with fibronectin, matrigel, human serum, or with no treatment. After 24 hr, cells attached with fibronectin and matrigel coating, but poor attachment was observed with human serum treatment or without treatment (Figure C-10). After 3 days,

cells were confluent on fibronectin- and matrigel-coated silicone rubber (Figure C-11). Cells were subsequently differentiated for 7 days, at which time many cells stained positive for PDX1 (Figure C-12). Throughout culture, cell detachment was not observed with fibronectin or Matrigel treatment. This data demonstrates that the ViaCyte protocol can be performed on silicone rubber plates, and we do not expect problems to arise due to the use of these plates.

C.5. Tables and Figures

Table C-1. Oxygen consumption rate of CyT49 hESC during differentiation

Stage	Differentiation Time (days)	Oxygen Consumption Rate (amol $cell^{-1}$ sec^{-1})
0	0	21.0 ± 2.6
1	2	18.5 ± 1.5
3	8	20.9 ± 1.0
4	14	19.2 ± 4.3

Cells differentiated on polystyrene at pO_{2gas}=142 mmHg with Novocell protocol.

Data presented as average ± stdev.

n=2 for all except 0 days, in which n=7.

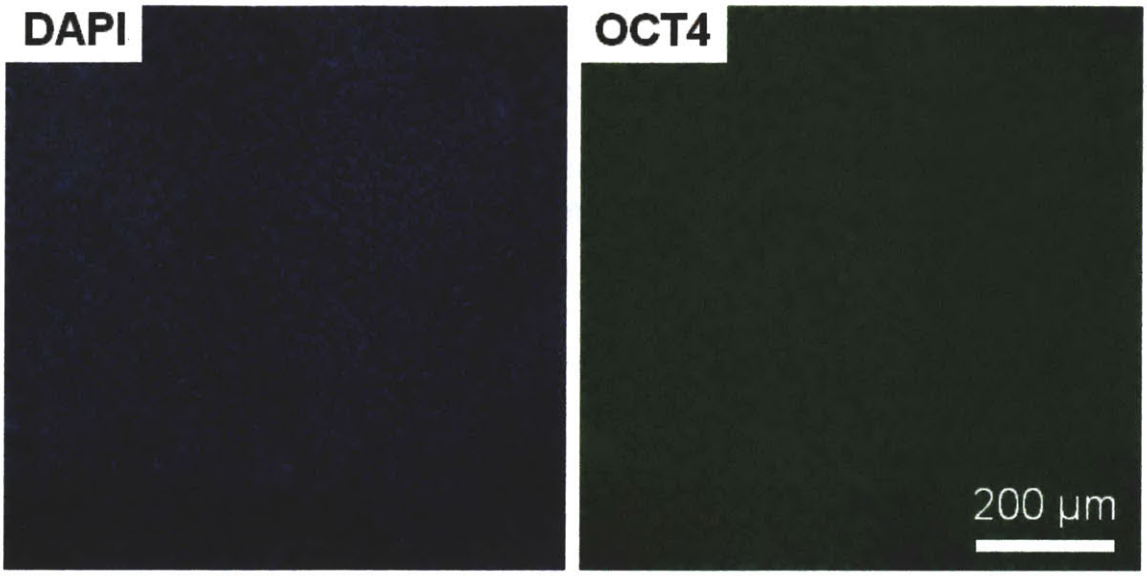

Figure C-1. En face immunofluorescence images of undifferentiated CyT49 cells.

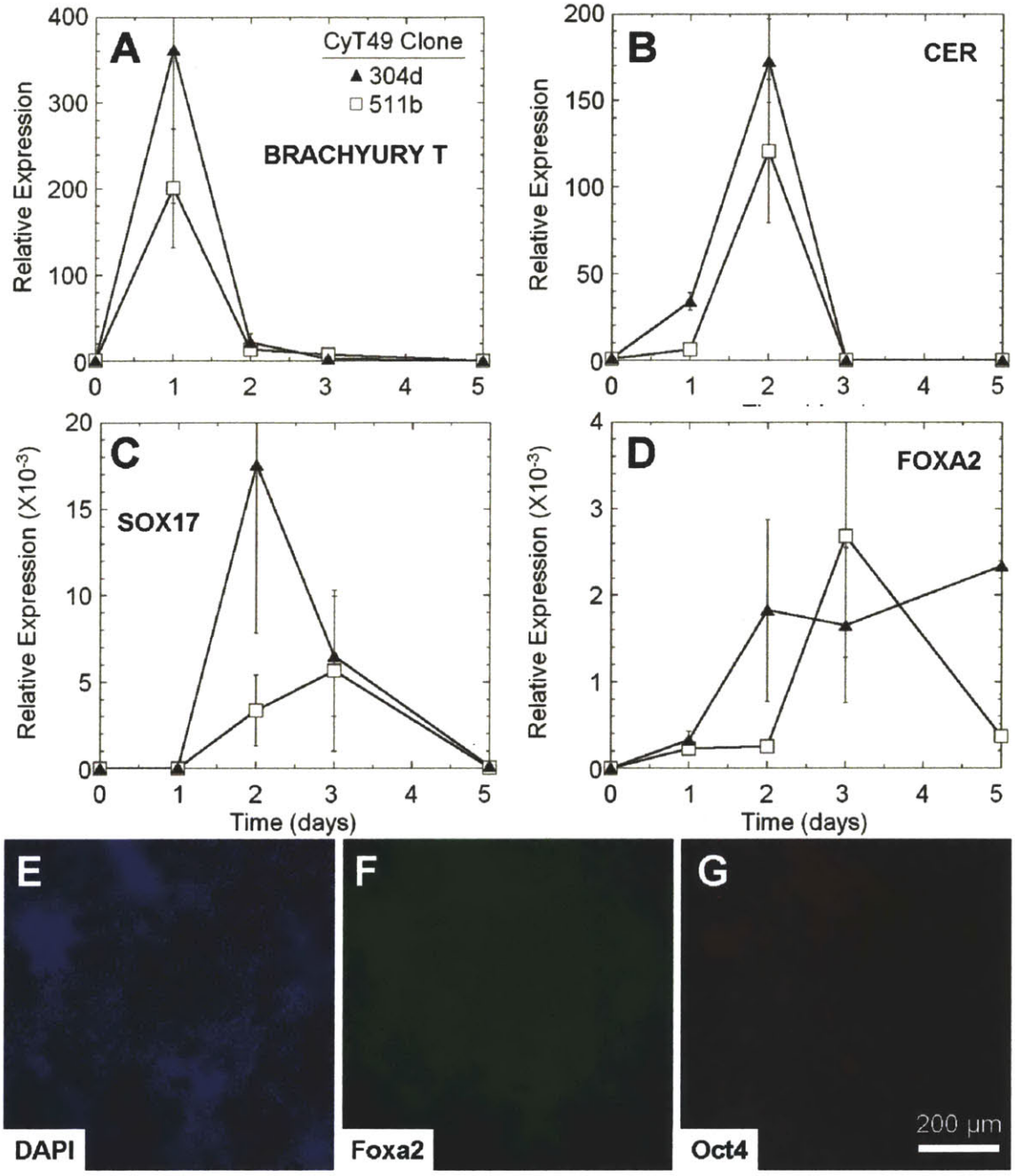

Figure C-2. Expression of stage 1 markers in differentiating CyT49 cells.

(A-D) Relative expression of BRACHYURY T, CER, SOX17, AND FOXA2 mRNA measured with real-time PCR (n=4). (E-G) En face images of cells differentiated 5 days and stained with DAPI or immunostained against FOXA2 or OCT4 protein.

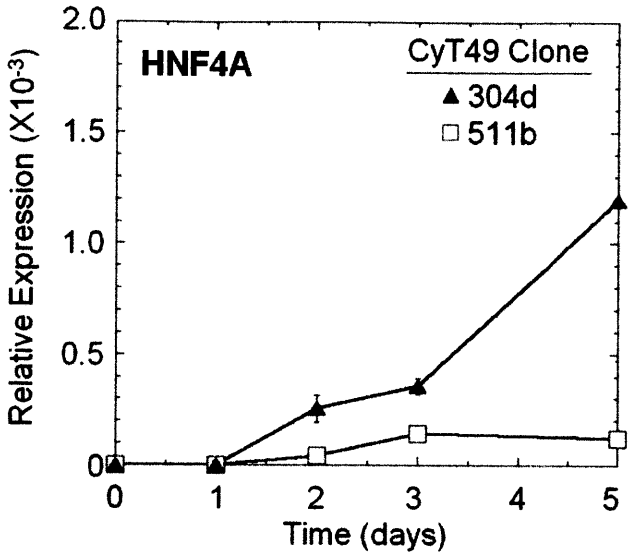

Figure C-3. Relative expression of the stage 2 marker HNF4A mRNA measured with real-time PCR in differentiating CyT49 cells (n=4).

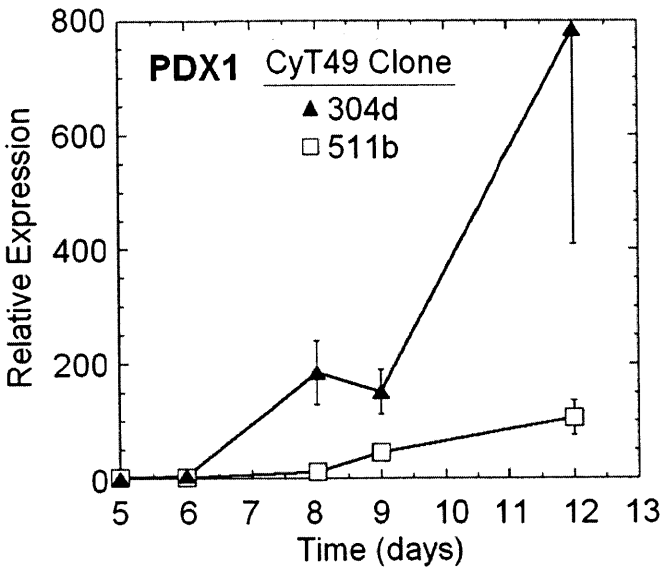

Figure C-4. Relative expression of the stage 3 marker PDX1 mRNA measured with real-time PCR in differentiating CyT49 cells (n=4).

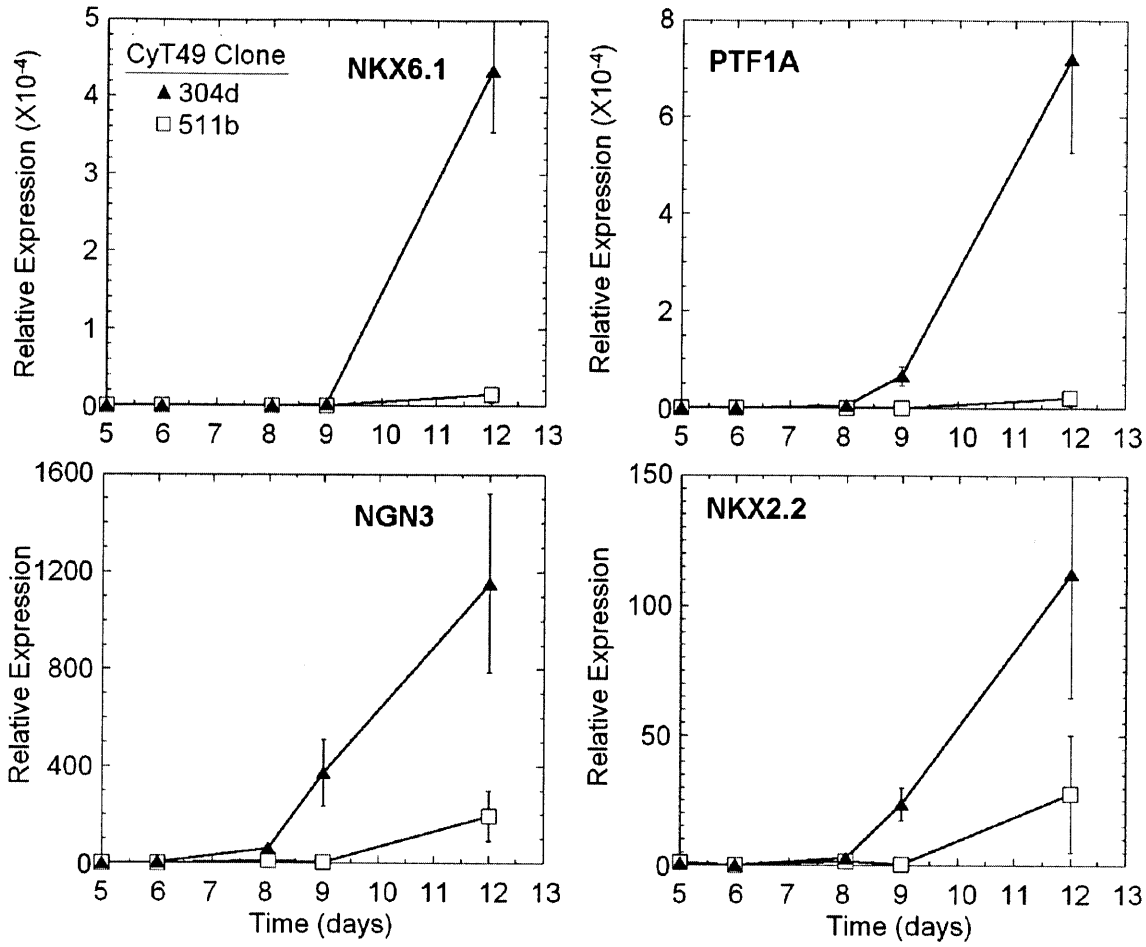

Figure C-5. Relative expression of the stage 4 markers NKX6.1, PTF1A, NGN3, NKX2.2 mRNA measured with real-time PCR (n=4).

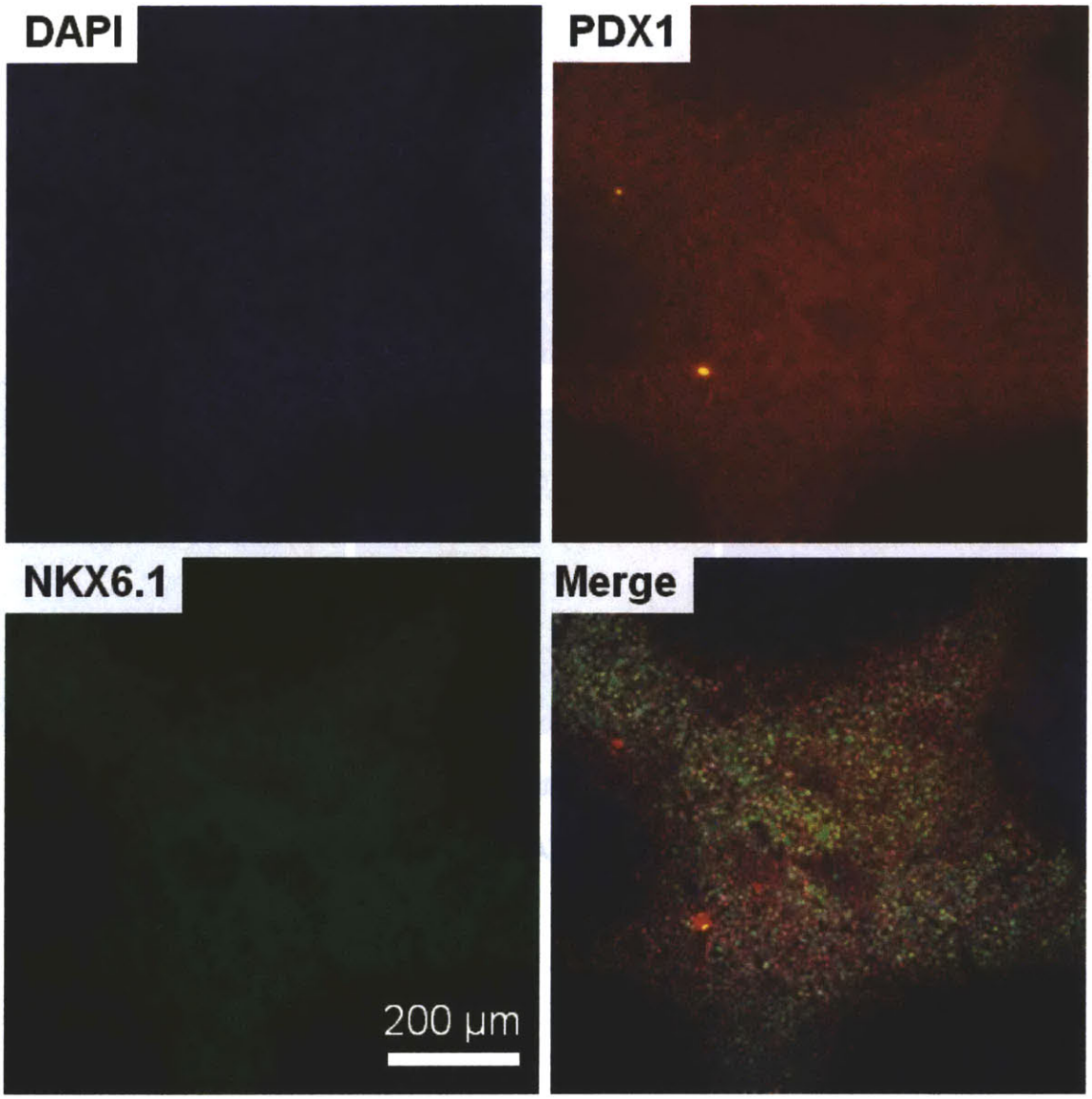

Figure C-6. En face images of cells differentiated 12 days and stained with DAPI and immunostained against PDX1 or NKX6.1 protein.

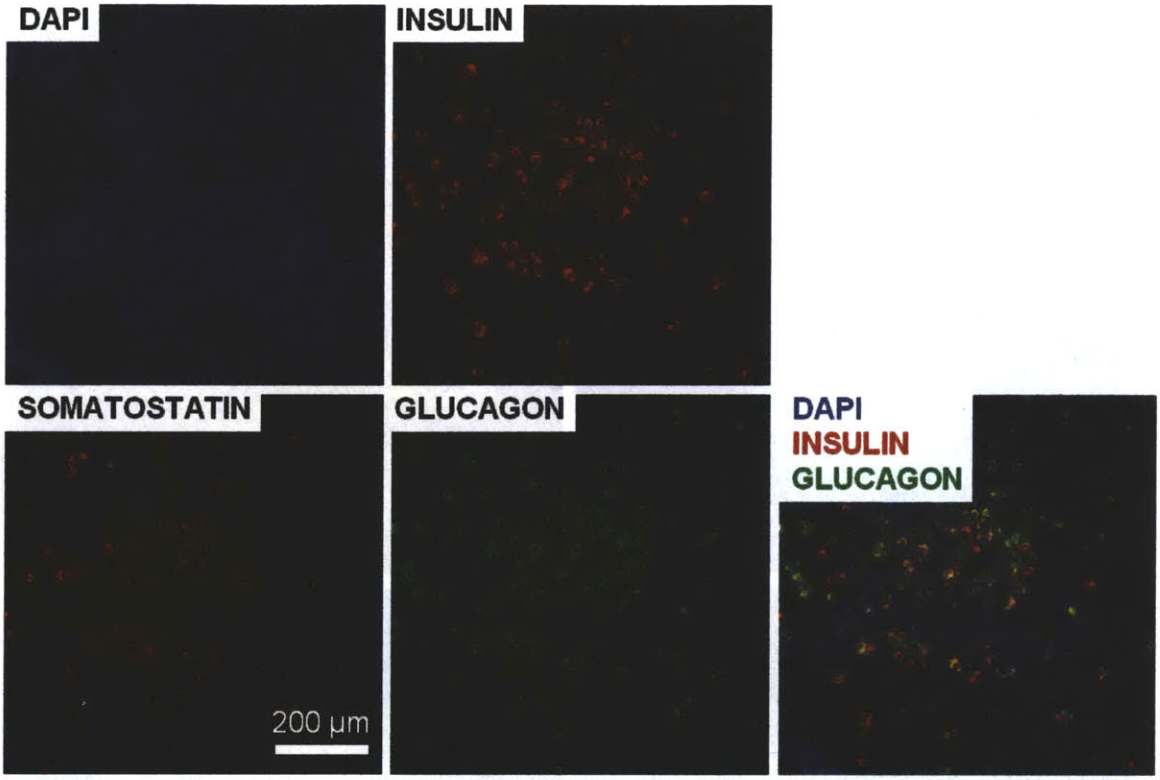

Figure C-7. En face images of cells differentiated 16 days and stained with DAPI and immunostained with INSULIN, SOMATOSTATIN, or GLUCAGON protein.

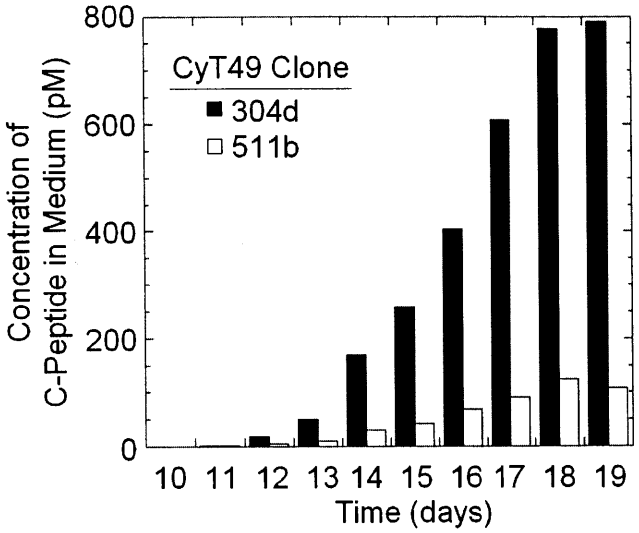

Figure C-8. Concentration of c-peptide in medium determined by ELISA for CyT49 cells differentiated with ViaCyte protocol (n=1)

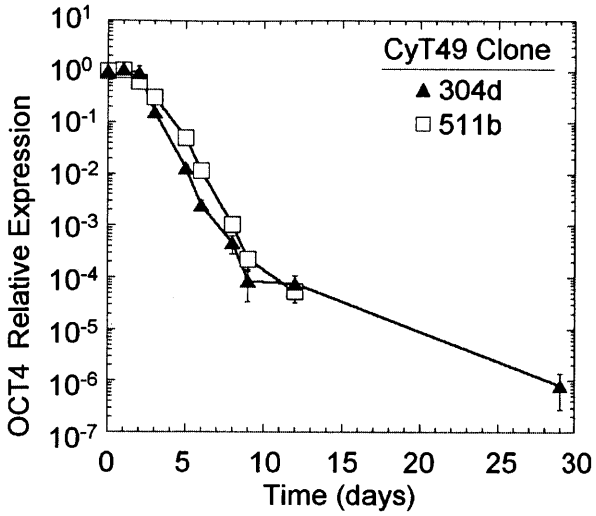

Figure C-9. Real-time PCR analysis of OCT4 expression of CyT49 hESCs during differentiation with ViaCyte protocol on polystyrene at pO_{2gas}=142 mmHg. After the 12-day protocol was completed, cells from clone 304d were maintained for another 17 days under conditions used to reach stage 4 (n=2).

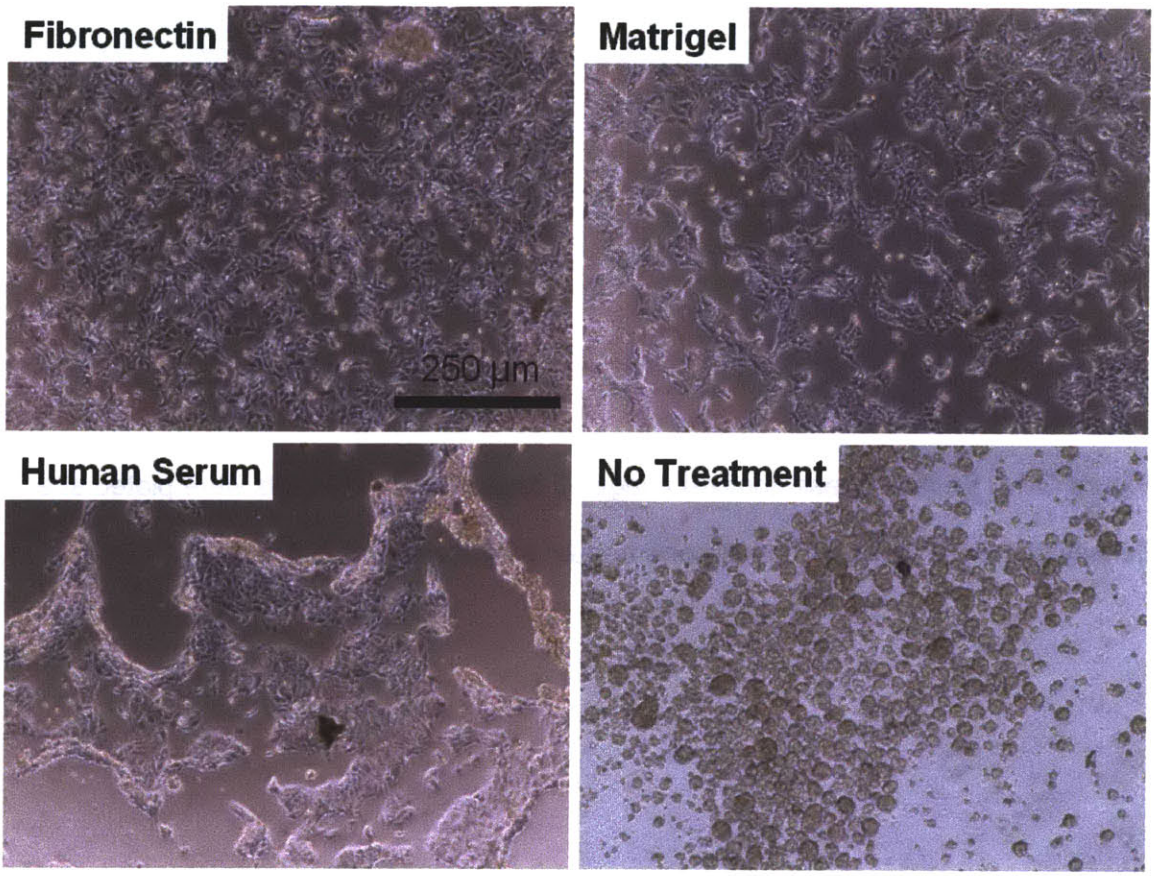

Figure C-10. En face phase contrast images 24 hr after CyT49 cells were plated at a density of $1.3x10^5$ cells cm^{-2} on silicone treated with fibronectin, Matrigel, human serum, or with no treatment.

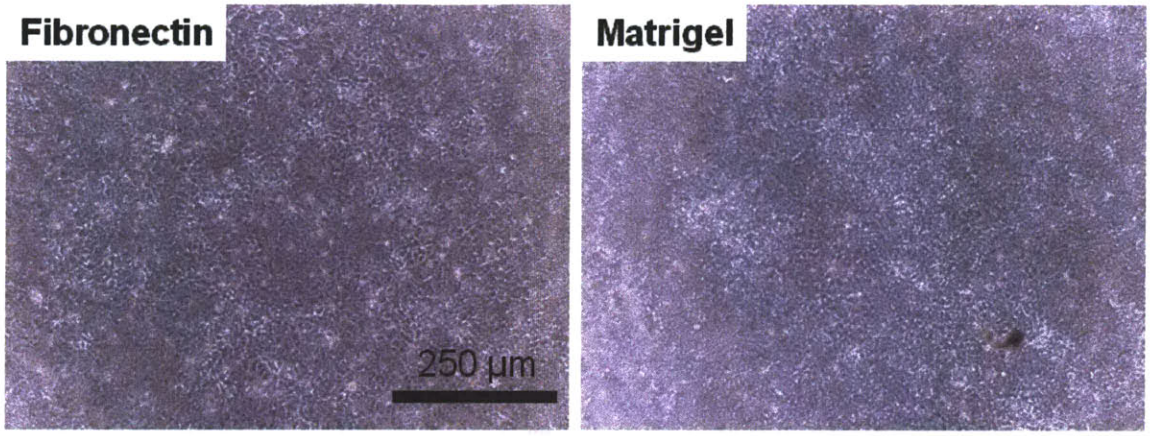

Figure C-11. En face phase contrast images 3 days after CyT49 cells were plated at a density of $1.3x10^5$ cells cm^{-2} on silicone treated with fibronectin or Matrigel.

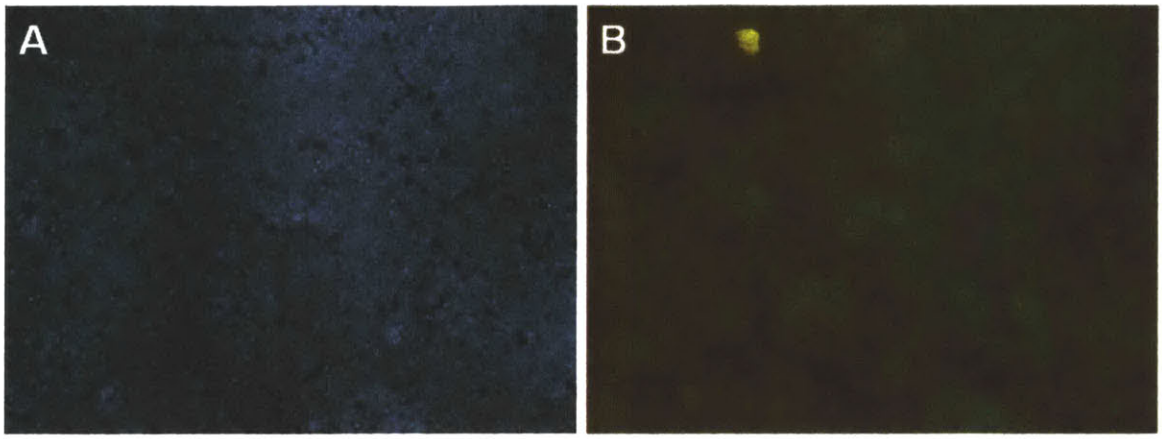

Figure C-12. En face immunofluorescence image of CyT49 cells differentiated 7 days to stage 3 with ViaCyte protocol on Matrigel-coated silicone rubber at 142 mmHg pO_{2gas}. (A) DAPI. (B) PDX1. 20x zoom.

-Page Intentionally Left Blank-

D. Experiments with the BioSpherix Xvivo

D.1. Introduction

The Xvivo incubation system is fabricated by BioSpherix, Inc and allows for the continuous cellular culture under reduced oxygen. It combines incubators with interconnecting, sealed glove box and microscope chambers in which pO_2 can be continuously controlled electronically. When the cells must be removed from the incubator and manipulated, sudden transient spikes in the oxygen concentration are avoided. We hypothesize that this feature is important for low oxygen culture because HIF-1α is rapidly degraded at atmospheric oxygen, and it takes hours to re-accumulate under low oxygen culture, which results in cells having depressed HIF-1α content for up to 8 hr [156]. Use of the Xvivo incubation system avoids these issues and allows for uninterrupted expression of HIF-1α and subsequent target genes. Combination of silicone rubber dishes [53] to the Xvivo system would provide a system to monitor and control the pO_2 to which the cells are exposed, a capability that does not now exist. The Xvivo incubation system can dynamically control the oxygen concentration of the incubator atmosphere. For example, when the cells are initially seeded at low density, a specific concentration of oxygen can be used. However, as the cell density increases, pO_{2cell} decreases. To compensate for this, the system could gradually increase pO_{2gas} according to an algorithm or based on sensor measurements to keep pO_{2cell} constant.

I performed several pilot studies to investigate the technical advantages of the Xvivo with and without silicone rubber membrane culture plates described hereafter.

D.2. The effect of low oxygen control methodologies on mESC VEGF secretion

D.2.1. Introduction

We investigated the secretion of VEGF protein by mESC cultured on silicone rubber membranes on top of polystyrene (SR-P) or silicone rubber alone (SR) using a flush box or Xvivo system. VEGF is an important signaling molecule that is secreted by cells at low oxygen and is involved in embryonic development and stem cell differentiation [42]. We hypothesized that VEGF expression during experiments involving low oxygen culture of cells in standard low oxygen incubators is likely affected by periodic high-oxygen exposure when the cells are handled (e.g. media changes) and that this problem is exacerbated if cell culture is being performed on oxygen-impermeable polystyrene dishes, since on the order of 20 hours can be required for the cells to return to low oxygen levels upon placement in a low oxygen environment [157]. We found that culture in the Xvivo and on SR dishes resulted in more VEGF production compared to the flush box

system and SR-P dishes because of their ability to better maintain pO_2 at low levels.

D.2.2. Methods

R1 mESC numbering $2.4x10^4$ were plated in a 24-well plate with culture surfaces consisting of either fibronectin-coated SR-P or SR, placed in a flush box or Xvivo incubator, and cultured in DMEM supplemented with 10% FBS and 10^3 units/mL of LIF at 142 or 7 mmHg pO_{2gas}. For SR-P, having silicone rubber on top of polystyrene controlled for differences in surface properties, while maintaining the oxygen transport characteristics of polystyrene. After 48 hours, the media was replaced with fresh media. Media exchange for the plates in the flush box was performed in an open biological safety cabinet at atmospheric pO_{2gas} (160 mmHg) and for cells in the Xvivo, was performed in the closed Xvivo system at 7 mmHg pO_{2gas}. After 24 additional hours of culture, media and cells were collected. The VEGF content of the media was assayed with ELISA (Calbiochem), and the viable cell number was determined with a membrane-integrity assay (Guava ViaCount).

D.2.3. Results

With incubation in the flush box, the VEGF content was higher under low oxygen compared to culture at 142 mmHg (Figure D-1). Among all 7 mmHg culture

conditions, culture on SR-P in the flush box had the smallest increase in VEGF content compared to 142, a factor of 1.9. Culture on SR in the flush box resulted in an even larger increase in VEGF content compared to 142, a factor of 5.1. VEGF content at low oxygen in the flush box is higher with SR compared to SR-P because pO_{2cell} rapidly reaches steady-state after exposure to atmospheric oxygen, requiring only minutes, while polystyrene requires on order 20 hours.

Incubation in the Xvivo system at 7 mmHg resulted in the higher VEGF content compared to 7 mmHg in the flush boxes for both SR-P and SR (Figure D-1). Culture in the Xvivo increased VEGF content by a factor of 2.8 and 1.2 on SR-P and SR, respectively, compared to culture in the flush box. There was no statistical difference between SR-P and SR at 7 mmHg in the Xvivo. In the Xvivo, cells were never exposed to atmospheric oxygen during media exchange, since the Xvivo allows media exchange to occur without changing pO_{2gas}. This allowed the cells to be at low pO_{2cell} during the entire duration of the experiment, longer than with the flush box.

D.2.4. Conclusions

With incubation at low pO_{2gas}, culture on SR and in the Xvivo system decreases and eliminates, respectively, periodic high-oxygen exposure that occurs with conventional culture in flush boxes. Because of this more consistent exposure to low oxygen with SR and the Xvivo, VEGF content was higher. These results

demonstrate the importance of oxygen-control methodologies, as they have large effects on cell phenotype.

D.2.5. Tables and Figures

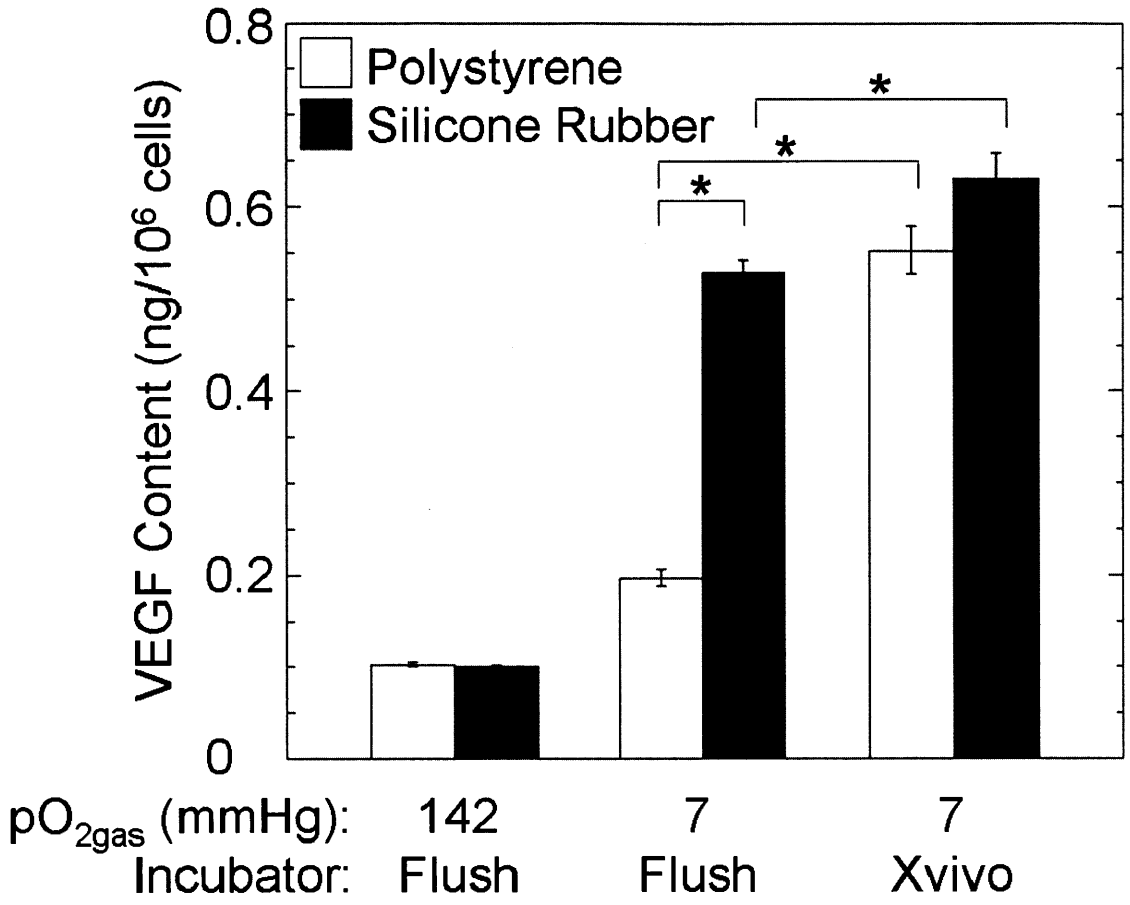

Figure D-1. VEGF content in culture medium for mESC cultured 24 hours at 142 or 7 mmHg pO_{2gas} determined with ELISA.

R1 mESC were culture on either fibronectin-coated polystyrene or silicone rubber in a flush box or Xvivo incubator. * $p<0.05$ between the two indicated conditions. n=3.

D.3. Experiments with oxygen sensors

D.3.1. Introduction

The pO_2 at the surface of cell culture dishes can differ from that in the gas phase, in particular if a culture vessel without a silicone rubber membrane bottom is used [157]. Mathematical models are available to predict pO_{2cell}; however, these require measurements of the OCR, which represents an added burden to stem cell researchers. Even when OCR is known, prediction of pO_2 within aggregates is more reliable if the pO_2 profile at the surface of the aggregate is measured.

The Xvivo culture system comes with 2-mm diameter oxygen sensors that can be inserted into open culture vessels to measure pO_2 in real time. The Xvivo can also change pO_{2gas} in response to sensor measurements, e.g., to keep pO_2 of the sensor ($pO_{2sensor}$) at a constant, set value. However, the presence of the oxygen sensor may significantly disrupt the oxygen gradient within culture medium normal to the cell surface that is present in static cell culture.

In the following pilot study, I investigated the disturbance of the oxygen gradient by the oxygen sensor and attempted to use oxygen sensor measurements coupled with Xvivo control of pO_{2gas} to maintain $pO_{2sensor}$ at a set value in mESC culture.

D.3.2. Methods

Finite element modeling was used to simulate pO_2 profiles and measurements for oxygen sensors ranging 0.1-1 mm in diameter in mESC culture using previously published oxygen permeability values [157]. To investigate oxygen sensor-based pO_2 control, $5x10^4$ mESC cm^{-2} were seeded on fibronectin-coated polystyrene or silicone rubber 24-well plates with a 2 mm medium height. After 24 hr, the medium was replaced with medium equilibrated at 76 mmHg pO_2 and a 2 mm-diameter oxygen sensor placed 0.5 mm above the cells (t=0). The cells were cultured for up to an additional 30 hr with either no process control or processor control where the set point was $pO_{2sensor}$=76 mmHg.

D.3.3. Effects of oxygen sensors on oxygen gradients

The presence of oxygen sensors disrupted the oxygen gradient and caused predicted pO_2 measurements lower than the actual pO_2 (Figure D-2). Sensors with a 1 and 0.5 mm diameter resulted in predicted measurements that were approximately 20 and 10 mmHg, respectively, lower than the actual pO_2 for all heights. The difference between the predicted measured and actual pO_2 increased the closer the sensors were to the cells. Small-diameter sensors had small (<10 mmHg) differences between predicted measured and actual pO_2 at all heights except near 0 μm, which had a difference greater than 10 mmHg.

Radial oxygen gradients were present on the surface of the oxygen sensor. Depletion of oxygen becomes increasingly severe towards the center of the probe surface with large diameter probes (0.5 and 1.0 mm), virtually reaching 0 mmHg. Smaller probes (0.1 mm and 0.2 mm) resulted in a less dramatic pO_2 drop between the bulk and the region directly underneath the sensor.

D.3.4. Control of $pO_{2sensor}$

Measurements of $pO_{2sensor}$ coupled with the Xvivo control of pO_{2gas} were used to control the value of $pO_{2sensor}$ to 76 mmHg (Figure D-3). Without process control, $pO_{2sensor}$ reached 0 mmHg by 18 hr on polystyrene (Figure D-3A). With process control at early times, large oscillations in the values of pO_{2gas} and $pO_{2sensor}$ were seen with polystyrene culture, with $pO_{2sensor}$ oscillating around 76 mmHg (Figure D-3B). By 30 hrs, pO_{2gas} had reached the maximum the system is capable of (660 mmHg), and the value of $pO_{2sensor}$ dropped to 0 mmHg (Figure D-3C). With silicone rubber culture plates, the value of $pO_{2sensor}$ was maintained at 76 mmHg both with and without process control (data not shown).

D.3.5. Conclusions

Physical insertion of oxygen sensors to measure pO_{2cell} is often not practical and disrupts the oxygen gradient, resulting in incorrect measurements of the actual pO_{2cell} in the absence of the probe. Sensors with larger diameters result in

diffusion limitations under the surface. Oxygen sensors with diameters smaller than 200 μm theoretically could avoid this problem but are likely too fragile. The development of practical microsensors or other alternative oxygen measurement methodologies is desirable.

In addition, coupling of these measurements to the Xvivo oxygen control system would provide researchers a way to precisely control the cell surface pO_2 in any commercially available culture dish. However, experiments coupling large 2 mm-diameter probes with the Xvivo control system were unable to control pO_2 in polystyrene dishes, presumably because of the large size of the probe. Use of silicone rubber dishes avoids the need for process control but are not commercially available.

D.3.6. Tables and Figures

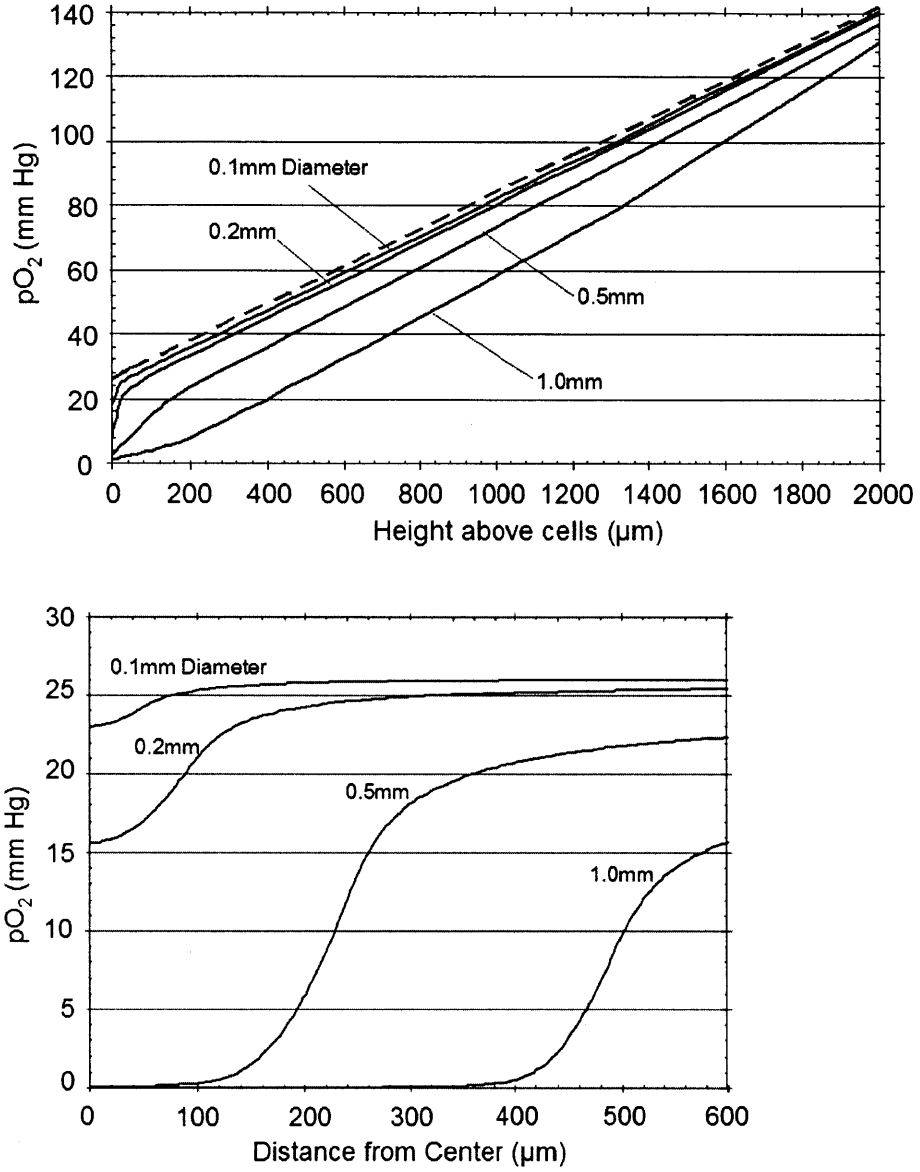

Figure D-2. Numerical simulations of oxygen sensors within oxygen gradient. (Top) Numerical simulation of pO_2 measurements by probes 0.1, 0.2, 0.5, and 1.0 mm in diameter as a function of height above respiring cells in 2 mm of media. The dashed line is the calculated pO_2 without any probe. (Bottom) Numerical simulation of the pO_2 profile across the surface of probes of different diameters placed 20 μm above the surface of respiring cells.

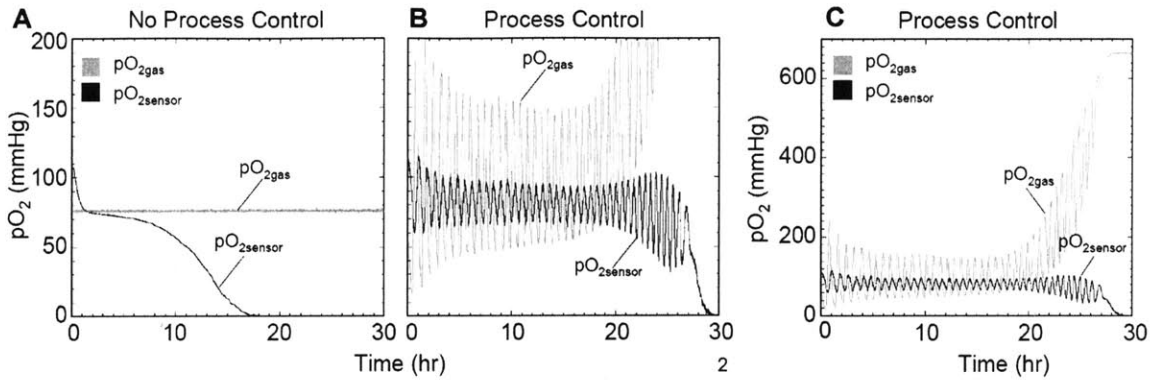

Figure D-3. Control of $pO_{2sensor}$ by controlling pO_{2gas}.

mESC plated on polystyrene were cultured for 30 hr with either (A) no process control or (B) process control. The controller attempted to keep $pO_{2sensor}$ at a set point of 76 mmHg by changing pO_{2gas}. The data plotted in (C) is the same data as in (B) but with a different scale.

D.4. The effect of continuous oxygen control on mESC differentiation to cardiomyocytes

D.4.1. Introduction

Chapter 2 demonstrates that low-pO_2 differentiation increases differentiation of mESC to cardiomyocytes. However, the incubation system employed was a flush box, which only controls pO_{2gas} while the cells are inside, but pO_{2gas} is 160 mmHg when the cells are removed for observation and medium exchange. We hypothesized that the continuous low oxygen culture environment afforded by the Xvivo would yield superior yields of cardiomyocytes compare to the period high oxygen exposure of the flush box. This periodic high oxygen exposure is of interest because continuous uninterrupted low oxygen culture is not currently available in most laboratories, and periodic high oxygen exposure is unavoidable.

D.4.2. Methods

J1 mESC were differentiated for 10 days with the differentiation protocol described in Chapter 2 on highly-oxygen permeable silicone rubber membranes with media supplemented with 0.2 mM ascorbic acid inside either flush box and Xvivo culture systems at 142 and 36 mmHg pO_{2gas}. Cells cultured in the flush box were removed and placed in a biological culture cabinet for 1 hour at room temperature and atmospheric O_2 and CO_2 every 24 hours, after which they were

returned to the flush box. Cells cultured in the Xvivo were cultured continuously at the indicated pO_{2gas} and 5% CO_2 or subjected to changes in pO_{2gas} or CO_2 as indicated. MF-20+ cells were counted with flow cytometric and cell number counted with nuclei counts, as described in Chapter 2.

D.4.3. Results

The fraction and number of MF-20+ cells was the same between cells cultured in the flush box and the Xvivo, regardless of the changes in pO_{2gas} and CO_2 (Table D-1). Based on these results, low-pO_2 differentiation of mESC to cardiomyocytes on silicone rubber membranes appears insensitive to these types of periodic high oxygen and low CO_2 perturbations. However, more acute processes, such as VEGF secretion (Appendix D.2), are sensitive to periodic high oxygen exposure. Moreover, mESC VEGF secretion was more sensitive to period high oxygen exposure when the cells were cultured on polystyrene culture plates, which required significantly more time to equilibrate back to low pO_{2gas} compared to silicone rubber membranes (Appendix A). Taken together, low-pO_2 differentiation of mESC to cardiomyocytes may be sensitive to period high oxygen exposure if the cells were instead cultured on polystyrene.

D.4.4. Tables

Table D-1. Comparison of different gas control strategies on mESC differentiation to cardiomyocytes

Culture System	pO_{2gas} (mmHg)	O_2 Constant?	CO_2 Constant?	Fraction MF-20+ (%)	Number MF-20+ ($x10^{-5}$ cells)
Flush Box	142	No	No	8.3 ± 3.2	1.0 ± 0.53
	36	No	No	16.2 ± 1.7	3.7 ± 0.068
Xvivo	142	Yes	Yes	8.0 *	1.5 *
	36	Yes	Yes	16.5 ± 3.5	3.8 ± 1.3
	36	No[a]	Yes	16.2 ± 1.4	4.2 ± 1.3
	36	Yes	No[b]	16.3 *	3.8 *

n=2 for all samples except where designated by *, where n=1 due to infection

[a] pO_{2gas} was changed to 160 mmHg for 1 hr every 24 hr

[b] CO_2 was changed to 0% for 1 hr every 24 hr